BNWL-1982

Mathematical and Experimental Investigations on Dispersion and Recirculation of Plumes from Dry Cooling Towers at Wyodak Power Plant in Wyoming

February 1976

Prepared for the Energy Research and Development Administration under Contract E(45-1):1830

Battelle
Pacific Northwest Laboratories

BNWL-1982

DISCLAIMER

NOTICE

PACIFIC NORTHWEST LABORATORY
operated by
BATTELLE
for the
ENERGY RESEARCH AND DEVELOPMENT ADMINISTRATION
Under Contract E(45-1)-1830

Printed in the United States of America
Available from
National Technical Information Service
U.S. Department of Commerce
5285 Port Royal Road
Springfield, Virginia 22151
Price: Printed Copy ~~$10.00~~ 9.00; Microfiche $2.25

ERDA-PL-RICHLAND, WA

BNWL-1982

MATHEMATICAL AND EXPERIMENTAL INVESTIGATIONS ON DISPERSION AND RECIRCULATION OF PLUMES FROM DRY COOLING TOWERS AT WYODAK POWER PLANT IN WYOMING

to
U.S. Energy Research and Development Administration

by
Yasuo Onishi
Donald S. Trent

February 1976

Battelle
Pacific Northwest Laboratories
Richland, Washington 99352

THIS PAGE

WAS INTENTIONALLY

LEFT BLANK

ABSTRACT

The use of dry cooling towers for dissipating waste heat produced from electric power generation can significantly reduce both the need for water and the stress on the environment caused by plant operation. However, effective arrangement of these cooling towers at a power plant site can be a critical design problem.

The present study was conducted (1) to develop a two-dimensional mathematical simulation model for determination of plume dispersion and recirculation from an existing code; (2) to investigate experimentally and mathematically the recirculation and temperature distributions of plumes from two dry cooling towers at the Wyodak Plant in Wyoming; and (3) to elucidate the effects of wind velocity, temperature of heated effluent, adjacent cooling towers and local topography on plume dispersion and recirculation.

The mathematical model is based on solution of the steady flow momentum and energy equations using the stream function-vorticity technique. Experiments were conducted in a 10-foot-wide hydraulic flume, using water as a model flow.

The study shows that plume recirculation and dispersion are strongly influenced by local topography and nearby structures such as adjacent cooling towers and buildings, as well as by the ambient wind velocity and effluent exit temperature. In the present study, nearby cooling towers and local topography produced up to approximately 18 percent of the recirculation ratio, which is a nondimensional temperature rise in the cooling tower's withdrawal air. This caused a 7 percent reduction in the cooling tower's heat rejection capability. This reduction of heat rejection capacity could be two to three times more for wet cooling towers. The study also

revealed very strong nonuniform distributions of cooling tower inlet air temperature within the cooling tower, implying that it may not be appropriate to assume that the ambient air temperature is the true inlet cooling air temperature, as is commonly done to evaluate cooling tower performance.

CONTENTS

LIST OF FIGURES

LIST OF TABLES

MATHEMATICAL AND EXPERIMENTAL INVESTIGATIONS ON DISPERSION AND RECIRCULATION OF PLUMES FROM DRY COOLING TOWERS AT WYODAK POWER PLANT IN WYOMING

1.0 INTRODUCTION

Dry cooling towers use air-cooled heat exchangers for rejecting waste heat from thermal power plants and the chemical process industry. As compared with once-through and wet cooling methods, the use of the dry cooling tower can significantly reduce water use and stress on the environment[1] and could make plant site selection easier. Dry cooling towers have been used in the United States process industry for decades. However, only a few electric power plants in Europe and one in the United States (Wyodak Plant, Wyoming) use the dry cooling system.

Large-scale electric power plants require many dry cooling tower modules to handle the quantity of heat generated by the power plant. Proper arrangement of these cooling towers on a power plant site can be a critical design problem. Improper arrangement can lead to recirculation of hot exhaust air into the intakes of the cooling tower or nearby cooling towers and cause an increase in the condenser temperatures.[2,3] This temperature rise in turn increases the turbine back-pressure and thereby reduces turbine efficiency and the plant's output of electricity.

During certain meteorological conditions, cooling tower performance can be adversely affected by the tower itself, adjacent towers, buildings, and the surrounding terrain.[4,5,6] When crosswinds are present, the heated effluent plume is deflected, or bent over, and the plume trajectory is shifted close to the intake faces of the cooling tower, resulting in recirculation of the plume into the tower intake. Recirculation

can become a significant problem if the tower or a portion of the plume is situated in a wake caused by adjacent structures and/or the local terrain. If one tower is located downwind of another, some of the effluent from the upwind tower may be ingested into the intake of the downwind tower, causing interference.

Severe recirculation and interference will occur if a captive eddy forms and persists between the cooling towers. When recirculation and/or interference occur, the true cooling air temperature available to the air-cooled heat exchangers increases and reduces cooling tower performance.

Little is known about the recirculation characteristics of large dry cooling towers for a power plant. The purpose of the present study has been (1) to develop a mathematical simulation model for plume dispersion and recirculation studies from an existing code; (2) to investigate experimentally and mathematically the plume recirculation and distributions of temperature and flow in the vicinity of the 330 MWe generating plant dry cooling tower at Wyodak, Wyoming, and the nearby 50 MWe ERDA dry cooling tower; and (3) to identify the effects of wind velocity, temperature of heated effluent, adjacent cooling towers, and local topography on plume dispersion and recirculation.

2.0 SUMMARY, CONCLUSIONS AND RECOMMENDATIONS

2.1 SUMMARY AND CONCLUSIONS

A two-dimensional simulation model for dispersion of plumes from dry cooling towers was evolved in this study. Dispersion, recirculation and interference of the plumes from the 50 MWe ERDA and the 330 MWe Wyodak plant dry cooling towers at Wyodak, Wyoming, were investigated both experimentally and mathematically, considering effects of various wind velocities, effluent exit temperatures, nearby cooling towers and local topographies.

The study reveals that the flow characteristics in the vicinity of the dry cooling towers at the Wyodak plant indicate strong three-dimensionality. The plume recirculation, and hence the cooling tower performance, are strongly affected by the adjacent cooling towers and local topography as well as by the velocity ratio of the heated effluent to the ambient flow, K, and the effluent densimetric Froude number, F_D. Two-dimensional heated jet experiments were also conducted to examine the validity of the numerical code developed in this study.

The main conclusions drawn from the investigation may be summarized as follows:

1) When K decreases (the ambient flow velocity increases), or F_D increases (effluent exit temperature decreases), the plumes from the cooling towers are deflected more closely to the ground. The mixing between the plumes and the ambient flow was also enhanced when K decreases.

2) Centerline trajectories of plume from both the Wyodak plant and the ERDA dry cooling towers reveal their strong dependency on the local topography and are expressed by Equation 4.4:

$$\frac{ZV_a^3}{F} = 1.5\left[\frac{XV_a^3}{F} \cdot \exp\frac{b}{a}\right]^{2/3}$$

where X and Z are longitudinal and vertical distances, respectively. V_a and F denote the ambient flow velocity and buoyancy flux of the plume, respectively. The distance between the cooling tower and the coal mine pit are represented by "a" and "b" is the depth of the coal mine pit at the Wyodak plant site. Hence, the plume rise is proportional to "2/3 power" of the longitudinal distance X.

3) The prevailing wind at the Wyodak plant site is northwesterly. When this is the case, the plume from the upwind ERDA dry cooling tower merges with the plume from the downwind Wyodak plant dry cooling tower, resulting in a higher plume rise of the merged plume and a lower temperature near the ground. Hence, the existence of the ERDA tower in this case may reduce the recirculation ratio, R (nondimensional temperature rise of cooling tower's inlet air flow defined by Equation 4.1) for the Wyodak plant cooling tower and may improve its performance. When the wind is southeasterly, the plume from the Wyodak plant tower covers the downwind ERDA tower. A fairly strong interference occurs in this case, causing higher recirculation ratios for both the Wyodak plant and the ERDA dry cooling towers.

4) It was found that there was severe nonuniform distribution of the cooling tower's withdrawal flow temperature (i.e., recirculation ratio, R) within the Wyodak plant cooling tower (see Figures 4.35 through 4.38). It is expected that the availability of the cooling air temperature varies for each module within a cooling tower. This implies that it may not be appropriate to assume the ambient air temperature to be the true inlet cooling air temperature, as is commonly done to evaluate the cooling tower performance.

5) The recirculation ratio, R, is small when K is large (or the ambient velocity is relatively small as compared with the heated effluent exit velocity). R first increases as K decreases (or the ambient wind velocity increases) from a large value of K and reaches its maximum value as K decreases. R then decreases as K further decreases (see Figure 4.40). This may be explained as follows: the plume rises relatively straight upward at a large value of K, resulting in a small recirculation ratio. When K decreases the plume is deflected more closely to the ground and R increases. As K further decreases, the plume is bent over more. However, mixing between the plume and the ambient flow is also greatly enhanced, resulting in the significant dilution of the plume and large reduction in temperature rise. Moreover, the strong ambient flow can supply more withdrawal flow from the upstream side intake face rather than withdrawing the flow from the wake behind the tower. Hence, R starts to decrease as K further decreases.

6) As shown in Figures 4.43 through 4.46, the recirculation ratio, R, for both cooling towers monotonically increases as the effluent densimetric Froude number, F_D increases (or the temperature difference between the effluent and the ambient flow, ΔT_o decreases) for the range covered by this study.

7) A large difference of R between the southeasterly wind with flat ground case (Run C) and the northwesterly wind with flat ground case (Run A) was found for both the Wyodak plant and the ERDA towers (see Figures 4.40 and 4.42). The maximum R values of the ERDA tower for Runs C and A were 19 and 1 percent, respectively. This 19 percent recirculation ratio is due to the strong

interference caused by the upwind Wyodak plant tower. The maximum R values of the Wyodak plant tower for Runs C and A were 6 and 2 percent, respectively. These differences were due to the locations of the nearby cooling towers (the Wyodak plant tower location for the ERDA tower's recirculation ratio and the ERDA tower location for the Wyodak plant tower's recirculation ratio) with respect to the wind direction. Actual topography in the vicinity of the Wyodak plant site reduced values of R for the southeasterly wind case (Run TD), but increased values of R for the northwesterly wind case (Run TU) as compared to those for the flat ground cases (Runs C and A).

8) A dry cooling tower performs poorly during the hot summer months. At the Wyodak plant site, northwesterly and southeasterly winds prevail in the summer. Figures 4.39 and 4.42 show that the worst performances of both the Wyodak plant tower and the ERDA tower are expected to occur at 10 mph and 37 mph southwesterly winds, respectively. The recirculation ratios in these cases are 6 and 19 percent. If the ambient wind temperature is assumed to be 85°F, reductions in the cooling capacities of the Wyodak plant and the ERDA towers are estimated at 2 and 7 percent, respectively. For conventional wet cooling towers, which usually have a much smaller initial temperature difference, the loss of heat rejection capacity due to recirculation could be two to three times more severe than that of a dry cooling tower for the same recirculation ratio. In both cases, proper arrangement of cooling towers can be a critical design problem.

9) As discussed in Conclusion 8, the worst recirculation conditions for the Wyodak plant and the ERDA towers occur at different ambient wind velocities. Moreover, the Wyodak plant tower, which has a much smaller recirculation ratio than that of the ERDA tower, will be used to reject 85 percent of the total plant exhaust heat. The overall cooling performance obtained by the two dry cooling towers is expected to perform most poorly when the wind is at 30 mph from the southeast during summer. However, even for this case, the loss of the overall plant's cooling capacity due to recirculation is only 2 percent. If the Wyodak plant tower is used to reject all the plant exhaust heat, without using the ERDA tower, the cooling capacity loss due to recirculation is only 1 percent. Hence, locations of the Wyodak plant and the ERDA towers have been properly arranged with respect to spacing, orientation and actual topography, so that plume recirculation causes almost no interference to the Wyodak power plant's overall operation.

10) The numerical simulation model evolved in this study demonstrated its capability to calculate temperature distribution of the plume from cooling towers and the flow patterns including wakes behind the towers, recirculation and interference. Comparison of the calculated and experimental results for the Wyodak plant dry cooling tower case revealed that plume heights agreed reasonably well. However, the computer results showed a large circulation pattern in the wake of the Wyodak tower and significant recirculation. This disagreement may be explained by the fact that the computer model is two-dimensional, whereas the hydraulic model revealed significant three-dimensional effects. These included significant

edge effects, such as lateral withdrawal and entrainment, because of the dry cooling tower's short length as compared to width. These effects tend to decrease temperatures within the plume.

11) Comparisons between computer and experimental results for the two-dimensional heated jet cases revealed that the water temperature distrubutions yield good agreement and that the simulation model is able to predict both flow pattern and temperature distributions for a plume dispersion study. However, these comparisons must be regarded as preliminary and further detailed tests are needed to verify the numerical model.

2.2 RECOMMENDATIONS

Local topography and nearby structures (e.g., adjacent cooling towers and buildings) are revealed to be important factors in recirculation, interference and plume rise. These factors may also cause a strong maldistribution of true cooling air temperature within a cooling tower. Since little is known about these problems, it is recommended that these recirculation and interference problems be studied numerically and experimentally for various topographies and nearby structures and that generalized cooling tower siting criteria be obtained. A study for determination of detailed flow and temperature distributions within a cooling tower is also needed. Interaction among plumes from a large number of cooling towers, such as those at possible energy centers, is extremely complex. Further experimental and mathematical studies are recommended to obtain accurate velocity and temperature distributions in the near field, which is strongly affected by the interaction among many cooling towers and by the local topography.

3.0 DESCRIPTION OF HYDRAULIC MODEL

3.1 DIMENSIONAL ANALYSIS AND MODELING CRITERIA

For fixed cooling tower geometry, surrounding topography and adjacent structures, the spatial distribution of the temperature difference, ΔT, where ΔT is defined as the difference between the temperature T at any point in the flow field and that of the ambient flow, T_a, can be expressed by

$$\Delta T = f(X, Y, Z, g, \nu_a, \nu_j, \rho_a \Delta\rho_o, V_a, V_j, \frac{\Delta T_a}{\Delta Z}, \gamma_d, \Delta T_o, L, D) \quad (3.1)$$

where

X, Y, Z = Cartesian coordinates in the longitudinal, lateral and vertical directions, respectively

g = gravitational acceleration

ν_a, ν_j = kinematic viscosity of the ambient fluid and tower discharge, respectively

ρ_a = reference ambient fluid density

$\Delta\rho_o$ = density difference between the tower discharge and the reference ambient fluid

V_a, V_j = velocities of the ambient flow and tower discharge, respectively

$\Delta T_a / \Delta Z$ = vertical temperature gradient of ambient flow

γ_d = dry adiabatic lapse rate

ΔT_o = temperature difference between the tower discharge and the ambient flow

L = characteristic length scale of the ambient flow

D = cooling tower stack diameter

Dimensional analysis with the Π theorem yields the following expressions from Equation 3.1:

$$\frac{\Delta T}{\Delta T_o} = f\left(\frac{X}{D}, \frac{Y}{D}, \frac{Z}{D}, \frac{V_j}{\sqrt{\frac{\Delta\rho_o}{\rho_a} gD}}, \frac{V_a L}{\nu_a}, \frac{V_j D}{\nu_j}, \frac{\Delta\rho_o}{\rho_a}, \frac{V_j}{V_a}, \frac{\Delta T_a}{\gamma_d \Delta Z}, \frac{\Delta T_a}{\gamma_d L}\right) \quad (3.2)$$

Since the effect of the density difference between the ambient flow and the tower discharge is incorporated in the term of $V_a/\sqrt{(\Delta\rho_o/\rho_a)gD}$, the term $\Delta\rho_o/\rho_a$ in Equation 3.2 can be deleted. The term $\Delta T_a/\gamma_d L$ is important only if L is a vertical distance. However, for this case this term expresses the same meaning as that of the term $\Delta T_a/\gamma_d \Delta Z$. Therefore, the term $\Delta T_a/\gamma_d L$ can be deleted. For the present experiments, neutral stratification of the ambient air flow was imposed. Hence, the ambient flow stability parameter $\Delta T_a/\gamma_d \Delta Z$ will be deleted from Equation 3.2. Equation 3.2 then becomes

$$\frac{\Delta T}{\Delta T_o} = f\left(\frac{X}{D}, \frac{Y}{D}, \frac{Z}{D}, \mathbb{F}_D, \mathbb{R}_a, \mathbb{R}_j, K\right) \quad (3.3)$$

where

$$\mathbb{F}_D = \frac{V_j}{\sqrt{\frac{\Delta\rho_o}{\rho_a} gD}}, \text{ densimetric Froude number} \quad (3.4)$$

$$\mathbb{R}_a = \frac{V_a L}{\nu_a}, \text{ ambient flow Reynolds number} \quad (3.5)$$

$$\mathbb{R}_j = \frac{V_j D}{\nu_j}, \text{ jet Reynolds number} \quad (3.6)$$

$$K = \frac{V_j}{V_a}, \text{ velocity ratio of the effluent to the ambient flow} \quad (3.7)$$

Hence, to obtain similarity between the prototype and the model, the last four similarity criteria in the right hand side of Equation 3.3, in addition to geometric similarity, must be satisfied. However, it is not possible to exactly satisfy all similarity conditions described in Equation 3.3; it is intended to satisfy the Reynolds criteria, $\mathbb{R}_a$ and $\mathbb{R}_j$, only to the extent that the ambient and jet flows in the model will be maintained as turbulent flows.

In the experiments, water was used as a model fluid to simulate the prototypic air flow movement because with water it is relatively easier, and requires smaller models, to satisfy the densimetric Froude number and Reynolds number criteria for the model. Flow and temperature measurements and flow observations are also more readily conducted in water than in air. The models of the two proposed dry cooling towers at the Wyodak plant in Wyoming have a model-to-prototype length scale ratio of 1/600. Actual prototype and model flow conditions and similitude will be described in Chapter 4.

3.2 EXPERIMENTAL EQUIPMENT

The principal item of equipment used in the experimental study was a hydraulic flume located in the Battelle, Pacific Northwest Laboratories.

3.2.1 Hydraulic Flume

Figure 3.1 shows the multi-purpose hydraulic flume which was designed for research in hydrodynamics and physical model studies of free surface flow phenomena such as thermal dispersion, sediment and pollutant transport, river and estuary hydraulics, hydraulic structures, etc. This recirculating flume with an open-channel section 10 feet wide, 1.5 feet deep and 42 feet long has adjustable slope and is capable of flow rates up to 10 cfs. As shown in Figure 3.1, one side wall of

the flume has three glass windows through which flow movement can be observed and photographed. Flow discharge is measured by means of calibrated orifice meters in each of the two 10-inch return pipes. The flume is equipped with a motor driven carriage which rides the full length of the flume channel on rails. Remote sensing devices (e.g., an infrared camera) can be installed on the carriage to take temperature distributions of surface water at every location in the flume (Figure 3.2).

During the course of this study, three major pieces of equipment have been fabricated: (1) a glass-walled hydraulic flume with an open-channel section 4 feet wide, 5 feet deep and 40 feet long (Figures 3.3 and 3.4) and a maximum discharge of 10 cfs; (2) a PDP 11/10 Computer Data Aquisition and Control System for experiments conducted in the two hydraulic flumes; and (3) a 4-watt argon laser which can measure the flow velocity and concentration of various substance in the water at any location within the glass-walled flume.

3.2.2 Water Heat Exchanger

Three heat exchangers (two 90 kW and one 75 kW, in series) supplied heated water for temperature studies. The heat input to obtain a desired water temperature could be adjusted to any value between zero and 255 kW by an AC power controller. Heated water discharge was measured by flow meters, shown at the right side of Figure 3.5.

3.2.3 Thermistors

Temperature measurements were made with thermistors and an electronic data recording system (Figures 3.1 and 3.5). All thermistors used for this study were calibrated; their calibration curve is shown in Figure 3.6. The data obtained by this system were fed into a PDP 11/45 computer and the water temperature distributions were plotted by a Calcomp Plotter 936. The

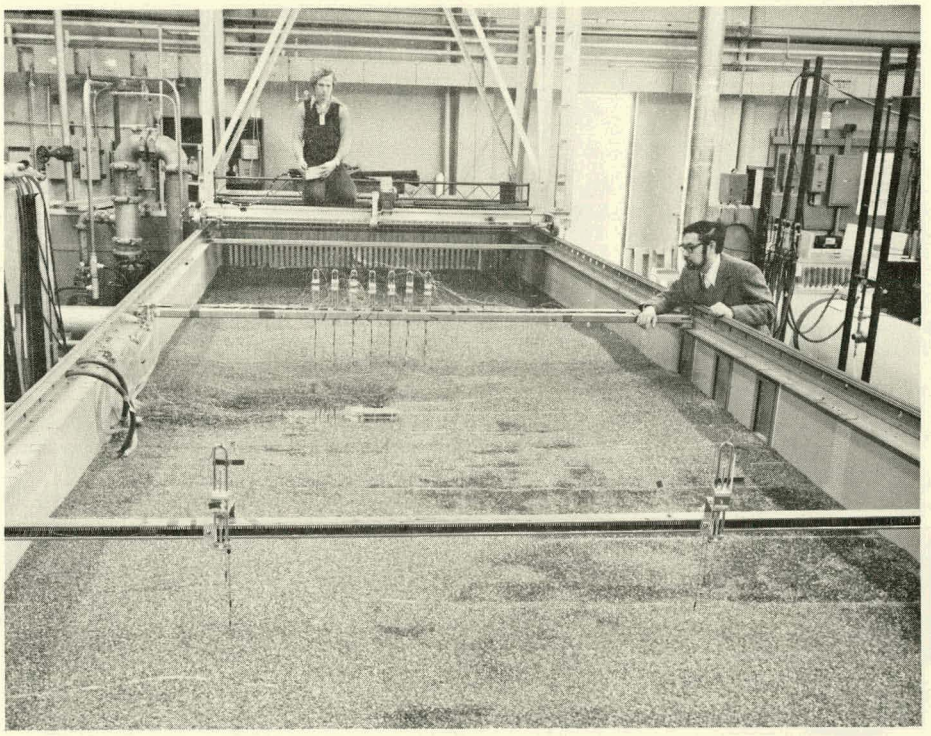

FIGURE 3.1 Photograph of the Multi-Purpose Hydraulic Flume and Experimental Set Up

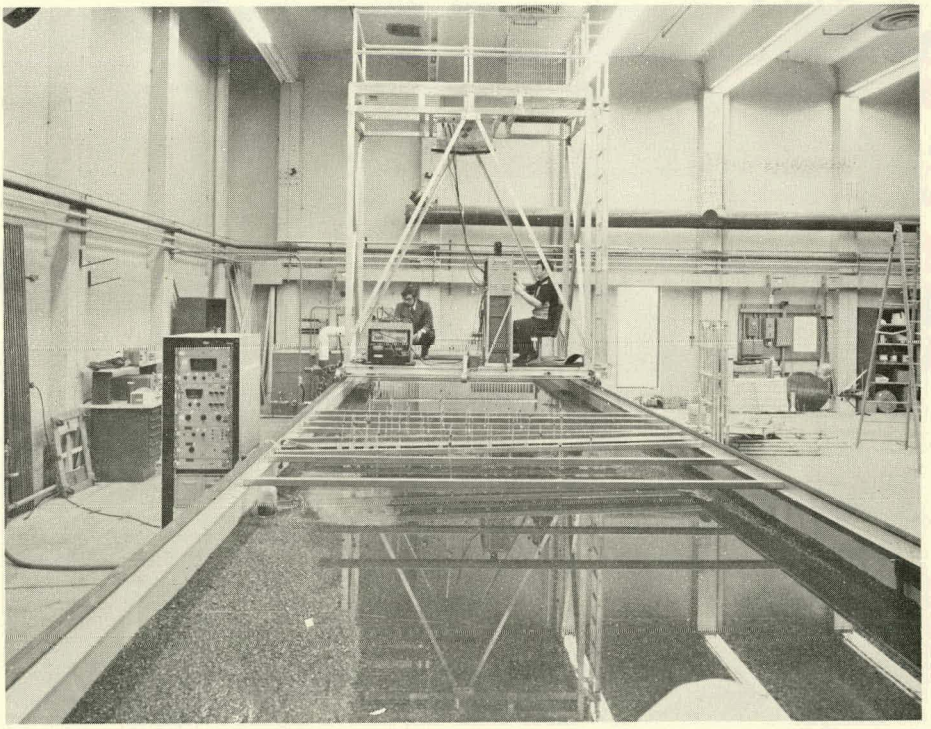

FIGURE 3.2 Photograph of the Multi-Purpose Hydraulic Flume and a Remote Sensing Device

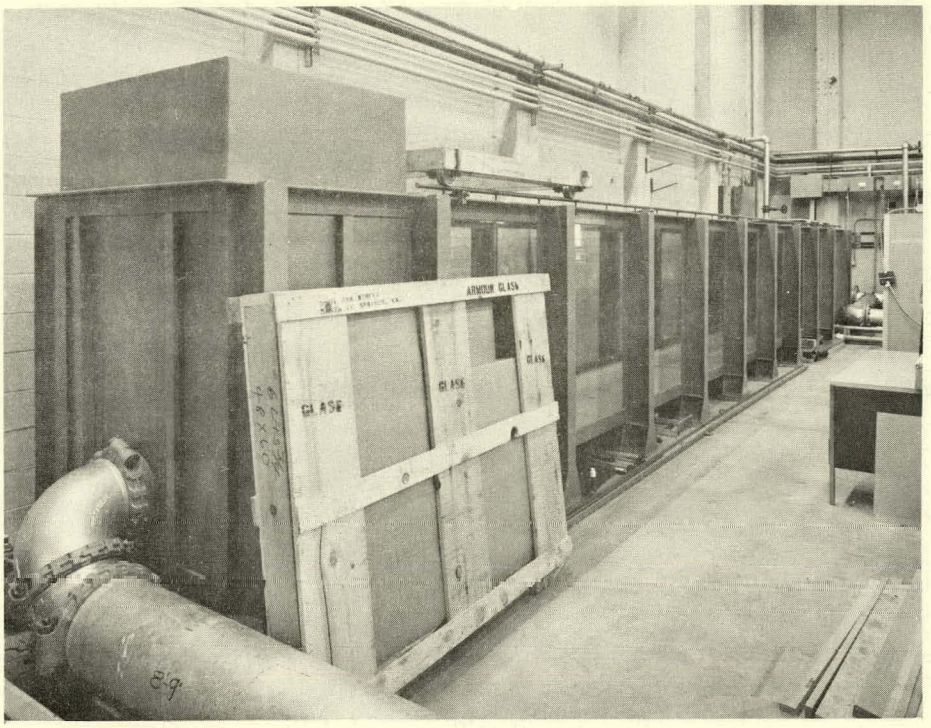

FIGURE 3.3 Photograph of the Glass-Walled Flume

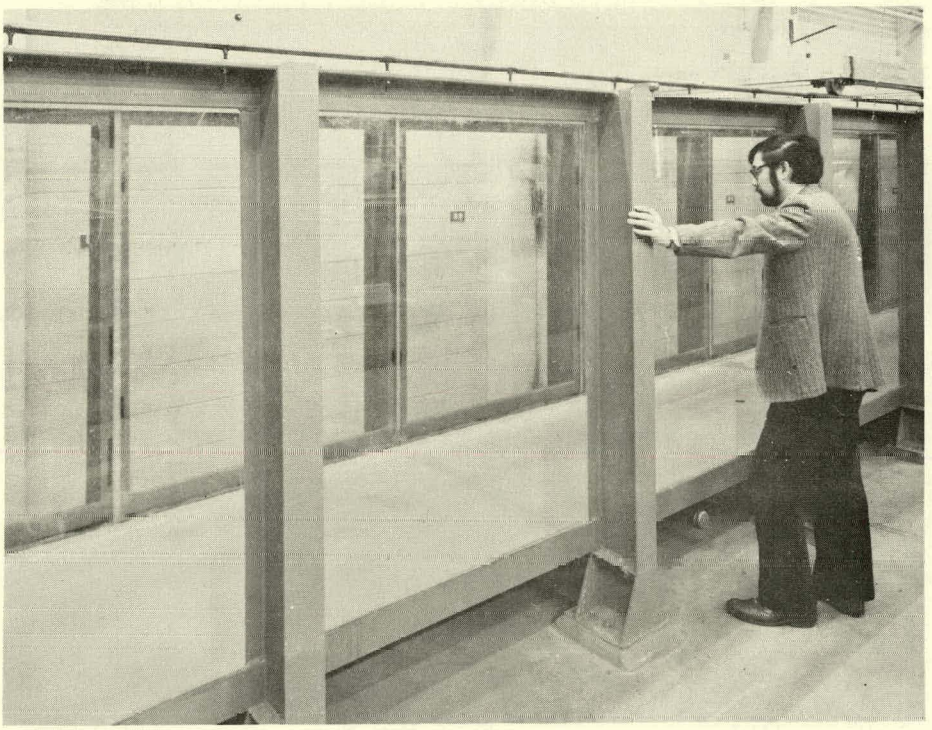

FIGURE 3.4 Photograph of a Section of the Glass-Walled Flume

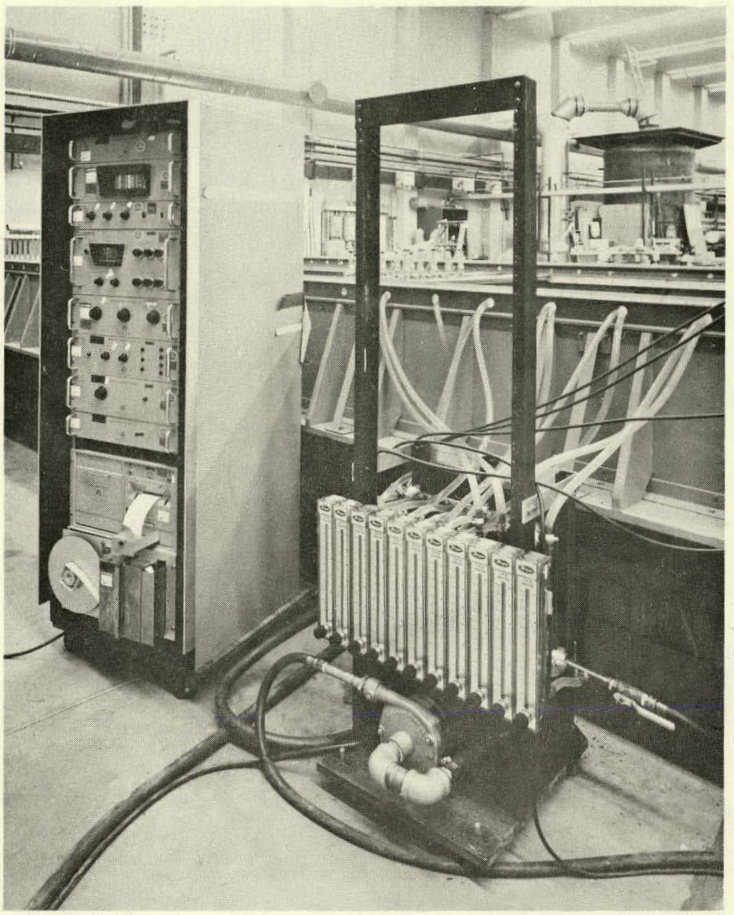

FIGURE 3.5 Photograph of the Data Aquisition System and Hot Water Distributor

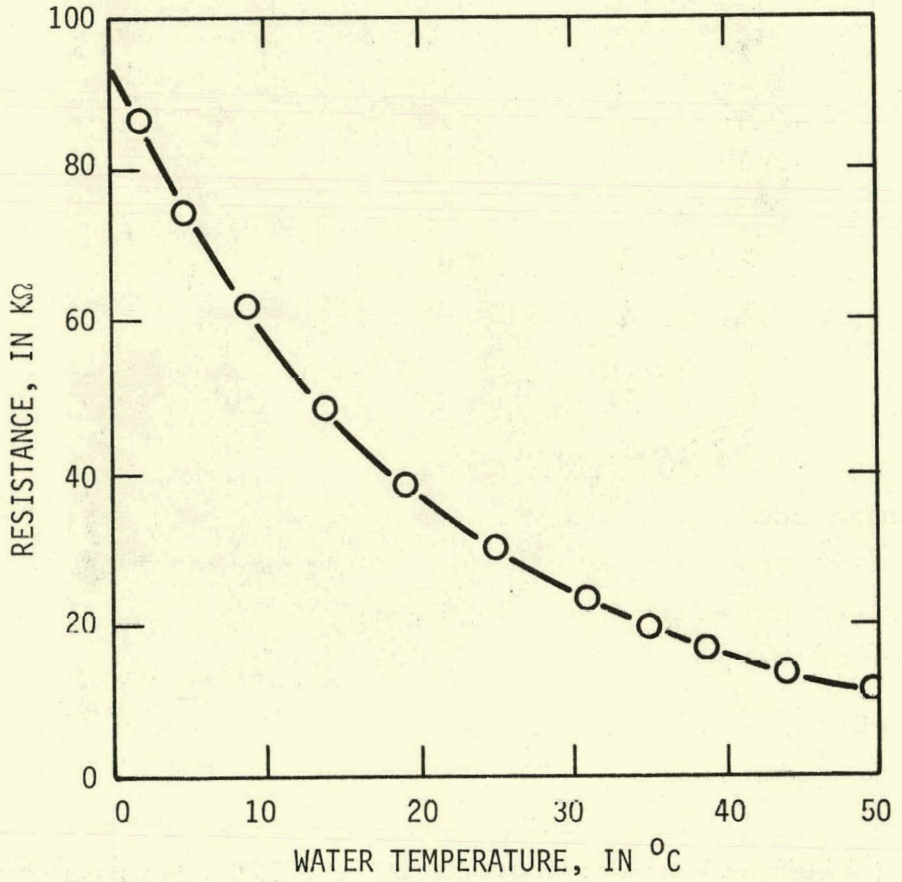

FIGURE 3.6. Calibration Curve of Thermistors

electronic data recording system is presently being replaced by the PDP 11/10 Computer Data Acquisition and Control System, which will be connected to the PDP 11/45 computer.

3.2.4 Dry Cooling Towers

Two mechanical draft dry cooling towers were tested in this study. One was a GEA direct mechanical draft dry cooling tower (GEA-Air Condenser) for the 330 MWe Wyodak plant. This tower is approximately 350 feet long, 180 feet wide and 85 feet high and is connected to a turbine room 110 feet long, 195 feet wide and 97 feet high. A drawing of these structures is shown in Figure 3.7. The second tower is a proposed dry cooling tower which will be developed for the Energy Research and Development Administration (ERDA). The ERDA tower will test the performance of various dry cooling towers by accommodating up to 15 percent of the waste heat from the 330 MWe power plant. Since the precise type of the ERDA dry cooling tower has not yet been determined, a hypothetical 50 MWe mechanical draft dry cooling tower was arbitrarily selected for this study. The assumed cooling tower is 100 feet long, 87 feet wide and 80 feet high and has two 50-foot diameter stacks. Photographs of two dry cooling tower models (model length scale of 1/600) are shown in Figure 3.8.

A schematic layout of experiments to investigate plume dispersion, recirculation, and interference at the Wyodak plant site is shown in Figure 3.9. In this configuration the ERDA tower is located upwind of the Wyodak plant cooling tower. Water was withdrawn through tubes (one tube for the ERDA tower and six tubes for the Wyodak plant tower) connected to the intake faces of the cooling towers. These tubes lay beneath the sand bed with which both flat ground and actual prototypic ground were modeled. In the prototype, the air is drawn to the tower and forced through the cooling tower heat exchanger cells by fans. This operation was modeled by adjusting the

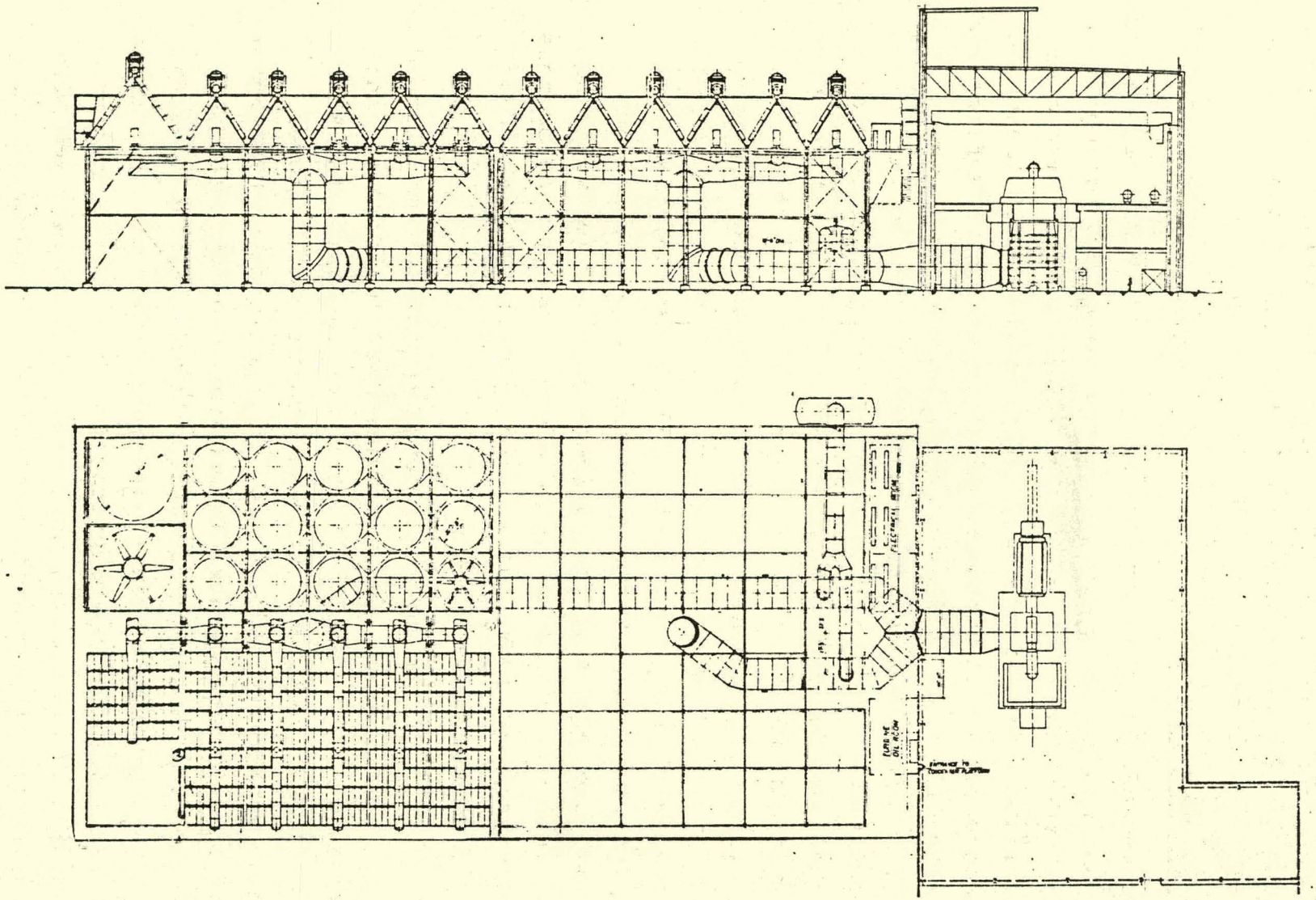

FIGURE 3.7 Drawing of the Wyodak Plant Dry Cooling Tower

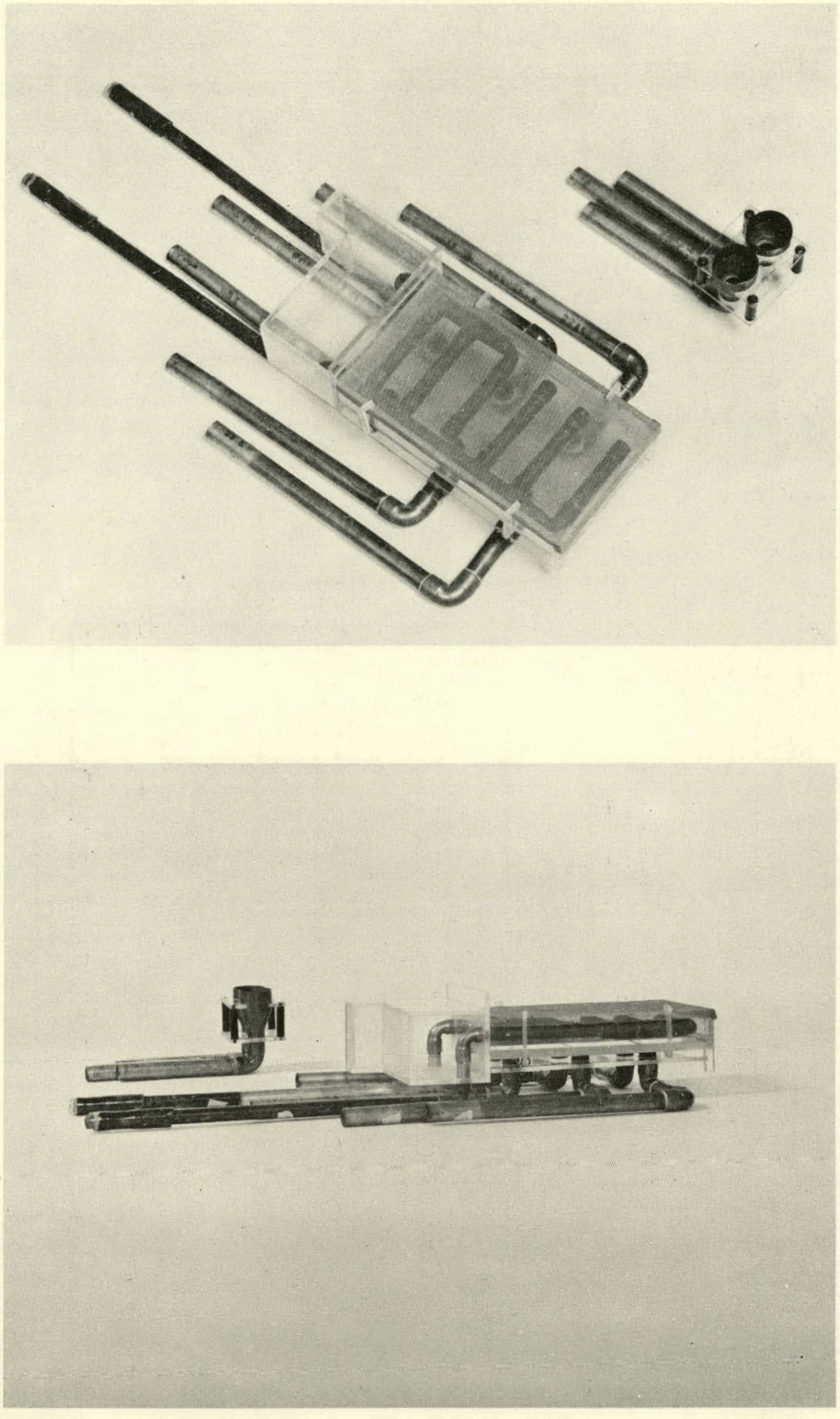

FIGURE 3.8 Photographs of the Wyodak Plant and ERDA Dry Cooling Tower Models

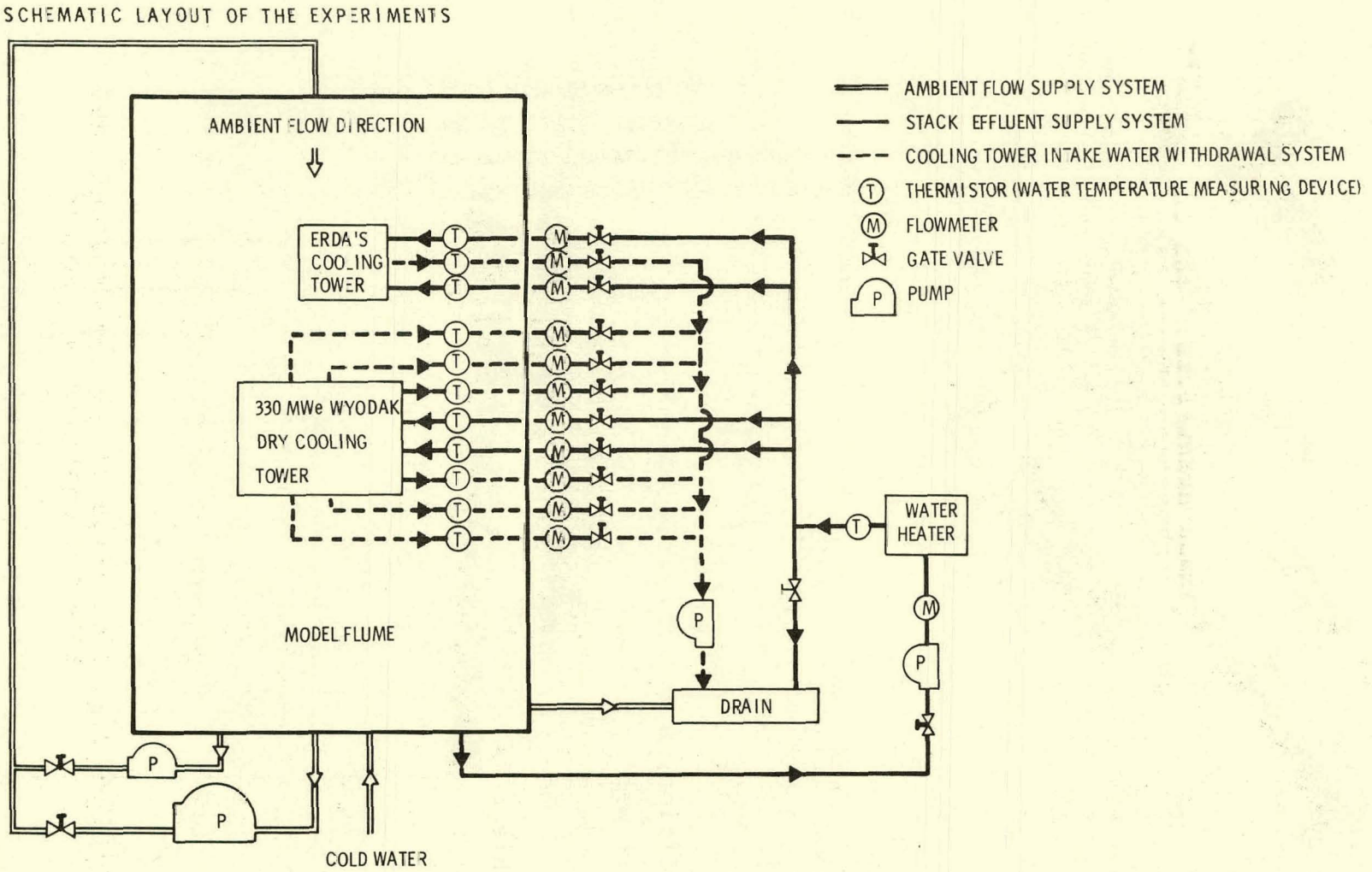

FIGURE 3.9 Schematic Layout of the Experiments

total effluent discharge equal to the total withdrawal. Temperatures of both the withdrawn and discharged water were measured by thermistors embedded in the effluent supply and withdrawal water systems (Figure 3.9). Figures 3.1 and 3.10 show photographs of the actual model setup. Figure 3.11 shows locations of the two dry cooling towers in relation to the surrounding topography at the Wyodak plant site. The variation of the topography along a northwest-southeast line passing through the center of the ERDA tower is shown in Figure 3.12.

3.3 EXPERIMENTAL PROCEDURE

In order to investigate characteristics of plume dispersion and recirculation and their effects on the cooling towers, experiments were conducted on effluent discharged from the dry cooling towers of the Wyodak plant site with:

1) surrounding topography assumed to be flat, and
2) the actual ground topography.

In addition, a two-dimensional hot water jet case was tested. The jet was injected vertically into an ambient flow from the bed through a 1/4-inch slit with a 40-inch lateral length. Flat ground was assumed for this case. The experimental results for this case were used to evaluate the two-dimensional simulation model evolved in this study for cooling tower plume analysis.

Figures 3.13 through 3.15 present the wind direction measured at a Wyodak site meteorological tower. These figures reveal that during the period September 1974 through June 1975 the prevailing wind was northwesterly, while during July 1975 dominant winds were north to northwesterly and south to southeasterly. The main concern with the dry cooling towers is their performance during the summer months. Hence, in this

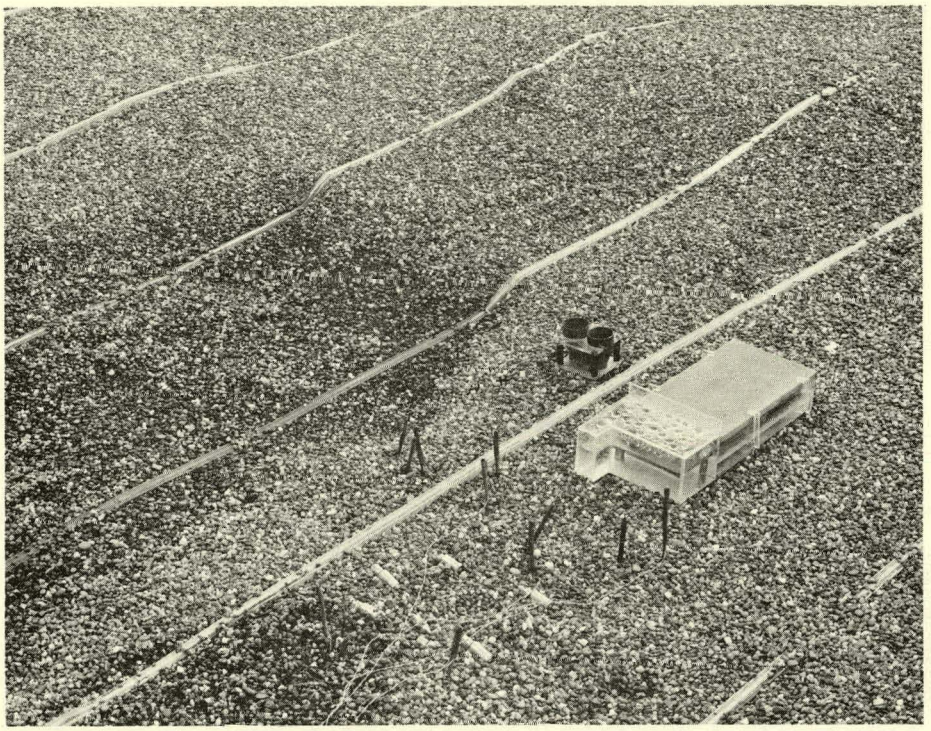

FIGURE 3.10 Photograph of the Model Cooling Towers and Model Topography

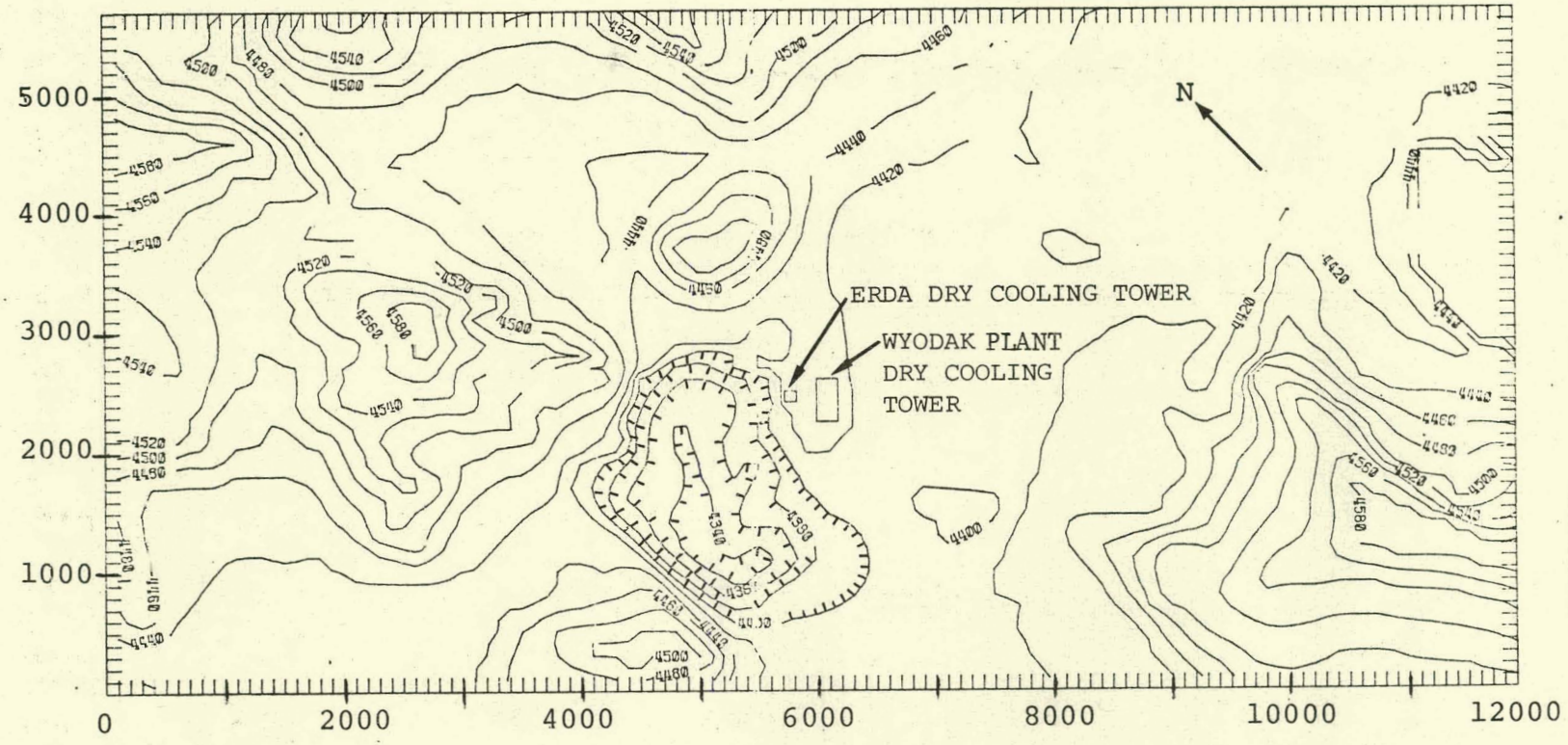

FIGURE 3.11 Topography in the Vicinity of the Wyodak Plant in Wyoming

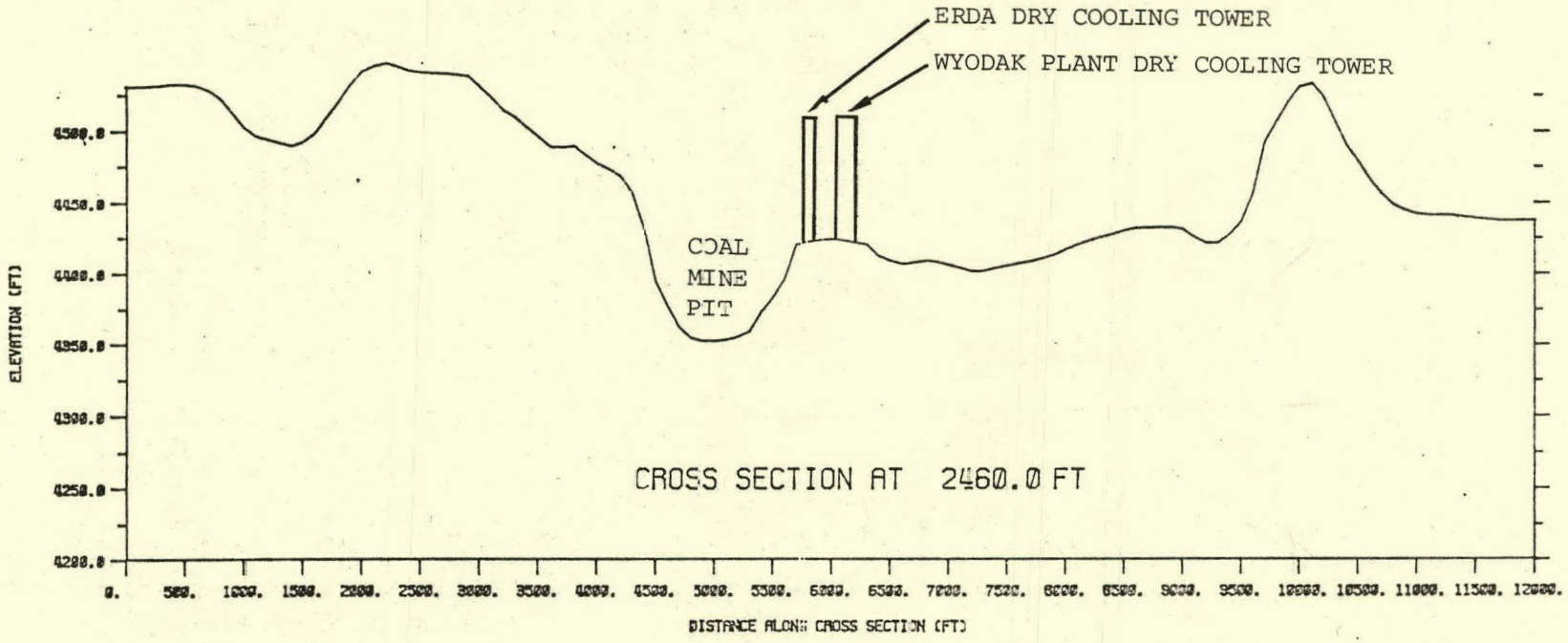

FIGURE 3.12 Variation of Cross Section From Northwest to Southeast

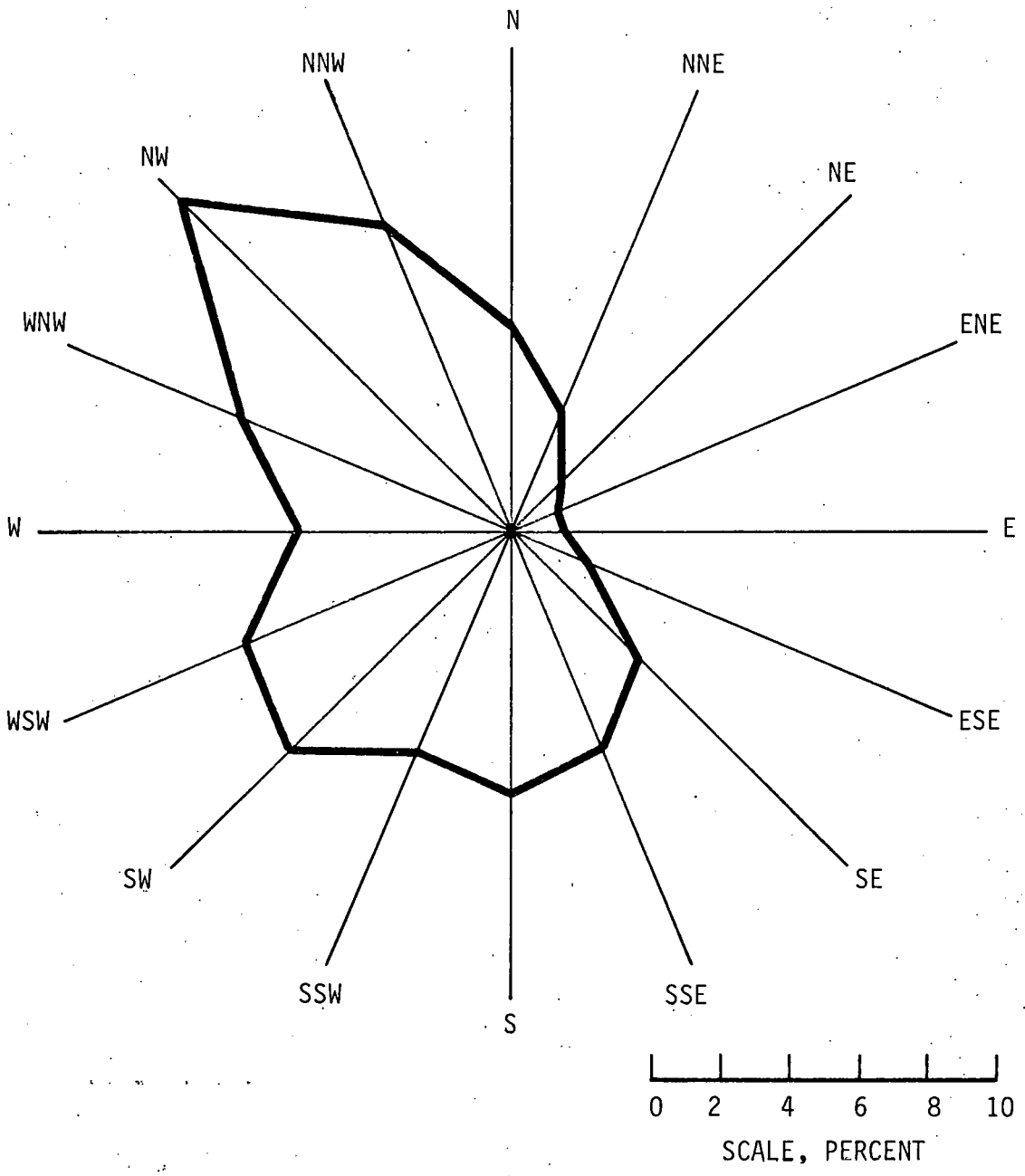

FIGURE 3.13 Percent Frequency of Occurrence for Wind Direction Measured at the Wyodak Plant Site During September 1, 1974, Through June 30, 1975

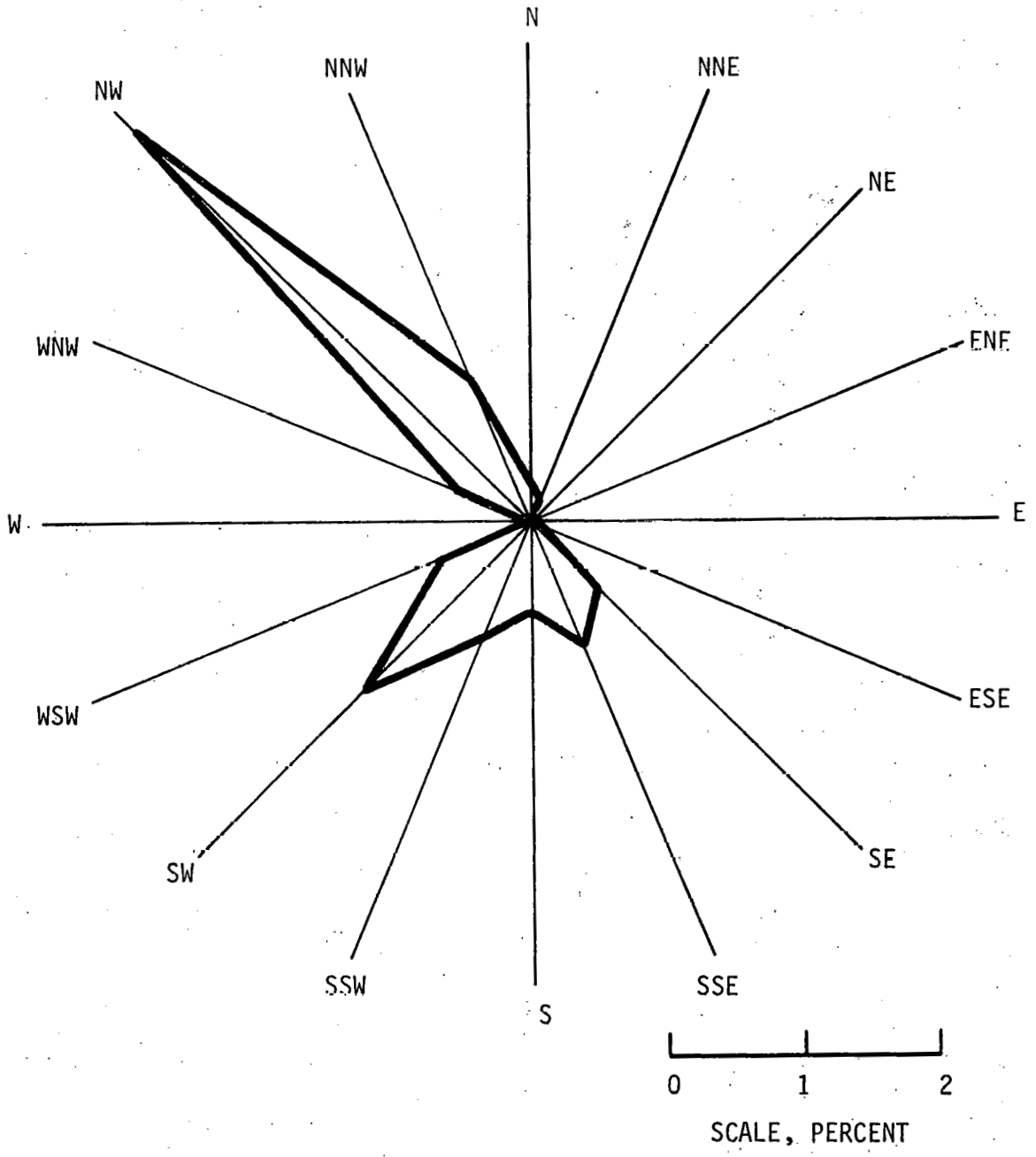

FIGURE 3.14 Percent Frequency of Occurrence for Direction of Wind Whose Speed Was Recorded to be More Than 24 MPH at the Wyodak Plant Site During September 1, 1974, Through June 30, 1975

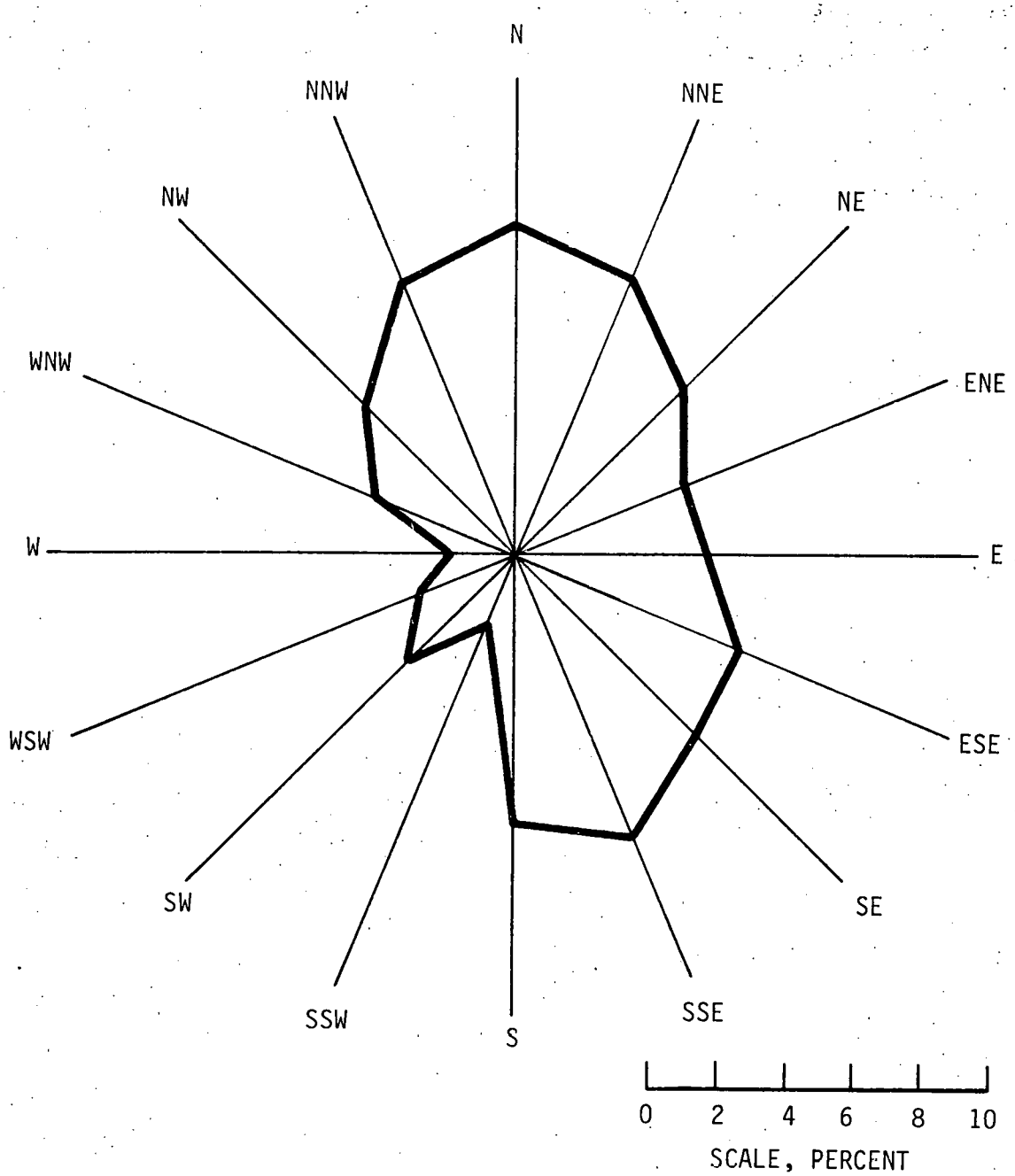

FIGURE 3.15 Percent Frequency of Occurrence for Wind Direction Measured at the Wyodak Plant Site During July 1, 1975, Through July 31, 1975

study northwesterly and southeasterly winds were selected as an ambient wind, with velocity varying from approximately 5 mph to 40 mph.

4.0 DISCUSSION OF EXPERIMENTAL RESULTS

Experiments were conducted to investigate effects of the ambient wind velocity (K in Equation 3.3), effluent discharge temperature (F_D), local topography and nearby structures on plume dispersion and recirculation for the dry cooling towers at the Wyodak plant site. In addition, temperatures of the two-dimensional plume case were measured for three different flow conditions. In this chapter, these experimental data are summarized and the results are analyzed.

4.1 DRY COOLING TOWER EXPERIMENTS

4.1.1 Summary of Experimental Data

Tables 4.1 through 4.4 summarize the experimental data obtained for the 330 MWe Wyodak plant and the 50 MWe ERDA dry cooling towers, together with the similitude of the model study. In Run A (Table 4.1) both the Wyodak plant and ERDA cooling towers were located on flat ground and the wind was northwesterly. The ERDA cooling tower was located upstream of the Wyodak plant tower for this case. For Run B, only the Wyodak plant cooling tower was considered on flat ground. The wind in this case was also northwesterly. In Run C (reported in Table 4.2) two cooling towers were located on flat ground and the wind was southeasterly (the ERDA tower was located downwind of the Wyodak plant tower). Runs TU and TD in Tables 4.3 and 4.4 included the actual topography at the Wyodak plant site. The former had a northwesterly wind, while the latter had a southeasterly wind.

In Tables 4.1 through 4.4, P and M in column 2 indicate prototype and model, respectively. W and E in column 3 mean the Wyodak plant and the ERDA dry cooling towers, respectively. Since the Wyodak plant dry cooling tower contains 69 stacks and the effluent jets discharged from all stacks are expected

TABLE 4.1 Summary of Experimental Data of the Wyodak Plant and ERDA Dry Cooling Towers for Northwesterly Wind and Flat Ground Case

Run No (1)	Prototype or Model (2)	Wyodak Plant or ERDA Tower (3)	Ambient Flow Velocity, V_a mph (4)	Ambient Flow Velocity, V_a fps (5)	Jet Velocity, V_j, fps (6)	Temperature Difference ΔT, °F (7)	Tower Stack Diameter D, ft (8)	Flow Depth, d, ft (9)	Velocity Ratio K (10)	Densimetric Froude Number, F_p (11)	Jet Reynolds Number, $R_j \times 10^3$ (12)	Ambient Flow Reynolds Number, $R_a \times 10^4$ (13)	Recirculation Ratio R, Percent: Upstream (14)	Downstream (15)	Average (16)
A-4	P	W	18.5	27.1	10.9	35.0	180	690	0.40	0.58	10500	45000			
	M	W		0.359	0.144	36.4	0.30	1.15	0.40	0.58	6.1	16.4			
	P	E	18.5	27.1	29.0	35.0	50	690	1.07	2.93	7800	45000			
	M	E		0.359	0.384	36.4	0.083	1.15	1.07	2.93	4.5	16.4			
A-5	P	W	28.1	41.2	10.9	35.0	180	600	0.26	0.58	10500	59000			
	M	W		0.548	0.142	36.4	0.30	1.00	0.26	0.58	6000	2.17			
	P	E	28.1	41.2	29.0	35.0	50	600	0.70	2.93	7800	59000			
	M	E		0.548	0.384	36.4	0.083	1.00	0.70	2.93	4500	2.17			
A-6	P	W	35.8	52.5	10.9	35.0	180	480	0.21	0.58	10500	60000			
	M	W		0.698	0.145	36.5	0.30	0.80	0.21	0.58	6.1	22.1			
	P	E	35.8	52.5	29.0	35.0	50	480	0.55	2.93	7800	60000			
	M	E		0.698	0.384	36.5	0.083	0.80	0.55	2.93	4.5	22.1			
A-7	P	W	4.8	7.03	10.9	35.0	180	678	1.55	0.58	10500	11000			
	M	W		0.053	0.144	37.6	0.30	1.13	1.55	0.58	6.1	4.2	0	2.1	1.1
	P	E	4.8	7.03	29.0	35.0	50	678	4.13	2.93	7800	11000			
	M	E		0.053	0.384	37.6	0.083	1.13	4.13	2.93	4.5	4.2			0.1
A-8	P	W	7.2	10.5	10.9	35.0	180	678	1.04	0.58	10500	17000			
	M	W		0.137	0.142	37.6	0.30	1.13	1.04	0.58	6.0	6.1	0	2.6	1.3
	P	E	7.2	10.5	29.0	35.0	50	678	2.76	2.93	7800	17000			
	M	E		0.137	0.378	37.6	0.083	1.13	2.76	2.93	4.4	6.1			0.4
A-9	P	W	9.7	14.3	10.9	35.0	180	678	0.76	0.58	10500	23000			
	M	W		0.188	0.142	37.4	0.30	1.13	0.76	0.58	6.0	8.4	0.1	3.1	1.6
	P	E	9.7	14.3	29.0	35.0	50	678	2.03	2.93	7800	23000			
	M	E		0.188	0.381	37.4	0.083	1.13	2.03	2.93	4.5	8.4			0.6
A-10	P	W	14.2	20.8	10.9	35.0	180	684	0.52	0.58	10500	34000			
	M	W		0.270	0.141	36.7	0.30	1.14	0.52	0.58	6.0	12.2	0	3.4	1.7
	P	E	14.2	20.8	29.0	35.0	50	684	1.39	2.93	7800	34000			
	M	E		0.270	0.376	36.7	0.083	1.14	1.39	2.93	4.4	12.2			0.6
A-11	P	W	19.0	27.9	10.9	35.0	180	606	0.39	0.58	10500	16000			
	M	W		0.372	0.145	37.8	0.30	1.01	0.39	0.58	6.1	14.9	0	4.0	2.0
	P	E	19.0	27.9	29.0	35.0	50	606	1.04	2.93	7800	16000			
	M	E		0.372	0.387	37.8	0.083	1.01	1.04	2.93	4.5	14.9			0.6
A-12	P	W	20.6	30.3	10.9	35.0	180	690	0.36	0.58	10500	50000			
	M	W		0.396	0.142	37.0	0.30	1.15	0.36	0.58	6.0	18.0	0	3.9	2.0
	P	E	20.6	30.3	29.0	35.0	50	690	0.96	2.93	7800	50000			
	M	E		0.396	0.379	37.0	0.083	1.15	0.96	2.93	4.4	18.0			0.7
A-13	P	W	29.0	42.5	10.9	35.0	180	490	0.26	0.58	10500	50000			
	M	W		0.572	0.147	38.0	0.30	0.8	0.26	0.58	6.2	18.3	0.1	3.5	1.8
	P	E	29.0	42.5	29.0	35.0	50	490	0.68	2.93	7800	50000			
	M	E		0.572	0.390	38.0	0.083	0.8	0.68	2.93	4.6	18.3			0.8
A-14	P	W	35.5	52.1	10.9	35.0	180	470	0.21	0.58	10500	58000			
	M	W		0.704	0.147	38.0	0.30	0.78	0.21	0.58	6.2	22.0	0.4	2.4	1.4
	P	E	35.5	52.1	29.0	35.0	50	470	0.56	2.93	7800	58000			
	M	E		0.704	0.392	38.0	0.083	0.78	0.56	2.93	4.6	22.0			0.9
B	P	W	27.5	40.3	10.9	35.0	180	600	0.27	0.58	10500	58000			
	M	W		0.530	0.142	35.5	0.30	1.00	0.27	0.58	6.0	20.6			

TABLE 4.2 Summary of Experimental Data of the Wyodak Plant and ERDA Dry Cooling Towers for Southeasterly Wind and Flat Ground Case

Run No (1)	Prototype or Model (2)	Wyodak Plant or ERDA Tower (3)	Ambient Flow Velocity, V_a mph (4)	Ambient Flow Velocity, V_a fps (5)	Jet Velocity, V_j, fps (6)	Temperature Difference ΔT_o, °F (7)	Tower Stack Diameter D, ft (8)	Flow Depth, d, ft (9)	Velocity Ratio K (10)	Densimetric Froude Number, F_p (11)	Jet Reynolds Number, $R_j \times 10^3$ (12)	Ambient Flow Reynolds Number, $R_a \times 10^4$ (13)	Recirculation Ratio R, Percent: Upstream (14)	Recirculation Ratio R, Percent: Downstream (15)	Recirculation Ratio R, Percent: Average (16)
C-4	P	W	18.5	27.1	10.9	35.0	180	708	0.40	0.58	10500	46000			
	M	W		0.359	0.144	36.6	0.30	1.18	0.40	0.58	6.1	16.9			
	P	E		27.1	29.0	35.0	50	708	1.07	2.93	7800	46000			
	M	E		0.359	0.384	36.6	0.083	1.18	1.07	2.93	4.5	16.9			
C-5	P	W	28.0	41.0	10.9	35.0	180	606	0.27	0.58	10500	59000			
	M	W		0.546	0.145	36.7	0.30	1.01	0.27	0.58	6.1	22.1			
	P	E	28.0	41.0	29.0	35.0	50	606	0.71	2.93	7800	59000			
	M	E		0.546	0.386	36.7	0.083	1.01	0.71	2.93	4.5	22.1			
C-6	P	W	36.0	52.8	10.9	35.0	180	490	0.21	0.58	10500	62000			
	M	W		0.695	0.143	36.3	0.30	0.82	0.21	0.58	6.0	22.8			
	P	E	36.0	52.8	29.0	35.0	50	490	0.55	2.93	7800	62000			
	M	E		0.695	0.382	36.3	0.083	0.82	0.55	2.93	4.5	22.8			
C-7	P	W	4.7	6.9	10.9	35.0	180	690	1.58	0.58	10500	11000			
	M	W		0.091	0.144	39.2	0.30	1.15	1.58	0.58	6.1	4.1	0	5.4	2.7
	P	E	4.7	6.9	29.0	35.0	50	690	4.20	2.93	7800	11000			
	M	E		0.091	0.382	39.2	0.083	1.15	4.20	2.93	4.5	4.1			2.4
C-8	P	W	9.8	14.4	10.9	35.0	180	678	0.76	0.58	10500	23000			
	M	W		0.192	0.145	38.9	0.30	1.13	0.76	0.58	6.1	8.6	0	11.7	5.9
	P	E	9.8	14.4	29.0	35.0	50	678	2.01	2.93	7800	23000			
	M	E		0.192	0.386	38.9	0.083	1.13	2.01	2.93	4.5	8.6			3.5
C-9	P	W	14.2	20.8	10.9	35.0	180	690	0.52	0.58	10500	34000			
	M	W		0.280	0.147	39.2	0.30	1.15	0.52	0.58	6.2	12.6	0	9.8	4.9
	P	E	14.2	20.8	29.0	35.0	50	690	1.39	2.93	7800	34000			
	M	E		0.280	0.390	39.2	0.083	1.15	1.39	2.93	4.6	12.6			11.5
C-10	P	W	19.2	28.1	10.9	35.0	180	590	0.39	0.58	10500	39000			
	M	W		0.384	0.149	39.8	0.30	0.99	0.39	0.58	6.3	14.9	0	7.1	3.6
	P	E	19.2	28.1	29.0	35.0	50	590	1.03	2.93	7800	39000			
	M	E		0.384	0.396	39.8	0.083	0.99	1.03	2.93	4.6	14.9			18.2
C-11	P	W	28.0	41.1	10.9	35.0	180	480	0.27	0.58	10500	47000			
	M	W		0.572	0.152	40.3	0.30	0.80	0.27	0.58	6.4	17.9	0	5.0	2.5
	P	E	28.0	41.1	29.0	35.0	50	480	0.71	2.93	7800	47000			
	M	E		0.572	0.404	40.3	0.083	0.80	0.71	2.93	4.7	17.9			18.6
C-12	P	W	34.3	50.3	10.9	35.0	180	470	0.22	0.58	10500	56000			
	M	W		0.699	0.151	40.0	0.30	0.78	0.22	0.58	6.4	21.4	0.1	4.4	2.3
	P	E	34.3	50.3	29.0	35.0	50	470	0.58	2.93	7800	56000			
	M	E		0.699	0.403	40.0	0.083	0.78	0.58	2.93	4.7	21.4			18.5

TABLE 4.3 Summary of Experimental Data of the Wyodak Plant and ERDA Dry Cooling Towers for Northwesterly Wind and Actual Topography Case

Run No (1)	Prototype or Model (2)	Wyodak Plant or ERDA Tower (3)	Ambient Flow Velocity, V_a mph (4)	Ambient Flow Velocity, V_a fps (5)	Jet Velocity, V_j, fps (6)	Temperature Difference ΔT_o, °F (7)	Tower Stack Diameter D, ft (8)	Flow Depth, d, ft (9)	Velocity Ratio R (10)	Densimetric Froude Number, F_p (11)	Jet Reynolds Number, $R_j \times 10^3$ (12)	Ambient Flow Reynolds Number, $R_a \times 10^4$ (13)	Recirculation Ratio R, Percent: Upstream (14)	Downstream (15)	Average (16)
	P	W	5.4	7.9	10.9	35.0	180	666	1.38	C.5E	10500	13000			
	M	W		0.102	0.141	38.2	0.30	1.11	1.38	C.56	5.8	4.0	0.8	3.4	2.1
TU-1	P	E	5.4	7.9	29.0	35.0	50	666	3.67	2.93	7800	13000			
	M	E		0.102	0.374	38.2	0.083	1.11	3.67	2.93	4.3	4.0			1.0
	P	W	9.5	13.9	10.9	35.0	180	666	0.78	C.58	10500	22000			
	M	W		0.178	0.140	37.5	0.30	1.11	0.78	C.58	5.8	7.0	0.9	3.7	2.3
TU-2	P	E	9.5	13.9	29.0	35.0	50	666	2.09	2.93	7800	22000			
	M	E		0.178	0.372	37.5	0.083	1.11	2.09	2.93	4.2	7.0			1.0
	P	W	13.E	20.2	10.9	35.0	180	696	0.54	0.58	10500	33000			
	M	W		0.261	0.141	38.6	0.30	1.16	0.54	0.58	5.8	10.7	1.4	4.6	3.0
TU-3	P	E	13.E	20.2	29.0	35.0	50	696	1.44	2.93	7800	33000			
	M	E		0.261	0.376	38.6	0.083	1.16	1.44	2.93	4.3	10.7			1.0
	P	W	19.E	28.8	10.9	35.0	180	660	0.38	0.58	10500	45000			
	M	W		0.359	0.136	37.2	0.30	1.10	0.38	0.58	5.6	14.0	1.6	5.4	3.5
TU-4	P	E	19.E	28.8	29.0	35.0	50	660	1.01	2.93	7800	45000			
	M	E		0.359	0.361	37.2	0.083	1.10	1.01	2.93	4.1	14.0			0.9
	P	W	29.E	43.8	10.9	35.0	180	580	0.25	0.58	10500	60300			
	M	W		0.545	0.136	37.7	0.30	0.96	0.25	0.58	5.6	18.5	1.5	4.9	3.2
TU-5	P	E	29.E	43.8	29.0	35.0	50	580	0.66	2.93	7800	60300			
	M	E		0.545	0.361	37.7	0.083	0.96	0.66	2.93	4.1	18.5			0.8
	P	W	39.	57.3	10.9	35.0	180	480	0.19	0.58	10500	65300			
	M	W		0.697	0.133	35.7	0.30	0.80	0.19	0.58	5.5	19.7	1.5	4.0	2.8
TU-6	P	E	39.	57.3	29.0	35.0	50	480	0.51	2.93	7800	65300			
	M	E		0.697	0.353	35.7	0.083	0.80	0.51	2.93	4.0	19.7			0.9
	P	W	18.0	26.5	10.9	35.0	180	666	0.41	0.58	10500	42300			
	M	W		0.346	0.142	39.5	0.30	1.11	0.41	0.58	5.8	13.6	1.6	5.2	3.4
TU-7	P	E	18.3	26.5	29.0	35.0	50	666	1.09	2.93	7800	42300			
	M	E		0.346	0.377	39.5	0.083	1.11	1.09	2.93	4.3	13.6			0.9
	P	W	18.3	26.5	10.9	24.6	180	666	0.41	0.68	10900	42300			
	M	W		0.346	0.142	30.6	0.30	1.11	0.41	0.68	5.3	13.6	1.8	5.8	3.8
TU-8	P	E	18.3	26.5	29.0	24.6	50	666	1.09	3.42	8100	42300			
	M	E		0.346	0.377	30.6	0.083	1.11	1.09	3.42	4.0	13.6			1.1
	P	W	18.3	26.5	10.9	15.3	180	666	0.41	0.86	11200	42300			
	M	W		0.346	0.142	23.8	0.30	1.11	0.41	0.86	4.7	13.6	2.2	7.2	4.7
TU-9	P	E	18.3	26.5	29.0	15.3	50	666	1.09	3.32	8300	42300			
	M	E		0.346	0.377	23.8	0.083	1.11	1.09	3.32	3.5	13.6			0.9
	P	W	18.3	26.5	10.9	13.8	180	666	0.41	0.90	11300	42000			
	M	W		0.346	0.142	21.2	0.30	1.11	0.41	0.90	4.7	13.6	2.5	7.5	5.0
TU-10	P	E	18.3	26.5	29.0	13.8	50	666	1.09	3.53	8300	42000			
	M	E		0.346	0.377	21.2	0.083	1.11	1.09	3.53	3.5	13.6			1.0
	P	W	18.3	26.5	10.9	6.6	180	666	0.41	0.28	11500	42000			
	M	W		0.346	0.142	12.1	0.30	1.11	0.41	0.28	4.2	13.6	4.0	10.6	7.3
TU-11	P	E	18.3	26.5	29.0	6.6	50	666	1.09	5.48	8500	42000			
	M	E		0.346	0.377	12.1	0.083	1.11	1.09	5.48	3.1	13.6			1.1
	P	W	18.3	26.5	10.9	1.6	180	666	0.41	2.38	11700	42000			
	M	W		0.346	0.142	5.1	0.30	1.11	0.41	2.38	3.6	13.6	9.0	14.5	11.7
TU-12	P	E	18.3	26.5	29.0	1.6	50	666	1.05	12.00	8600	42000			
	M	E		0.346	0.377	5.1	0.083	1.11	1.05	12.00	2.6	13.6			2.1

TABLE 4.4 Summary of Experimental Data of the Wyodak Plant and ERDA Dry Cooling Towers for Southeasterly Wind and Actual Topography Case

Run No (1)	Prototype or Model (2)	Wyodak Plant or ERDA Tower (3)	Ambient Flow Velocity, V_a mph (4)	Ambient Flow Velocity, V_a fps (5)	Jet Velocity, V_j, fps (6)	Temperature Difference ΔT_o, °F (7)	Tower Stack Diameter D, ft (8)	Flow Depth, d, ft (9)	Velocity Ratio K (10)	Densimetric Froude Number, F_p (11)	Jet Reynolds Number, $R_j \times 10^3$ (12)	Ambient Flow Reynolds Number, $R_a \times 10^4$ (13)	Recirculation Ratio R, Percent: Upstream (14)	Downstream (15)	Average (16)
	P	W	5.5	8.1	10.9	35.0	180	666	1.35	0.58	10500	13000			
	M	W		0.099	0.133	35.4	0.30	1.11	1.35	0.58	5.5	4.0	1.7	2.4	2.1
TD-1	P	E	5.5	8.1	29.0	35.0	50	666	3.58	2.93	7800	13000			
	M	E		0.099	0.354	35.4	0.083	1.11	3.58	2.93	4.0	4.0			1.3
	P	W	10.3	15.1	10.9	35.0	180	672	0.72	0.58	10500	24000			
	M	W		0.183	0.132	34.8	0.30	1.12	0.72	0.58	5.5	7.5	1.6	6.1	3.9
TD-2	P	E	10.3	15.1	29.0	35.0	50	672	1.92	2.93	7800	24000			
	M	E		0.183	0.351	34.8	0.083	1.12	1.92	2.93	4.0	7.5			1.1
	P	W	15.6	22.8	10.9	35.0	180	660	0.48	0.58	10500	36000			
	M	W		0.279	0.133	35.1	0.30	1.10	0.48	0.58	5.5	11.2	1.5	6.2	3.9
TD-3	P	E	15.6	22.8	29.0	35.0	50	660	1.27	2.93	7800	36000			
	M	E		0.279	0.355	35.1	0.083	1.10	1.27	2.93	4.0	11.2			3.8
	P	W	19.8	29.0	10.9	35.0	180	660	0.38	0.58	10500	46000			
	M	W		0.357	0.134	35.4	0.30	1.10	0.38	0.58	5.5	14.3	1.5	5.8	3.6
TD-4	P	E	19.8	29.0	29.0	35.0	50	660	1.00	2.93	7800	46000			
	M	E		0.357	0.357	35.4	0.083	1.10	1.00	2.93	4.1	14.3			8.3
	P	W	29.2	42.8	10.9	35.0	180	580	0.26	0.58	10500	59000			
	M	W		0.542	0.138	35.8	0.30	0.96	0.26	0.58	5.7	18.9	1.5	3.7	2.6
TD-5	P	E	29.2	42.8	29.0	35.0	50	580	0.68	2.93	7800	59000			
	M	E		0.542	0.367	35.8	0.083	0.96	0.68	2.93	4.2	18.9			16.6
	P	W	37.1	54.4	10.9	35.0	180	470	0.20	0.58	10500	61000			
	M	W		0.692	0.139	35.9	0.30	0.79	0.20	0.58	5.7	19.9	1.6	3.2	2.4
TD-6	P	E	37.1	54.4	29.0	35.0	50	470	0.53	2.93	7800	61000			
	M	E		0.692	0.369	35.9	0.083	0.79	0.53	2.93	4.2	19.9			18.2
	P	W	19.8	29.0	10.9	23.6	180	660	0.38	0.64	10900	46000			
	M	W		0.357	0.134	29.8	0.30	1.10	0.38	0.64	5.3	14.3	1.9	6.9	4.4
TD-7	P	E	19.8	29.0	29.0	23.6	50	660	1.00	3.33	8100	46000			
	M	E		0.357	0.357	29.8	0.083	1.10	1.00	3.33	3.9	14.3			10.3
	P	W	19.8	29.0	10.9	18.3	180	660	0.38	0.78	11100	46000			
	M	W		0.357	0.134	21.3	0.30	1.10	0.38	0.78	4.7	14.3	2.4	6.9	4.7
TD-8	P	E	19.8	29.0	29.0	18.3	50	660	1.00	4.10	8200	46000			
	M	E		0.357	0.357	21.3	0.083	1.10	1.00	4.10	3.5	14.3			14.4
	P	W	19.8	29.0	10.9	16.8	180	660	0.38	0.82	11300	46000			
	M	W		0.357	0.134	20.3	0.30	1.10	0.38	0.82	4.7	14.3	2.6	7.1	4.8
TD-9	P	E	19.8	29.0	29.0	16.8	50	660	1.00	4.27	8300	46000			
	M	E		0.357	0.357	20.3	0.083	1.10	1.00	4.27	3.5	14.3			13.7
	P	W	19.8	29.0	10.9	9.6	180	660	0.38	1.07	11500	46000			
	M	W		0.357	0.134	13.5	0.30	1.10	0.38	1.07	4.3	14.3	4.0	8.8	6.4
TD-10	P	E	19.8	29.0	29.0	9.6	50	660	1.00	5.58	8500	46000			
	M	E		0.357	0.357	13.5	0.083	1.10	1.00	5.58	3.2	14.3			16.8

to join together immediately after discharge, the jet velocity for this case was obtained by dividing the total effluent discharge by the total area of the cooling tower top surface. The stack diameter, D, for this case was assumed to be the cooling tower width. The symbol d denotes the ambient flow depth in the model and its corresponding height in the prototype. It was assumed that L = 4d to calculate the ambient flow Reynolds number, R_a in Equation 3.5; calculated values are shown in column 13. The recirculation ratio, R, in columns 14, 15 and 16 were defined by

$$R = \frac{T_w - T_a}{\Delta T_o} \tag{4.1}$$

where T_w is the temperature of withdrawal water as discussed in Section 3.2.4. As shown in Figure 3.9, for the Wyodak plant cooling tower case, there were three suction tubes for each upstream and downstream half of the cooling tower. Columns 14 and 15 show values of R for the upstream and downstream rows, respectively. Column 16 is the average of the values shown in columns 14 and 15. Values of R in these three columns are the averages of 3 to 50 repeated experiments.

As discussed in Chapter 3, four important factors influence turbulent dispersion of the cooling tower plume. The first is the momentum of effluent and ambient flows. The relative intensity of momentum of these two flows are dominant factors near the cooling tower stacks. K in Equation 3.7 is the square root of the ratio of the effluent flow momentum to the ambient flow momentum, provided the Boussinesq assumption is adopted (that is, the density difference between these two flows is important for consideration of the buoyancy force but not for the flow momentum).

Another important factor is the effluent buoyancy force due to density difference between the discharge jet and the

ambient flows, especially in the near field. The relative strength of the effluent momentum to the effluent buoyancy force is expressed by the densimetric Froude number, IF_D as shown in Equation 3.4. A third factor is the turbulent intensity of the Jet flow, which is expressed by the jet Reynolds number, IR_j in Equation 3.6. This is important also in the near field. The final factor is a combination of ambient flow characteristics, including the ambient flow turbulence, wakes behind the towers and topographical features, and wind shear stress. Since the cooling towers selected for this study were rectangular with sharp corners, flow separation is independent of the Reynolds number as long as the flow is turbulent. The wind shear stress in the turbulent flow is also independent of the Reynolds number but depends on the relative size of topographical projections. The ambient flow turbulence is the dominant mechanism for dispersing the plume in the far field. However, it is not important in this near field study.

Tables 4.1 through 4.4 reveal that these four similarity criteria (see Equation 3.3) were all satisfied to assure the dynamic similarity between the prototype and model flows.

4.1.2 Flow Patterns

Observation of flow patterns in the vicinity of the cooling towers revealed the importance of K and IF_D to plume dispersion and recirculation. When the ambient flow velocity increased (or K decreased) the plumes from the cooling towers were deflected more closely to the ground on the downstream side. These plumes also acted as solid obstacles, producing wakes behind them. Moreover, a large wake was generated by the separation of flow from the edge of the rectangularly-shaped Wyodak plant cooling tower. This captive eddy zone continuously withdrew a portion of the plume until it reached an equilibrium condition. This was the primary cause of recirculation. Photographs of plume dispersion

patterns for various ambient velocities are shown in Figures 4.1 through 4.19. These photographs were obtained by injecting dye into the plumes prior to their emission from the towers. Figures 4.1 through 4.11 present the TU cases (northwesterly wind and actual topography imposed in the model; see Table 4.3) and Figures 4.12 through 4.19 show the TD cases (southeasterly wind and actual topography imposed in the model; see Table 4.4). These figures clearly indicate the plume deflection due to cross winds. The plume from the ERDA tower reached a higher elevation than the one from the Wyodak plant tower because the ERDA effluent had a larger K value. The effects of K tended to overcome the effects of higher F_D, which generally lowers the plume rise. Figures 4.7 through 4.10 were obtained by injecting dye into only one of the two plumes being discharged. These photographs show the following different dispersion patterns between the two plumes; the Wyodak plant tower plume was swept away by the ambient flow and its lateral dispersion was much smaller than that of the ERDA tower plume. The ERDA tower plume (Figures 4.9 and 4.10) was rolled up to form a pair of counter-rotating vortices, whereas the Wyodak plant tower plume did not indicate this process strongly. These differences between the two dispersion patterns are believed to be due to the different values of K for the plumes.

Figure 4.1 shows the plume dispersion for a 5.4 mph northwesterly wind. Although both ERDA tower stacks discharged the same amount of effluent, one effluent contained more dye than the other for this particular case. The plumes from the ERDA tower and the Wyodak plant towers dispersed independently of each other and almost no recirculation nor interference occurred. When the wind velocity increased to 13.8 mph, the plumes were deflected closer to the ground and some plume recirculation occurred for the Wyodak plant tower, but no interference, as shown in Figure 4.3. Figures 4.5 through 4.11 show similar phenomena.

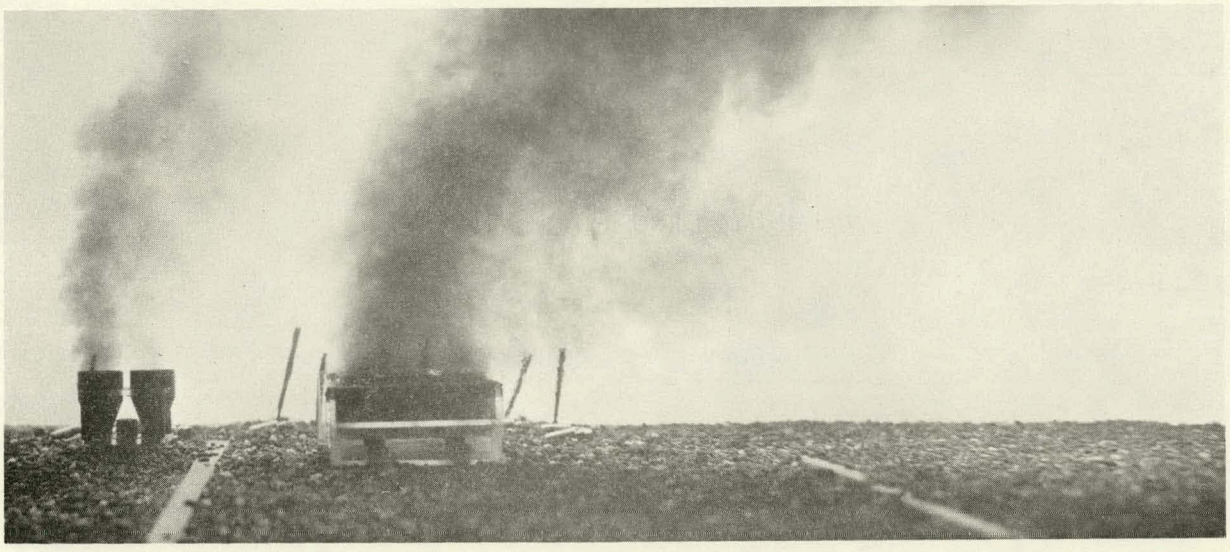

FIGURE 4.1 Photograph of Plumes from the Two Dry Cooling Towers for Run TU-1. V_a = 5.4 MPH.

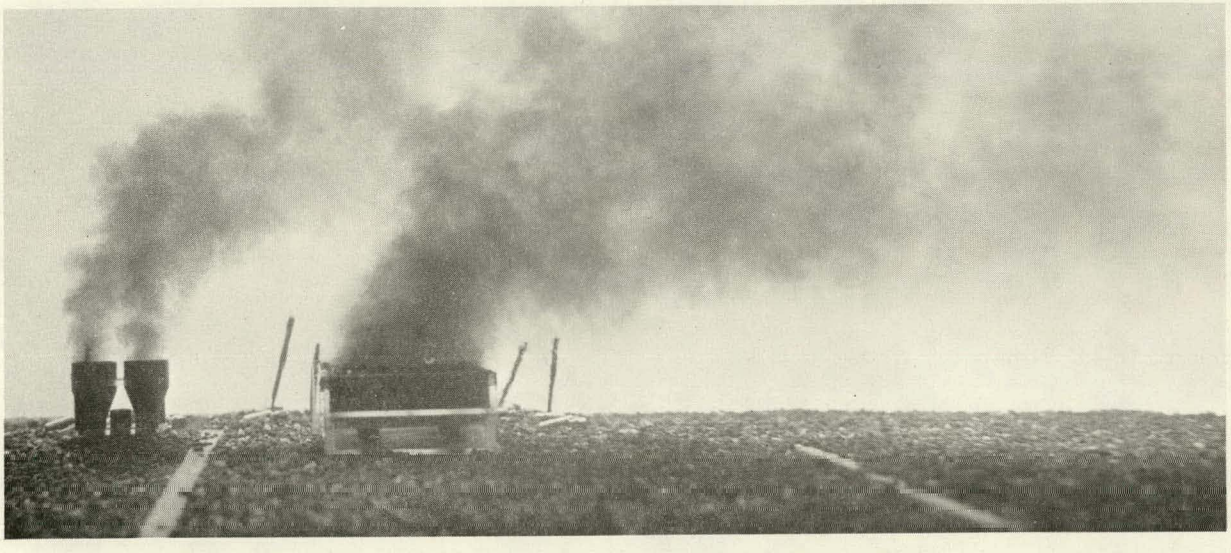

FIGURE 4.2 Photograph of Plumes from the Two Dry Cooling Towers for Run TU-2. V_a = 9.5 MPH.

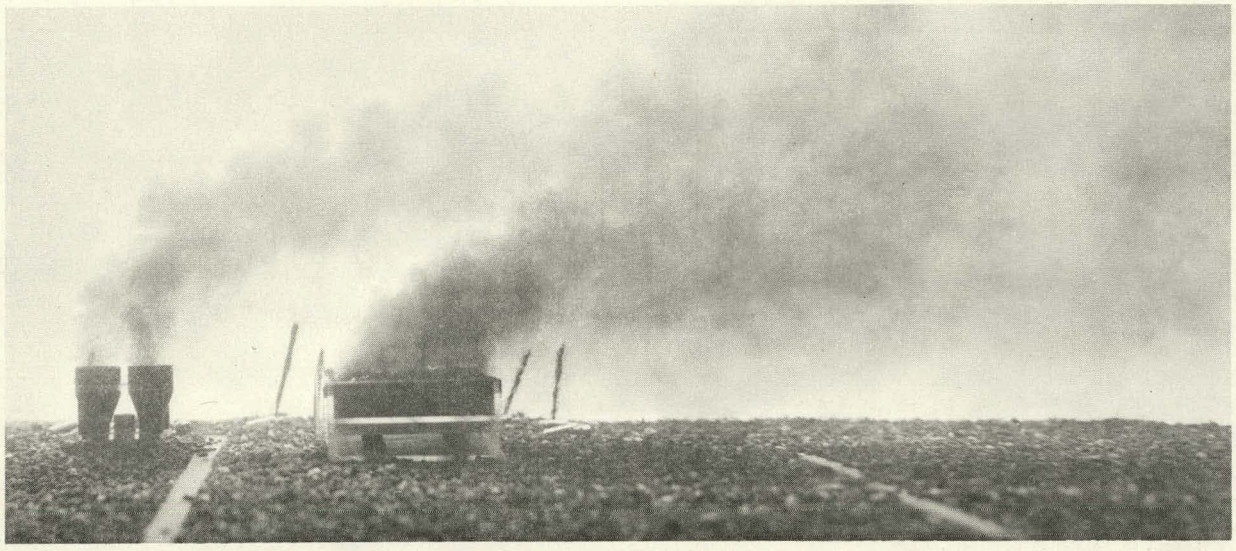

FIGURE 4.3 Photograph of Plumes from the Two Dry Cooling Towers for Run TU-3. V_a = 13.8 MPH.

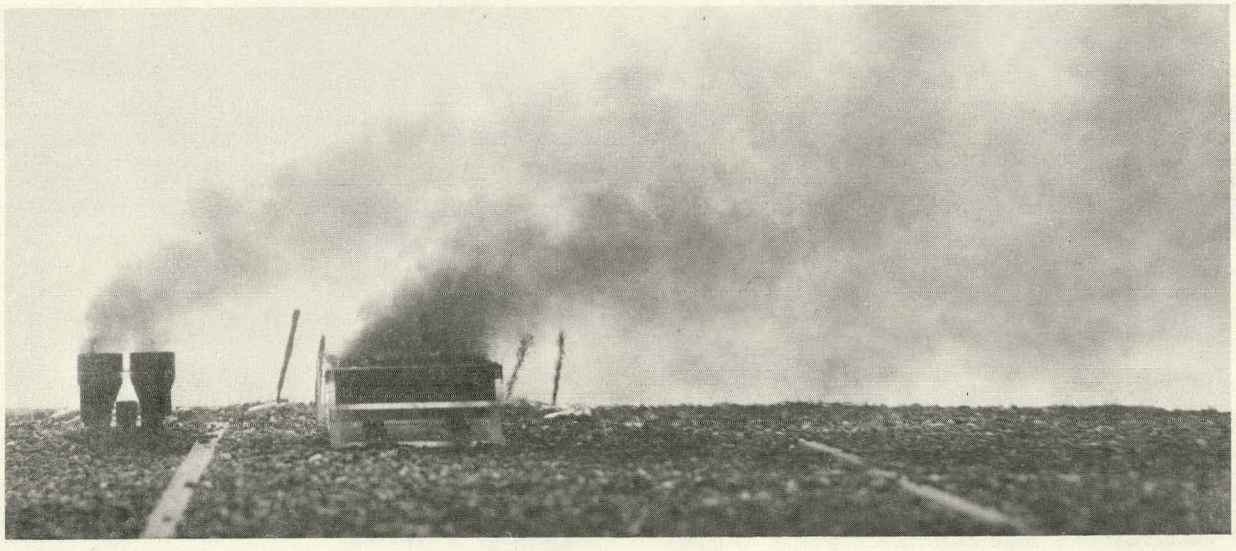

FIGURE 4.4 Photograph of Plumes from the Two Dry Cooling Towers for Run TU-4. V_a = 19.6 MPH.

FIGURE 4.5 Photograph of Plumes from the Two Dry Cooling Towers for Run TU-5. V_a = 29.8 MPH.

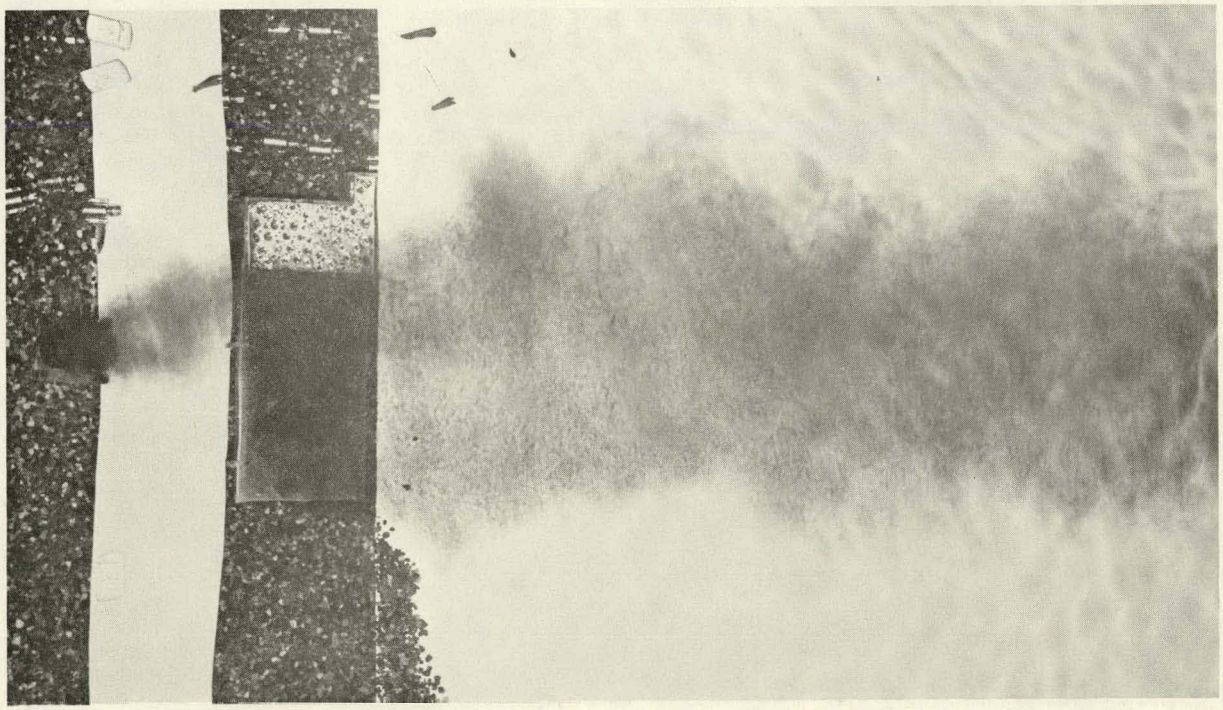

FIGURE 4.6 Photograph of the Top View for Plumes from the Cooling Towers for Run TU-5. V_a = 29.8 MPH.

FIGURE 4.7 Photograph of a Plume from the Wyodak Plant Dry Cooling Tower for Run TU-5. V_a = 29.8 MPH.

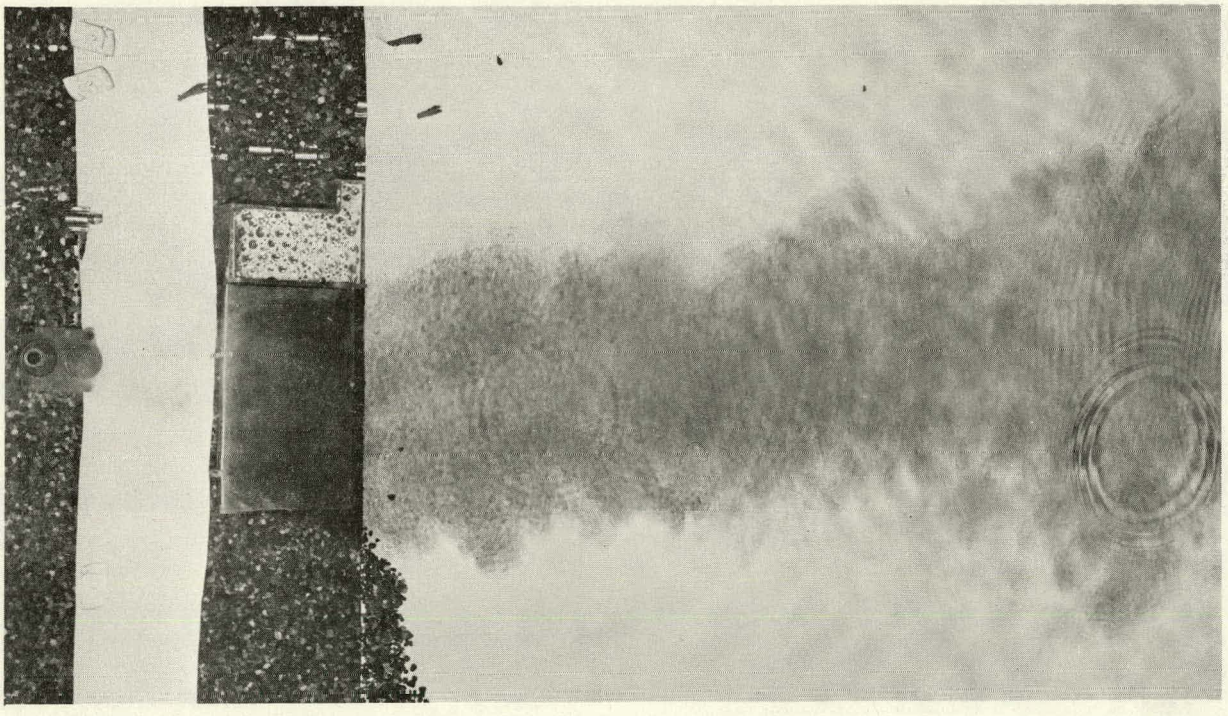

FIGURE 4.8 Photograph of the Top View for a Plume from the Wyodak Plant Dry Cooling Tower for Run TU-5. V_a = 29.8 MPH.

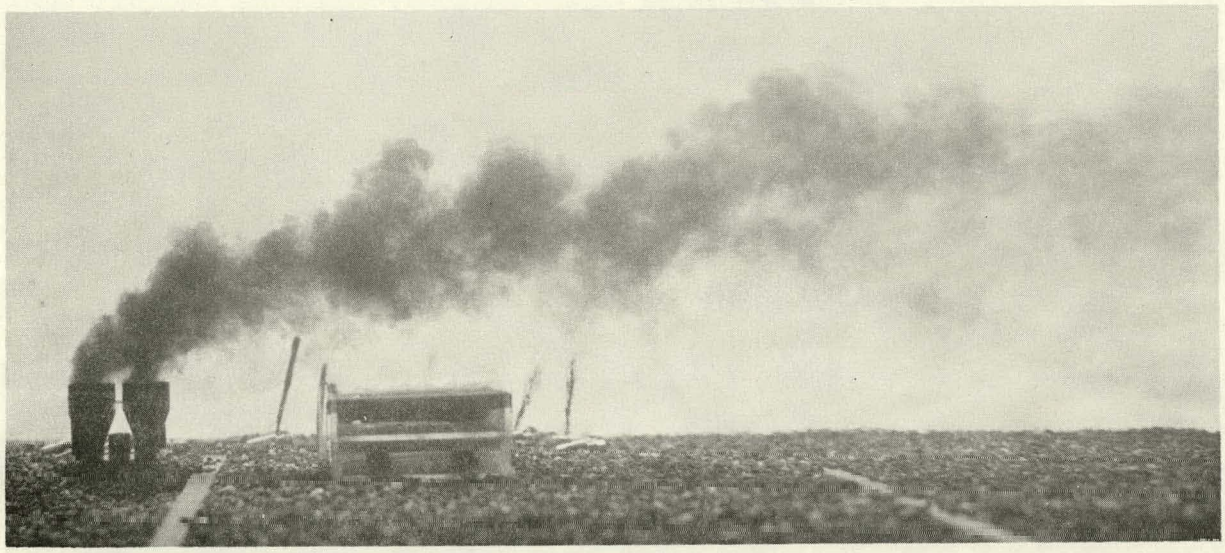

FIGURE 4.9 Photograph of a Plume from the ERDA Dry Cooling Tower for Run TU-5. V_a = 29.8 MPH.

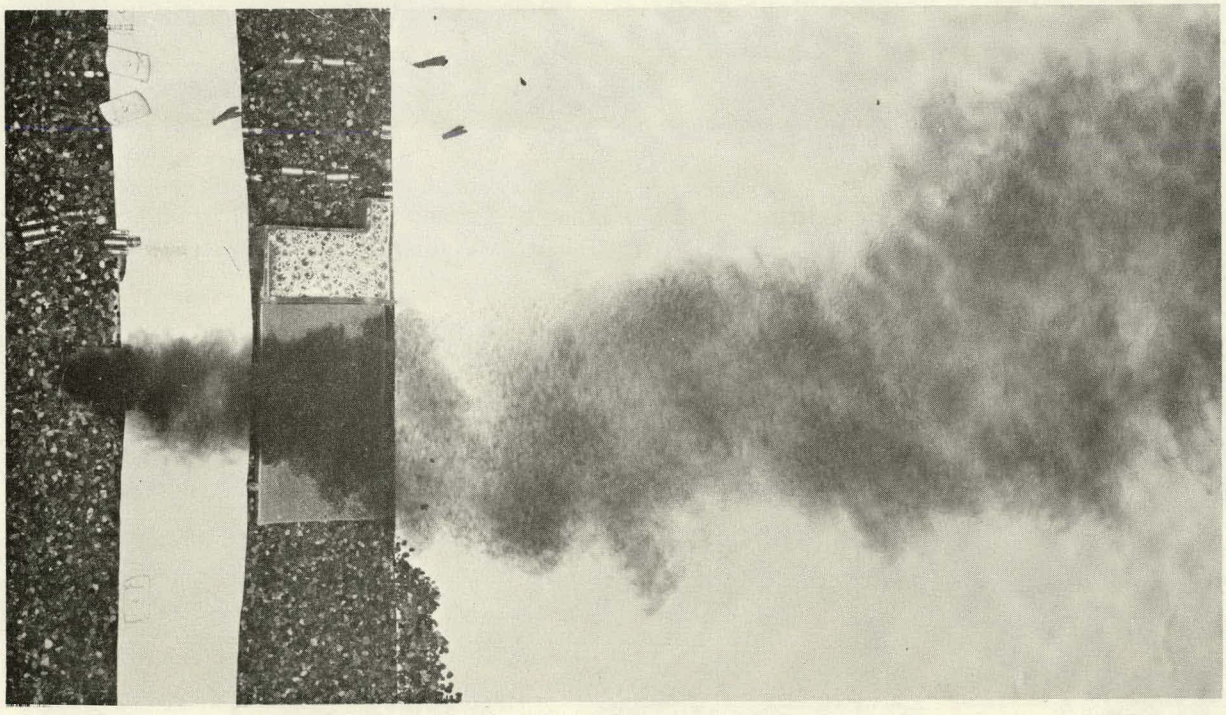

FIGURE 4.10 Photograph of the Top View for a Plume from the ERDA Dry Cooling Tower for Run TU-5. V_a = 29.8 MPH.

FIGURE 4.11 Photograph of Plumes from the Two Cooling Towers for Run TU-6. V_a = 39.1 MPH.

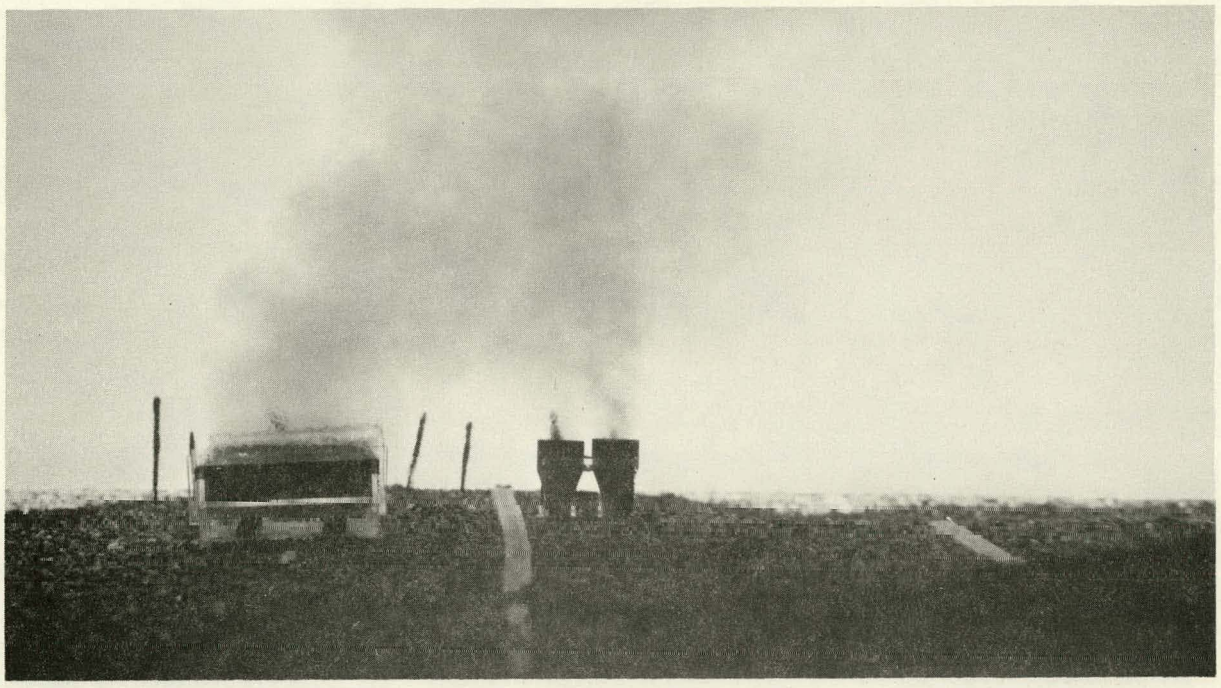

FIGURE 4.12 Photograph of Plumes from the Two Dry Cooling Towers for Run TD-1. V_a = 5.5 MPH.

FIGURE 4.13 Photograph of Plumes from the Two Dry Cooling Towers for Run TD-2. V_a = 10.3 MPH.

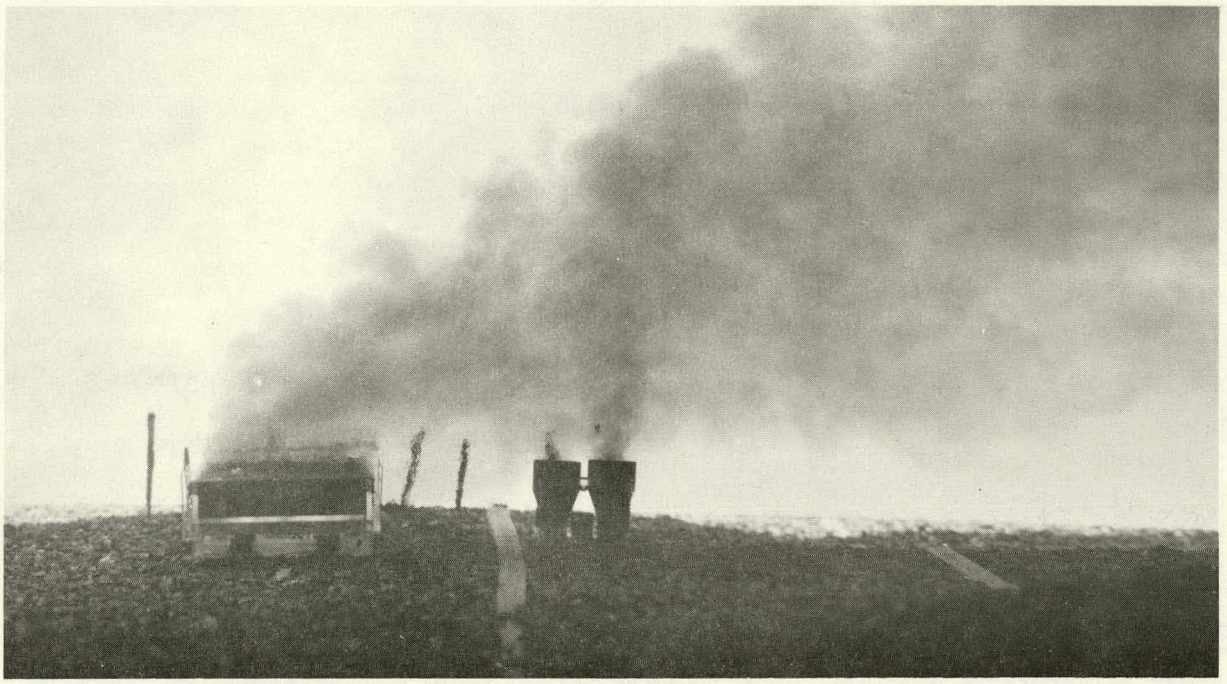

FIGURE 4.14 Photograph of Plumes from the Two Dry Cooling Towers for Run TD-3. V_a = 15.6 MPH.

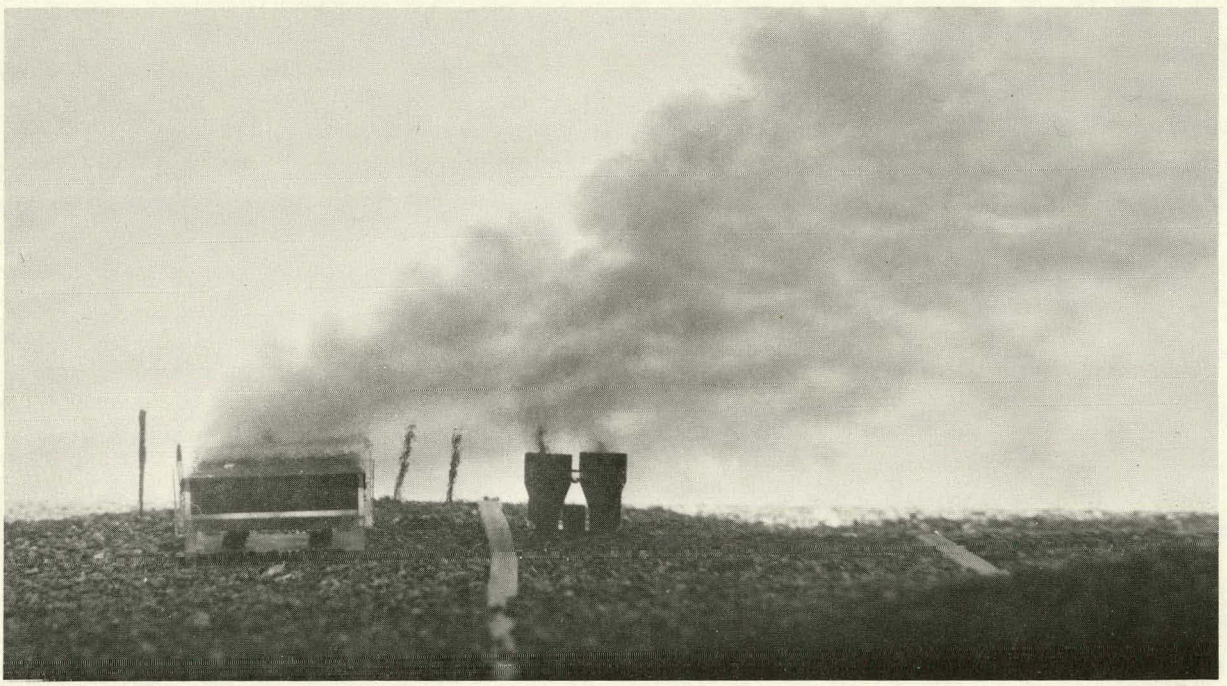

FIGURE 4.15 Photograph of Plumes from the Two Dry Cooling Towers for Run TD-4. V_a = 19.8 MPH.

FIGURE 4.16 Photograph of Plumes from the Two Dry Cooling Towers for Run TD-5. V_a = 29.2 MPH.

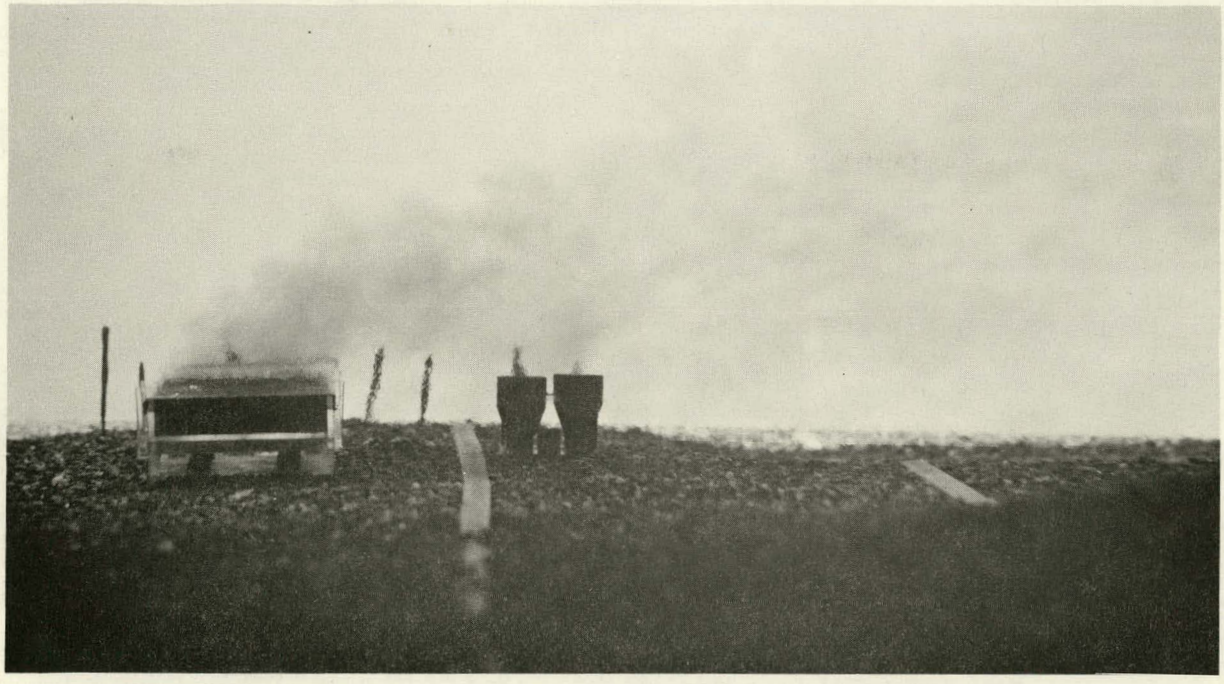

FIGURE 4.17 Photograph of a Plume from the Wyodak Plant Dry Cooling Tower for Run TD-5. V_a = 29.2 MPH.

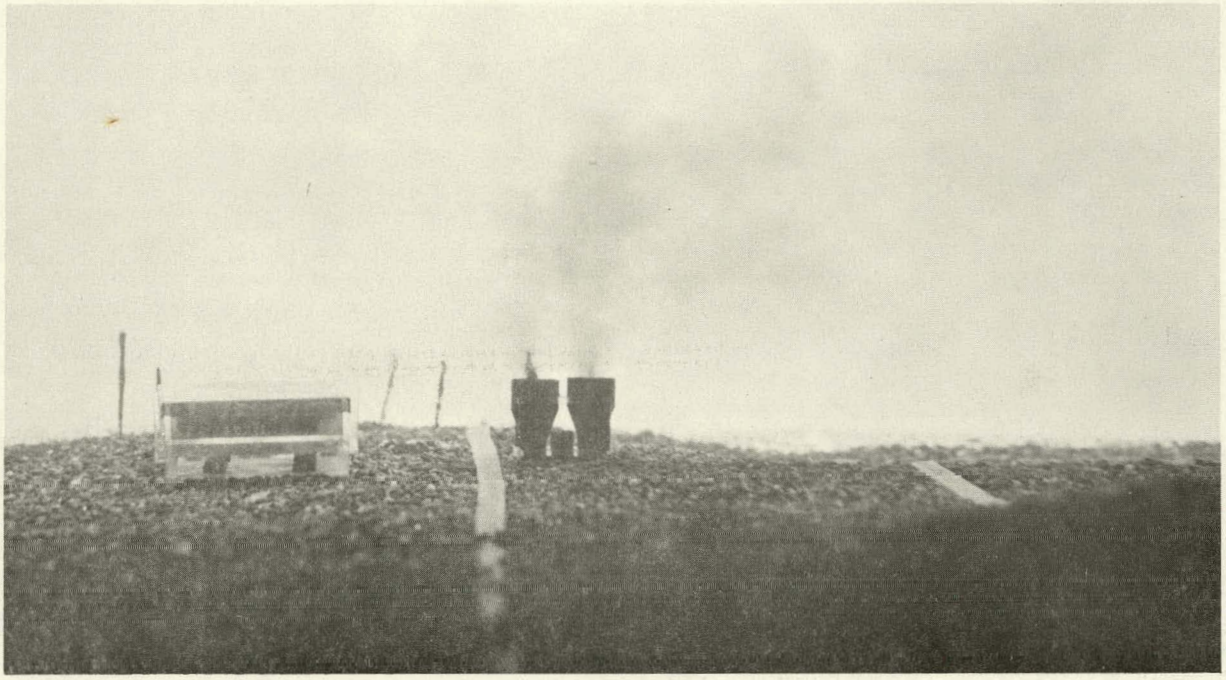

FIGURE 4.18 Photograph of a Plume from the ERDA Dry Cooling Tower for Run TD-5. V_a = 29.2 MPH.

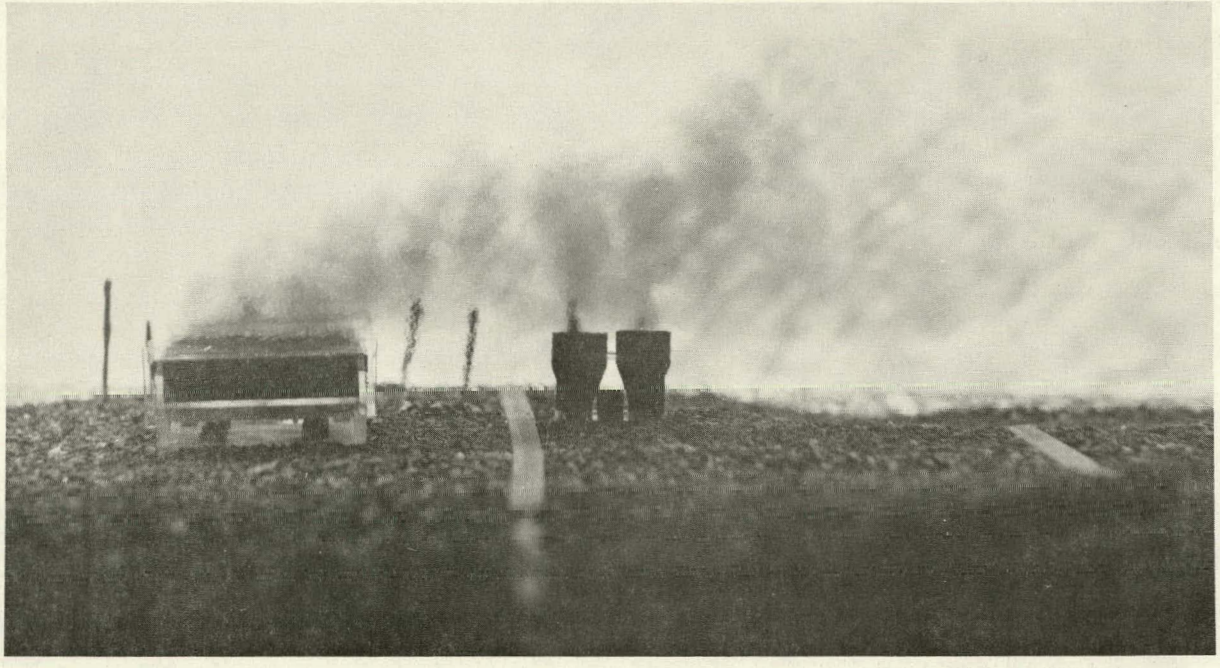

FIGURE 4.19 Photograph of Plumes from the Two Dry Cooling Towers for Run TD-6. V_a = 37.1 MPH.

These photographs for the northwesterly wind cases also reveal that since the plume from the ERDA tower merged with the plume from the Wyodak plant cooling tower without being withdrawn into the downwind Wyodak plant tower inlets, the merged plume may have a higher temperature than it otherwise would. Comparison of measured temperature distrubutions for the two tower cases (Run A-4, Figure 4.22) with those for the Wyodak plant tower alone (Run B, Figure 4.25) also supports this observation. This additional temperature rise tends to lift the plume and to reduce the temperature near the ground. Hence, the existence of the ERDA cooling tower for these cases may be advantageous to the Wyodak plant cooling tower's performance because it reduces the plume recirculation to the Wyodak plant tower.

However, when the wind is southeasterly, the plume from the upwind Wyodak plant tower is drawn into the ERDA cooling tower, thereby generating interference and strong adverse effects on the ERDA cooling tower's performance. As will be discussed in detail later, the ERDA tower recirculation ratio became 18 percent for the 30 mph southeasterly wind, resulting in a reduction of approximately 7 percent in the ERDA tower's cooling capacity for this case. It was also observed in this case that the plume from the ERDA tower was somewhat sheltered by the plume from the Wyodak plant tower.

Effects of tower effluent temperature (or F_D) on the plume dispersion were also clearly observed in the experiments. When the tower jet temperature was higher, then the buoyancy force relative to the ambient flow momentum increased. This caused a higher plume rise and less deflection of the plume, resulting in less recirculation.

In order to identify the effects of topography, plume centerline trajectories for Runs TU-3 through TU-6 were obtained from photographs (Figures 4.3 through 4.11) for both the Wyodak plant

and ERDA towers. For these cases, the winds were 13.8, 19.6, 29.8 and 39.1 mph from the northwest and the actual topography was installed in the model. The open coal mine pit for these cases was located upwind of the ERDA tower which was in turn located upwind of the Wyodak plant tower (see Figures 3.11 and 3.12). The trajectories of plumes were defined as the mid-point of the upper and lower plume edges. They are plotted as ZV_a^3/F versus XV_a^3/F in Figure 4.20, where X and Z are longitudinal and vertical distances and F is the buoyancy flux of the plume defined by

$$F = \frac{\Delta\rho}{\rho} \cdot \frac{V_j g D^2}{4}$$

In cases of flat or fairly flat ground, Briggs[5] derived the following semi-empirical expression of plume trajectory for neutral stratification of ambient flow:

$$\frac{ZV_a^3}{F} = 1.8 \left(\frac{XV_a^3}{F} \right)^{2/3} \tag{4.2}$$

or

$$\frac{Z}{D} = 1.8 \, K_I F_D^{-2/3} \left(\frac{X}{D} \right)^{2/3} \tag{4.3}$$

This equation was plotted in Figure 4.20 as a straight line, in order to compare it with experimental results. Figure 4.20 reveals that the trajectories of plumes from the ERDA tower deviate significantly from the straight line, whereas those from the Wyodak plant tower show fairly good agreement with the Briggs expression. The difference between the ERDA tower and Wyodak plant tower cases is believed to be attributable to topographical effects; i.e., existence of the coal mine pit changed the approaching ambient flow conditions (direction and magnitude of ambient flow). This effect may be strongly felt in the plumes from the ERDA tower which is located immediately downwind of the mine pit. Since the Wyodak tower is located

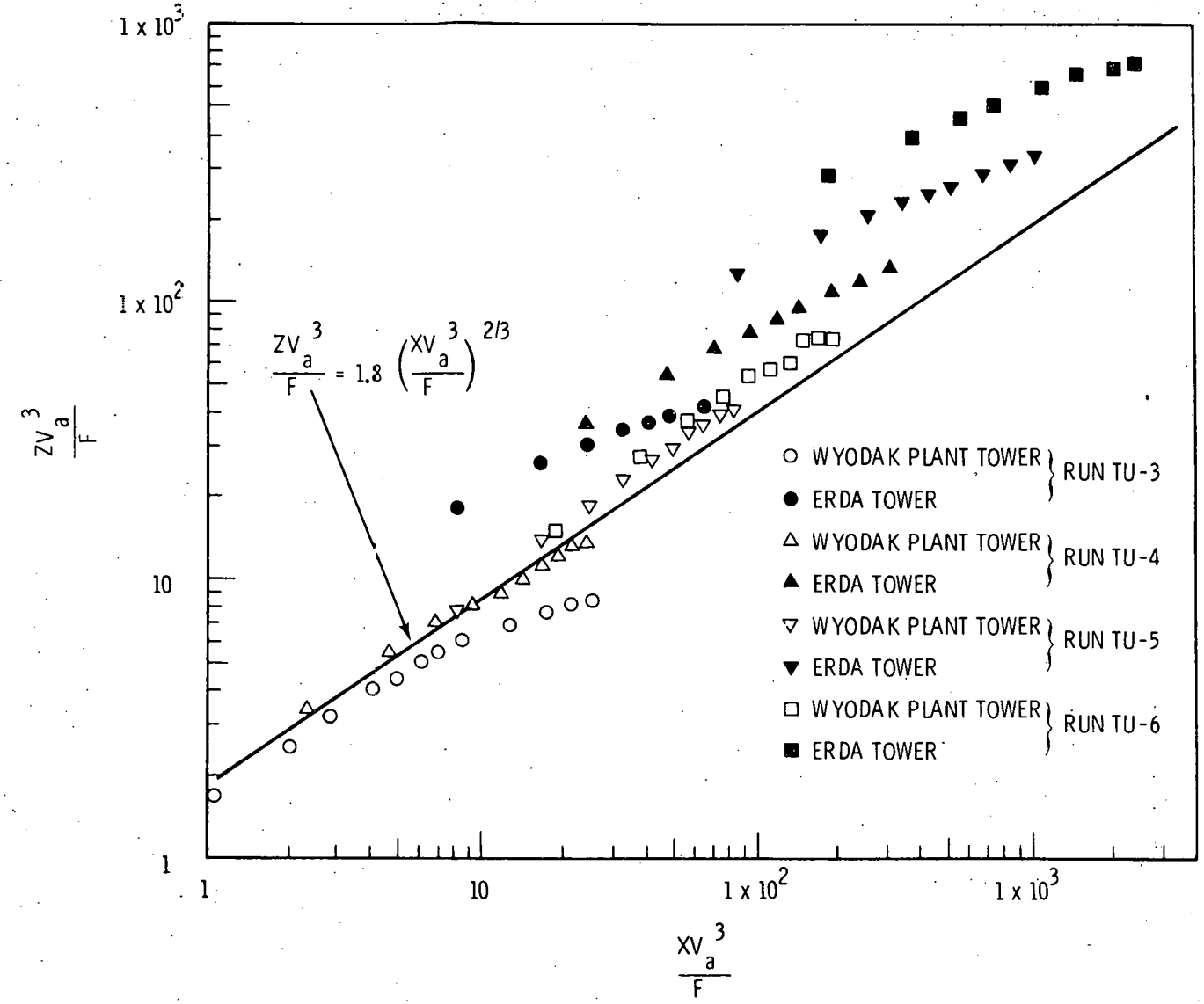

FIGURE 4.20. Trajectories of Bent-Over Plumes from the Wyodak Plant and ERDA Dry Cooling Towers with Actual Topography; Northwesterly Wind Cases

further downwind, this effect was considerably less intense in the Wyodak tower plumes, resulting in fairly good agreement with the Briggs expression (Equation 4.3).

In order to take into account the effect of the local topography on the plume trajectories, a simple equation, exp (b/a) was introduced, where "a" is the distance between the open pit and the cooling towers and "b" is the depth of the pit. The previous figure was replotted using the new function $(XV_a^3/F) \cdot \exp(b/a)$; the results for the ERDA and Wyodak plant plumes are shown in Figure 4.21. If the ground is flat, exp (b/a) becomes unity, resulting in XV_a^3/F. A straight line in the figure was drawn to fit the present experimental data. As shown in Figure 4.21, the data points for the ERDA tower plume indicate a better agreement with the straight line, showing a marked improvement as compared to Figure 4.20. The Wyodak plant plume also shows fairly good agreement. The shadowed area in the figure represents the width of the scatter of various wet cooling tower plume data reported by Briggs.[5] The straight line obtained from this study is expressed by

$$\frac{ZV_a^3}{F} = 1.5 \left[\frac{XV_a^3}{F} \cdot \exp \frac{b}{a} \right]^{2/3} \tag{4.4}$$

or

$$\frac{Z}{D} = 1.5\ K^{2/3} F_D^{-2/3} \left(\exp \frac{b}{a}\right)^{2/3} \left(\frac{X}{D}\right)^{2/3} \tag{4.5}$$

Hence the plume rise is proportional to "2/3 power" of the longitudinal distance X. Although there is a large amount of scatter for the present data, especially the slope of the ERDA plume, Figure 4.21 reveals that even such a simple function, exp (b/a), can improve the results significantly, indicating the very strong effects of local topography on the plume dispersion. This is one area that needs further study.

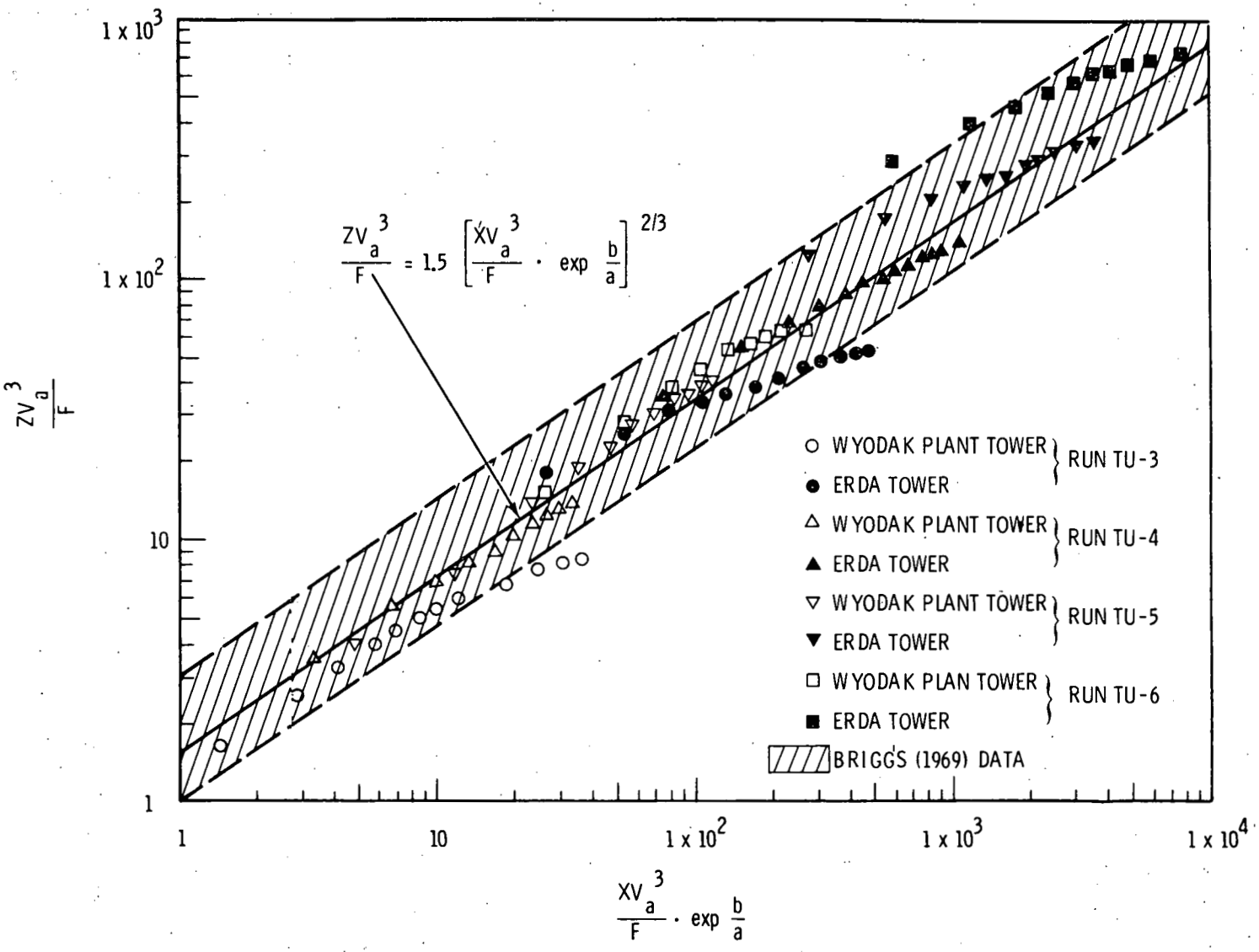

FIGURE 4.21. Variation of Nondimensional Plume Rise with Nondimensional Downstream Distance in the Cases of Actual Topography and Northwesterly Wind

4.1.3 Temperature Distribution

Figures 4.22 through 4.34 in Appendix 1 present normalized temperature distributions for Runs A-4, A-5, A-6, B, C-4, C-5, C-6, TU-4, TU-5, TU-6, TD-4, TD-5 and TD-6. Numbers shown in these figures are values of $\Delta T/\Delta T_o$. Plus marks (+) indicate the measurement points. The origin of the longitudinal axis is the upwind intake face of the upwind cooling tower; i.e., for Runs A, B, and TU, the upwind intake face of the ERDA cooling tower and for Runs C and TD, the upwind face of the Wyodak plant cooling tower. For Runs TU and TD, both cooling towers were drawn in the figures. Vertical temperature distributions shown in Figures 4.22 through 4.34 were obtained on a vertical plane which contains the centerline of the ERDA dry cooling tower. The elevations in these figures were measured above the local ground level at each measurement point.

Comparison of Figures 4.22, 4.23 and 4.24 indicates that when K decreases, the plume deflects more toward the downstream direction, resulting in less plume rise. Moreover, as K decreases, more vigorous mixing between the plume and the ambient occurs and rapidly reduces the temperature rise in the downstream area. These phenomena were also observed for the other set of data.

Comparison of Runs A-5 and B (Figures 4.23 and 4.25) shows that when the plume from the upwind ERDA tower merges with the plume from the Wyodak Plant tower, the resultant plume has a higher temperature than does the plume from the Wyodak tower alone. This higher temperature lifts the merged plume to a higher elevation, resulting in a lower temperature near the ground. This effect reduces the recirculation ratio defined by Equation 4.1 and improves the downwind cooling tower performance.

One effect of the local topography on plume dispersion is seen in Runs TU and TD (Figures 4.29 through 4.34). Comparison

of Runs A and TU reveals that the topography of the Wyodak plant site reduced mixing of the plume with the ambient. One possible reason is that a coal mine pit upwind of the cooling towers was considered in Run TU. Hence, the ambient flow direction at the cooling towers was somewhat upward, reducing the effective ambient velocity perpendicular to the plume. This in turn reduced the amount of mixing between the plume and the ambient flow.

When the wind was southeasterly, the actual topography upwind of the cooling tower was fairly flat. This may explain why there was only a minor difference between the temperature distributions of Runs C and TD for the 20, 30 and 40 mph wind cases. However, as will be discussed in the next section, the recirculation ratio for Runs C and TD differed when the ambient velocity was less than 20 mph.

4.1.4 Recirculation Ratio

In this section, effects of wind velocity (or K), effluent exist temperature (or F_D), adjacent cooling towers and local topography on recirculation and interference are examined.

As mentioned above, when cross-winds are present, the heated effluent plume is bent over and the plume trajectory is shifted closer to the intake faces of the cooling tower, causing some recirculation of the plume into the cooling tower. Recirculation may become a significant problem if the tower or a portion of the plume is situated in a wake caused by adjacent structures and/or the local terrain. severe interference may occur if some of the effluent from the upwind tower is taken into the downwind cooling tower.

Figures 4.35 and 4.36 (Runs A and C) show the variation in the recirculation ratio defined by Equation 4.1 with the velocity ratio, K for the Wyodak plant dry cooling tower located on flat ground. As shown in Figure 3.9, the Wyodak

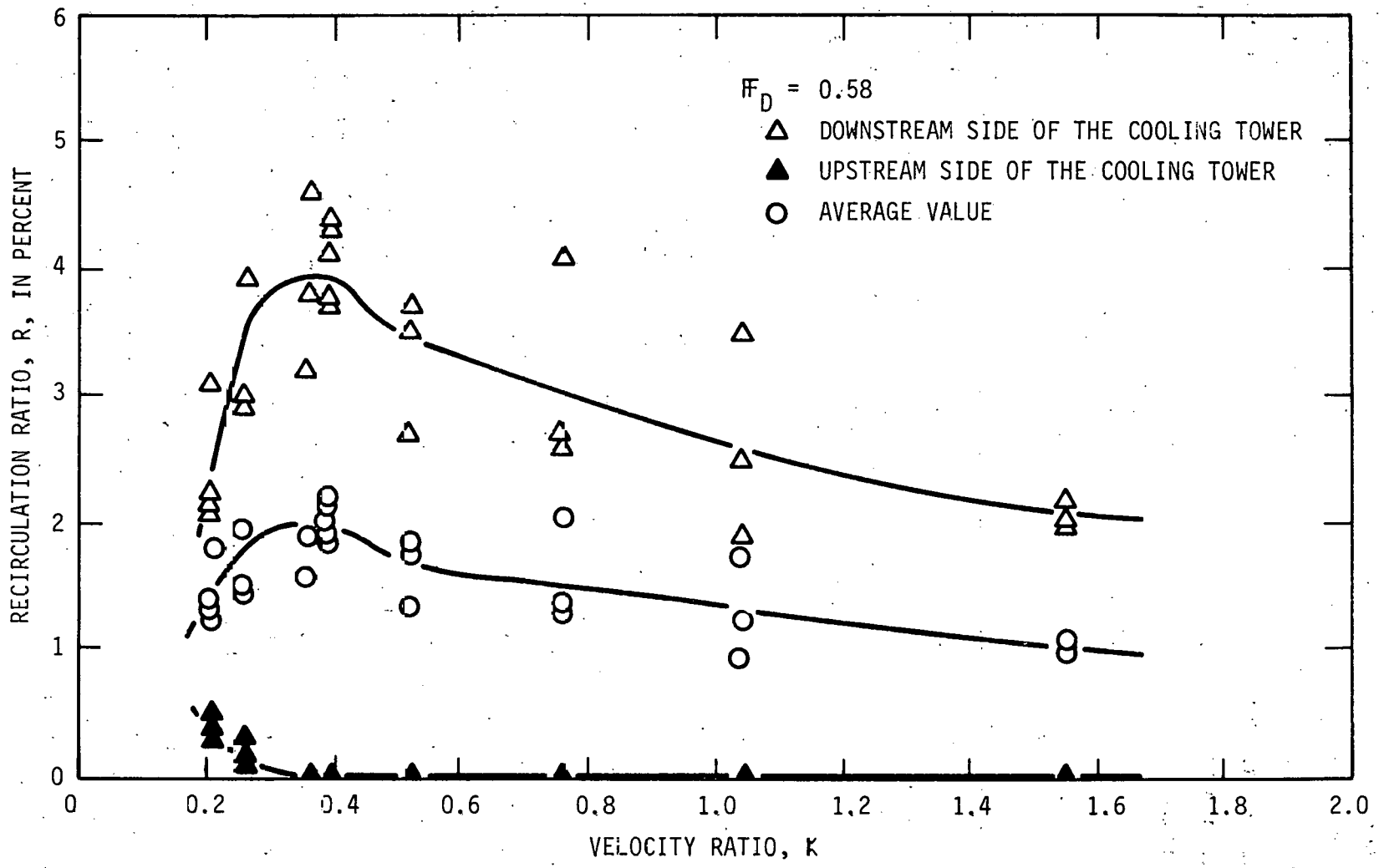

FIGURE 4.35. Variation of Recirculation Ratio, R, With Velocity Ratio, K, for the Wyodak Plant Dry Cooling Tower With Flat Ground; Northwesterly Wind Case (Run A)

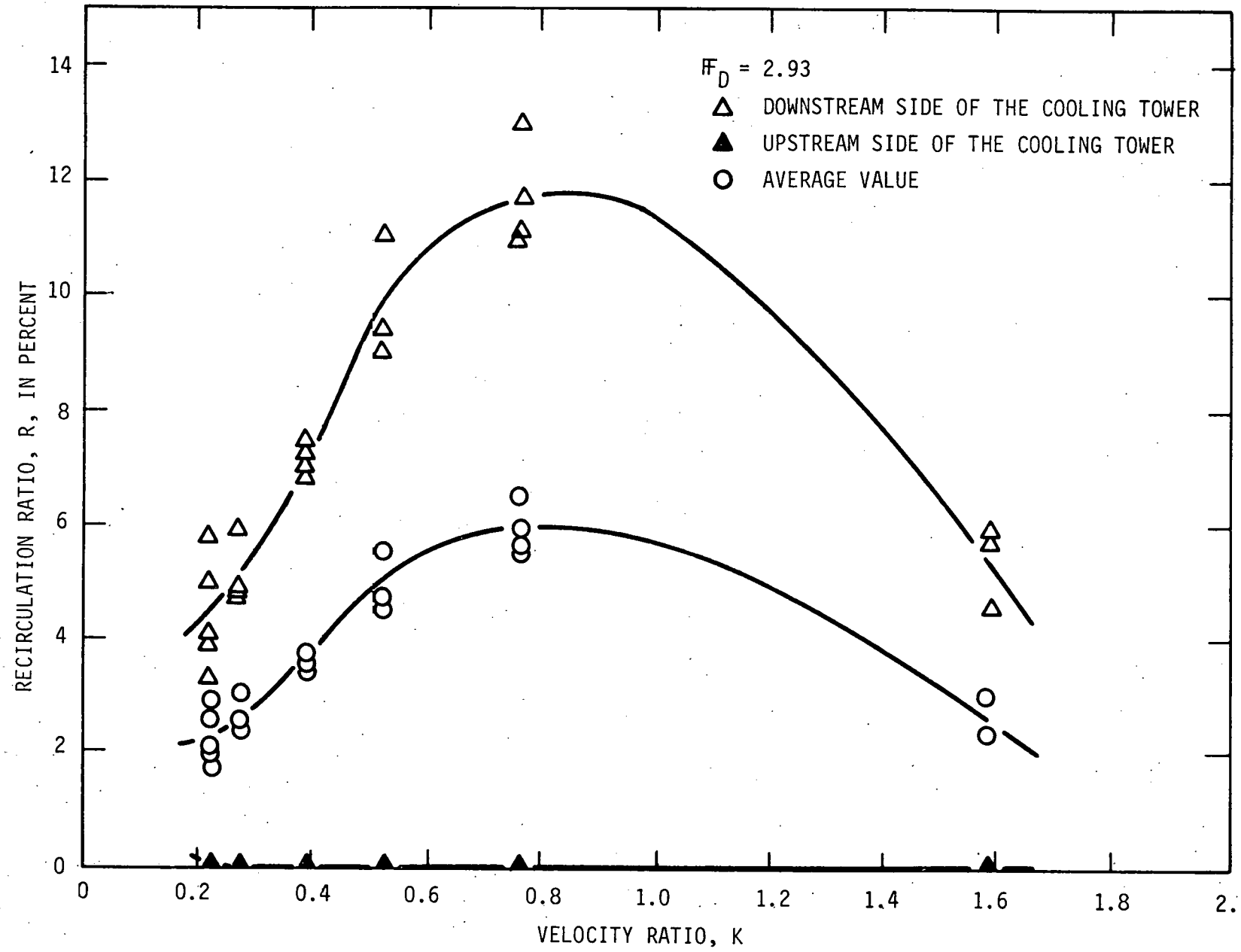

FIGURE 4.36. Variation of Recirculation Ratio, R, With Velocity Ratio, K, for the Wyodak Plant Dry Cooling Tower With Flat Ground Topography; Southeasterly Wind Case (Run C)

plant tower model had six pipes to withdraw the ambient flow into the cooling tower, three pipes located on the upstream side and three located on the downstream side of the tower. Figures 4.35 and 4.36 show values of R measured at the upstream and downstream sides, as well as average values for the tower. In both cases, the recirculation ratio, R, first increases as K decreases from a large value (or relatively small ambient velocity as compared to the heated effluent velocity). R reaches its maximum value as K decreases (or the ambient wind velocity increases). R then decreases as K further increases. At large values of K the plume rises nearly straight up, as shown in Figures 4.1 and 4.12. Hence, there is very little recirculation. When K decreases, the plume is deflected more closely to the ground, which is to be expected since the ratio of the momentum of the ambient flow to the jet momentum increases as the wind speed increases, while the effect of buoyancy is kept unchanged. Hence, R increases as K decreases. As K decreases further, the plume is bent over more and approaches the ground more closely. However, mixing between the plume and the ambient flow is also greatly enhanced, resulting in a significant dilution of the plume and large reduction in temperature rise. Moreover, the strong ambient flow can supply more flow from the upstream side to the intake face, rather than withdrawing the flow from the wake behind the tower. Hence, R starts to decrease. For Runs A and C, R reaches its maximum value at around K = 0.35 and 0.8, respectively.

One striking result in this case is that values of R for the upstream and downstream sides of the tower differ significantly, and there is a severe maldistribution of the temperature within the cooling tower. For example, Figure 4.36 shows that for K = 0.8, values of R measured at the downstream and upstream sides are 12 and 0 percent, respectively. This implies that it may not be appropriate to assume that the

ambient air temperature is the true inlet cooling air temperature as is commonly done to evaluate cooling tower performance. The availability of the cooling air temperature varies for each module within a cooling tower. Since very little is known about this distribution problem, a further study is needed to provide more detailed information so that power plant engineers can obtain more accurate evaluation of cooling tower performance. Figures 4.37 and 4.38 show the variation of R with K for the Wyodak plant tower located on the actual prototypic topography (Runs TU and TD). These figures reveal trends of R similar to those for the flat ground cases (Figures 4.35 and 4.36). R reached its maximum values at approximately K = 0.35 and 0.6 for Runs TU and TD.

Figures 4.39 and 4.40 show the effects of the velocity ratio, K (or wind velocity), an adjacent tower and local topography on the average values of the recirculation ratio, R, and hence on the performance of the Wyodak plant tower. Comparison of R values in the southeasterly wind, flat ground case (Run C) and the northwesterly wind, flat ground case (Run A) indicates that the values of R for Run C are much higher than those for Run A. This difference is due to the location of the small adjacent ERDA tower with respect to the wind direction and the Wyodak plant tower location. For Run A, the plume from the upwind ERDA tower helps to raise the plume from the downwind Wyodak plant cooling tower. The approaching ambient flow is also affected by the ERDA tower before it reaches the Wyodak plant tower. However, for Run C, not only does the plume from the ERDA tower not enhance the plume rise immediately behind the Wyodak plant tower, the existence of the ERDA tower itself may generate a captive eddy behind the Wyodak plant tower and thus cause stronger recirculation and interference.

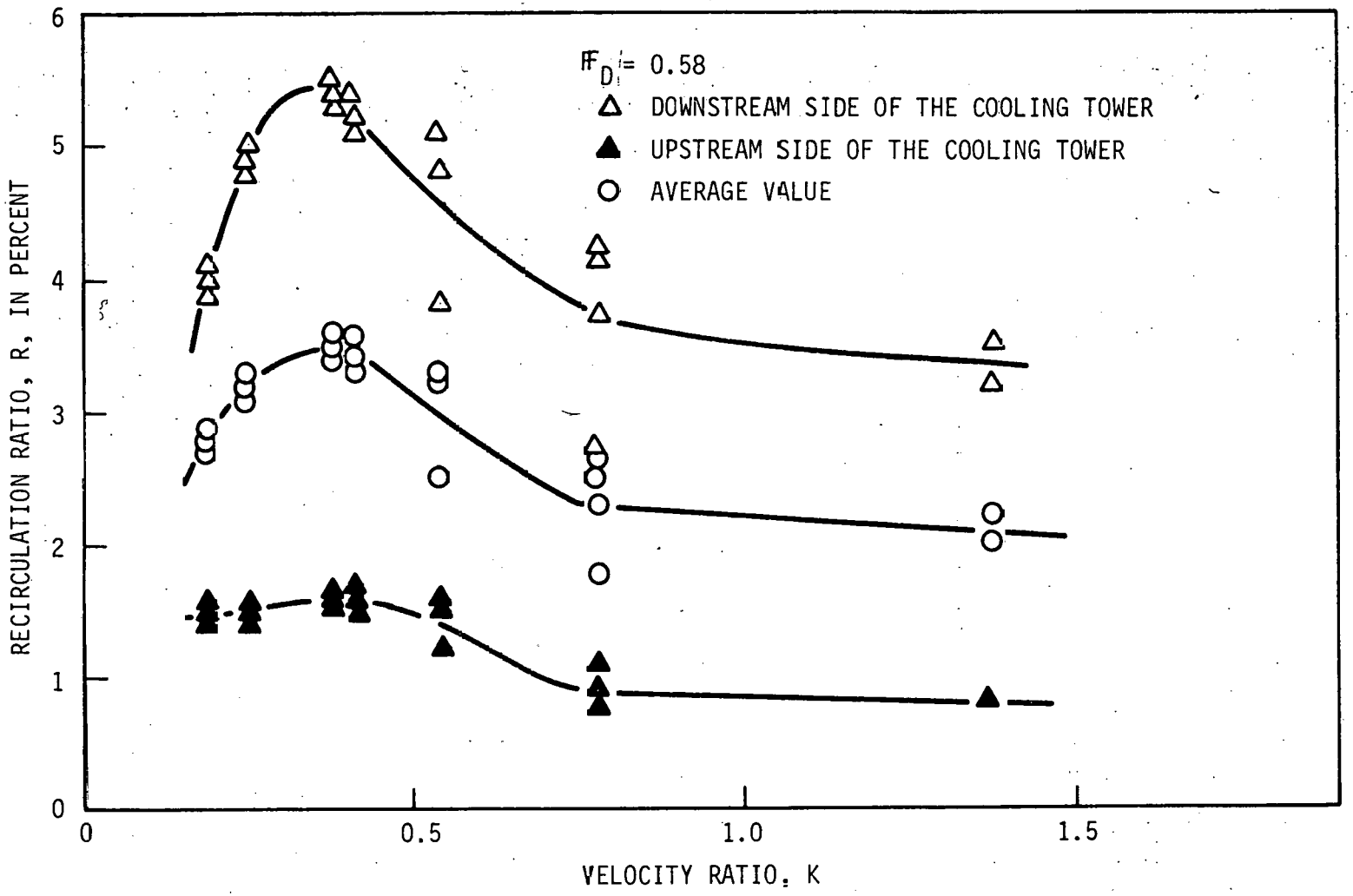

FIGURE 4.37. Variation of Recirculation Ratio, R, With Velocity Ratio, K, for the Wyodak Plant Dry Cooling Tower With the Actual Topography; Northwesterly Wind Case (Run TU)

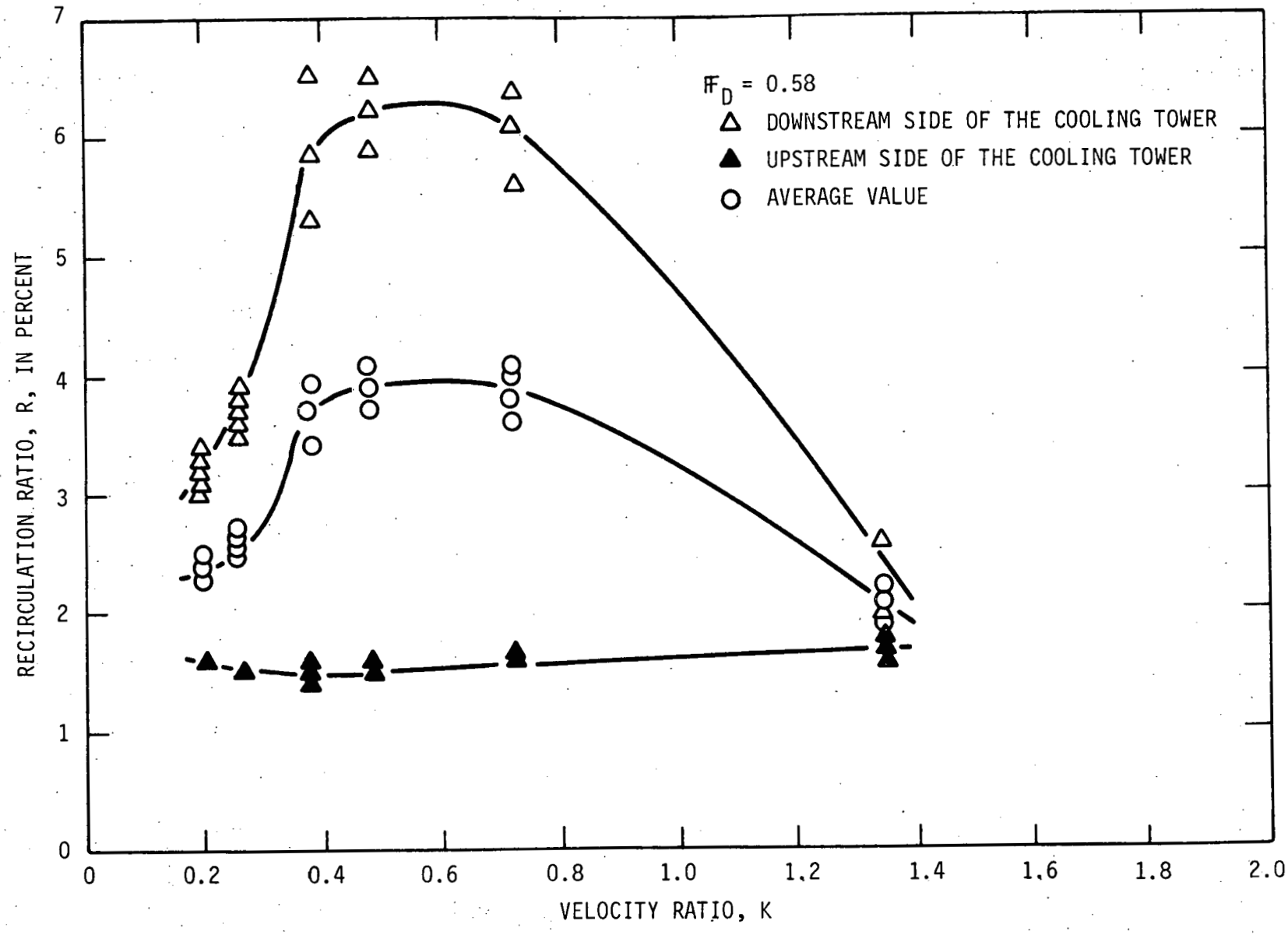

FIGURE 4.38. Variation of Recirculation Ratio, R, With Velocity Ratio, K, for the Wyodak Plant Dry Cooling Tower With the Actual Topography; Southeasterly Wind Case (Run TD)

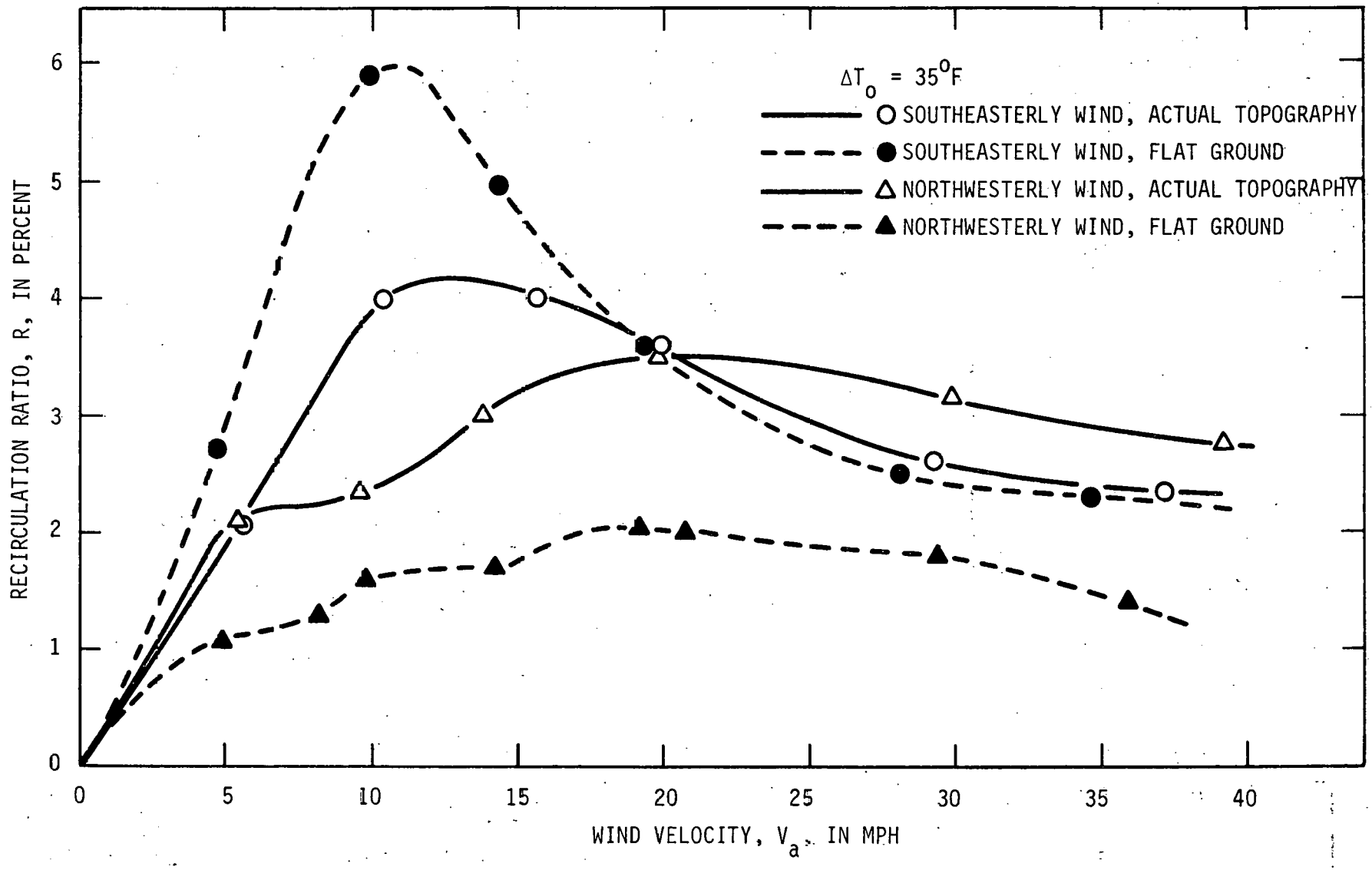

FIGURE 4.39. Variation of Recirculation Ratio, R, With Wind Velocity, V_a for the Wyodak Plant Dry Cooling Tower

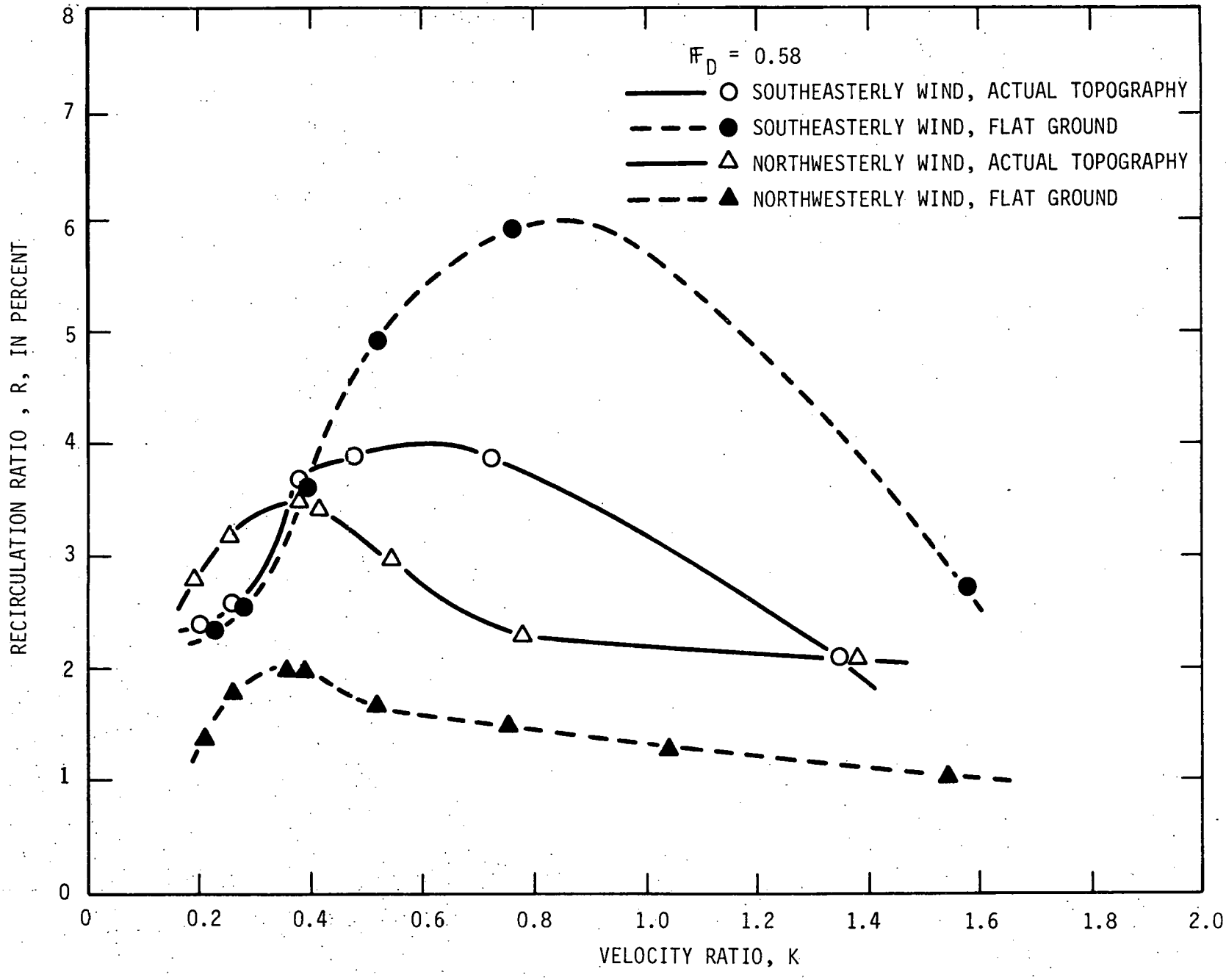

FIGURE 4.40. Comparison of Recirculation Ratio, R, of the Wyodak Plant Dry Cooling Tower

These advantageous effects of the ERDA tower for Run A and adverse effects for Run C were, however, offset by imposing the actual topography at the site. Comparison of the average values of R for these four cases (Runs A, C, TU and TD), as illustrated by Figures 4.39 and 4.40, reveals that the value of R for the northwesterly wind case with the actual topography (Run TU) is greater than for the flat ground case (Run A). This may be due to the fact that the coal mine pit just in front of the cooling towers changes the approaching ambient flow direction from the horizontal to the upward direction, as was discussed in Section 4.1.2.

The value of R for Run TD (southeasterly wind with actual topography) decreases from that of Run A (southeasterly wind with a flat ground) for a large K. This is again due mainly to the coal mine pit, which is located downwind of the two cooling towers in this case. The pit, however, works favorably to reduce R. This coal mine pit provides a larger area for an eddy to cover and lowers the temperature in the eddy zone for a large K. However, when K decreases, the mixing is enhanced and the effect of the pit is diminished.

Figures 4.41 and 4.42 show the variation of R with wind velocity and topography for the ERDA cooling tower. The trend is basically the same as for the Wyodak plant tower. However, the ratio of jet momentum to the ambient flow momentum (K) is larger for this case than for the Wyodak plant tower. Hence, R for the ERDA tower does not produce the peak point for the experimental range covered in this study. As shown in these figures, for the southeasterly wind cases (Runs C and TD), the average value of R reached 19 percent, indicating the very strong interference causes by the upwind Wyodak plant tower.

The plume recirculation affects the initial temperature difference, ITD, which in turn controls the heat rejection

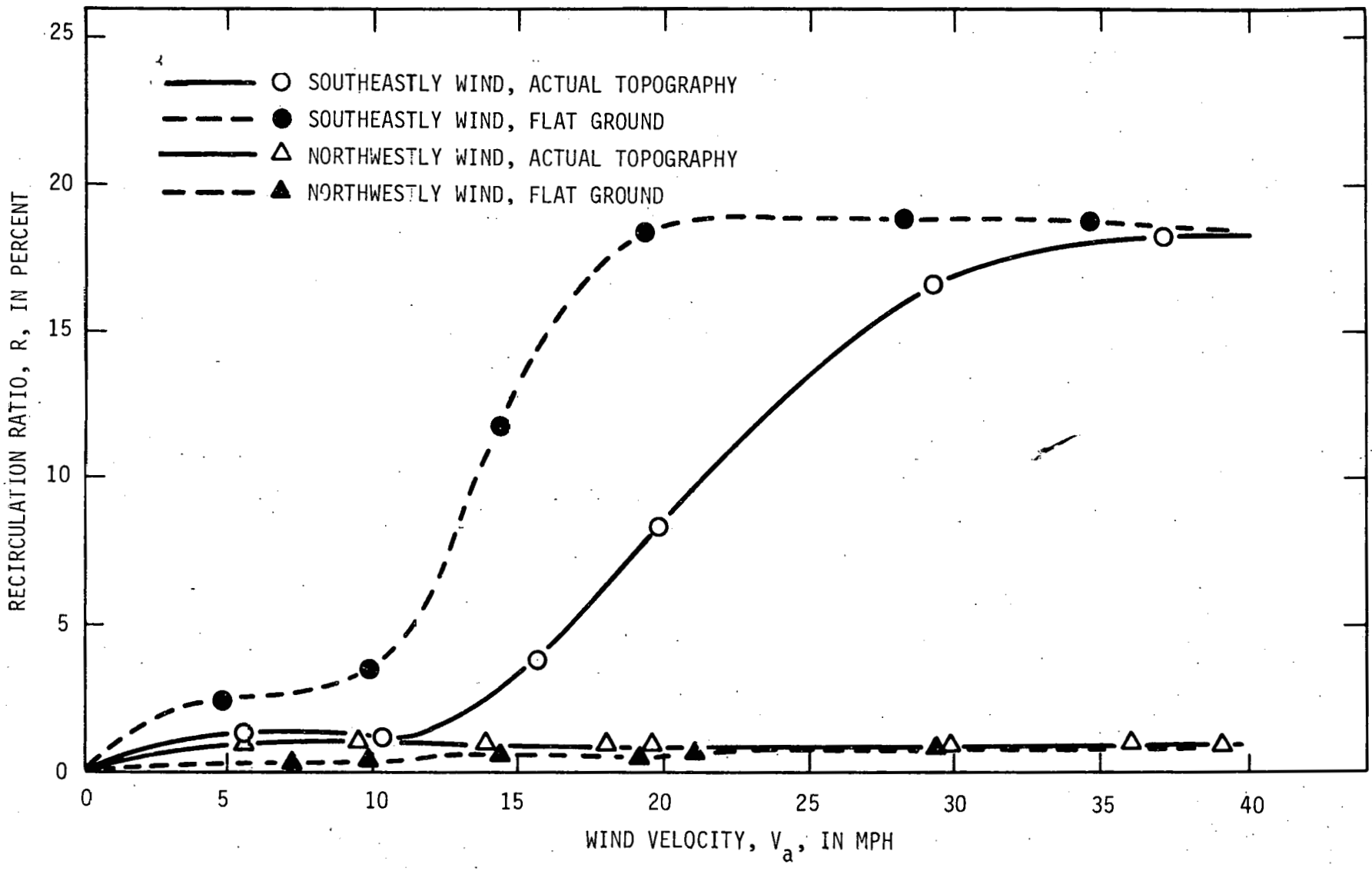

FIGURE 4.41. Variation of Recirculation Ratio, R, With Wind Velocity, V_a, for the ERDA Dry Cooling Tower (Runs A, C, TU and TD)

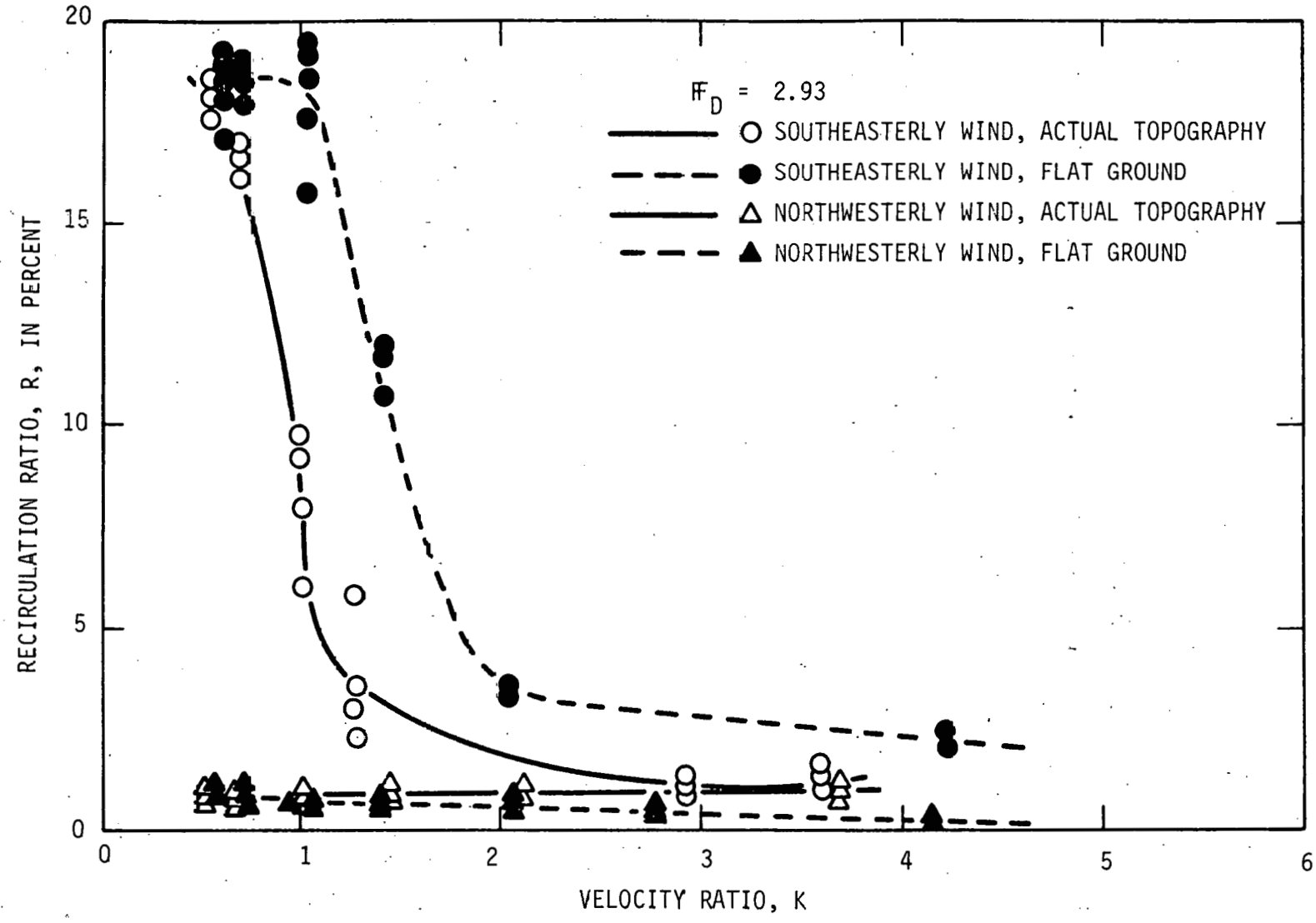

FIGURE 4.42. Variation of Recirculation Ratio, R, With Velocity Ratio, K, for the ERDA Dry Cocling Tower (Runs A, C, TU and TD)

capacity, Q_D of the cooling towers. For a mechanical draft dry cooling tower, Q_D in Btu/hr may be assumed by

$$Q_D = K_1(ITD) \tag{4.6}$$

where K_1 is a constant. For the two dry cooling towers being considered, ITD is large because of a high back turbine pressure (say, 7.4 psi). The cooling tower input water temperature, T_i is assumed to be 173.0°F.

The worst performance of dry cooling towers will be experienced during hot summer days. At the Wyodak plant site, the southeasterly wind is one of the prevailing winds during summer. Assuming an ambient temperature of 85°F and the effluent exit temperature of 120°F, ITD (= $T_i - T_a$) becomes 88°F without recirculation. Hence, the cooling capacity of the Wyodak plant tower without plume recirculation is

$$Q_D = K_1 \ (88.0) \qquad : \text{without recirculation}$$

When the southeasterly wind becomes 10 mph (or K = 0.72), R for the Wyodak plant tower becomes 4 percent (see Figures 4.39 and 4.40). For this case the true cooling air temperature is estimated as 86.4°F, and ITD becomes 86.6°F. The cooling capacity for this case then becomes

$$Q_D = K_1 \ (86.6) \qquad : \text{with recirculation}$$

Hence, a 4 percent recirculation ratio for the Wyodak plant tower reduces its cooling capacity by only 2 percent. However, for the ERDA tower, recirculation and interference become more severe problems. For the 37.1 mph (or K = 0.53) southeasterly wind case, R for the ERDA tower becomes 18.2 percent (see Figures 4.41 and 4.42). The true cooling air temperature is then 91.4°F instead of 85°F ambient temperature. The cooling capacities for cases without and with recirculation become

$$Q_D = K_2\ (88) \qquad \text{: without recirculation}$$

$$Q_D = K_2\ (81.6) \qquad \text{: with recirculation}$$

where K_2 is a constant which may be equal to K_1 in Equation 4.6 if both towers have similar heat rejection characteristics. The loss of heat rejection capacity due to recirculation for this case is approximately 7 percent. For conventional wet cooling towers, the turbine back pressure is much lower, resulting in a lower value of ITD (say ITD = 35°F). Note that for a wet tower, wet bulb temperature instead of dry bulb temperature must be used to get ITD. Hence the loss of heat rejection capacity of a wet cooling tower due to recirculation could be two to three times more severe than the capacity loss of a dry cooling tower for the same recirculation ratio. Fortunately, the worst recirculation conditions for the Wyodak plant and ERDA towers occur at different ambient wind velocities. Moreover, it is planned that the Wyodak plant tower, which has a smaller recirculation ratio than that of the ERDA tower, will be used to reject 85 percent of the total plant exhaust heat and the ERDA tower will reject only 15 percent of the total heat. Hence, even one of the worst cases may have a rather insignificant effect on the total power plant operation.

Example: For simplicity, assume the constant K_1 in Equation 4.6 is the same for both the Wyodak plant and ERDA towers.

Assume $T_a = 85.0°F$, $\Delta T_o = 35°F$, $V_a = 30$ mph (or 44.0 fps) and $T_i = 173.0°F$

Case 1. No Recirculation

For the Wyodak plant tower

$$Q_D = 0.85\ K_1(ITD) = 0.85\ K_1(173.0 - 85.0) = 74.8\ K_1$$

For the ERDA tower

$$Q_D = 0.15\ K_1(ITD) = 0.15\ K_1(173.0 - 85.0) = 13.2\ K_1$$

Total capacity

$$Q_D = 74.8\ K_1 + 13.2\ K_1 = 88.0\ K_1$$

Case 2. With Recirculation

For the Wyodak plant tower

$$K = \frac{10.9}{44.0} = 0.248$$

From Figure 4.40, R = 0.0255

$$ITD = 173.0 - 0.0255 \times 35.0 = 87.1°F$$

$$Q_D = 0.85\ K_1(87.1) = 74.0\ K_1$$

For the ERDA tower

$$K = \frac{29.0}{44.0} = 0.659$$

From Figure 4.42, R = 0.172

$$ITD = 85.0 + 0.172 \times 35.0 = 82.0°F$$

$$Q_D = 0.15\ K_1(82.0) = 12.3\ K_1$$

Total capacity

$$Q_D = 74.0\ K_1 + 12.3\ K_1 = 86.3\ K_1$$

Case 3. The Wyodak plant tower, with recirculation, rejects 100 percent of the plant exhaust heat (no ERDA tower operation)

For the Wyodak plant tower

$$V_j = 10.9 \times \frac{1.00}{0.85} = 12.8\ fps$$

$$K = \frac{12.8}{44.0} = 0.291$$

From Figure 4.40, R = 0.0275

$$ITD = 173.0 - 0.0275 \times 35.0 = 87.0°F$$

$$Q_D = 1.00\ K_1(87.0) = 87.0\ K_1$$

For the ERDA tower

$$Q_D = 0$$

Total cooling capacity

$$Q_D = 87.0\ K_1 + 0 = 87.0\ K_1$$

Hence, cooling capacity losses for Cases 2 and 3, as compared to Case 1, are only 2 and 1 percent, respectively, for the present Wyodak plant operation because of the reasons discussed above.

Variations of R with IF_D (or ΔT_o) for the Wyodak plant and the ERDA cooling towers are shown in Figures 4.43 through 4.46. These figures reveal that R increases as IF_D increases (or ΔT_o increases). This is because when IF_D decreases, the buoyancy force relative to the flow momentum increases and the plume rises higher and moves straight upward. Hence, the value of R decreases. Also, comparison of Runs TU and TD (Figures 4.43 and 4.44) shows that values of R for these cases are quite similar, despite the different wind directions.

This study reveals the strong effects of local topography and nearby cooling towers, as well as those of the ambient velocity and effluent exhaust air temperature, on plume recirculation. A further study is recommended to elucidate these effects on recirculation for other cases.

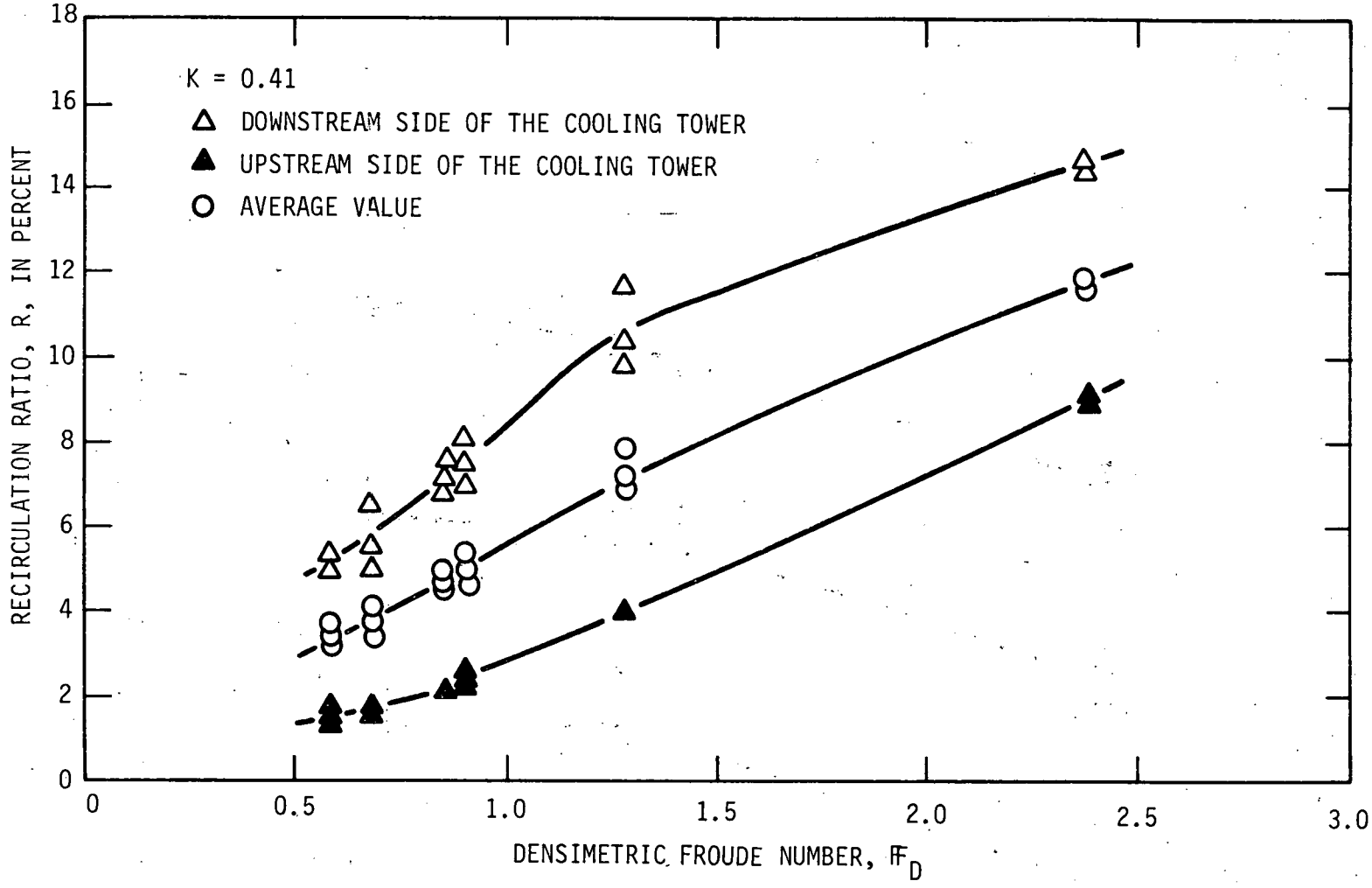

FIGURE 4.43. Variation of Recirculation Ratio, R, With Densimetric Froude Number, F_D, for the Wyodak Plant Dry Cooling Tower With the Actual Topography; Northwesterly Wind Case

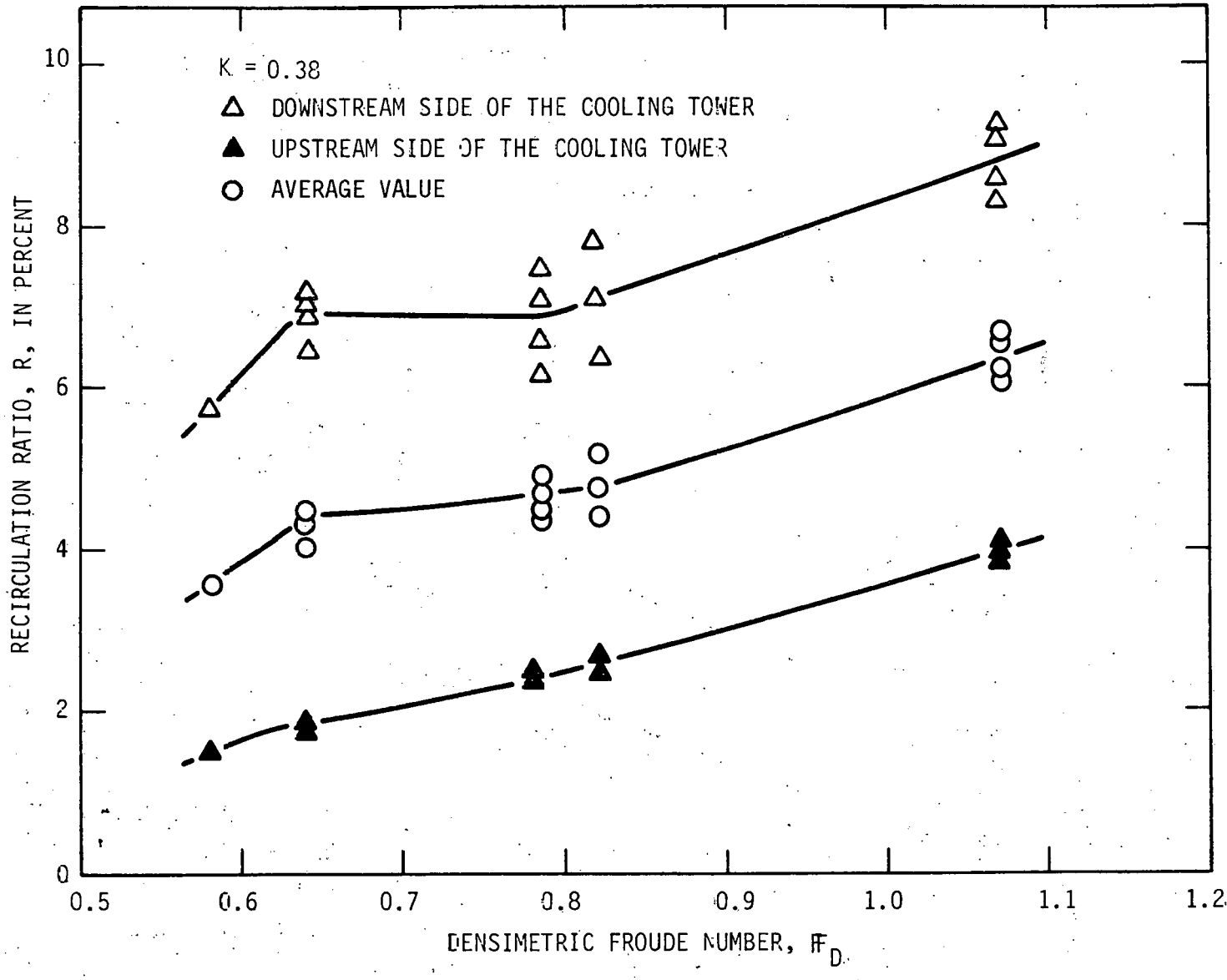

FIGURE 4.44. Variation of Recirculation Ratio, R, With Densimetric Froude Number, F_D, for the Wyodak Plant Dry Cooling Tower With the Actual Topography; Southeasterly Wind Case

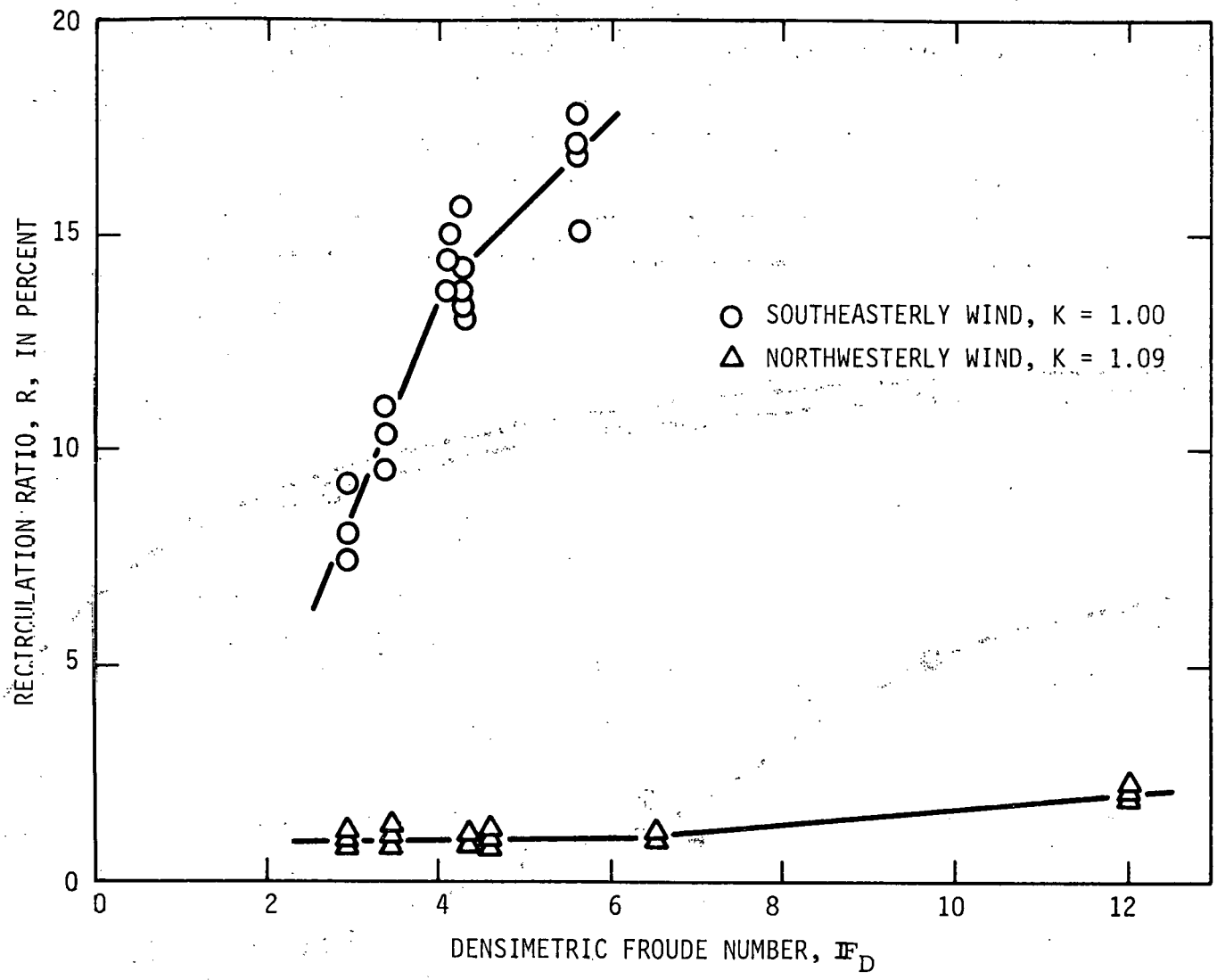

FIGURE 4.45. Variation of Recirculation Ratio, R, With Densimetric Froude Number, F_D, for the ERDA Dry Cooling Tower With the Actual Topography (Runs TU and TD)

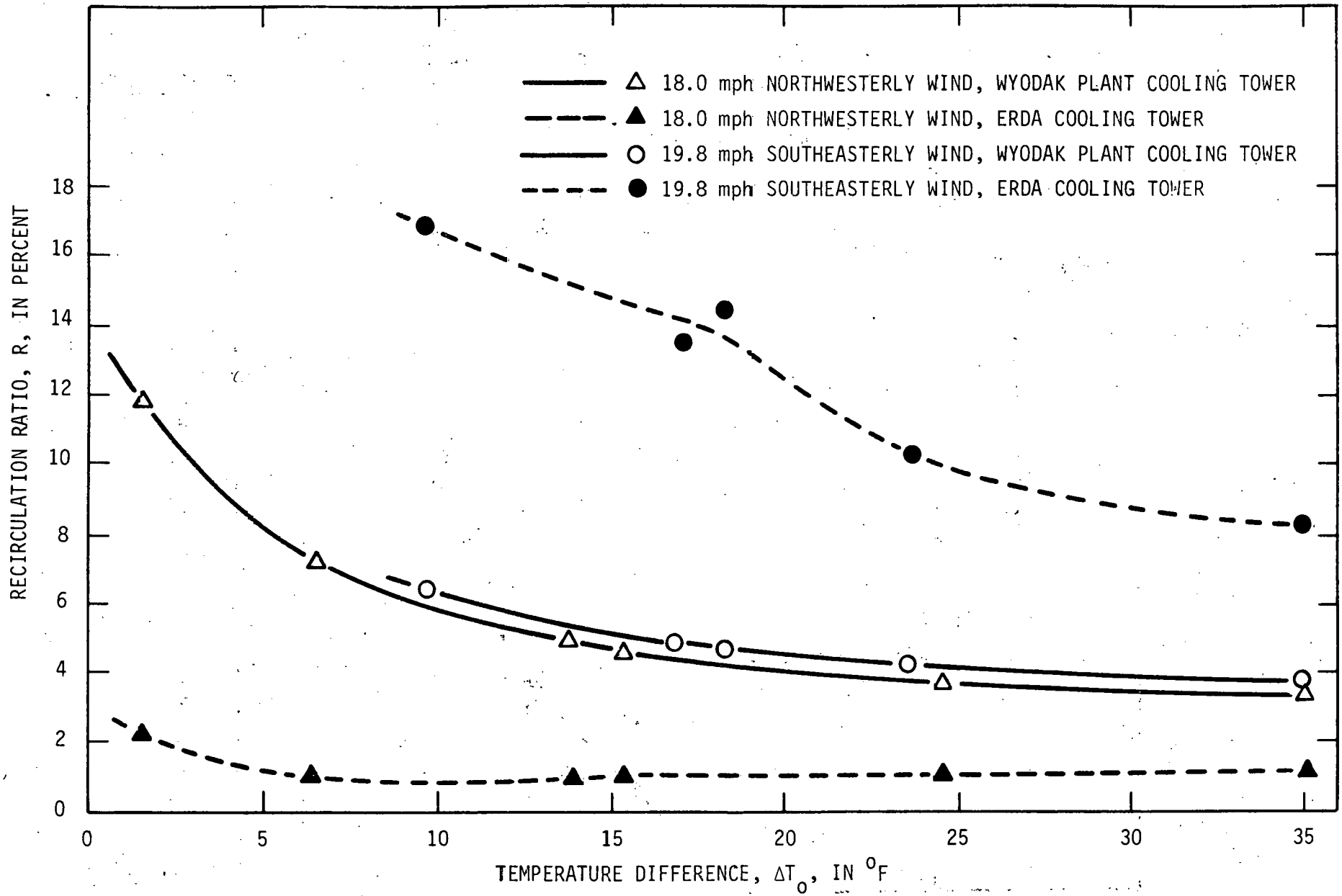

FIGURE 4.46. Variation of Recirculation Ratio, R, With the Temperature Difference, ΔT_o, for the Wycdak Plant and ERDA Dry Cooling Towers With the Actual Topography (Runs TU and TD)

4.2 TWO-DIMENSIONAL HEATED JET DISPERSION

A two-dimensional cooling tower plume simulation model was developed in this study. In order to examine the validity of this numerical code, three experiments for two-dimensional plumes were also conducted. As was discussed in Section 3.2, two-dimensional laminar heated jets were directed upward into a turbulent cross-ambient flow. Hydraulic conditions for these three experiments are shown in Table 4.5.

Water temperatures downstream of the jet discharge slit were measured along six different vertical planes. The measured 6 vertical distributions of water temperature and their average value are shown in Figures 4.47, 4.48 and 4.49 (Appendix 1). Unfortunately, these figures indicate some discrepancy from the true two-dimensional plume dispersion process.

Temperature distrubutions on the ground for these three average cases were plotted as $\Delta T/\Delta T_o$ versus $K^{1/2} \mathbb{F}_D^{-1/4} \mathbb{R}_j^{1/4} (X/D)$ (Figure 4.50). The water temperature on the ground decreases as X increases and its variation is correlated by the equation

$$\frac{\Delta T}{\Delta T_o} = 3.7 \, K^{-1/3} \mathbb{F}_D^{1/6} \mathbb{R}_j^{-1/6} \left(\frac{X}{D}\right)^{-2/3} \qquad (4.7)$$

Hence, the temperature distribution on the ground is proportional to "-2/3 power" of longitudinal distance X. This is somewhat expected because of the fact that a plume centerline trajectory is generally expected to be proportional to 2/3 the power of X (the "2/3 law") as shown in Equations 4.3 and 4.5.

As indicated by Equation 4.7, $\Delta T/\Delta T_o$ is proportional to $\mathbb{F}_D$ but inversely proportional to K, $\mathbb{R}_j$ and (X/D). Among these parameters, (X/D) has a dominant effect on $\Delta T/\Delta T_o$, followed by K. $\mathbb{F}_D$ and $\mathbb{R}_j$ have less effect on $\Delta T/\Delta T_o$ than those of (X/D) and K. The inverse effect of K on $\Delta T/\Delta T_o$ is explained as follows: For the range of K tested, the decrease in K deflects the plume more closely to the ground and hence $\Delta T/\Delta T_o$ on the

TABLE 4.5. Summary of Experimental Data for Two-Dimensional Heated Jet Case

Run No.	Ambient Flow Velocity, V_a, fps	Jet Velocity, V_j, fps	Temperature Difference, ΔT_o, °F	Discharge Slit Opening D, ft	Flow Depth, d, ft	Velocity Ratio K	Densimetric Froude Number, F_p	Jet Reynolds Number, R_j	Ambient Flow Reynolds Number, $R_a \times 10^4$
Y-1	0.465	0.335	22.8	0.021	1.09	0.72	6.7	910	19.9
Y-2	0.466	0.335	44.9	0.021	1.09	0.72	4.5	1130	19.9
Y-3	0.202	0.335	44.9	0.021	1.09	1.65	4.5	1130	8.6

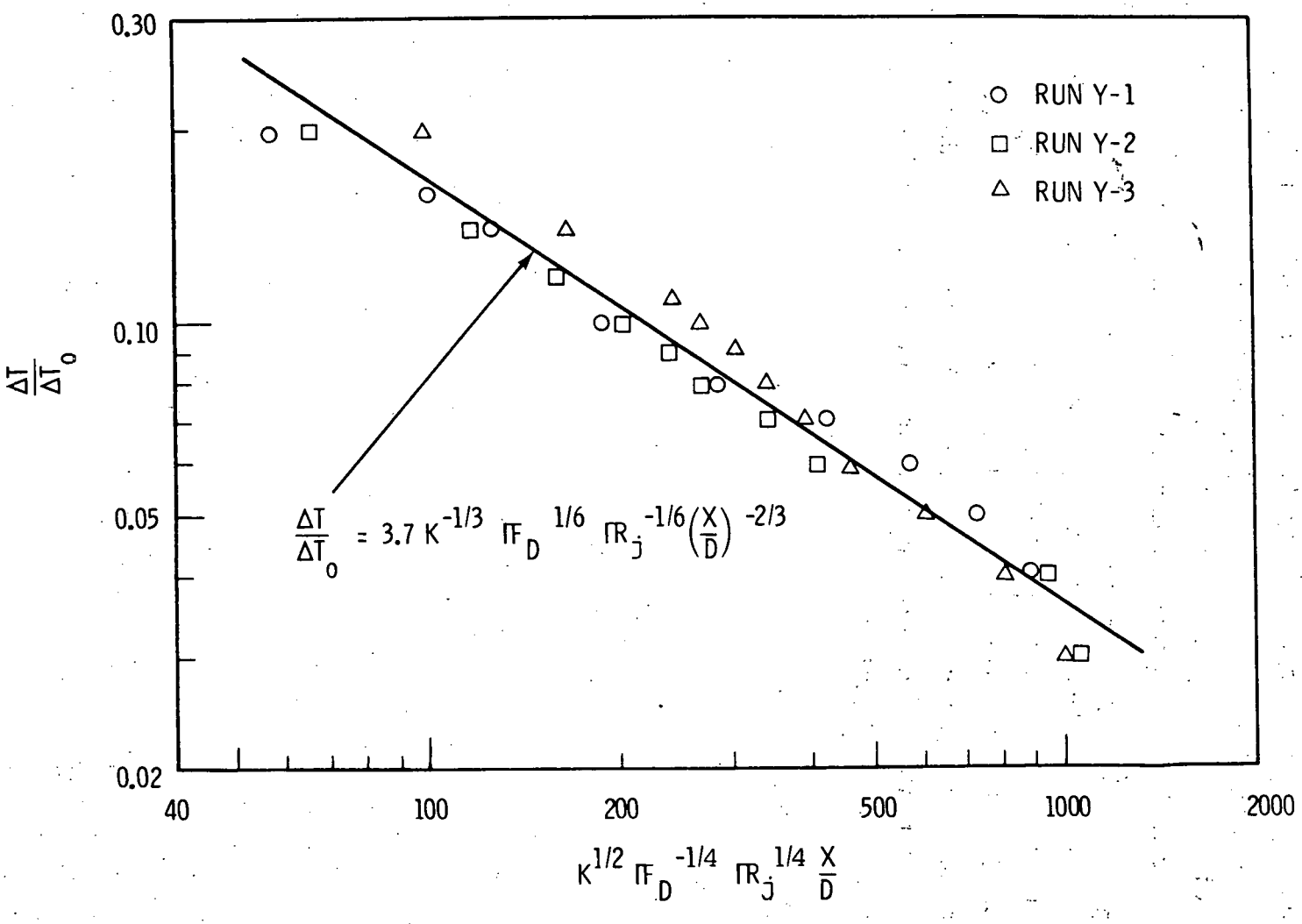

FIGURE 4.50. Variation of Temperature Distributions on the Ground

ground increase. When the buoyancy force increases (or $\mathbb{F}_D$ decreases), the plume rises more straight upward, resulting in the reduction of $\Delta T/\Delta T_o$ on the ground. Hence, $\Delta T/\Delta T_o$ is proportional to $\mathbb{F}_D$, as shown in Equation 4.7. The inverse effect of $\mathbb{R}_j$ on $\Delta T/\Delta T_o$ may be due to the following reason: For a laminar jet, the mixing of the jet with an ambient flow will be enhanced as $\mathbb{R}_j$ increases and thus values of $\Delta T/\Delta T_o$ will be reduced. If the jet is turbulent, $\mathbb{R}_j$ in Equation 4.7 will be deleted, as discussed in Section 3.1. Detailed descriptions of development of the computer code and testing of its validity are given in Chapters 5 and 6.

5.0 MATHEMATICAL MODEL

This section describes the theoretical basis and computational procedure of the VECTRA computer program. VECTRA (Vorticity-Energy Code for Transport Analysis) is designed for applying numerical simulation to a broad range of cooling tower flow configurations and adjacent topographical and structural influences. The code's computational procedure is based on finite-difference approximation of the vorticity-stream function partial differential equations which govern two-dimensional steady flow of incompressible, viscous fluids in conjunction with the transport of heat and other constituents.

Hydrodynamic and thermodynamic behaviors of cooling tower flows are inherently three-dimensional and nonlinear. They are further complicated by such phenomena as turbulence, buoyancy, and ambient conditions as well as local topographical features and adjacent structures. Because of these and other complications the possibility of resolving detailed temperature and velocity patterns for certain systems is rather remote without the aid of three-dimensional computational techniques. Recent developments in large core, high speed computer systems make the numerical simulation of three-dimensional hydrodynamic phenomena feasible[7,8] and have set the stage for broad practical application.

A working tool for tower flow assessment should be as simple as possible, yet be able to satisfactorily resolve the phenomena in question.[9,10,11] Within this framework many fluid dynamic analyses can be adequately performed through use of two-dimensional, steady or psuedo-steady flow techniques. In view of the inherent numerical complexities and economics associated with three-dimensional simulation, it seems prudent to attain the greatest practical proficiency in dealing with two-dimensional techniques and to exploit such methods to the greatest possible degree.

The VECTRA code provides a foundation computational tool that can be readily modified and incrementally improved to include capabilities for analyzing a broad range of tower external/internal flow configurations.

5.1 THEORETICAL DEVELOPMENT

The differential equations which govern momentum and heat transport appropriate for two-dimensional cooling tower flow are based on the following three physical laws:

- conservation of mass (continuity),
- Newton's second law (conservation of momentum), and
- the first law of thermodynamics (conservation of energy).

In addition, an appropriate equation of state is required to relate fluid density in terms of temperature.

The assumptions made at this stage of the development are:

- incompressible flow;
- turbulent flow;
- Reynolds stresses may be related to mean flow in terms of eddy diffusivities for momentum;
- eddy diffusivities include molecular effects and, in the absence of turbulence, collapse to the appropriate value of molecular kinematic viscosity;
- local change in density, ρ, is small compared to the absolute value of density (i.e., the Boussinesq approximation, $|\Delta\rho|/\rho << 1$); and
- turbulent heat and mass transfer coefficients are related to eddy diffusivities by an eddy Prandtl number.

The two-dimensional coordinate system considered is defined as a plane (or radial segment) normal to the geopotential surface. The two coordinates are defined as x and z where x lies in the horizontal plane and z is vertical. Corresponding velocity

components, u and v, are in the x and z directions, respectively. The governing equations are:

- Continuity

$$\frac{\partial u}{\partial x} + \frac{\partial v}{\partial z} + \xi \frac{u}{x} = 0$$

Where ξ is a binary function defined by:

$\xi = 1$: axisymmetric coordinates

$\xi = 0$: rectangular coordinates 5.1

- Momentum

x-direction:

$$\frac{\partial u}{\partial t} + \frac{\partial u \cdot u}{\partial x} + \frac{\partial v \cdot u}{\partial z} + \xi \frac{u^2}{r} = - \frac{\partial P^\circ}{\partial x} + F_x$$

$$+\varepsilon \left\{ \frac{\partial^2 u}{\partial x^2} + \frac{\partial^2 u}{\partial z^2} + \xi \left(\frac{1}{x} \frac{\partial u}{\partial x} - \frac{u}{x^2} \right) \right\} \quad 5.2$$

z-direction:

$$\frac{\partial v}{\partial t} + \frac{\partial u \cdot v}{\partial x} + \frac{\partial v \cdot v}{\partial z^2} + \xi \frac{u \cdot v}{x} = - \frac{\partial P^\circ}{\partial z} + \frac{\rho}{\rho_\circ} g_z + F_z$$

$$+\varepsilon \left\{ \frac{\partial^2 v}{\partial x^2} + \frac{\partial^2 v}{\partial z^2} + \frac{\xi}{x} \frac{\partial v}{\partial x} \right\} \quad 5.3$$

- Energy

$$\frac{\partial T}{\partial t} + \frac{\partial uT}{\partial x} + \frac{\partial vT}{\partial z} + \xi \frac{uT}{x} = \dot{q}$$

$$+ K \left\{ \frac{\partial^2 T}{\partial x^2} + \frac{\partial^2 T}{\partial z^2} + \frac{\xi}{x} \frac{\partial T}{\partial x} \right\} \quad 5.4$$

- State

$$P = \rho RT \qquad 5.5$$

Symbols used in the above equations are defined as follows:

$P^\circ = P/\rho_o$

P = pressure

ρ_o = reference density

F_x, F_z = drag forces

ε = eddy diffusion coefficient for momentum

K = eddy diffusion coefficient for heat

R = gas constant

T = temperature

A second state equation of the form $\rho = f(T)$ is used for modeling in water.

The momentum equations (5.2 and 5.3) in conjunction with the continuity equation (5.1) are converted to the following vorticity-stream function set:

- Stream Function, ψ

$$\frac{\partial^2\psi}{\partial x^2} + \frac{\partial^2\psi}{\partial z^2} - \frac{\xi}{x}\frac{\partial\psi}{\partial x} = \left\{\xi(x-1) + 1\right\}\omega \qquad 5.6$$

- Vorticity, ω

$$\frac{\partial\omega}{\partial t} + \frac{\partial u\omega}{\partial x} + \frac{\partial v\omega}{\partial z} = \varepsilon\left\{\frac{\partial^2\omega}{\partial x^2} + \frac{\partial^2\omega}{\partial z^2} + \frac{\xi}{x}\frac{\partial\omega}{\partial x} - \frac{\xi\omega}{x^2}\right\} - \frac{g}{\rho_o}\frac{\partial\rho}{\partial x} \qquad 5.7$$

$$+ \frac{\partial F_x}{\partial z} - \frac{\partial F_z}{\partial x}$$

where:

$$\omega = \frac{\partial u}{\partial z} - \frac{\partial v}{\partial x}$$

The velocity field u,v is computed from the stream function distribution using the following equations:

$$u = -\left\{\xi\left(\frac{1}{x} - 1\right) + 1\right\} \frac{\partial \psi}{\partial z} \qquad 5.8$$

$$v = \left\{\xi\left(\frac{1}{x} - 1\right) + 1\right\} \frac{\partial \psi}{\partial x} \qquad 5.9$$

For the purpose of computer simulation, Equations 5.5, 5.6, 5.7, 5.8 and 5.9 are cast into dimensionless forms using the following variables:

$$X = x/L$$

$$Z = z/L$$

$$U = u/v_o$$

$$V = v/v_o$$

$$\Psi = \psi/(Lv_o)$$

$$\Omega = \omega L/v_o$$

where v_o and L are reference velocity and length, respectively.

Dimensionless parameters used are:

$RE_x = \frac{v_o L}{\epsilon_x}$, horizontal reference Reynolds number

$RE_z = \frac{v_o L}{\epsilon_z}$, vertical reference Reynolds number

$PR_x = \frac{\epsilon_x}{k_x}$, horizontal reference Prandtl number

$PR_z = \frac{\epsilon_z}{k_z}$, vertical reference Prandtl number

$$F_o = \frac{v_o^2}{\left(\frac{\rho_r - \rho_o}{\rho_o}\right) gL}$$, reference densimetric Froude number

Based on the preceding dimensionless variables and parameters, the steady flow governing equations are

- Stream Function

$$\frac{\partial^2 \Psi}{\partial X^2} + \frac{\partial^2 \Psi}{\partial Z^2} - \frac{\xi}{X} \cdot \frac{\partial \Psi}{\partial X} = - \left\{ \xi (X - 1) + 1 \right\} \Omega \qquad 5.10$$

- Vorticity

$$\frac{\partial}{\partial X} (U\Omega) + \frac{\partial}{\partial Z} (V\Omega) = - \frac{1}{F_o} \frac{\partial \Delta}{\partial X} + \frac{1}{RE_x} \left\{ \frac{\partial^2 \Omega}{\partial X^2} + \frac{\xi}{X} \frac{\partial \Omega}{\partial X} - \frac{\xi \Omega}{X^2} \right\}$$

$$+ \frac{1}{RE_z} \frac{\partial^2 \Omega}{\partial Z^2} + \left(\frac{\partial F_x}{\partial z} - \frac{\partial F_z}{\partial x} \right) \qquad 5.11$$

- Energy

$$\frac{\partial}{\partial X} (UT) + \frac{\partial}{\partial Z} (VT) + \frac{\xi UT}{X} = \frac{1}{RE_\kappa PR_\kappa} \left\{ \frac{\partial^2 \bar{T}}{\partial X^2} + \frac{\xi}{X} \frac{\partial \bar{T}}{\partial X} \right\}$$

$$+ \frac{1}{RE_z PR_z} \frac{\partial^2 T}{\partial Z^2} \qquad 5.12$$

Where

$$\Delta = \frac{\rho_o - \rho}{\rho_o - \rho_r}$$

- Velocity

$$U = - \left\{ \xi \left(\frac{1}{X} - 1 \right) + 1 \right\} \frac{\partial \Psi}{\partial Z} \qquad 5.13$$

$$V = \left\{\xi\left(\frac{1}{X} - 1\right) + 1\right\} \frac{\partial \Psi}{\partial X} \qquad 5.14$$

For simplicity, eddy transport coefficients are assumed constant in the above equations.

5.2 FINITE-DIFFERENCE GRID SYSTEM

The finite-difference grid layout consists of two grid systems. One grid is used to calculate the stream function, Ψ, which provides information to compute velocity components U and V. This system coincides with the physical boundaries and is illustrated by the wider lines on Figure 5.1. The stream function is calculated at the interior intersection points designated by the solid round symbols. Solid box symbols represent boundary points.

Velocities are not calculated at these points. U components are computed at vertical (or coordinate) midpoints, which are designated by open circle symbols. The V components are computed at horizontal (or x coordinate) midpoints and designated by open box symbols. Thus, the stream function grid layout defines a system of cells with the stream function, Ψ, computed at each corner point (or set by boundary conditions, as the case may be) and velocities defined at the center of the cell face (see Figure 5.2).

The second grid system is used to calculate vorticity, Ω, and the temperature, T, and is illustrated in Figures 5.1 and 5.2 by narrow lines. This layout completely overlaps the grid (and physical system) with interior intersection points centered in the cells defined by the Ψ grid system. These interior grid points are indicated by crosses with boundary values at cross-and-box points.

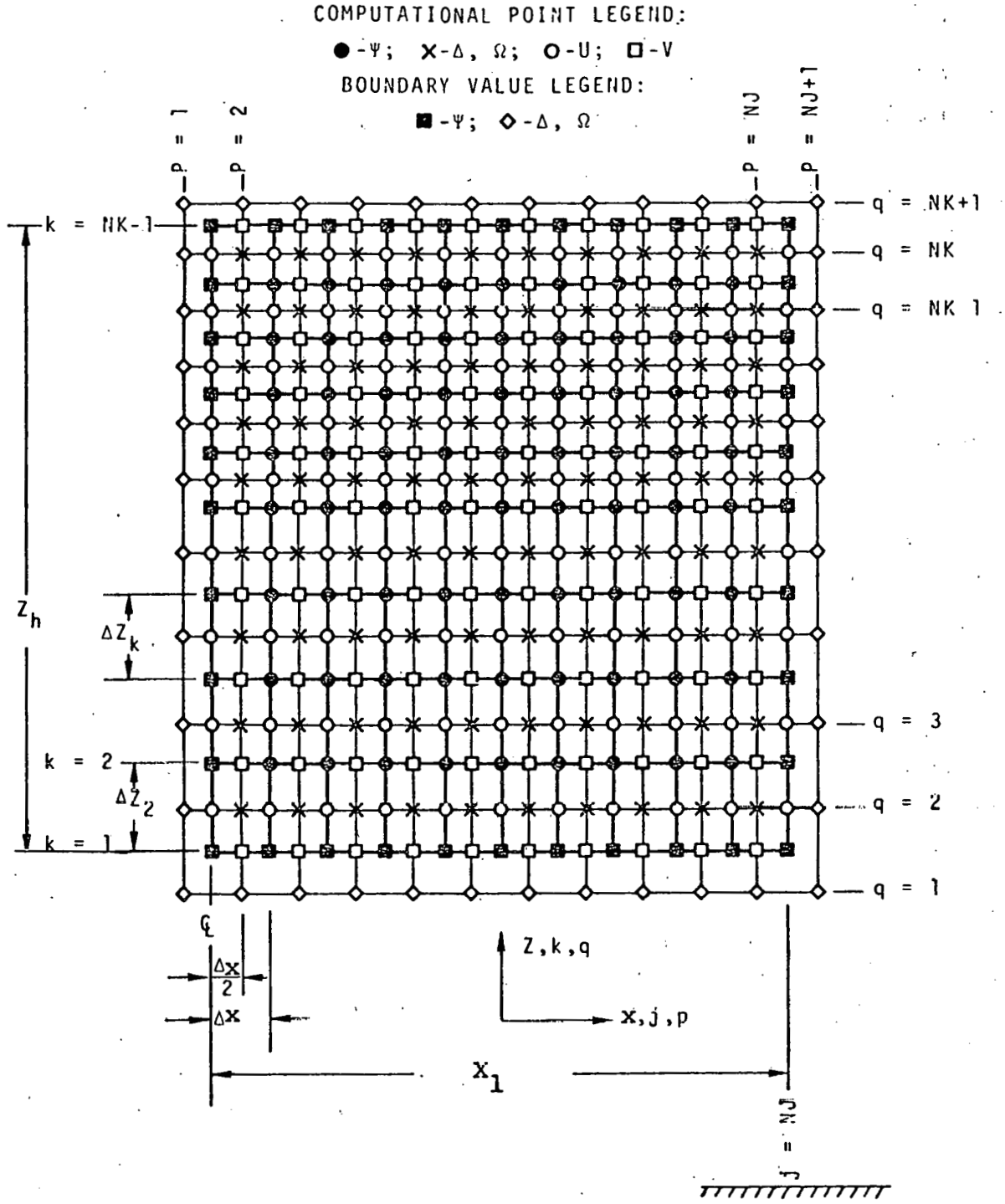

FIGURE 5.1 Computational Grid for Difference Equations

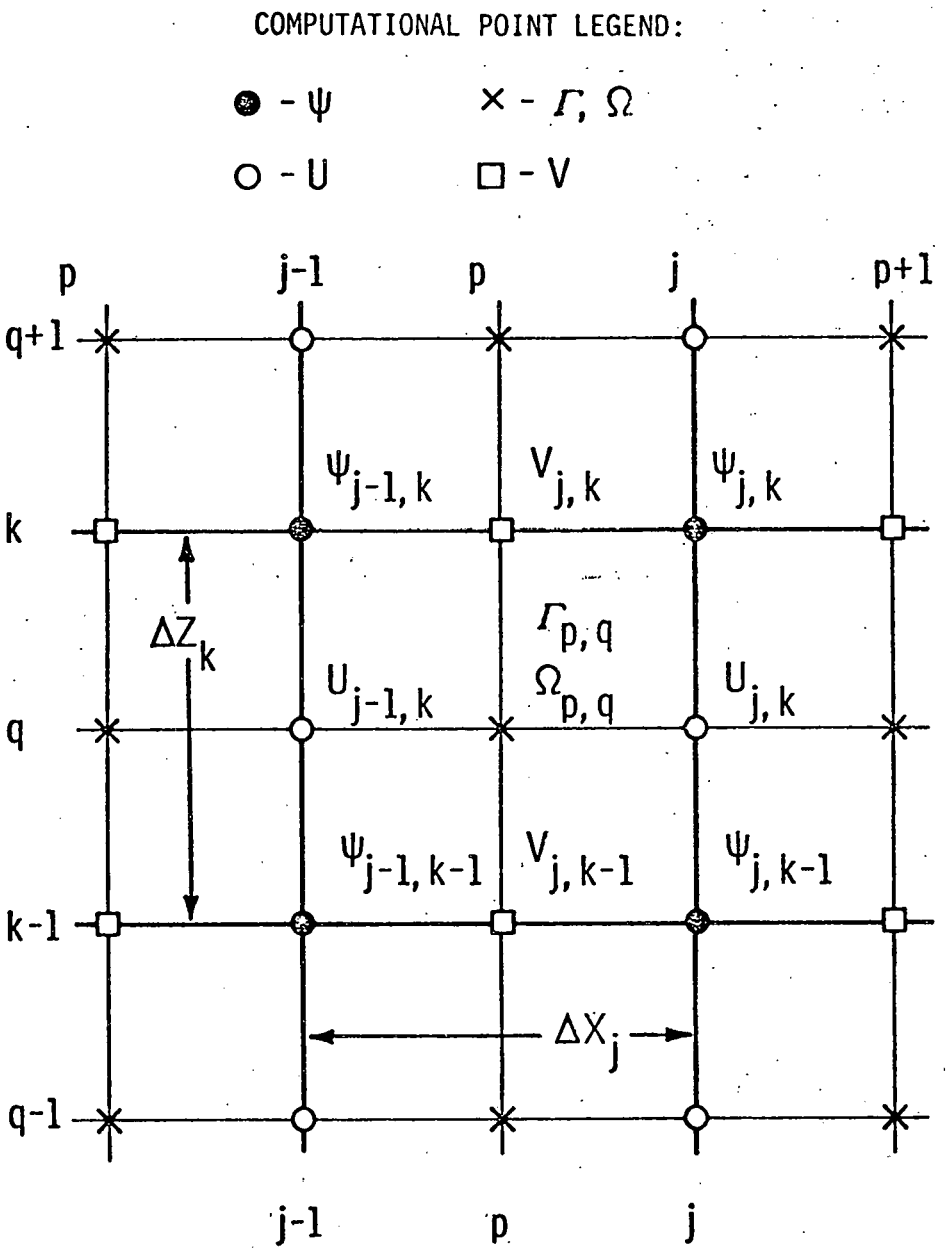

FIGURE 5.2 Typical Finite Difference Cell Illustrating Indices for ψ, Ω, Γ, U and V

The staggered grid system is used for computational convenience in treating boundary conditions and to permit convective transport terms to be evaluated at cell faces.

In Figure 5.2, the Ψ grid system is sized by NJ and NK grid points in the x and vertical directions, respectively. The Ω, T system has size NJ + 1 and NK + 1 in the respective directions. Points on the Ψ grid are indicated by J, k whereas points on the Ω, T grid are indicated by p, q. Grid spacing in either coordinate system may be variable. Figure 5.2 also illustrates indices, computed quantities, cell size and radial distances for a typical interior cell.

5.3 DIFFERENCING FOR CONSERVATIVE FORMS

The finite-difference methods employed in this work are based on central differencing techniques, except for the transport equation convection terms which have the conservative forms $\partial(U_j\Gamma)/\partial X_j$. The conservative form is in a direct result of a Γ balance in terms of infinitesimal quantities and has the correct form for proper conservation of a transported quantity in numerical analysis.

Convective balance of Γ in x, z coordinates is illustrated in Figure 5.3.

The steady flow convective balance equation for volume element p is given by

$$\int_{A_T} \Gamma(\vec{v}\cdot\hat{n})\,dA = \int_{A_1} \Gamma(\vec{v}\cdot\hat{n})\,dA + \int_{A_2} \Gamma(\vec{v}\cdot\hat{n})\,dA + \int_{A_3} \Gamma(\vec{v}\cdot\hat{n})\,dA + \int_{A_4} \Gamma(\vec{v}\cdot\hat{n})\,dA = 0. \qquad 5.15$$

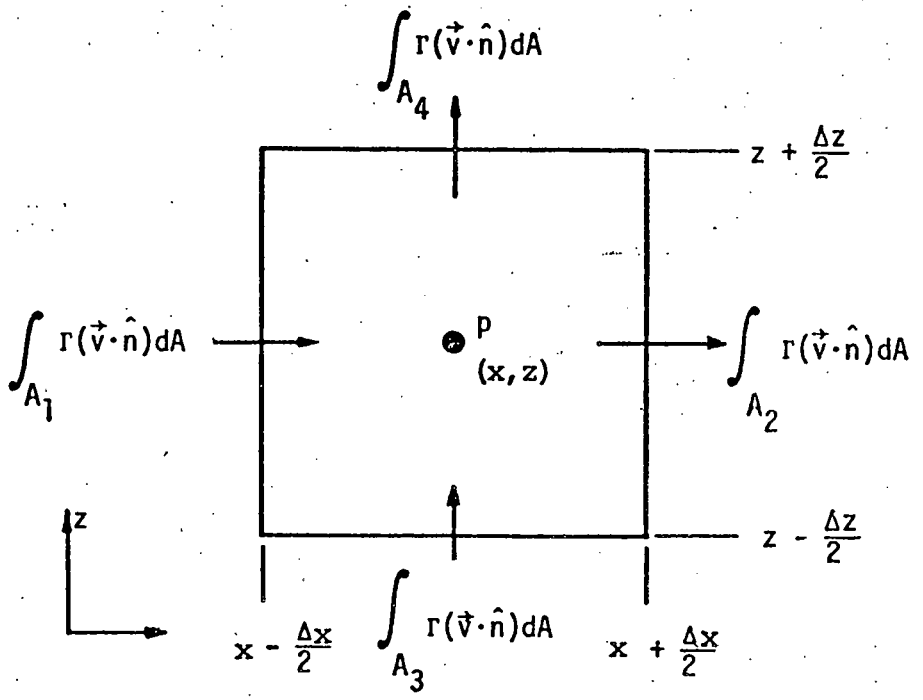

FIGURE 5.3 Convective Γ Flux for a Rectilinear x-z Volume Element

In Equation 5.4 and Figure 5.3, A_1, A_2, etc., are element areas corresponding to side 1, 2, etc., and $\hat{n}$ is a unit normal vector, with outward being the positive sense and inward, the negative. Like directional sense is used for the boundary velocity vector, $\vec{v}$.

The grid system shown in Figure 5.4 has constant Δx and Δz and velocities u and v are specified at the cell face, whereas Γ is cell-centered at point p. For the donor cell difference scheme based on Equation 5.14, the value of Γ at the upstream neighbor is convected into the cell, p, and the value of Γ at p is convected out of cell, p. Thus, the value of Γ to be used in Equation 5.15 is given by

$$\Gamma = \begin{cases} \Gamma_p, \text{ for } |\vec{v}\cdot\hat{n}| = \vec{v}\cdot\hat{n} \\ \\ \text{value at upstream neighbor for } |\vec{v}\cdot\hat{n}| \neq \vec{v}\cdot\hat{n}. \end{cases}$$

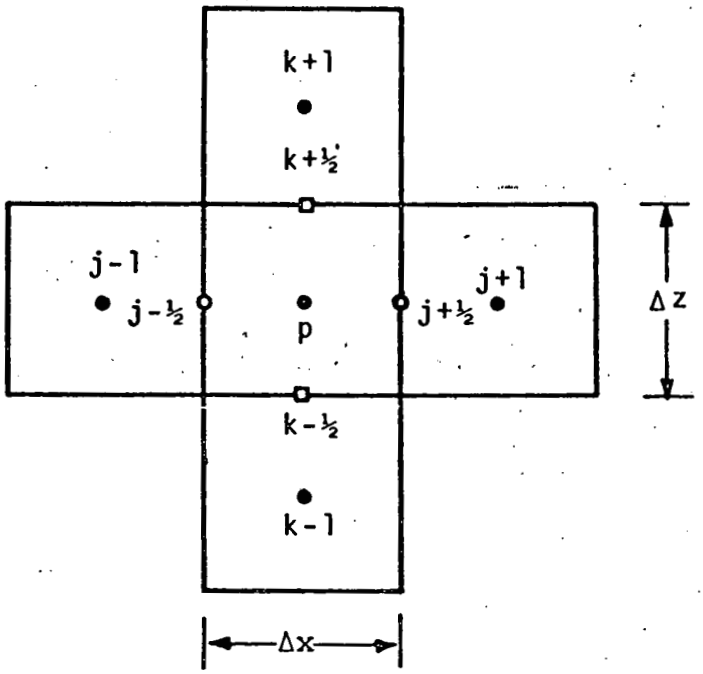

FIGURE 5.4. x-z Finite-Difference Cell with the Four Immediate Neighbor Cells

Using the ideas expressed by Equation 5.14, the above equation is expressed in finite-difference form as

$$\frac{\frac{1}{2}\left\{\Gamma_p(|u_{j-1/2}| - u_{j-1/2}) - \Gamma_{j-1}(|u_{j-1/2}| + u_{j-1/2})\right\}}{\Delta x}$$

$$+ \frac{\frac{1}{2}\left\{\Gamma_p(|u_{j+1/2}| + u_{j+1/2}) - \Gamma_{j+1}(|u_{j+1/2}| - u_{j+1/2})\right\}}{\Delta x}$$

$$+ \frac{\frac{1}{2}\left\{\Gamma_p(|v_{k-1/2}| - v_{k-1/2}) - \Gamma_{k-1}(|v_{k-1/2}| + v_{k-1/2})\right\}}{\Delta z}$$

$$+ \frac{\frac{1}{2}\left\{\Gamma_p(|v_{k+1/2}| + v_{k+1/2}) - \Gamma_{k+1}(|v_{k+1/2}| - v_{k+1/2})\right\}}{\Delta z}$$

$$\Leftrightarrow \quad \left.\frac{\partial(u\Gamma)}{\partial x} + \frac{\partial(v\Gamma)}{\partial z}\right|_p \qquad 5.16$$

5.4 DIFFERENCE EQUATIONS FOR RECTILINEAR COORDINATES

Finite-difference models are based on Equations 5.10, 5.11 and 5.12, along with the auxiliary Equations 5.13 and 5.14, which are needed for computing velocity components. In this discussion, only a steady flow condition will be considered with constant eddy transport coefficients. The difference equations for a uniform grid system (a variable grid is used in the computer code) are summarized as follows:

- Stream Function

$$\Psi_{j,k} = \frac{\Psi_{j-1,k} + \Psi_{j+1,k}}{2\left(\frac{1}{\Delta X^2} + \frac{1}{\Delta Z^2}\right)\Delta X^2} + \frac{\Psi_{j,k-1} + \Psi_{j,k+1}}{2\left(\frac{1}{\Delta X^2} + \frac{1}{\Delta Z^2}\right)\Delta Z^2}$$

$$+ \frac{\bar{\Omega}_{j,k}}{2\left(\frac{1}{\Delta X^2} + \frac{1}{\Delta Z^2}\right)} \qquad 5.17$$

Vorticity, $\bar{\Omega}_{j,k}$, is the average value for the four surrounding cells (see Figure 5.2) and is given as

$$\bar{\Omega}_{j,k} = \frac{1}{4}\left(\Omega_{p,q} + \Omega_{p,q+1} + \Omega_{p+1,q} + \Omega_{p+1,q+1}\right) \qquad 5.18$$

- Velocity

$$U_{j,k} = -\frac{1}{\Delta Z}\left(\Psi_{j,k} - \Psi_{j,k-1}\right) \qquad 5.19$$

$$V_{j,k} = \frac{1}{\Delta X}\left(\Psi_{j,k} - \Psi_{j-1,k}\right) \qquad 5.20$$

- Vorticity

$$\left[\frac{1}{2\Delta X}\left(|U_{j,k}| + U_{j,k} + |U_{j-1,k}| - U_{j-1,k}\right)\right.$$
$$+ \frac{1}{2\Delta Z}\left(|V_{j,k}| + V_{j,k} + |V_{j,k-1}| - V_{j,k-1}\right)$$
$$\left. + \frac{2}{RE_x \Delta X^2} + \frac{2}{RE_z \Delta Z^2}\right] \Omega_{p,q}$$
$$= \left[\frac{1}{2\Delta X}\left(|U_{j-1,k}| + U_{j-1,k}\right) + \frac{1}{RE_x \Delta X^2}\right] \Omega_{p-1,q}$$
$$+ \left[\frac{1}{2\Delta X}\left(|U_{j,k}| - U_{j,k}\right) + \frac{1}{RE_x \Delta X^2}\right] \Omega_{p+1,q}$$
$$+ \left[\frac{1}{2\Delta Z}\left(|V_{j,k-1}| + V_{j,k-1}\right) + \frac{1}{RE_z \Delta Z^2}\right] \Omega_{p,q-1}$$
$$+ \left[\frac{1}{2\Delta Z}\left(|V_{j,k}| - V_{j,k}\right) + \frac{1}{RE_z \Delta Z^2}\right] \Omega_{p,q+1}$$
$$- \frac{1}{2F_o \Delta X}\left(\Delta_{p+1,q} - \Delta_{p-1,q}\right). \qquad 5.21$$

- Temperature, T

$$\left[\frac{1}{2\Delta X}\left(|U_{j,k}| + U_{j,k} + |U_{j-1,k}| - U_{j-1,k}\right)\right.$$
$$+ \frac{1}{2\Delta Z}\left(|V_{j,k}| + V_{j,k} + |V_{j,k-1}| - V_{j,k-1}\right)$$
$$\left. + \frac{2}{RE_x PR_x \Delta X^2} + \frac{2}{RE_z PR_z \Delta Z^2}\right] T_{p,q}$$
$$= \left[\frac{1}{2\Delta X}\left(|U_{j-1,k}| + U_{j-1,k}\right) + \frac{1}{RE_x PR_x \Delta X^2}\right] T_{p-1,q}$$
$$+ \left[\frac{1}{2\Delta X}\left(|U_{j,k}| - U_{j,k}\right) + \frac{1}{RE_x PR_x \Delta X^2}\right] T_{p+1,q}$$

$$+\left[\frac{1}{2\Delta Z}\left(|V_{j,k-1}| + V_{j,k-1}\right)+ \frac{1}{RE_z PR_z \Delta Z^2}\right]T_{p,q-1}$$

$$+\left[\frac{1}{2\Delta Z}\left(|V_{j,k}| - V_{j,k}\right) + \frac{1}{RE_z PR_z \Delta Z^2}\right]T_{p,q+1} \qquad 5.22$$

Boundary conditions are

- Free-surface ($Z=Z_h$)

  Ψ = constant = Ψ_1

  $\Omega = 0$ (free slip condition)

  $\frac{\partial T}{\partial Z} = 0$ (adiabatic condition, for present work)

- Specified flow boundary

Discharge/intake velocity V_b and Δ are assumed known from data or empirical relationships.

$$\Psi = \Psi_1 + \int_o^Z V_b dZ$$

$$\Omega = \frac{\partial U}{\partial Z} - \frac{\partial V}{\partial X}$$

$$T = T_b$$

- No-slip boundary

$$\Psi = \Psi_1 + \int_o^{Z_h} V_b dZ = \text{constant} = \Psi_3$$

$$\Omega = \frac{\partial U}{\partial Z} - \frac{\partial V}{\partial X} \quad \text{(no-slip condition)}$$

$$\frac{\partial T}{\partial Z} = 0$$

- Free-flow boundary

$\frac{\partial \Psi}{\partial X}$ = constant (that is, streamlines do not change slope as they cross this boundary)

$\Omega = 0$, flow into system is irrotational

$$= \frac{\rho_r - \rho_\infty}{\rho_r - \rho_o}$$

6. CODE DESCRIPTION AND COMPUTATIONAL RESULTS

The computer program described in this section is designed to obtain the solution of the difference equations (5.17, 5.19, 5.20, 5.21 and 5.22) for the quantities ψ, U, V, Ω, and T (or Γ), respectively. The program consists of subroutines and/or functions which in part are managed by the executive routine VECTRA.

6.1 COMPUTATIONAL PROCEDURE

The task of the computer program is the simultaneous solution of one elliptic partial differential equation for the stream function, ψ, (Equation 5.17 and parabolic transport equations for the vorticity, Ω, and temperature, T, (Equations 5.21 and 5.22). Equations for U and V (5.19 and 5.20, respectively) are auxiliary but are also solved simultaneously during iteration. For neutral buoyancy, the buoyancy parameter equation need not be solved simultaneously with the vorticity and stream function equation. The Gauss-Seidel iterative technique is used for all quantities defined by second order partial differential equations. Liebmann acceleration is employed with the alternatives of both under- and over-relaxation.

Assuming all boundary conditions are set and pertinent variables are initialized, the procedure for solving the buoyancy coupled equation is

1) Compute $T_{p,q}$ (and $\Gamma_{p,q}$) using Equation 5.22 based on previously calculated values of $U_{j,k}, V_{j,k}$ and appropriate transport coefficients.

2) Compute $\Omega_{p,q}$ using Equation 5.21 and the previously computed values of $U_{j,k}, V_{j,k}, T_{p,q}$ and appropriate transport coefficients.

3) Update necessary boundary values for T, Γ, and Ω.

4) Use the newly computed values of Ω to compute the stream function distribution from Equation 5.17. One or more iterations may be required to arrive at a satisfactory solution for Ψ. Compute a new velocity field $V_{j,k}$ and $U_{j,k}$ from the newly calculated Ψ distribution.

5) If the eddy transport terms are not constant, compute multipliers FR and FZ from new velocity field (not implemented in present code version).

6) Repeat Steps 1 through 5 until a preset convergence criterion is satisfied or a specific number of iterations has been completed.

6.2 EXECUTIVE PROGRAM AND SUBROUTINE DESCRIPTION

The computer code consists of an executive routine called VECTRA and 18 subroutines and/or functions. A list of the primary duties served by each of these routines follows.

VECTRA Executive Routine

1) Reads case header and case set-up information.

2) Reads alphanumeric data for line printer output array option, plot file options, and program control.

3) Calls subroutines for data input, problem set-up and initialization, and program execution. The subroutines called in sequence are

   INPUT
   TYPE
   READY
   INDEXER
   BEST
   SEMBLE
   PLABAK

STREAM (for inviscid flow solution)
SSCOMP

4) Performs other miscellaneous tasks such as clock initialization, presetting variables, etc.

Subroutines

Primary duties of subroutines are given below.

Subroutine INPUT

General data input routine

- Reads restart file if required.
- Reads remaining input data from cards.
- Converts portions of input data to appropriate quantities and units.

Subroutine is called once during execution.

Subroutine TYPE

- Sets cell corner and cell center node types.

Subroutine called once during execution.

Subroutine READY

Problem set-up routine

- Sets all computed constants.
- Sets constant boundary conditions.
- Computes boundary coordinates for plotting.

Subroutine called once during execution.

Subroutine INDEXER

Computes boundary condition INDEX ARRAYS for hydrodynamics computational bookkeeping.

Subroutine called once during execution.

Subroutine BEST

Computes index arrays for transported quantities at free-flow boundary and sets fixed values.

Subroutine called once during execution.

Subroutine SEMBLE

Computes intercell conductances for heat and constituent transport.

Subroutine called once during execution.

Subroutine PLABAK

General information and debug output

- Writes to line printer various computed and input supplied variables and the operation modes of current case.
- Writes to line printer constant arrays used in the difference equation computations.
- Writes to line printer cell-corner and cell-center node type arrangement.
- Writes debug arrays.

Subroutine is called once or not at all, at the user's option.

Subroutine STREAM (IT, NSKIP)

Solves for stream function, Ψ

- Computes the viscous or inviscid stream function by Gauss-Siedel iteration. When called, this subroutine iterates on Ψ "IT" times.
- Upon completion of "IT" iterations, the velocity components $U_{j,k}$ and $V_{j,k}$ are computed by the auxiliary Equations 5.19 and 5.20.

Subroutine STREAM constitutes what is referred to in this manuscrip as the "inner iteration loop" (subroutine SSCOMP constitutes the "outer iteration loop") and is called at least once for each "outer iteration."

Subroutine SSCOMP

Calls subroutines for steady flow solution of all transport equations.

- Solves transport equation for Ω.
- Calls subroutine TRSPRT (T,Γ).
- Calls subroutine ROTATE (Ω).
- Calls subroutine STREAM to compute velocity field.
- Calls subroutine BOUSET to compute all boundary conditions.
- Writes out monitor node values.
- Calls subroutine OUTPUT for either interim or final array output.
- Generates plot data file.

This subroutine is referred to as the "outer iteration loop" and is called only once during a case execution. The code spends the majority of the execution time in this routine.

Subroutine TRSPRT

Computes quantities T and Γ.

Subroutine ROTATE

Solves vorticity transport equation for Ω.

Subroutine BOUSET (JUMP)

Sets all hydrodynamic and transport boundary conditions.

Subroutine OUTPUT (MODE)

This is the primary line printer output call routine.

- The primary purpose of this routine is to call selectively the output array writer subroutine, AROUT, based on the alpha input read in through the executive routine. The arrays and array header Holleriths are aligned in the call list of AROUT. This subroutine may be called selectively for array writing through input.

- The secondary purpose of subroutine OUTPUT is to write out selectively the convergence rate information computed in subroutine SSCOMP (i.e., maximum changes in and Ω and the nodal location of these changes, during successive iterations). The iteration numbers selected for output are specified by input.

Subroutine AROUT (list)

This is the general array writer.

This subroutine is used to write out all computed arrays specified for printing. The appropriate array, header and grid coordinates are aligned in the call list at subroutine OUTPUT. Miscellaneous computations are also performed here as necessary.

Subroutine MAPPER (list)

Prints cell corner and cell center node type identification to line printer.

Subroutine STATE (N)

This subroutine computes fluid density.

Subroutine ERROR

Floating point input data error check.

Subroutine IERROR

Integer data input error check.

6.3 COMPUTED RESULTS AND DISCUSSIONS

As of this time, the VECTRA code has been modified for application to cooling tower external flows in two-dimensional rectilinear and axisymmetric coordinates with constant transport coefficients. Preliminary results have been obtained for cases involving single and dual towers. One computer run has been conducted for comparison with a recent physical model test of the Wyodak plant tower.

Results for a test case of two towers oriented perpendicular to the crosswind are illustrated in Figures 6.1-A and B. These results illustrate the capability of the VECTRA code to predict recirculation, interference and plume rise. Note that the two-dimensionality of the solution allows for no edge effects, thus the formation of a strong vortex between towers. This behavior would be expected for long prototypic towers, but the vortex would undoubtedly be much weaker in the case of short towers where edge effects are significant.

Figures 6.2-A and B illustrate the case of dual two-dimensional towers at the Wyodak site; the downwind tower simulates a possible configuration of the proposed ERDA test facility. Again the two-dimensionality of the solution is apparent in the strong vortex formation and recirculation between towers.

Computed results shown in Figures 6.3-A and B correspond to the physical model test case for a crosswind of 28 mph (Table 4.1). The computer simulation used a tower discharge temperature excess of 37°F which differs slightly from the modeled 35°F ΔT_o.

The crosswind was prescribed at the upstream boundary by the gradient wind equation

$$U_{amb}(Z) = C\ Z^{.28}$$

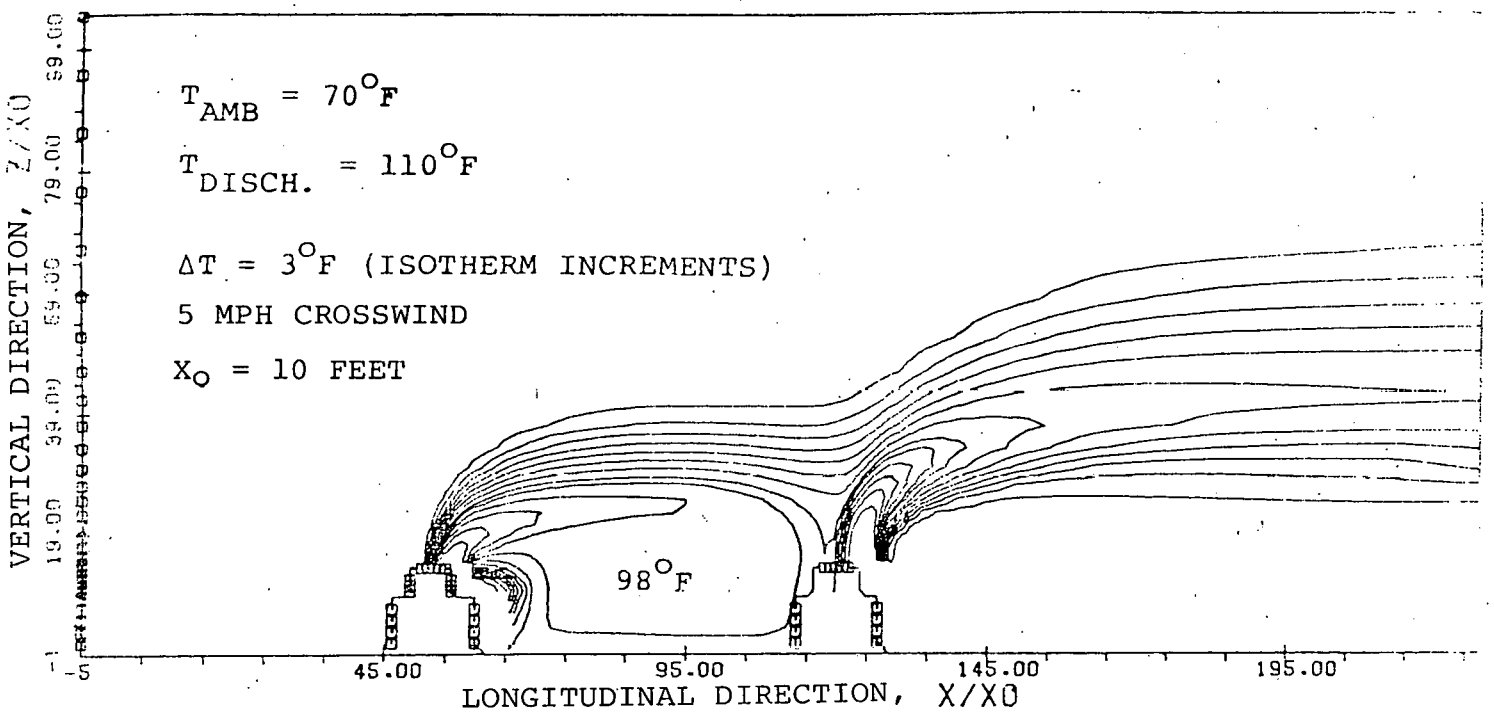

FIGURE 6.1-A Isotherms for Dual Cooling Towers

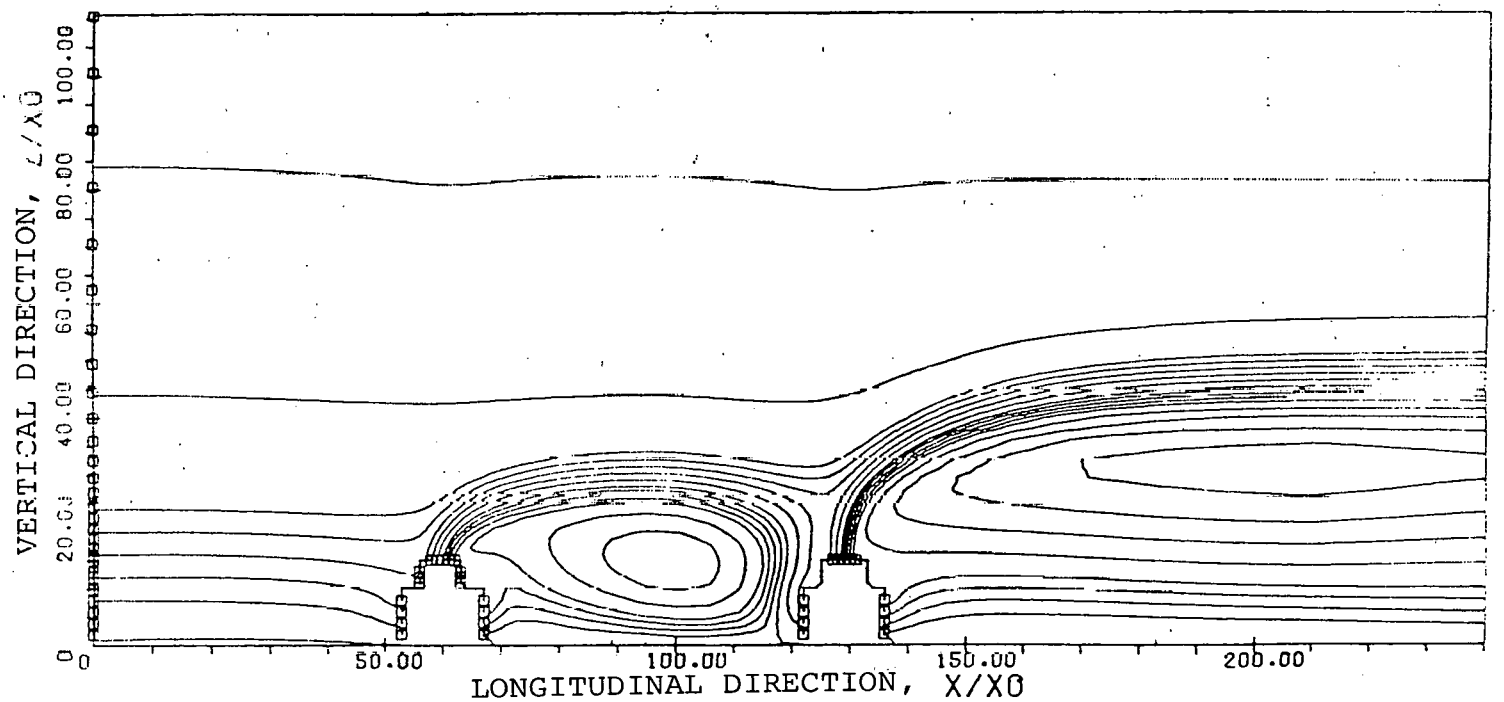

FIGURE 6.1-B Streamlines for Dual Cooling Towers

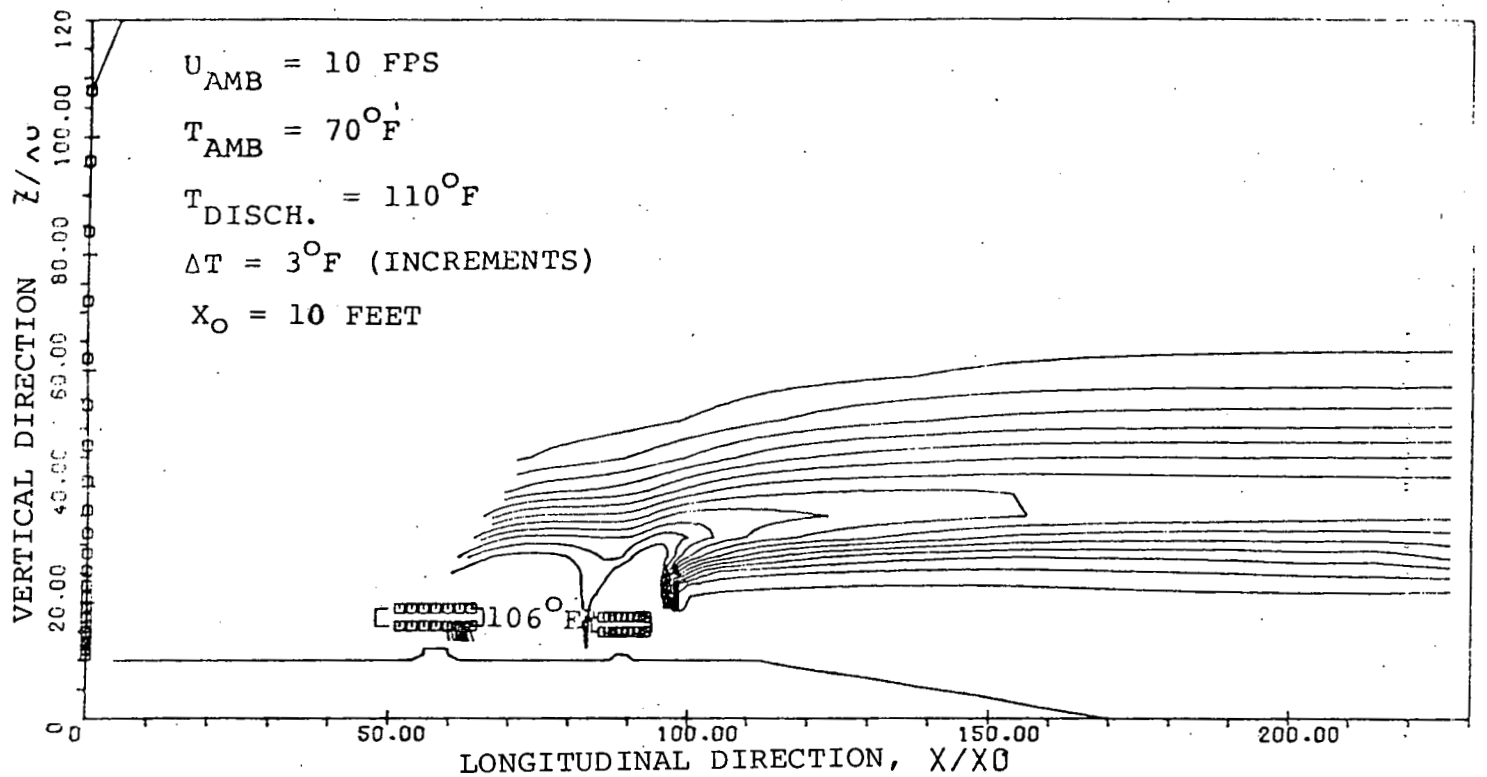

FIGURE 6.2-A Isotherms for the Wyodak Plant and the ERDA Dry Cooling Towers with Actual Topography, Southeasterly Wind

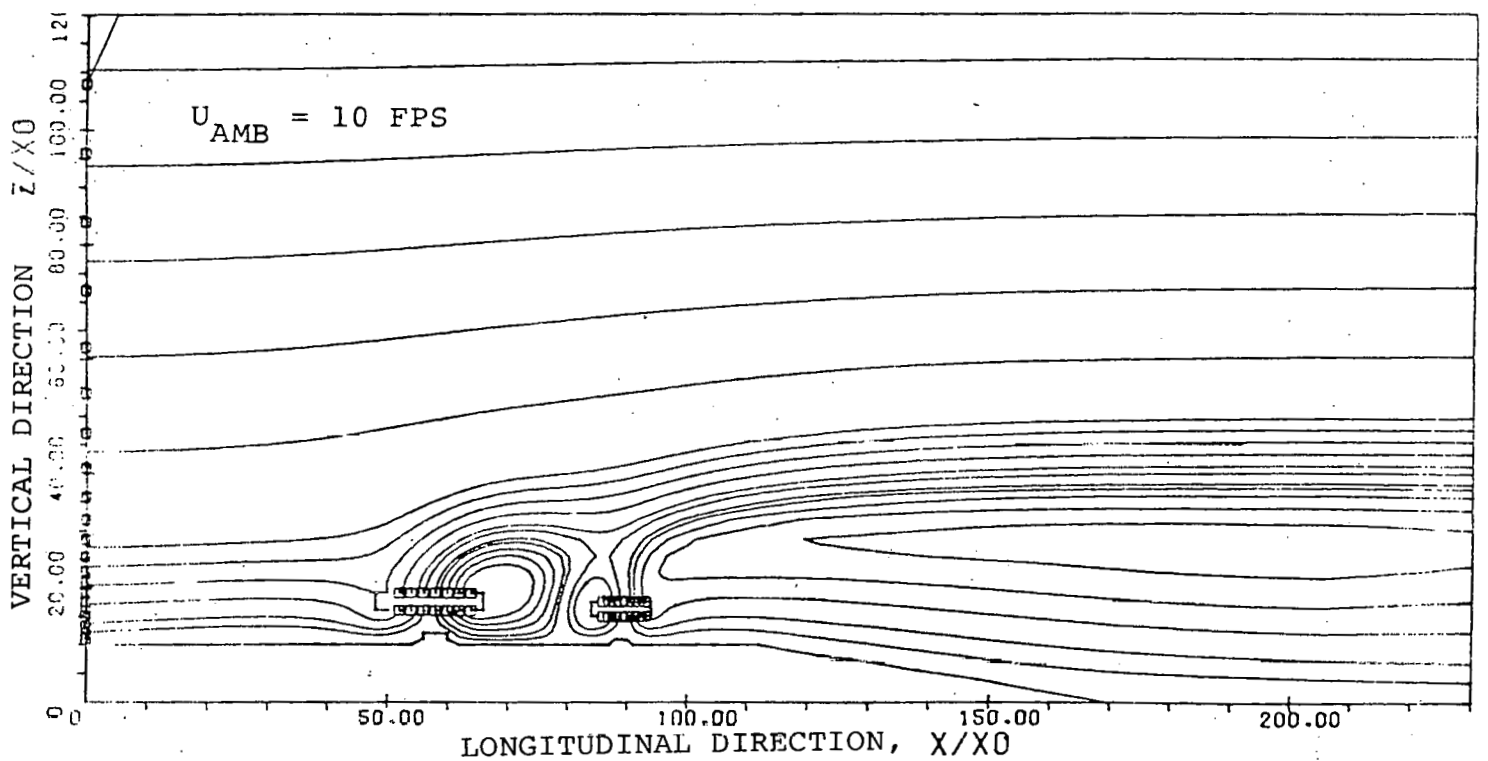

FIGURE 6.2-B Isotherms for the Wyodak Plant and the ERDA Dry Cooling Towers with Actual Topography, Southeasterly Wind

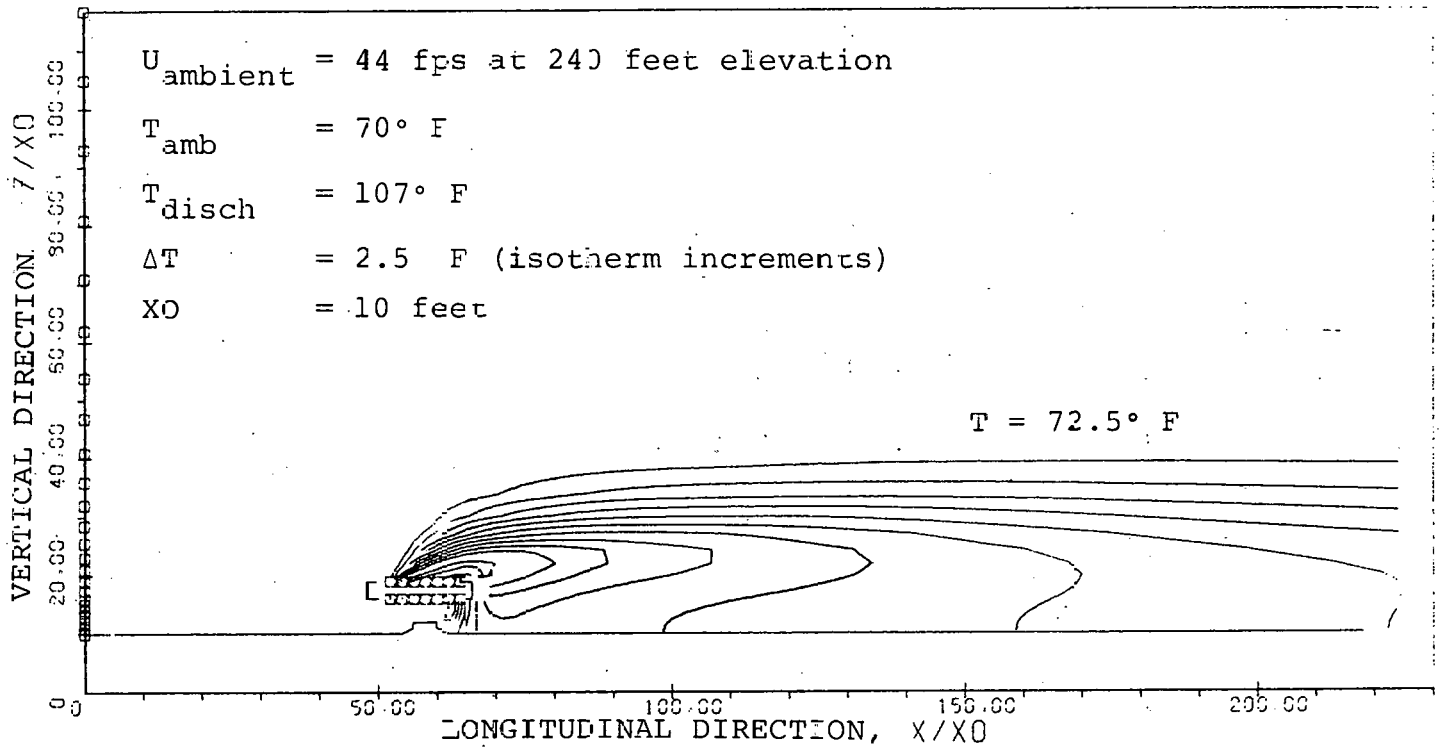

FIGURE 6.3-A Isotherms for the Wyodak Plant Dry Cooling Tower, 28 MPH Wind Case, XO = 10 Feet, Flat Ground

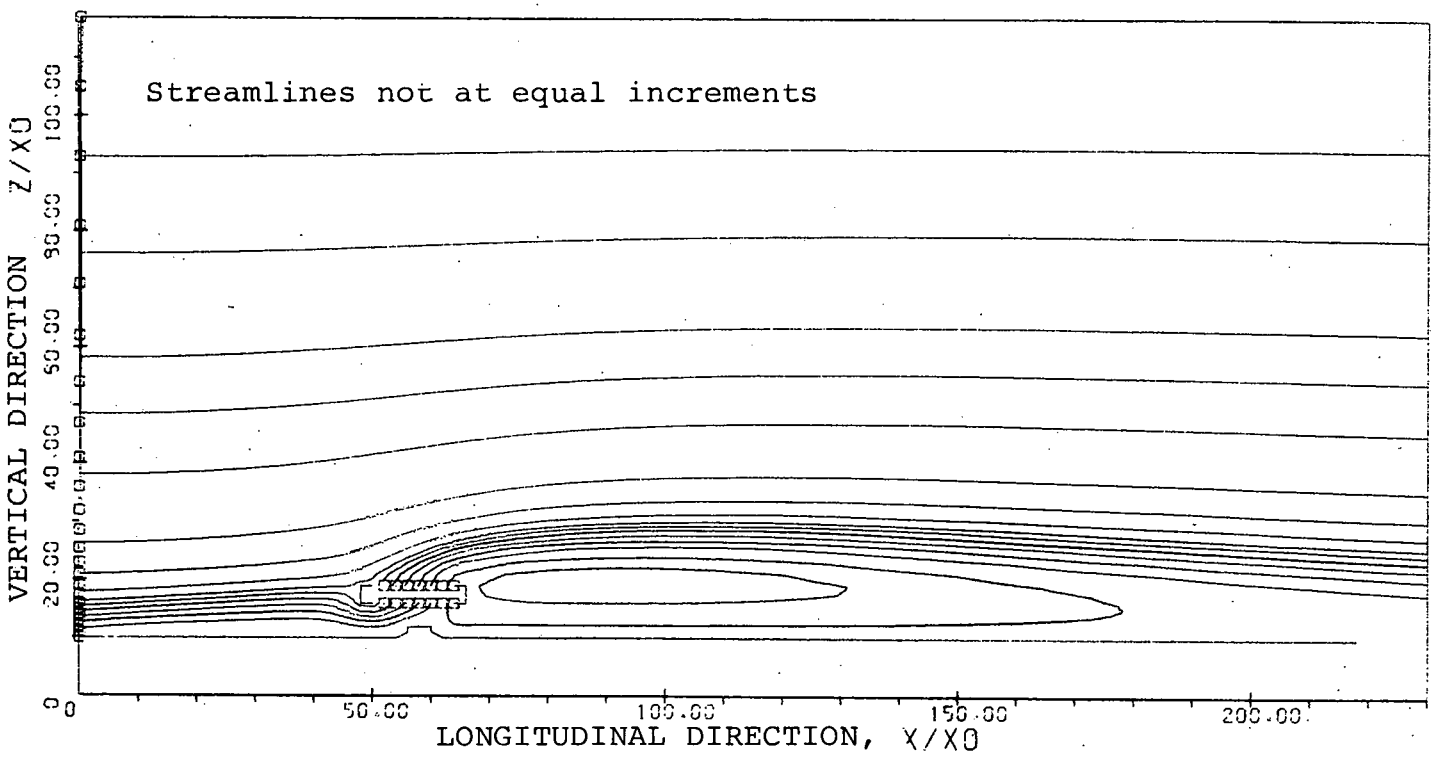

FIGURE 6.3-B Streamlines for the Wyodak Plant Dry Cooling Tower. 28 MPH Wind Case. XO = 10 Feet. Flat Ground

where U_{amb} is the vertical distribution of crosswind, C is a constant and Z is the vertical dimension. For conditions modeled, C = 9.4, which gives a crosswind of approximately 28 mph at a 180-ft height. The computer results show a large circulation pattern in the wake of the tower and significant recirculation. Computed isotherms were compared with physical model test results. Although the agreement is reasonably good for height of plume rise, there is disagreement in the downstream region, particularly in the region of the computed wake. This disagreement is explained by the fact that the computer model is two-dimensional, whereas the physical model reveals significant three-dimensional effects. The length of the Wyodak tower is short compared to its width, and thus there are significant "edge" effects, such as lateral withdrawal and entrainment, which tend to decrease temperatures within the plume.

The departure of the two-dimensional computed results from the Wyodak physical model simulations prompted further model studies designed to establish the limitations and validity of the two-dimensional computer program. In this regard, two-dimensional physical tests were initiated as described in Section 4.2. At this writing, results for three test runs have been obtained for comparison. These results are, however, preliminary and are not considered entirely satisfactory for an in-depth comparison for eventual validation of the two-dimensional model.

Computed mean streamlines and dimensionless isotherms corresponding to the experimental test runs Y-1, Y-2, and Y-3 are illustrated by Figures 6.4, 6.5, and 6.6. The computed isotherms do not compare as well as desired with the corresponding experimental results regarding the general shape and magnitude of the plume. In each case the computed results give a plume of larger magnitude; that is, isotherms having larger enclosed areas. An energy balance check revealed that the computer code conserves energy well within 1% of the total amount discharged.

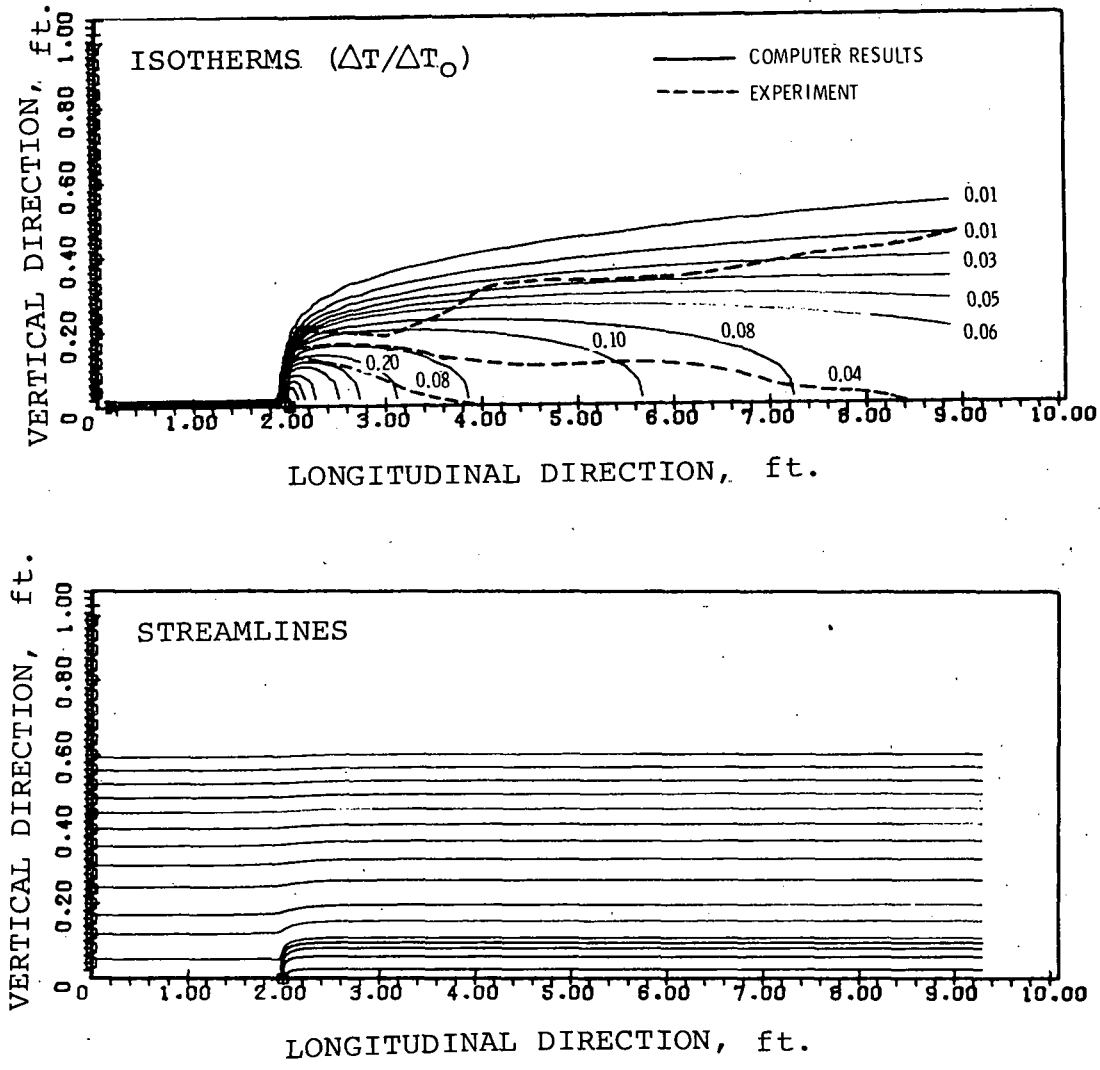

FIGURE 6.4 Isotherm and Streamline Plots for Two-Dimensional Flow Test Y-1 (No-Slip Boundary Condition).

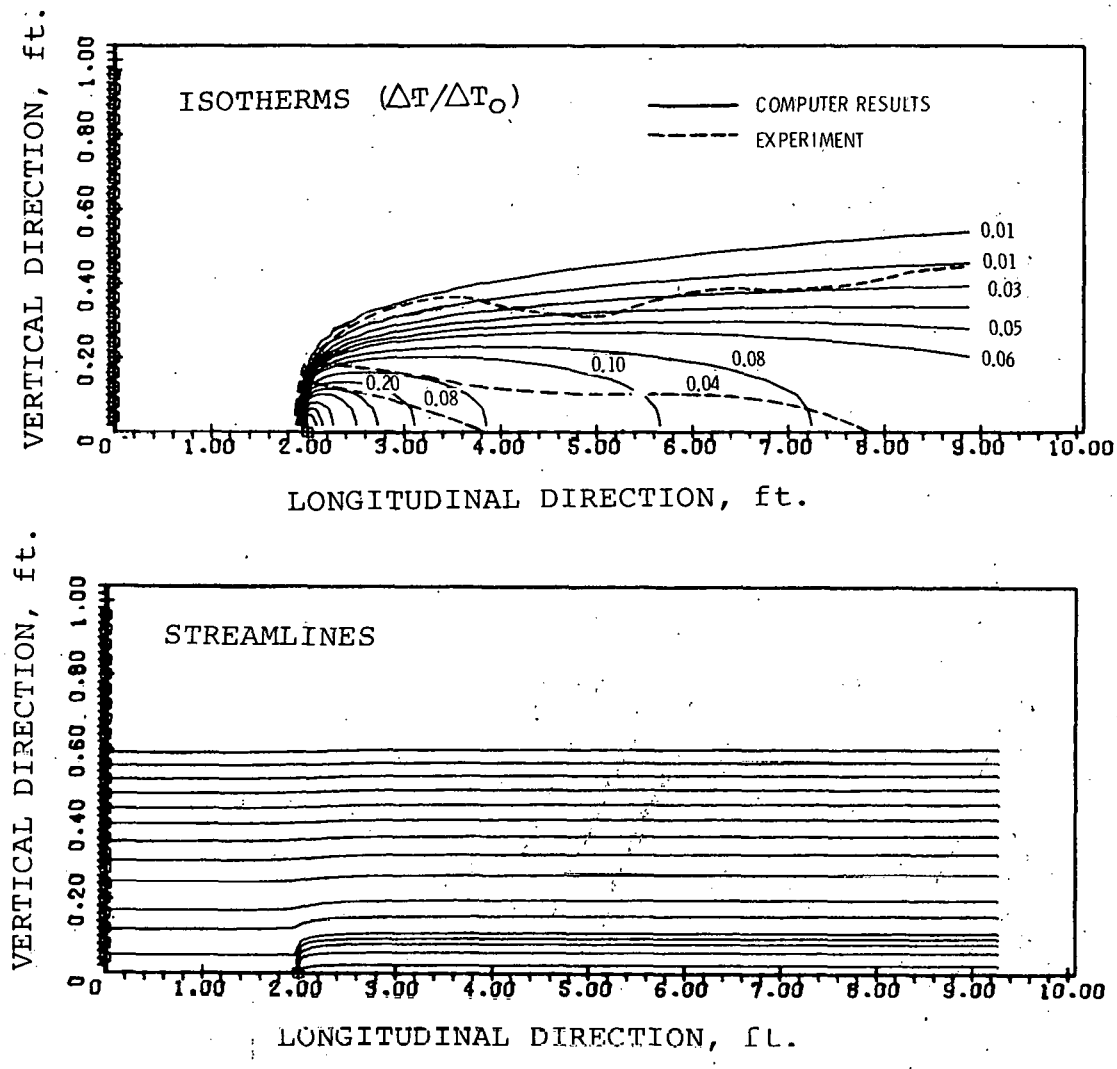

FIGURE 6.5 Isotherm and Streamline Plots for Two-Dimensional Flow Test Y=2 (No-Slip Boundary Condition).

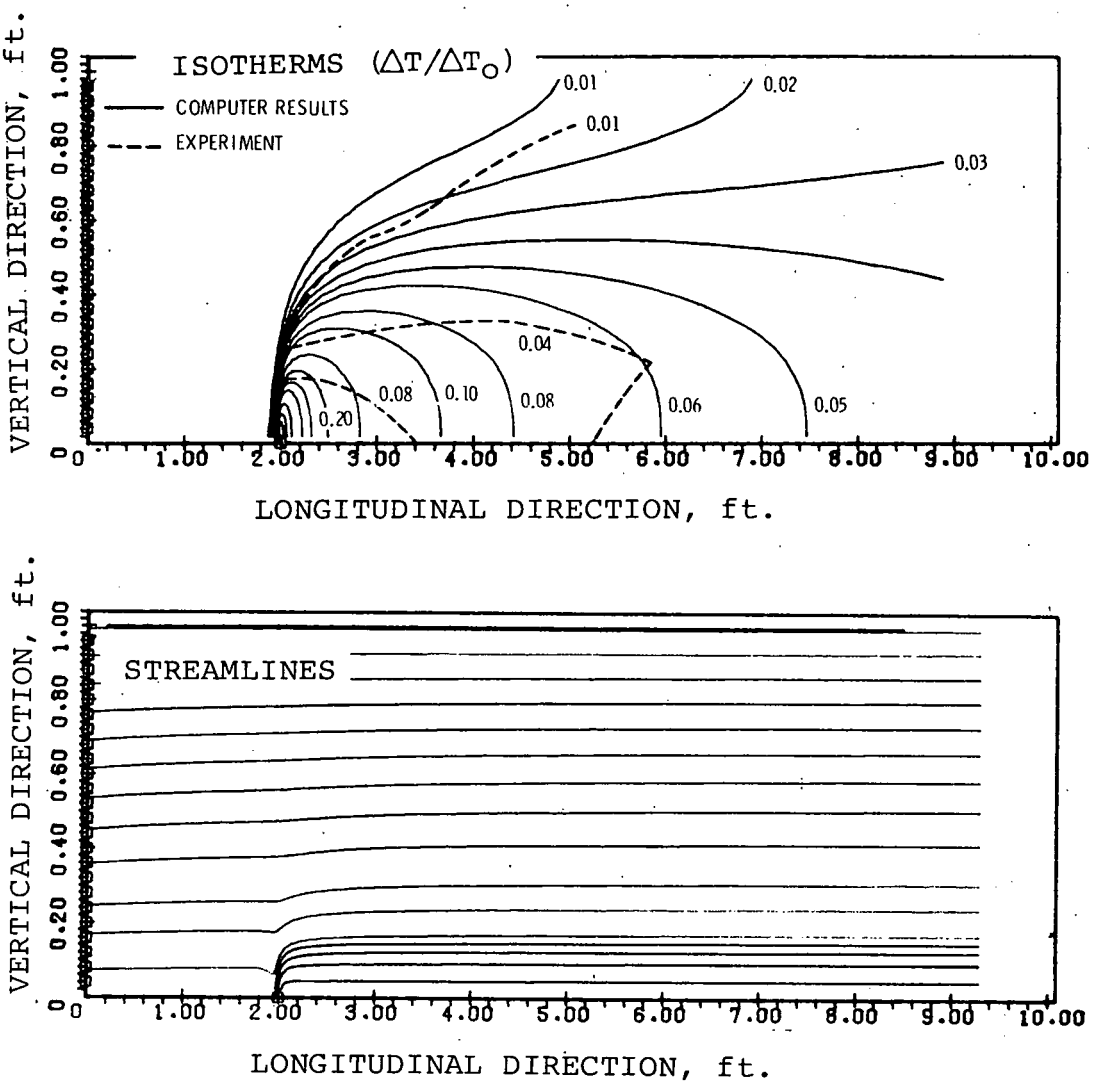

FIGURE 6.6 Isotherm and Streamline Plots for Two-Dimensional Flow Test Y-3 (No-Slip Boundary Condition).

The results illustrated in Figures 6.4 through 6.6 were computed using a "no-slip" condition at the bottom boundary which leads to development of a near parabolic velocity profile in the ambient flow. To more closely simulate actual test conditions the cases Y-1, Y-2, and Y-3 were recomputed using a slip condition at the bottom boundary. A comparison of resulting profiles for both situations is illustrated in Figures 6.7 and 6.8 for Cases Y-1 and Y-3, respectively. Observe the near parabolic velocity profile in the no-slip case as opposed to the very flat profile in the slip case. The parabolic distribution results because of using a constant value of eddy momentum diffusivity in conjunction with the no-slip condition.

Velocity profiles in the physical model were not measured during the preliminary testing but the channel flow was established as turbulent based upon the Channel Reynolds number (199,000 and 86,000 for Cases Y-1 and Y-3, respectively). Based upon these values of the Reynolds number a typical channel velocity profile is estimated for each case as shown in Figures 6.7 and 6.8. Note that the slip condition more accurately approximates the channel flow than does the no-slip condition. Thus, computed results obtained through use of the slip condition (see Figures 6.9 through 6.11) are in much better agreement with the experimental data primarily because of improved ambient velocity field simulation. One should not conclude from the results that a slip condition at the bottom boundary is correct, but that a slip condition more accurately simulates a turbulent profile than does the no-slip condition when using a constant eddy diffusion coefficient for momentum. These results thus indicate the need for more accurate turbulence modeling.

Although the slip condition yields generally good comparison with experimental data, computed isotherms still result in enclosed areas that are slightly larger than experimentally determined average values. The experimental results used for comparison

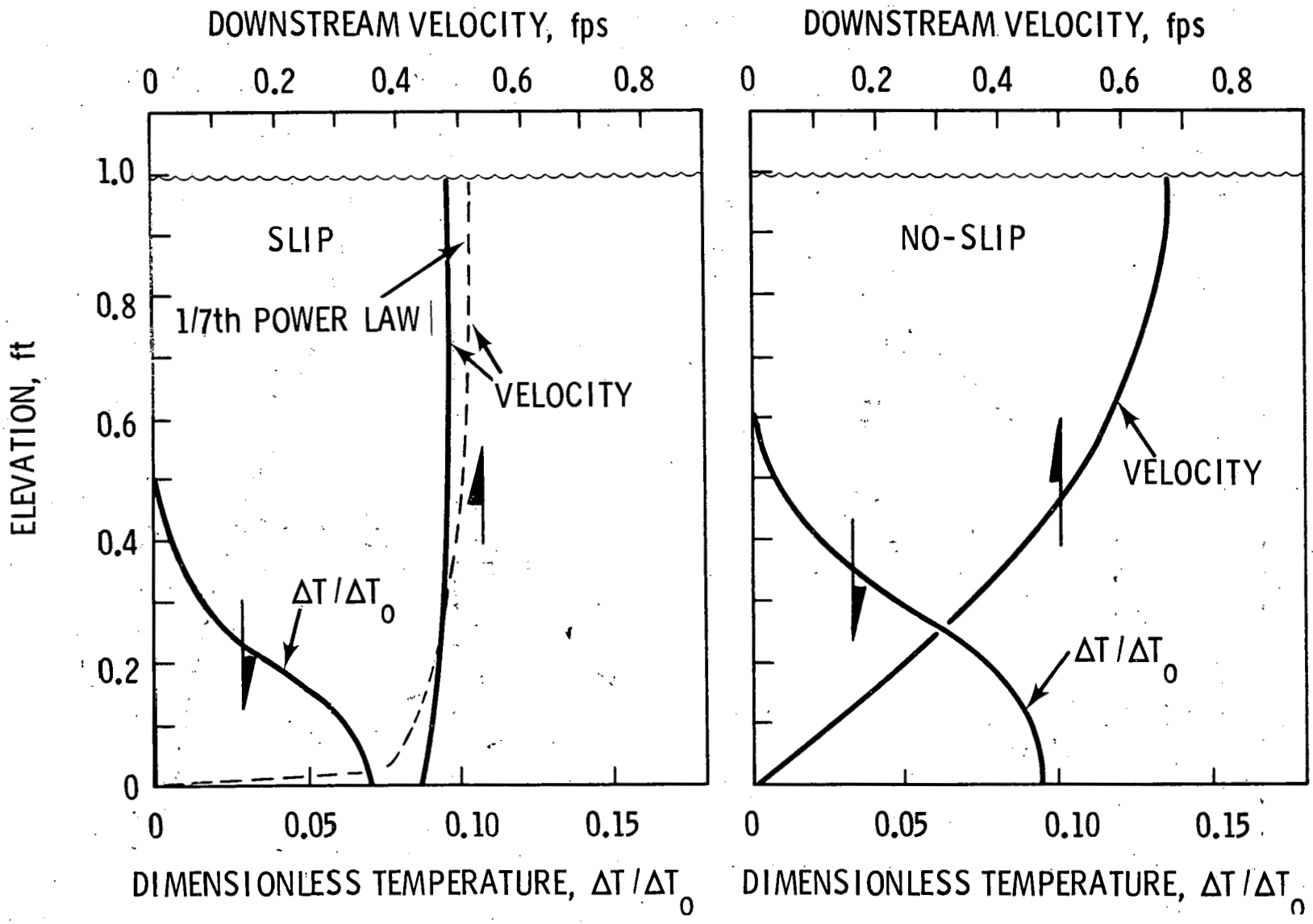

FIGURE 6.7 Comparison of Computed Velocity and Temperature Profiles for Slip and No-Slip Bottom Boundary Conditions. Approximately 4 Feet Downstream, Case Y-1.

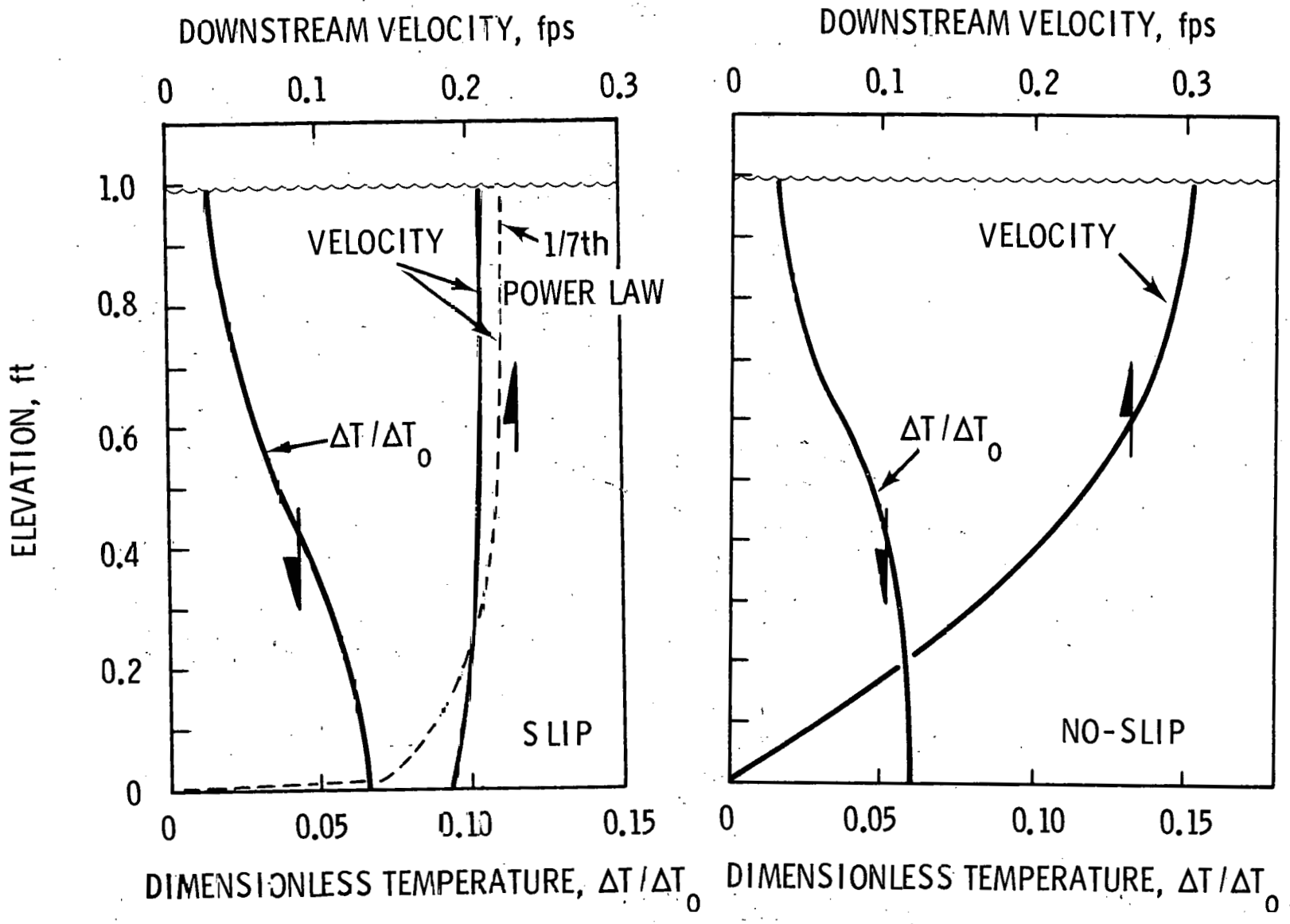

FIGURE 6.8 Comparison of Computed Velocity and Temperature Profiles for Slip and No-Slip Bottom Boundary Conditions. Approximately 4 Feet Downstream, Case Y-3.

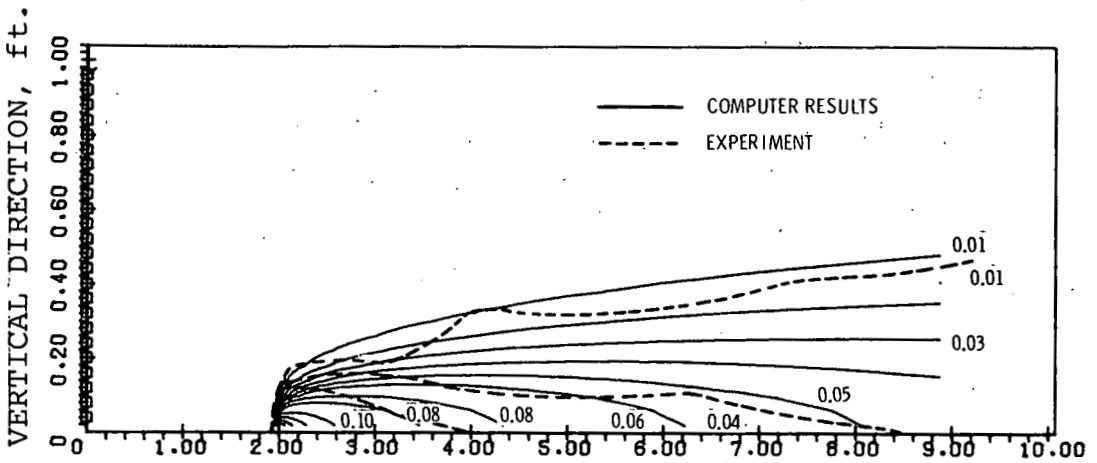

FIGURE 6.9 Isotherms ($\Delta T/\Delta T_o$) for Two-Dimensional Flow Test Y-1 (Slip Boundary Condition).

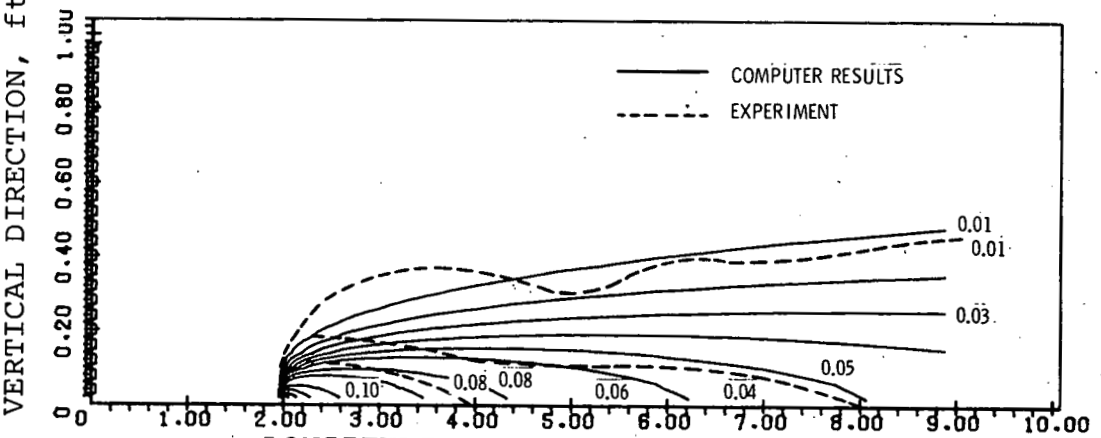

FIGURE 6.10 Isotherms ($\Delta T/\Delta T_o$) for Two-Dimensional Flow Test Y-2 (Slip Boundary Condition).

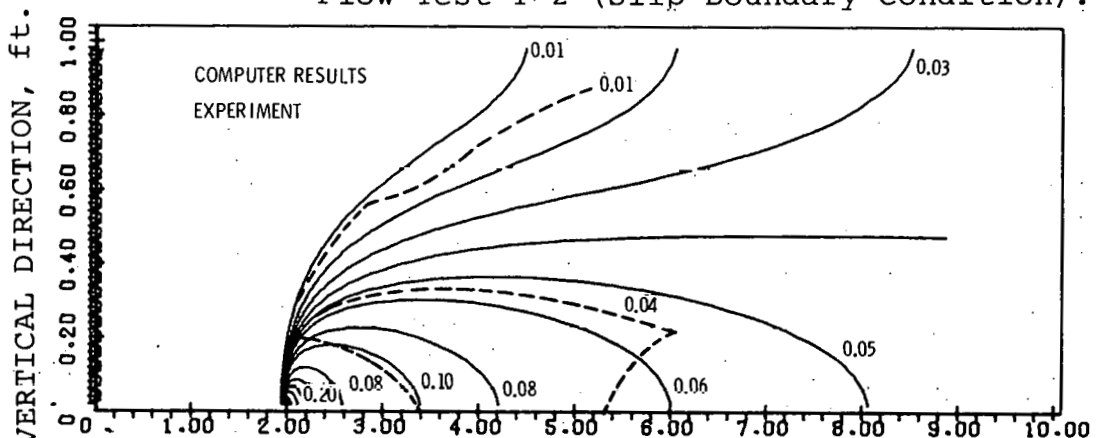

FIGURE 6.11 Isotherms ($\Delta T/\Delta T_o$) for Two-Dimensional Flow Test Y-3 (Slip Boundary Condition).

are based on average of values obtained as described in Section 4.2. Since the discharge did not occupy the full width of the flume, values along the edge are affected by the ambient and tend to reduce the overall average isotherm size. Comparison with isotherms more centrally located along the diffuser indicate still better agreement between the experiments and computations (Figure 6.12).

Based upon results of this preliminary testing, it is concluded that

1. the numerical model is capable of simulating two-dimensional transport with reasonable good accuracy,
2. the accuracy may be improved by incorporating improved turbulence modeling.

With regard to the latter point above, it is planned to incorporate a two-equation model for turbulence in the near future.

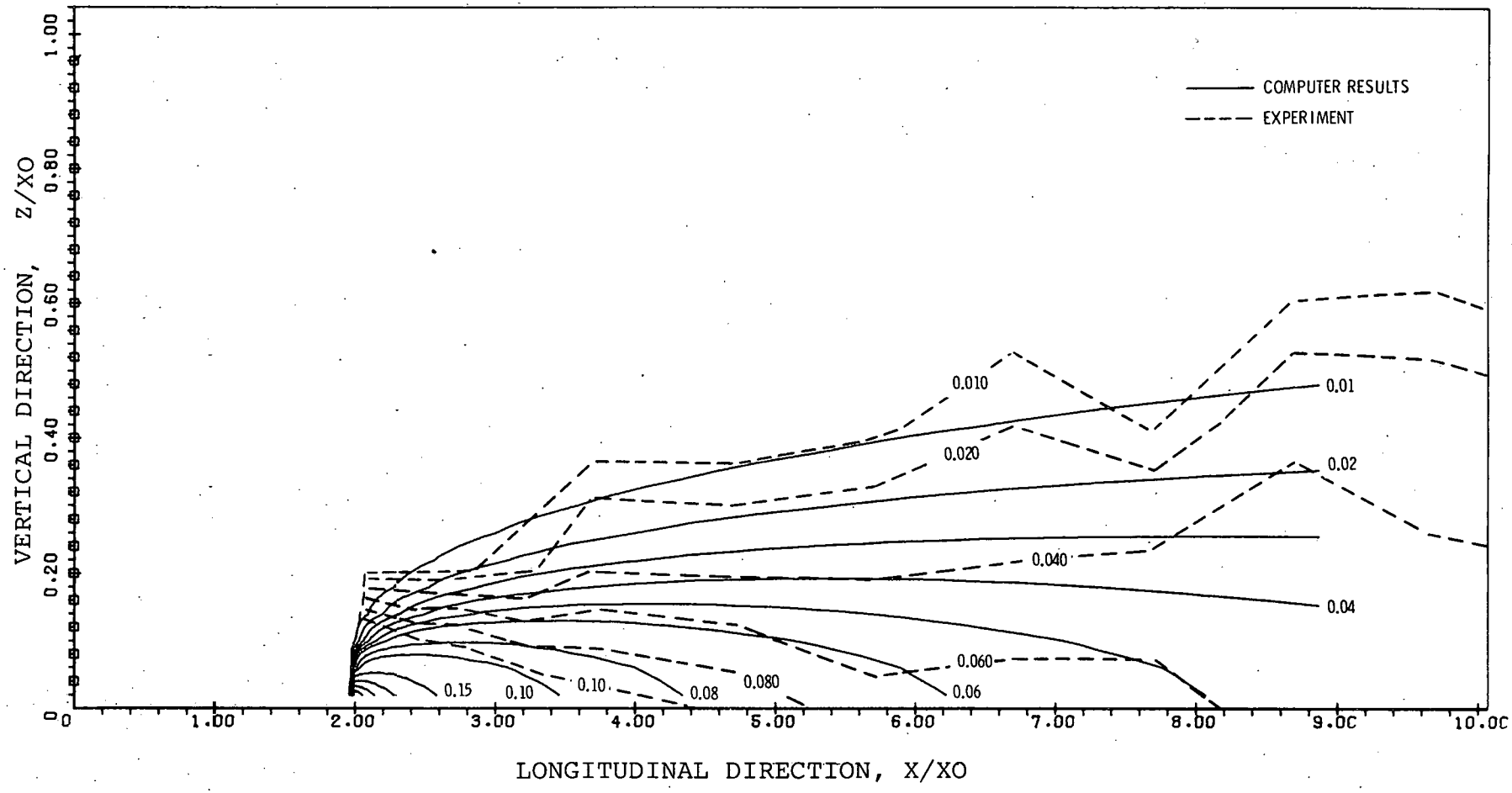

FIGURE 6.12. Isotherms ($\Delta T/\Delta T_o$) for Two-Dimensional Flow Test Y-1. Centerline of Discharge. (Slip Boundary Condition)

APPENDIX 1

FIGURES OF MEASURED TEMPERATURE DISTRIBUTIONS

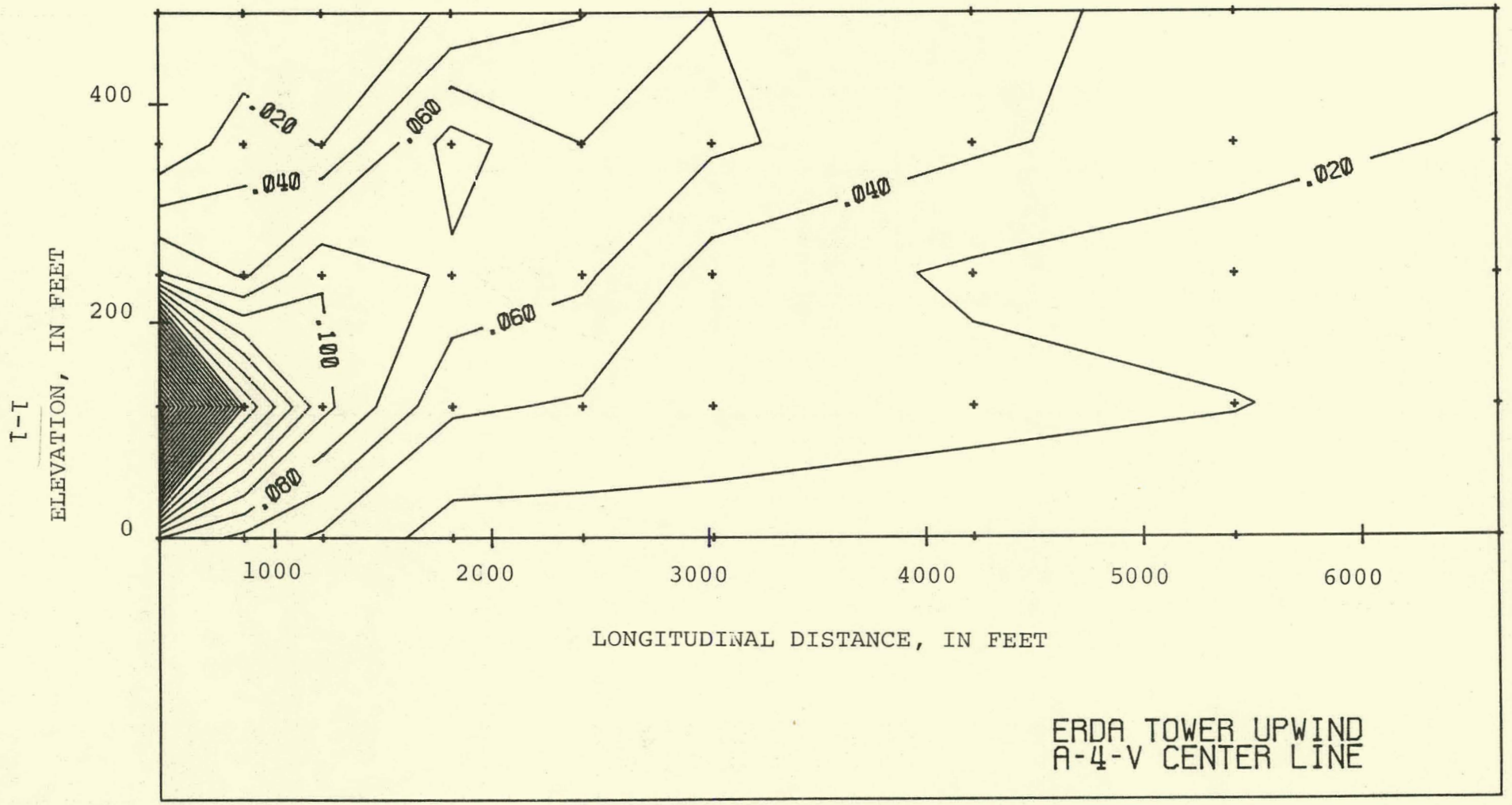

(a) Vertical Distribution

FIGURE 4.22 Temperature Distribution for Run A-4. V_a = 18.5 MPH.

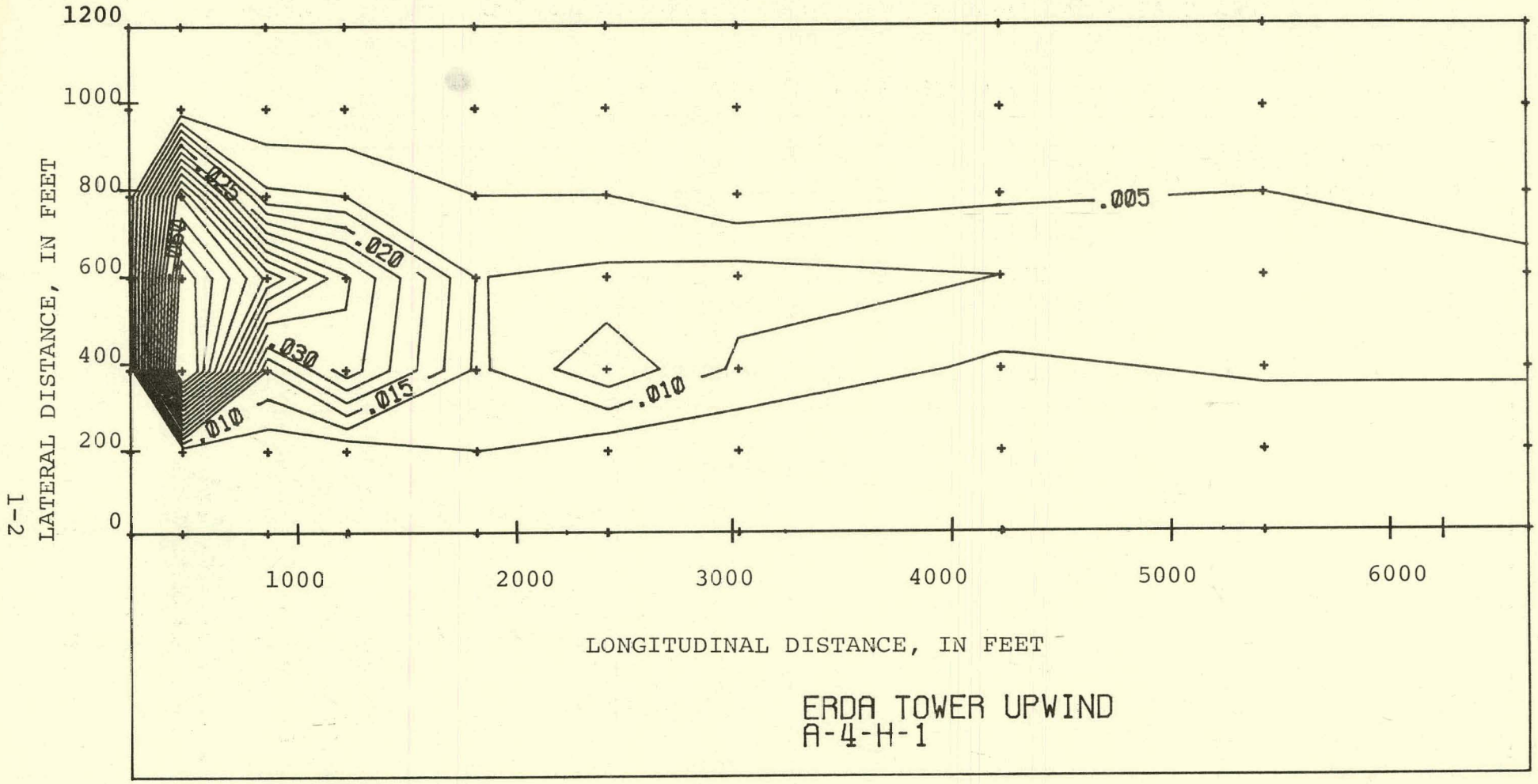

(b) Horizontal Distribution, Ground Level

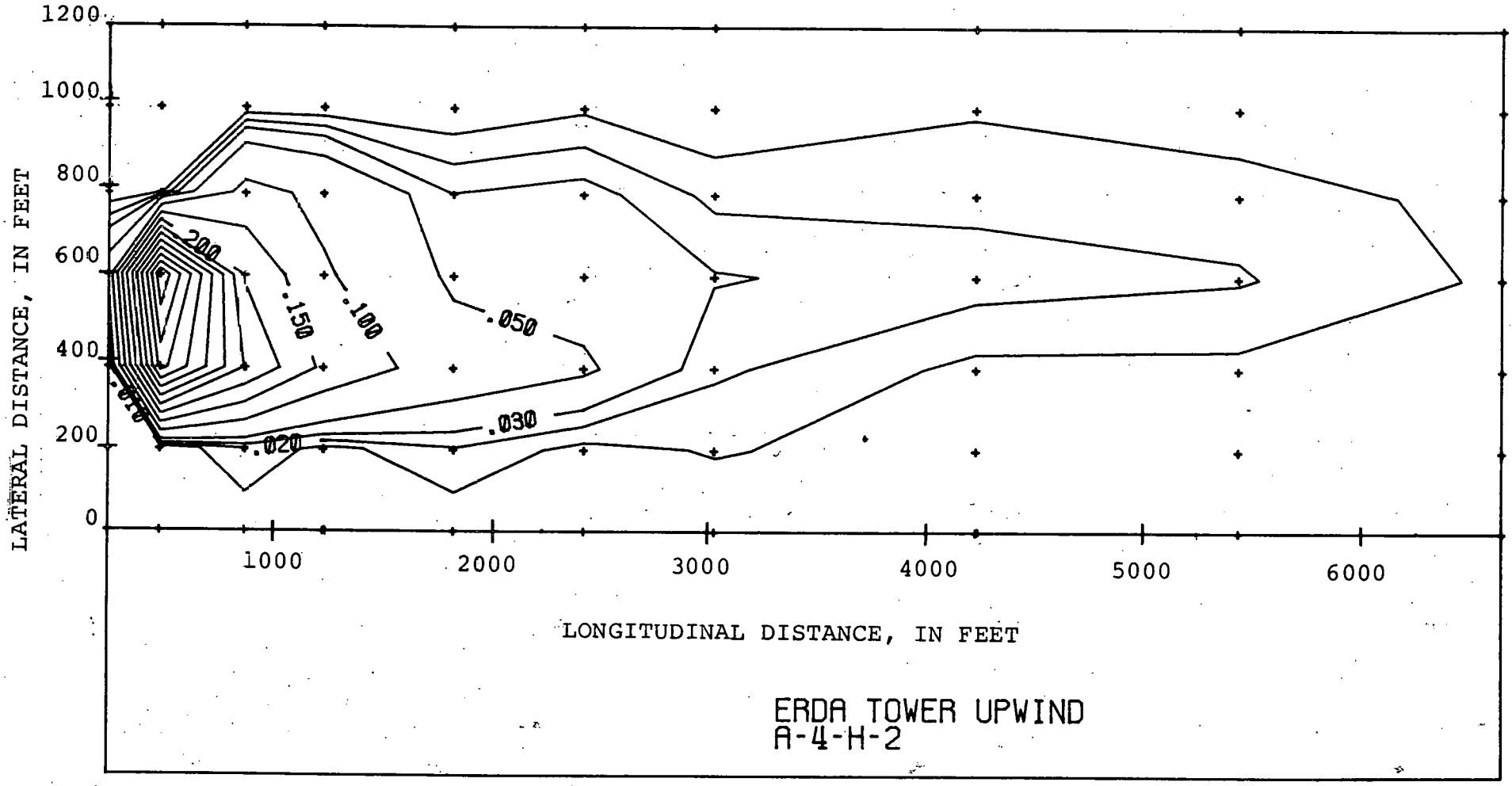

(c) Horizontal Distribution, 120 Feet Above the Ground

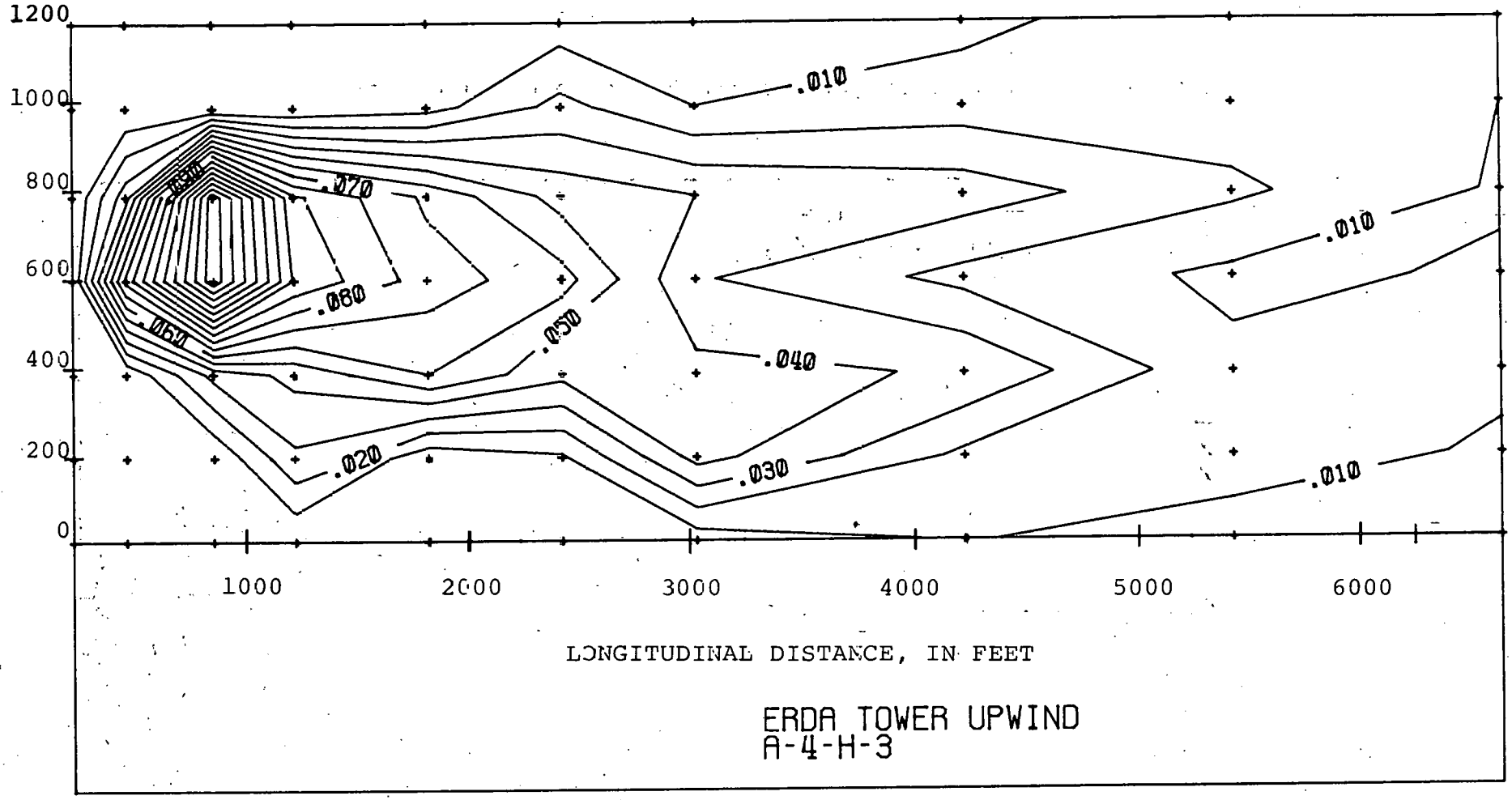

(d) Horizontal Distribution, 240 Feet Above the Ground

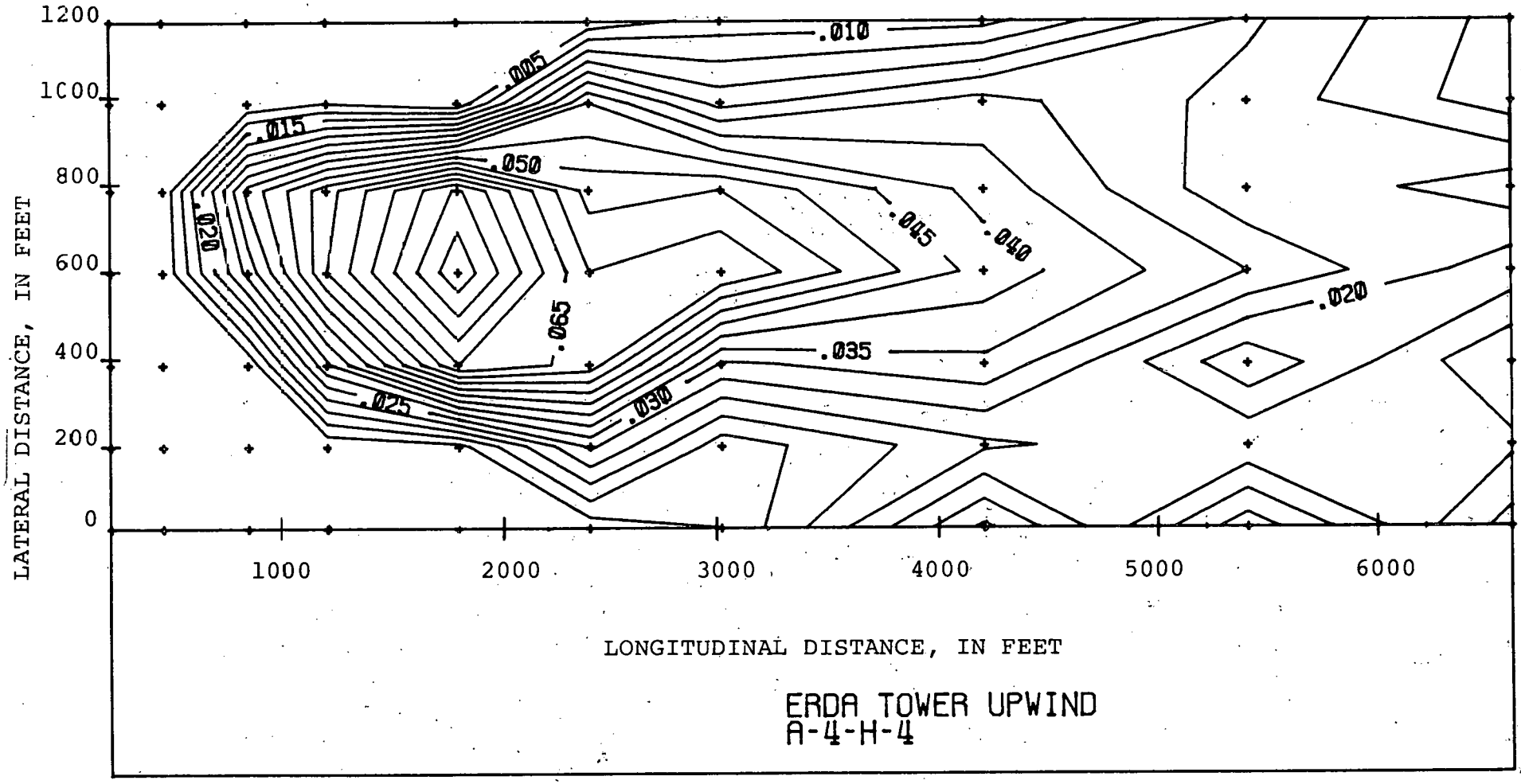

(e) Horizontal Distribution, 360 Feet Above the Ground

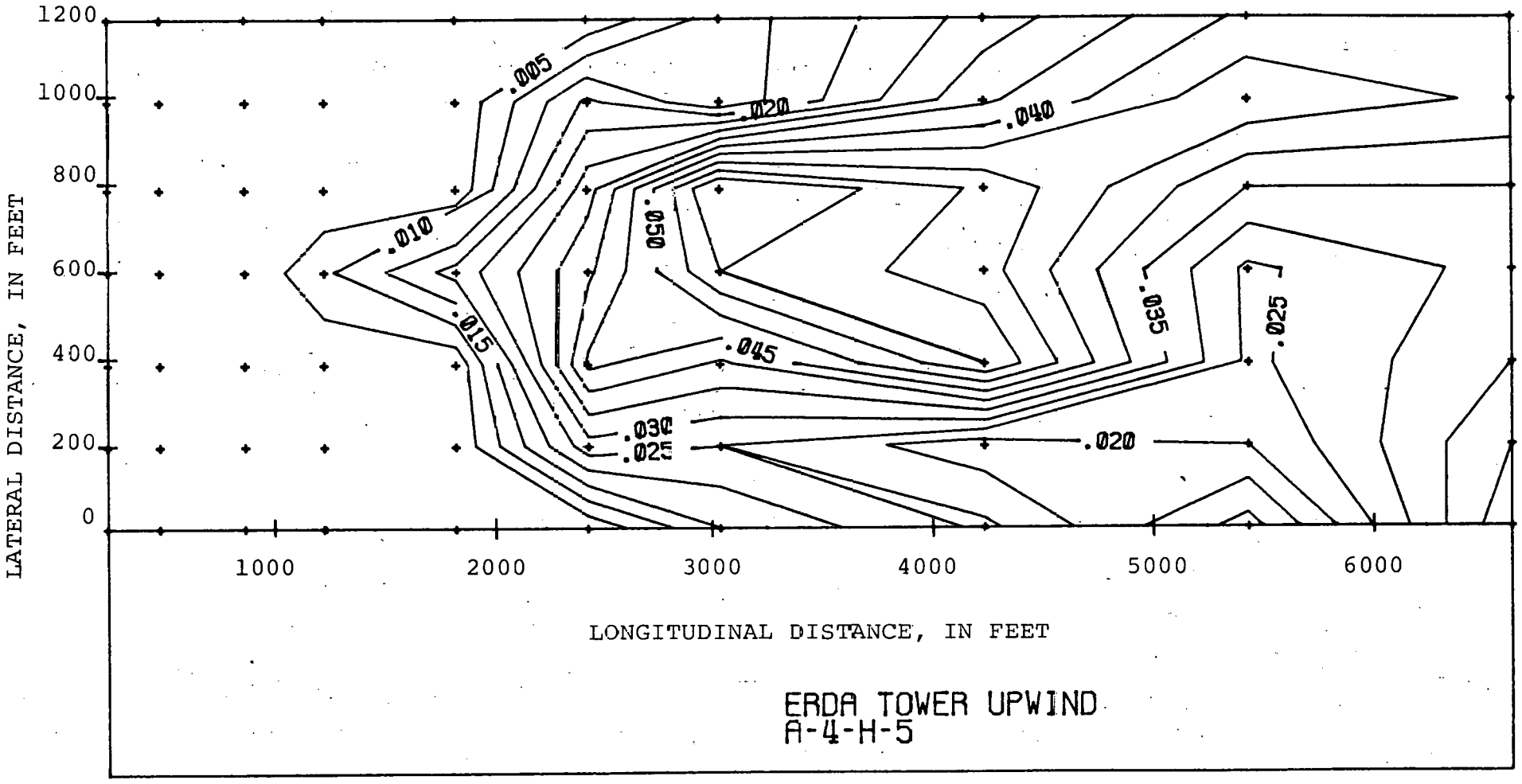

(f) Horizontal Distribution, 480 Feet Above the Ground

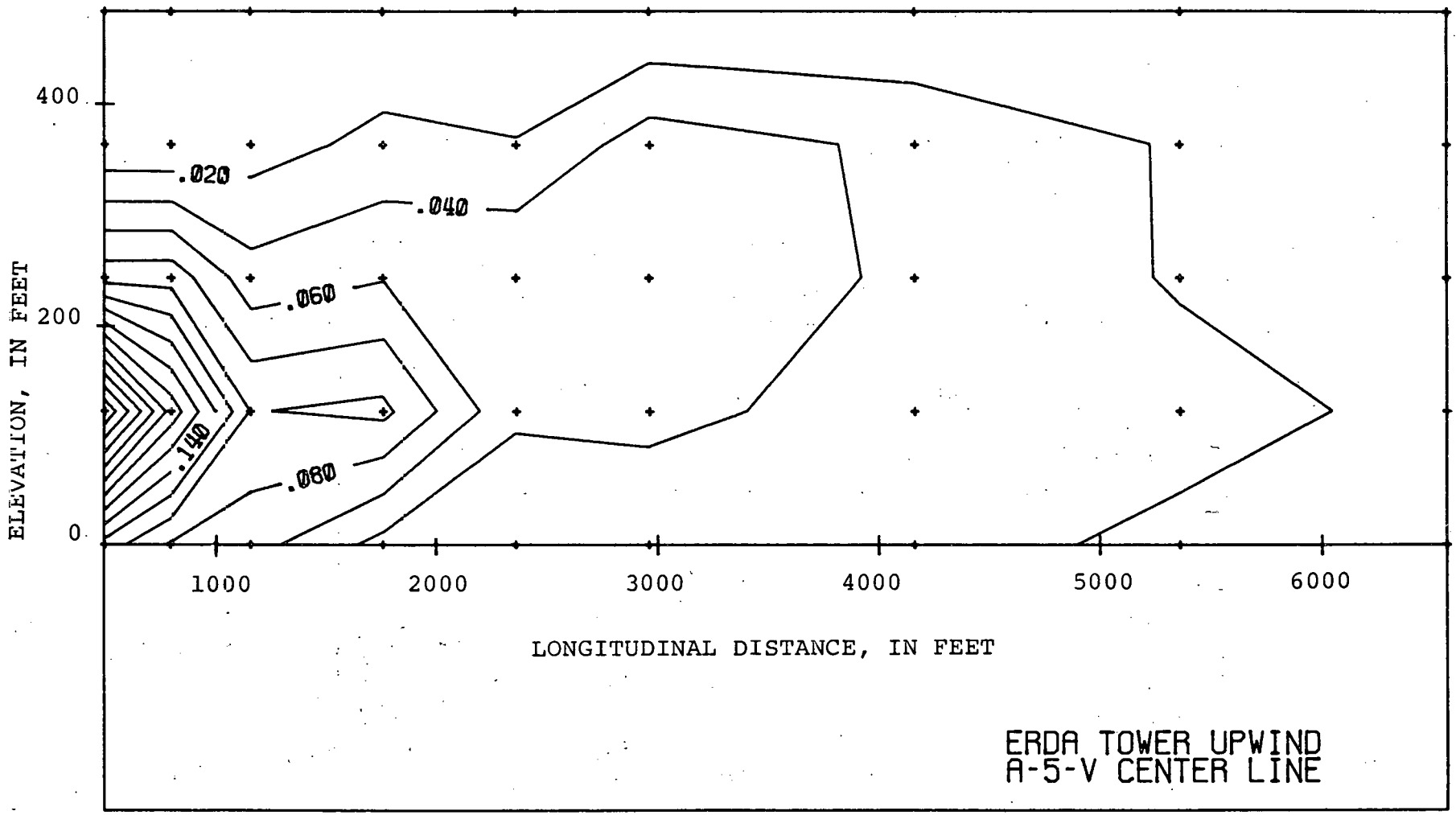

(a) Vertical Distribution

FIGURE 4.23 Temperature Distribution for Run A-5. V_a = 28.1 MPH.

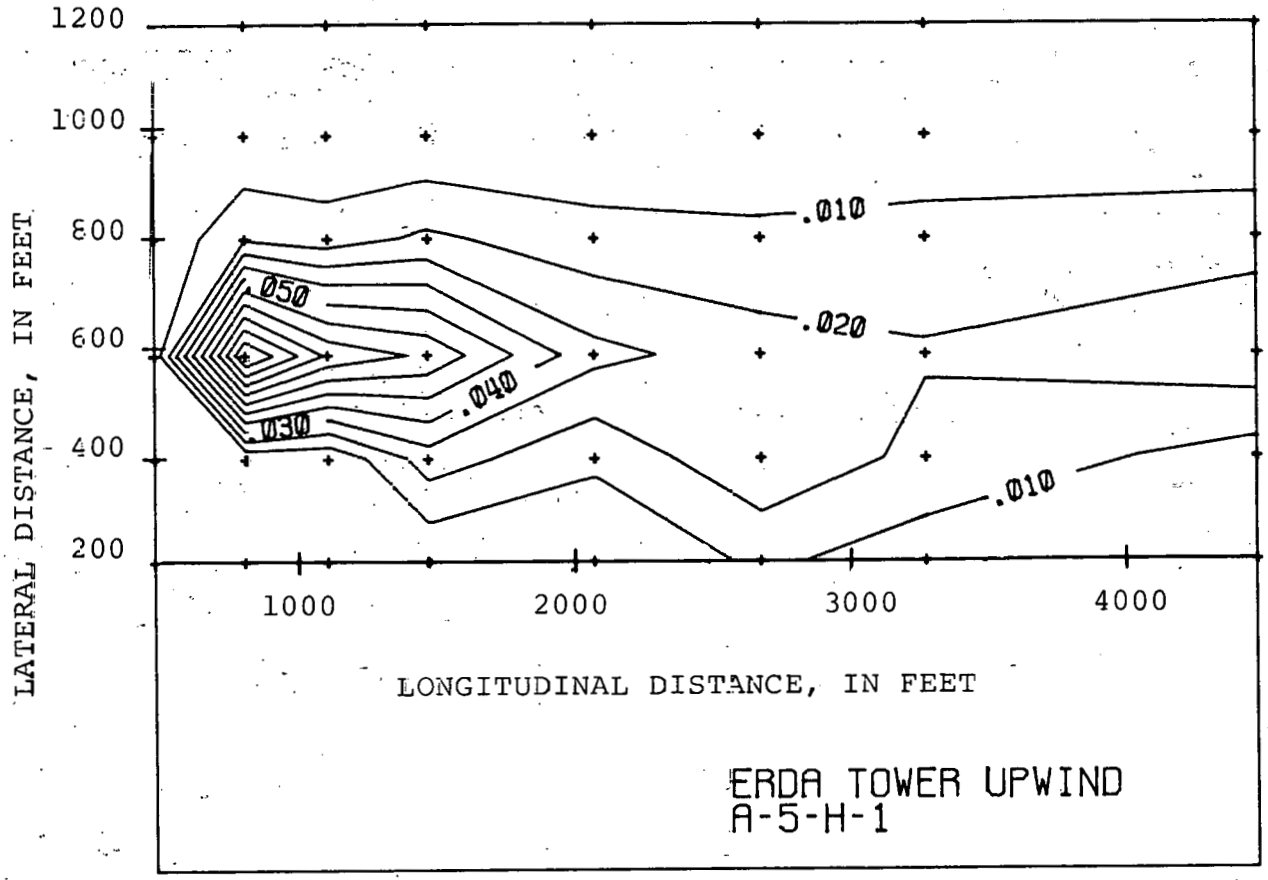

(b) Horizontal Distribution, Ground Level

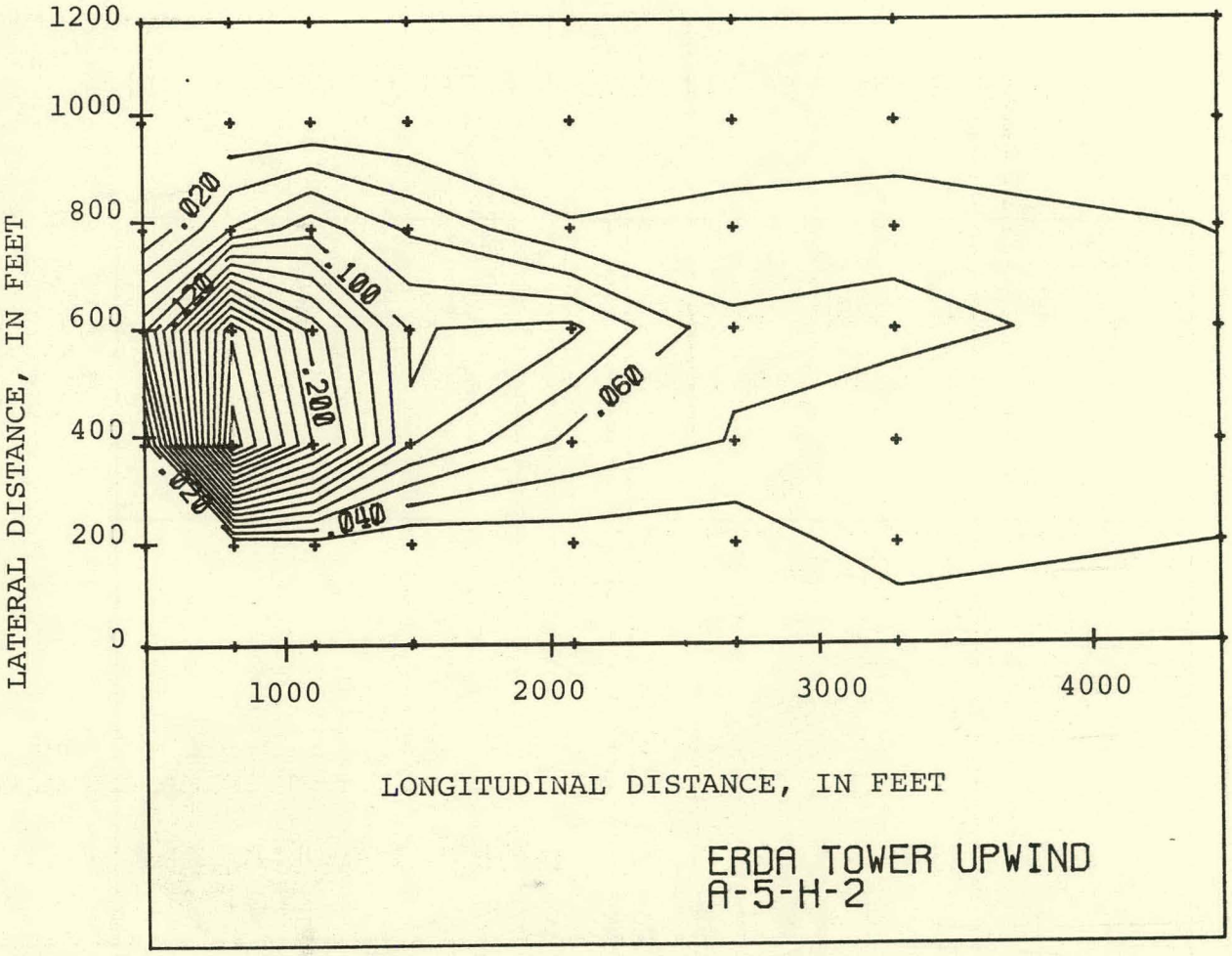

(c) Horizontal Distribution, 120 Feet Above the Ground

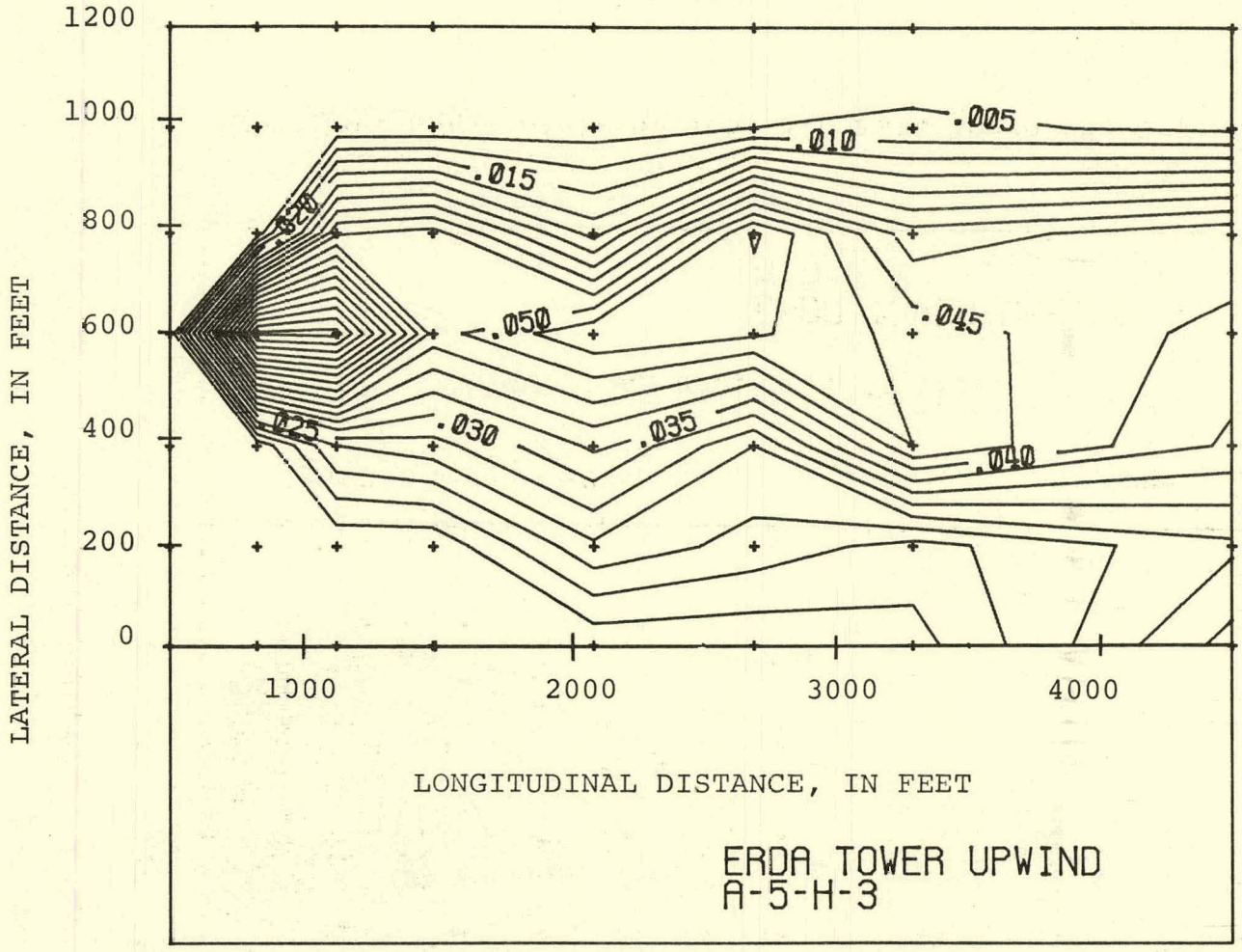

(d) Horizontal Distribution, 240 Feet Above the Ground

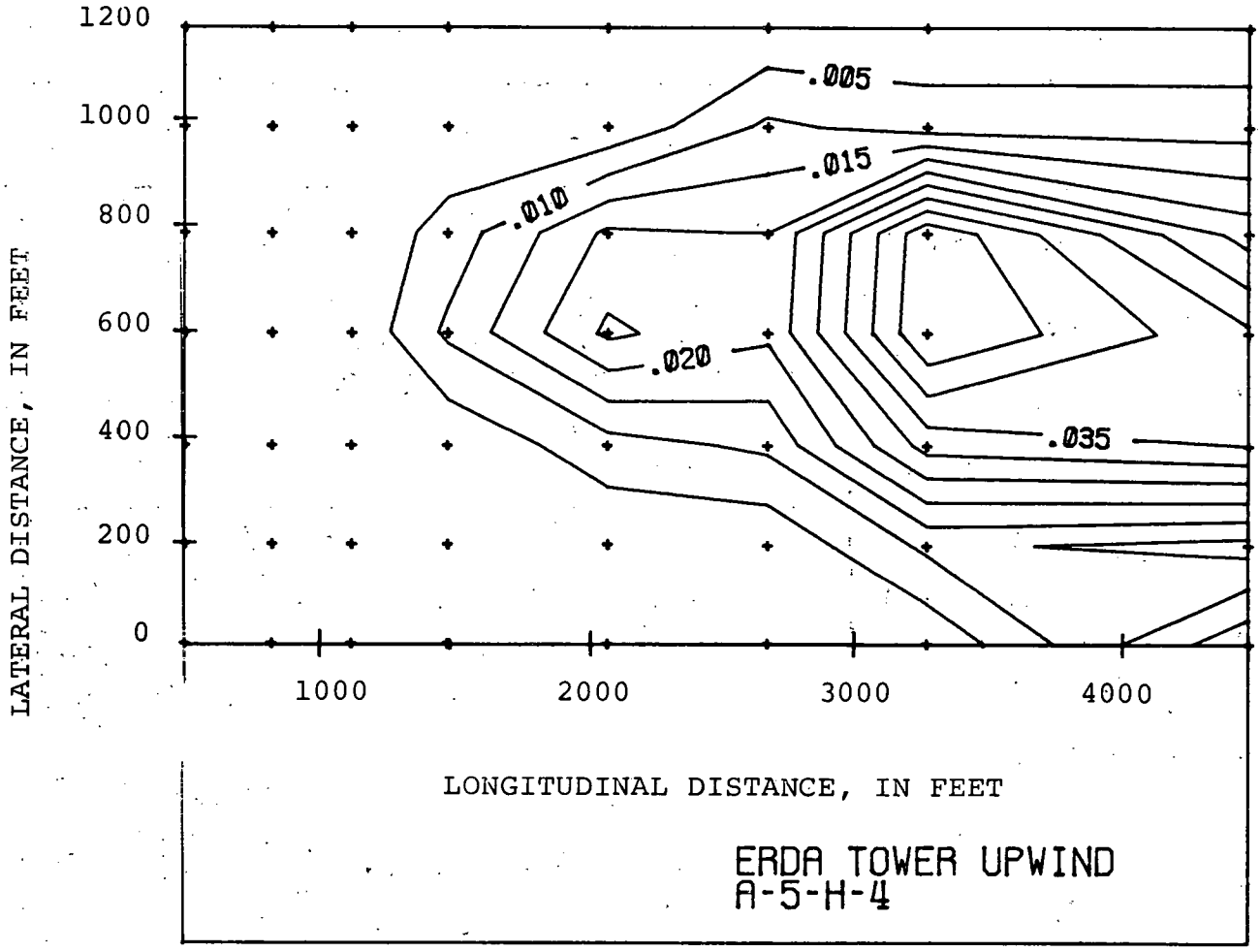

(e) Horizontal Distribution, 360 Feet Above the Ground

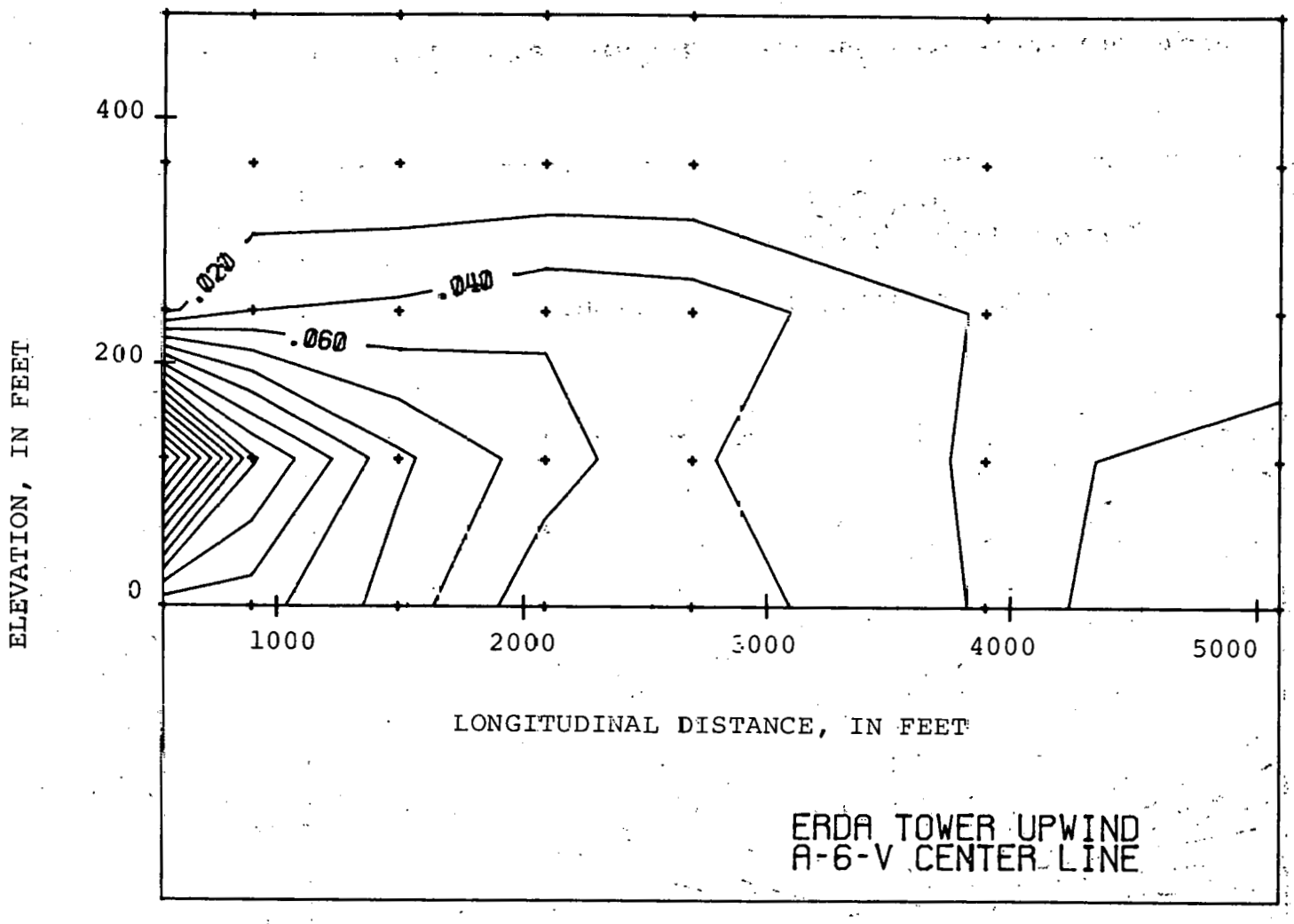

(a) Vertical Distribution

FIGURE 4.24 Temperature Distribution for Run A-6. V_a = 35.8 MPH.

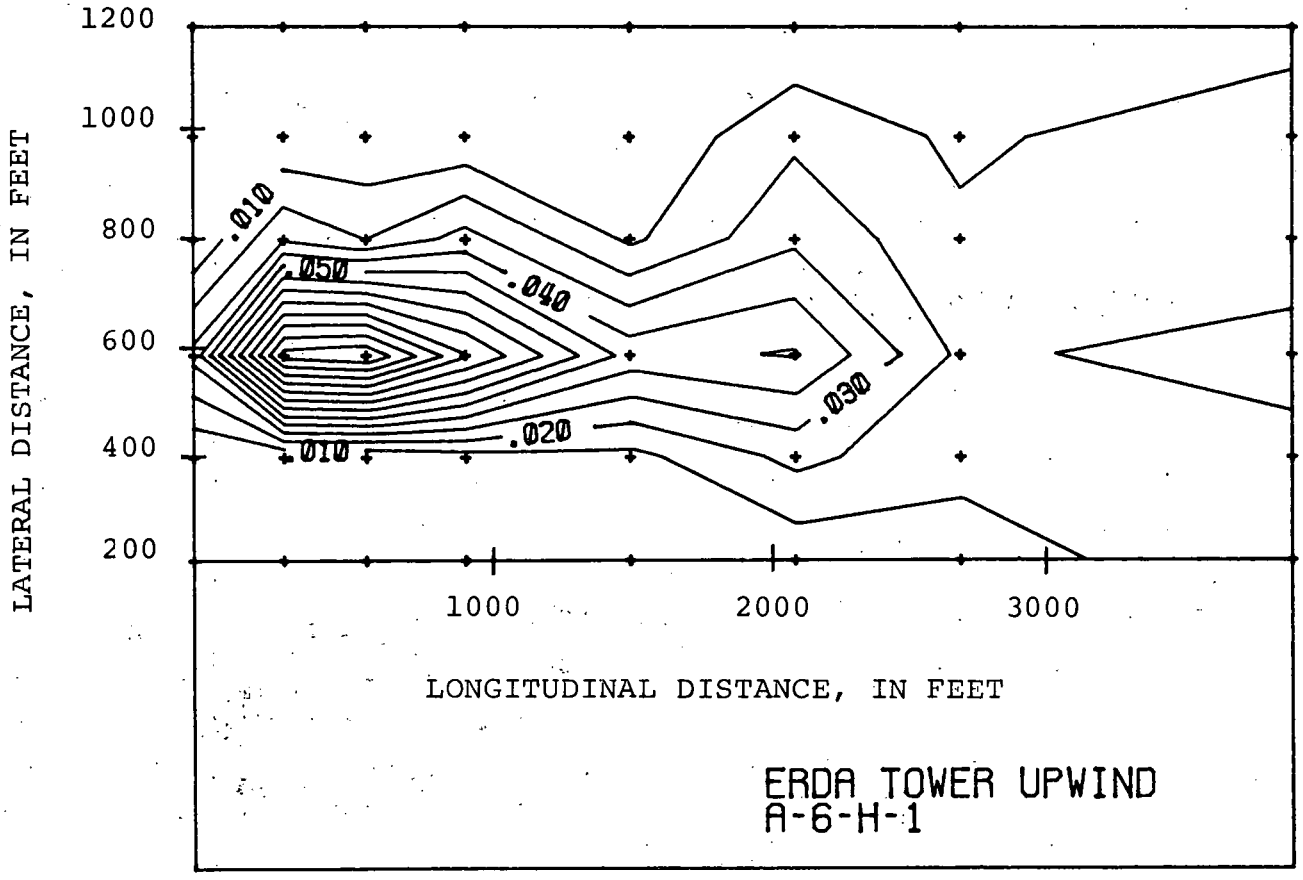

(b) Horizontal Distribution, Ground Level

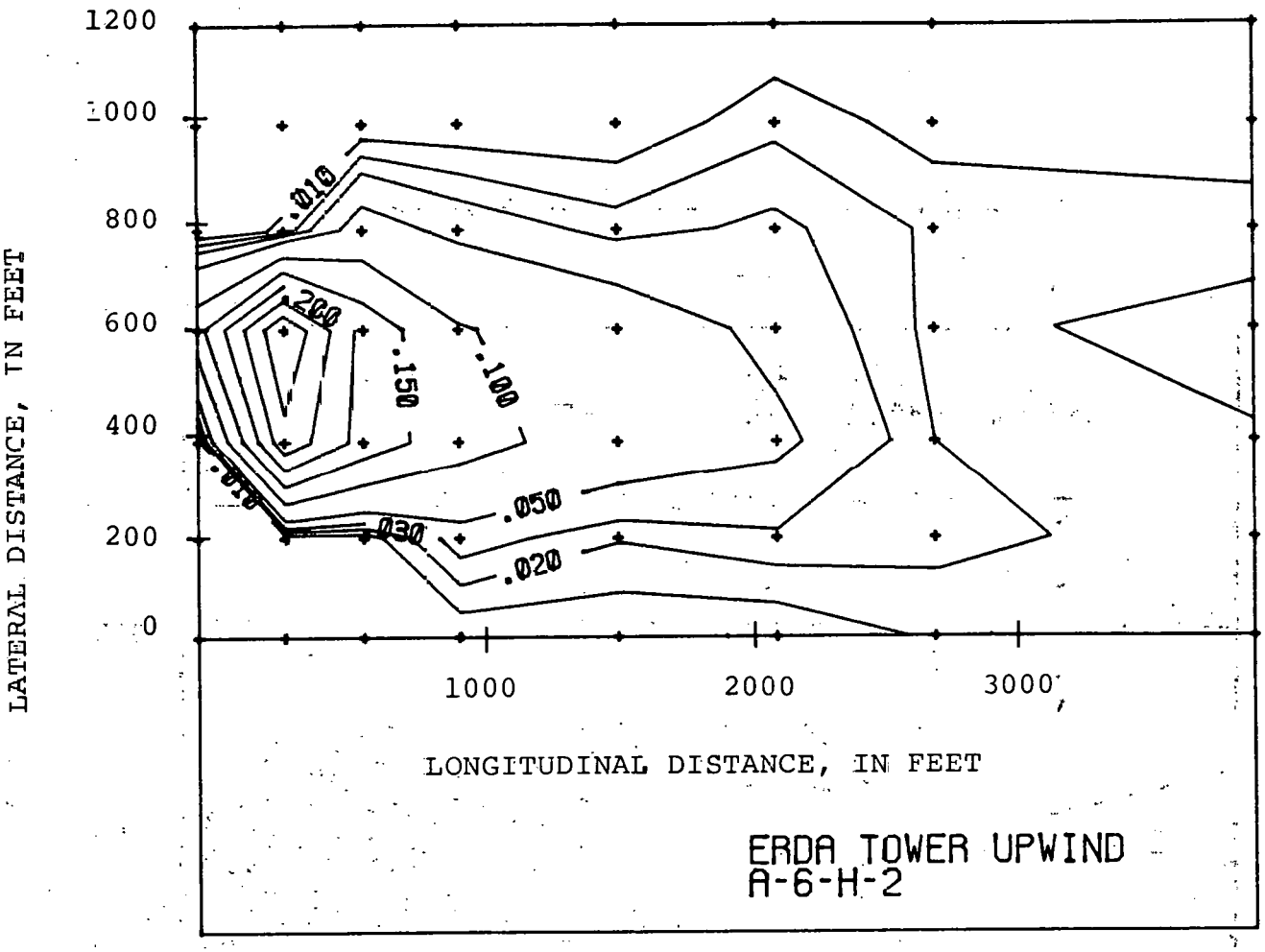

(c) Horizontal Distribution, 120 Feet Above the Ground

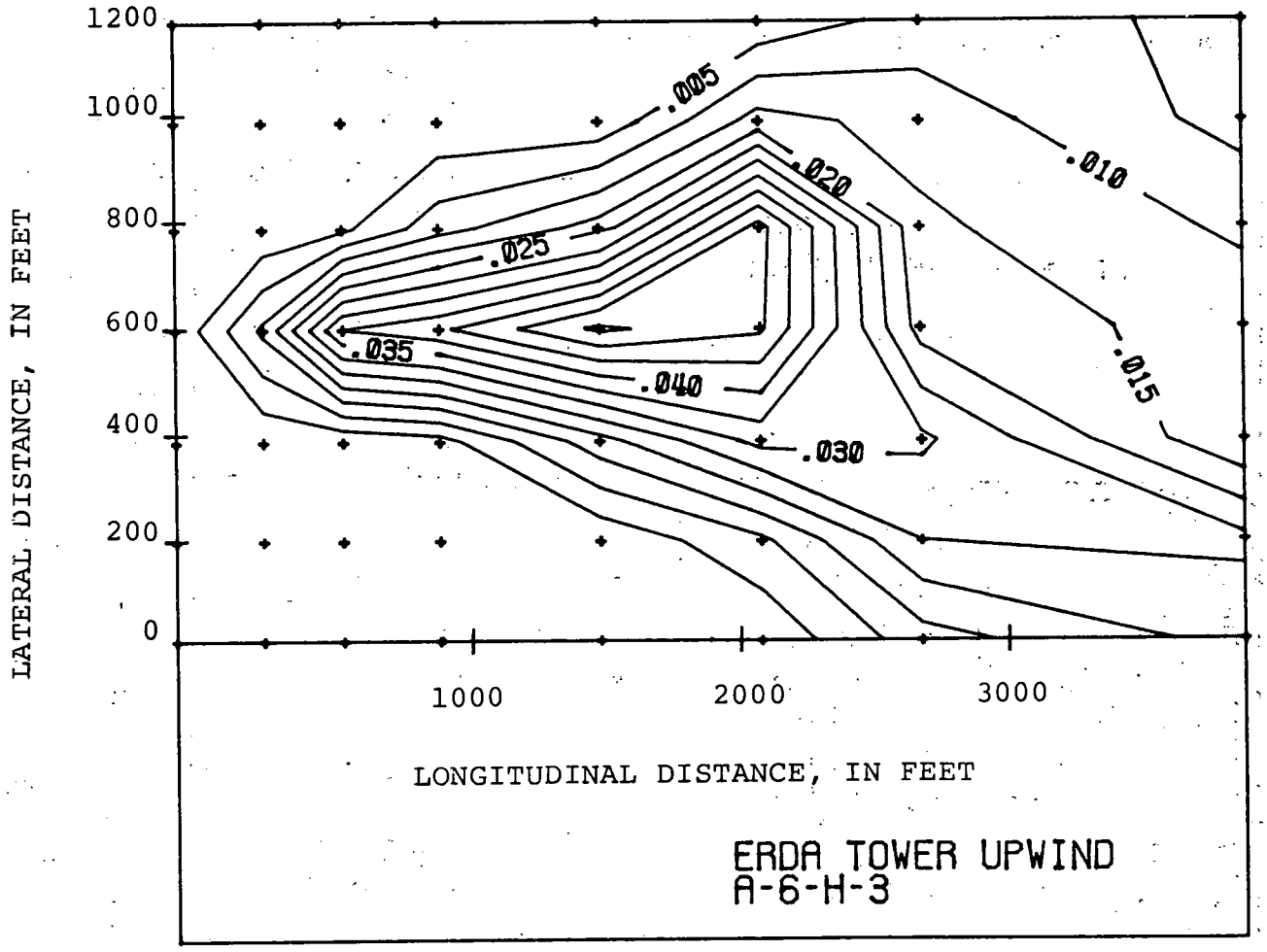

(d) Horizontal Distribution, 240 Feet Above the Ground

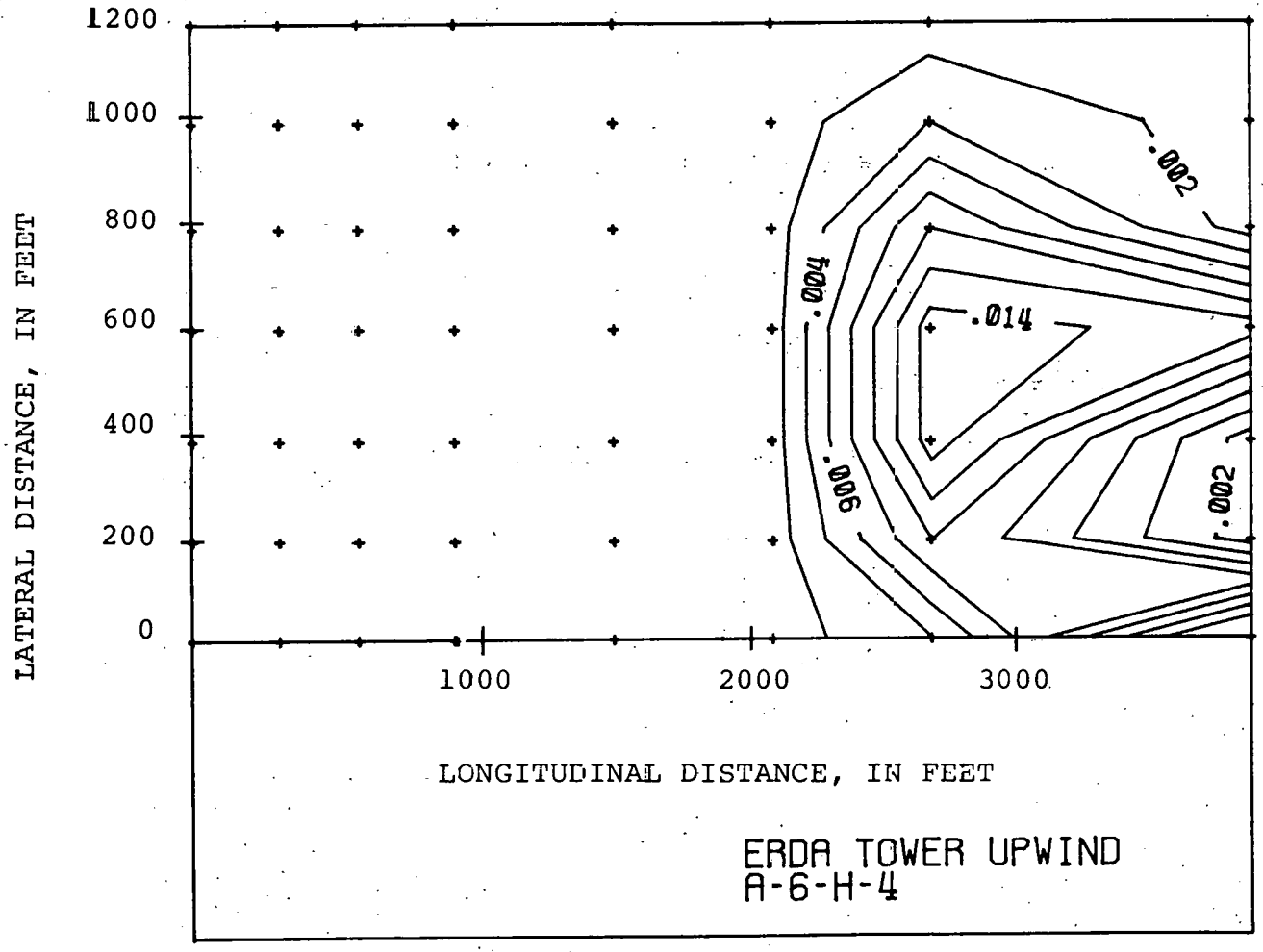

(e) Horizontal Distribution, 360 Feet Above the Ground

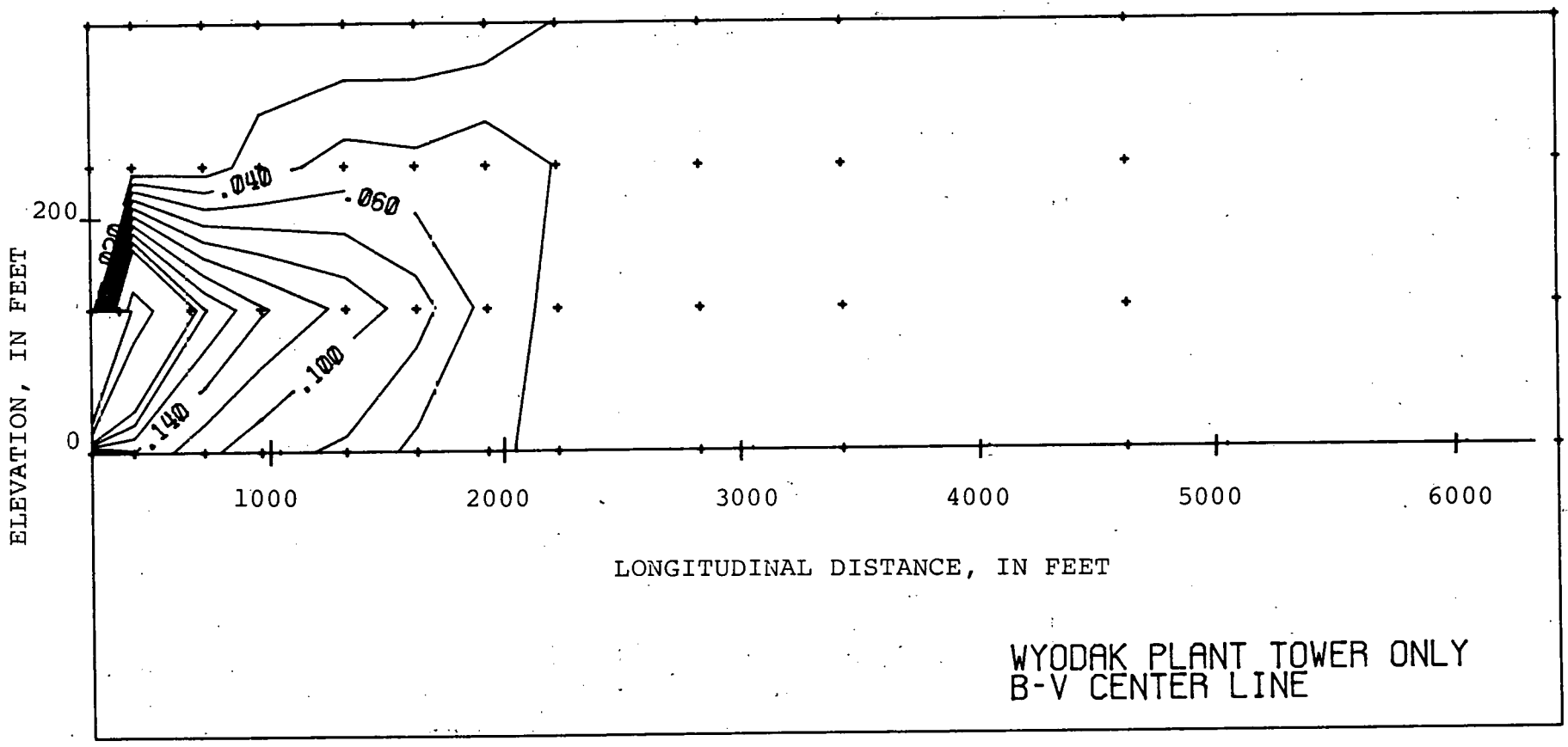

(a) Vertical Distribution

FIGURE 4.25 Temperature Distribution for Run B. V_a = 27.5 MPH.

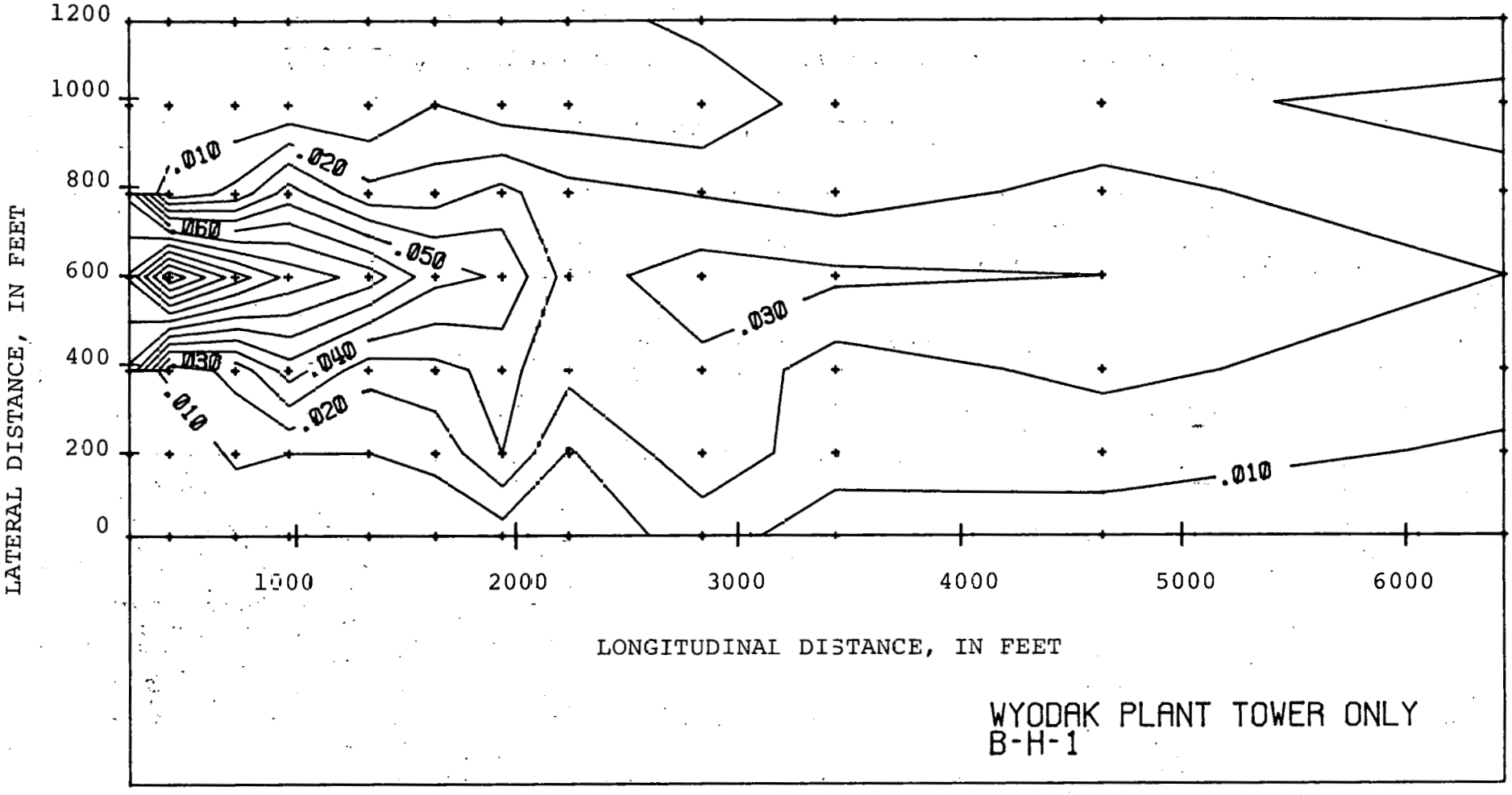

(b) Horizontal Distribution, Ground Level

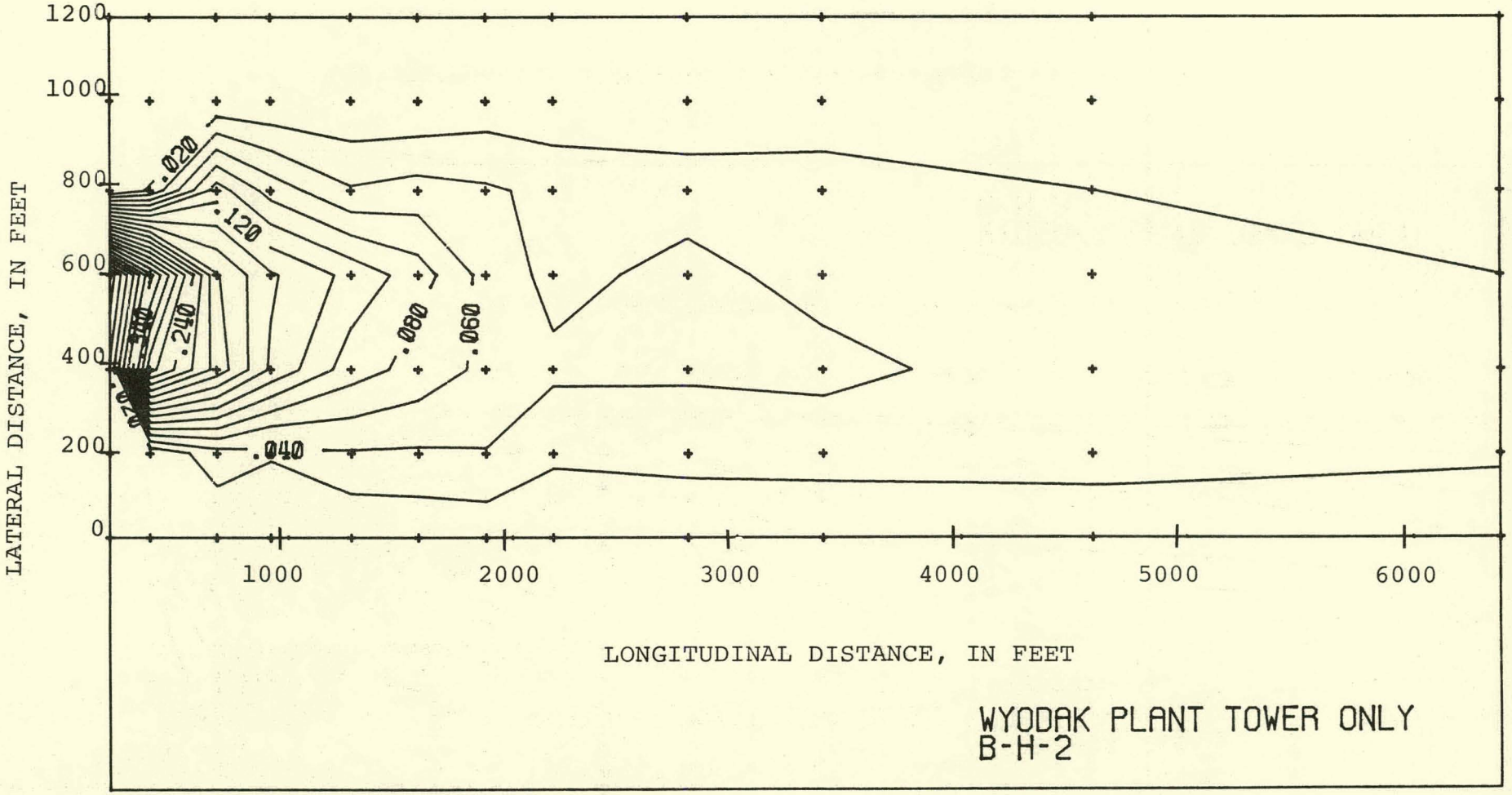

(c) Horizontal Distribution, 120 Feet Above the Ground

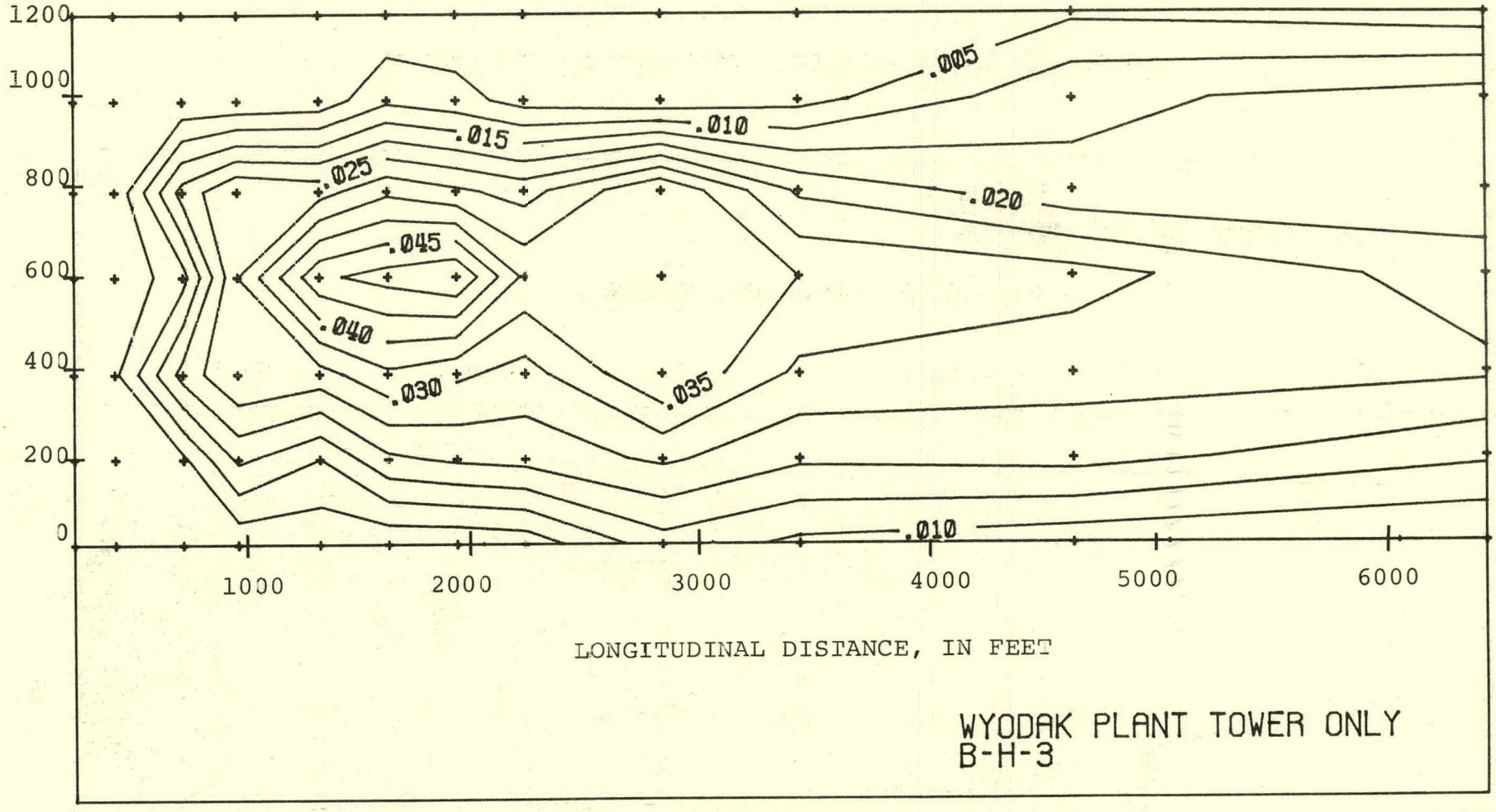

(d) Horizontal Distribution, 240 Feet Above the Ground

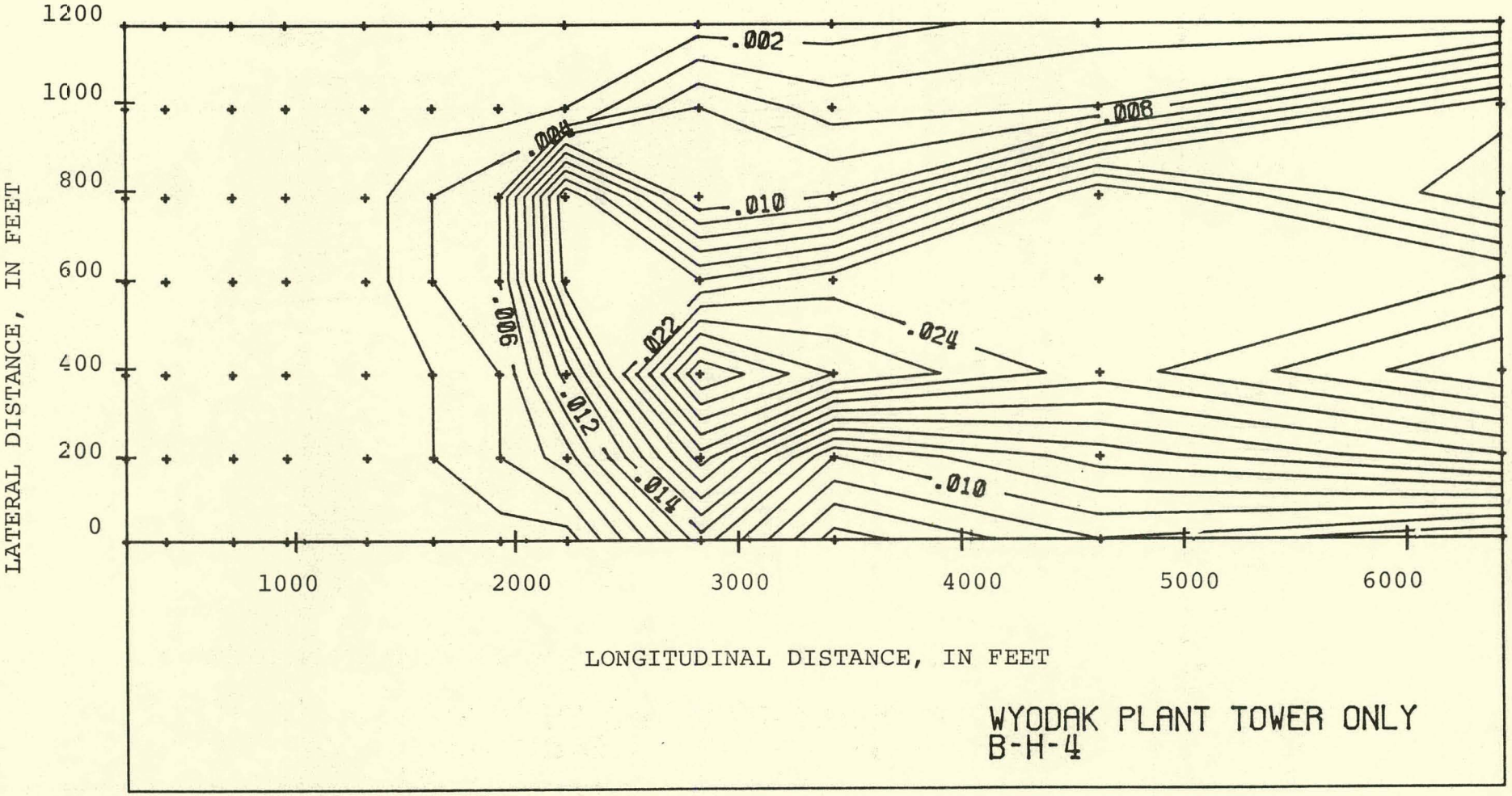

(e) Horizontal Distribution, 360 Feet Above the Ground

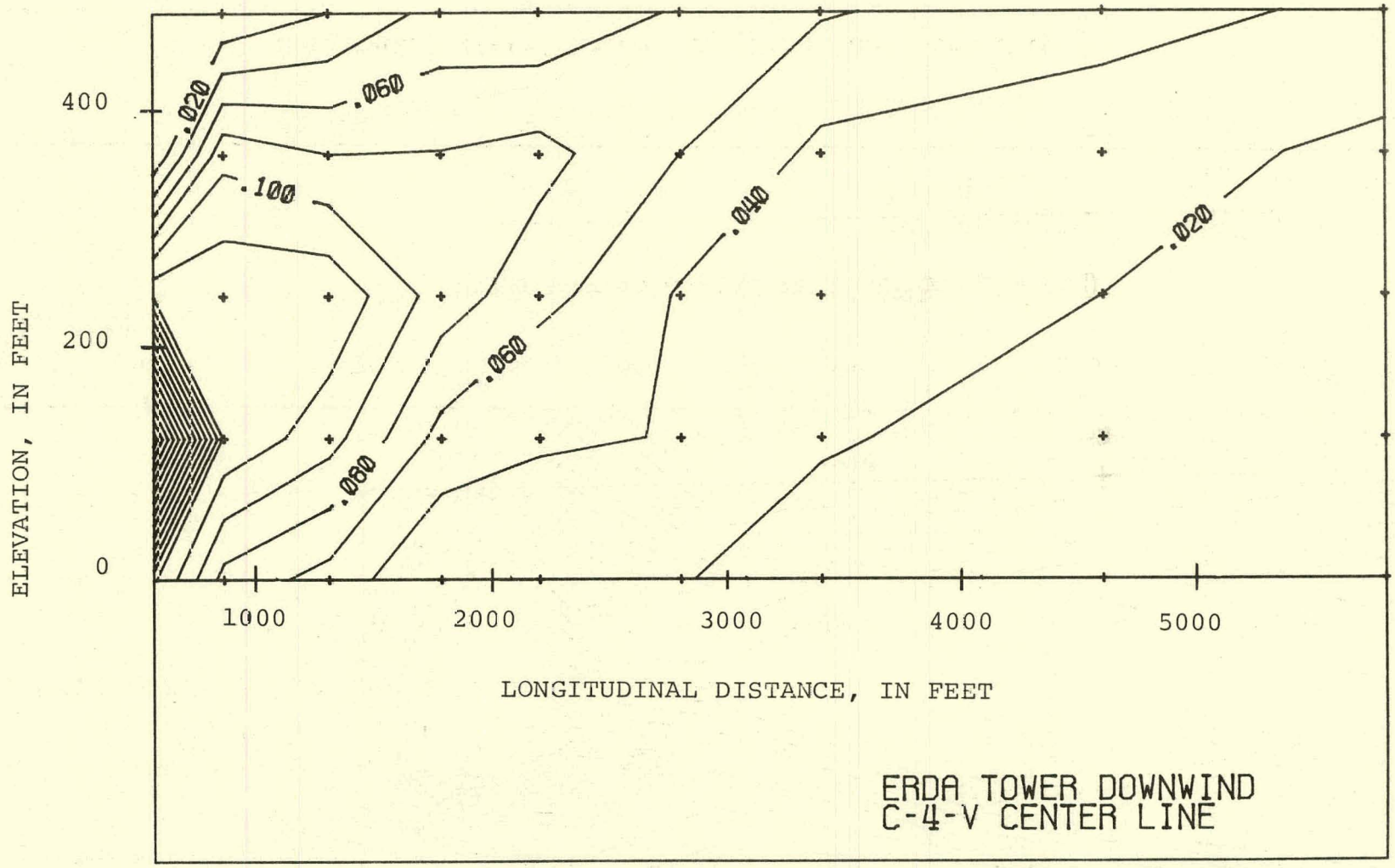

(a) Vertical Distribution

FIGURE 4.26 Temperature Distribution for Run C-4. V_a = 18.5 MPH.

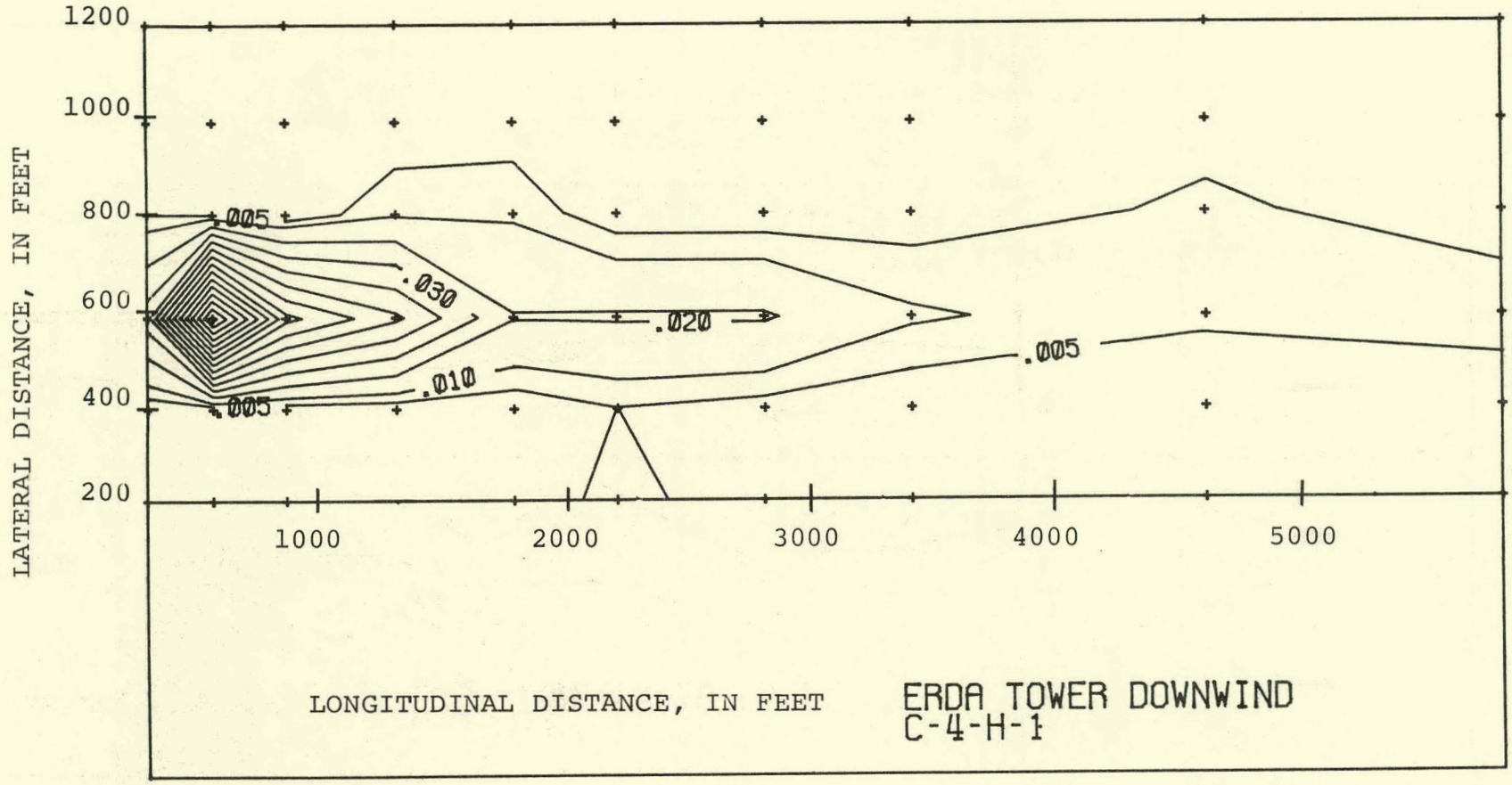

(b) Horizontal Distribution, Ground Level

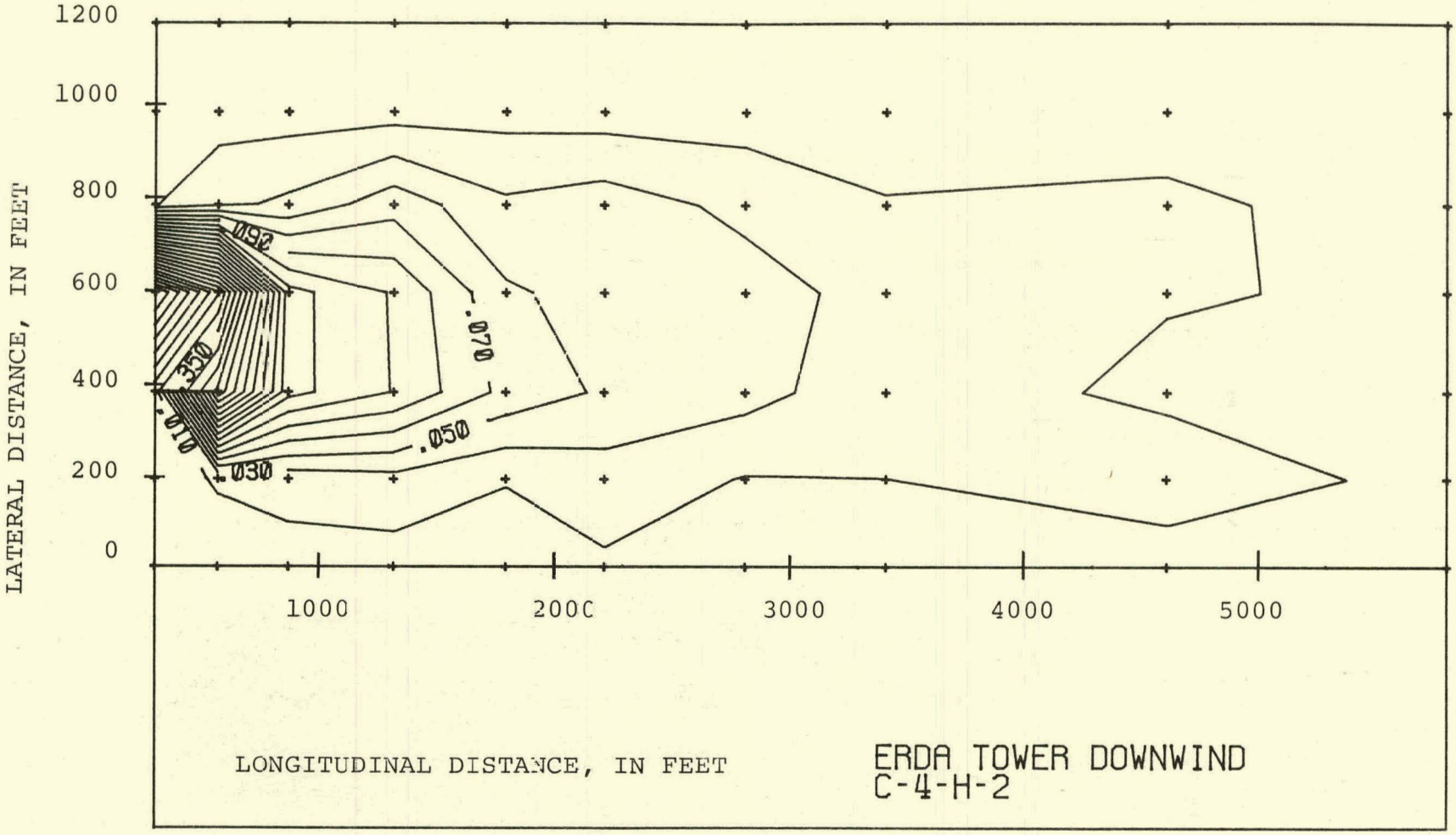

(c) Horizontal Distribution, 120 Feet Above the Ground

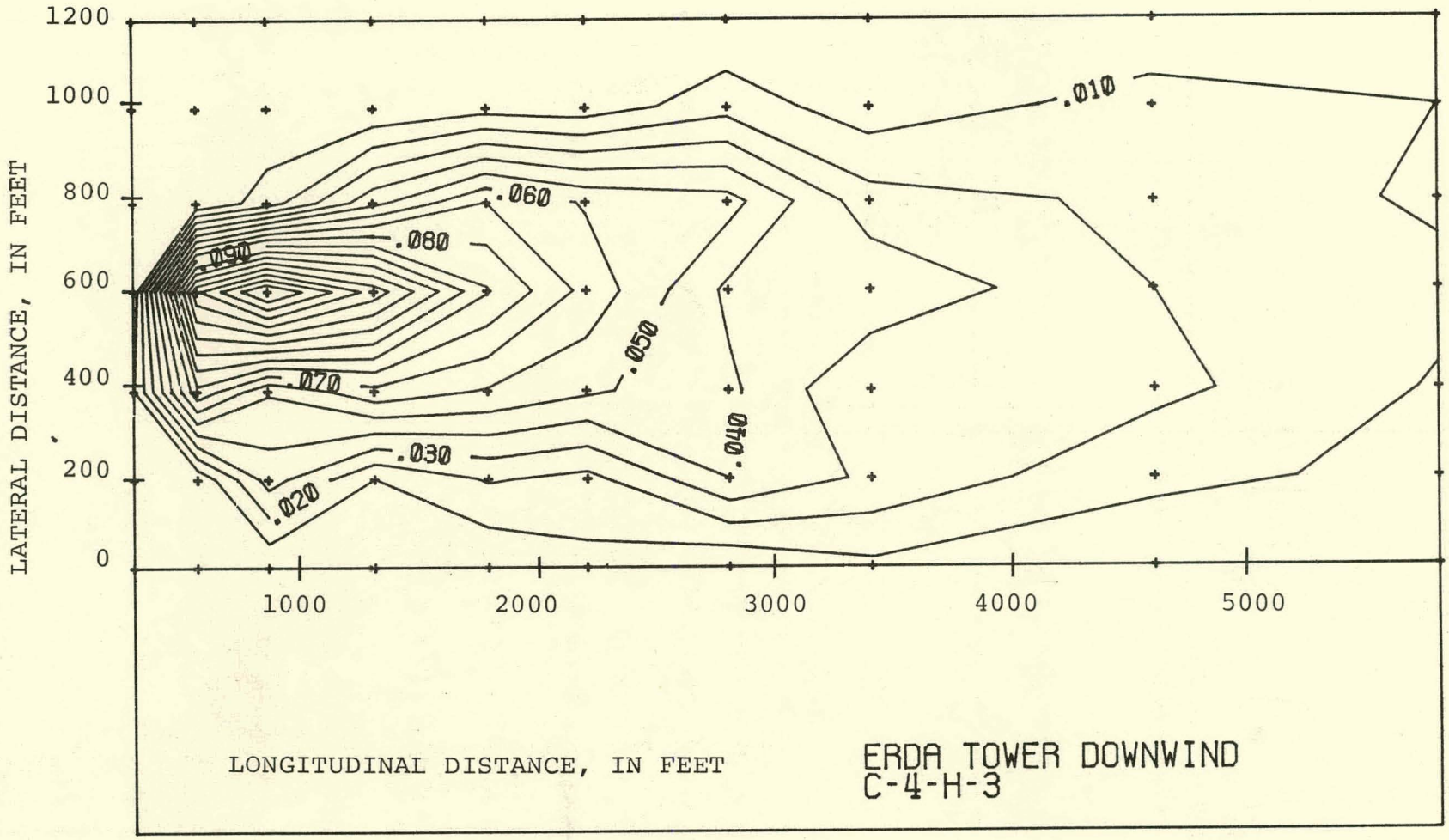

(d) Horizontal Distribution, 240 Feet Above the Ground

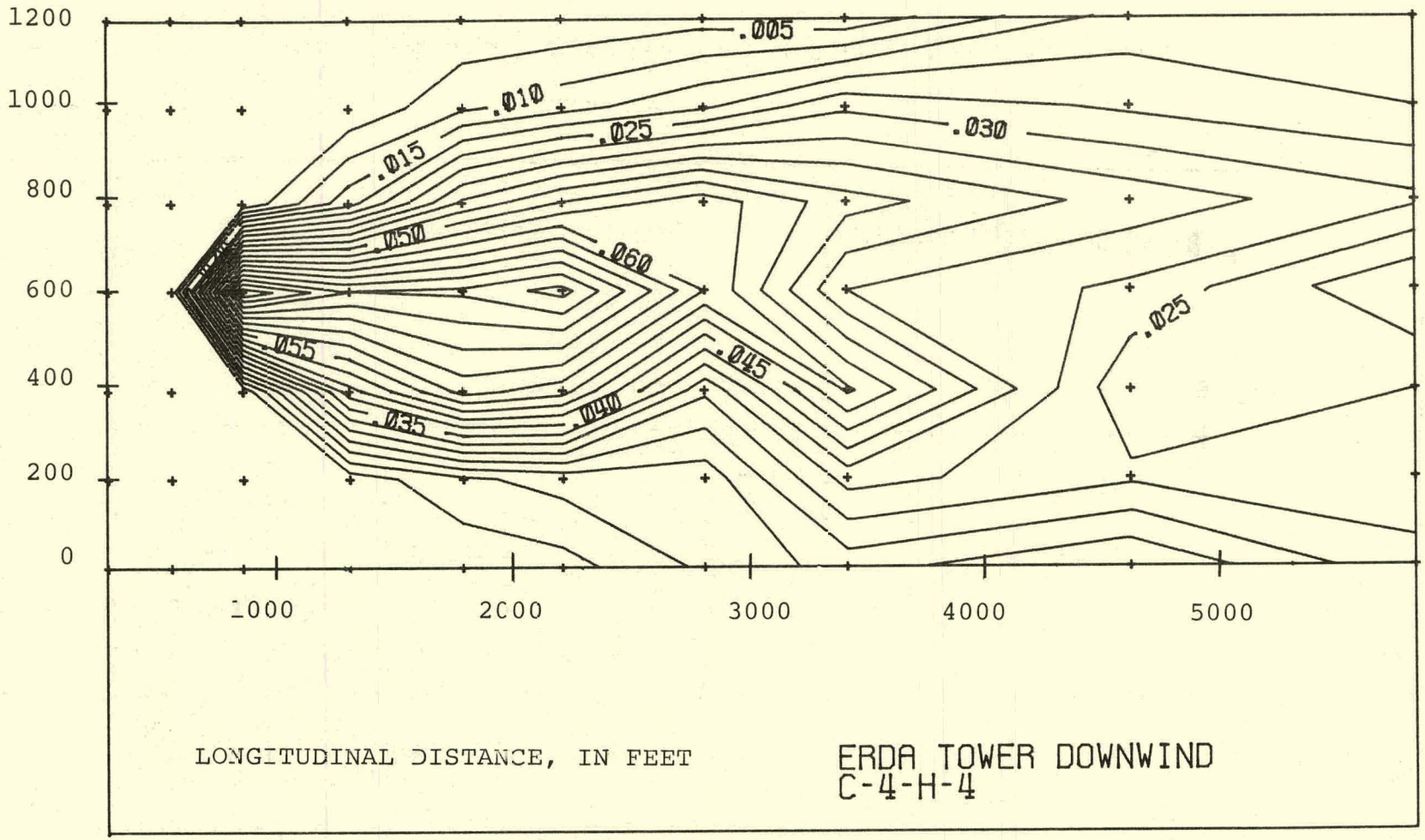

(e) Horizontal Distribution, 360 Feet Above the Ground

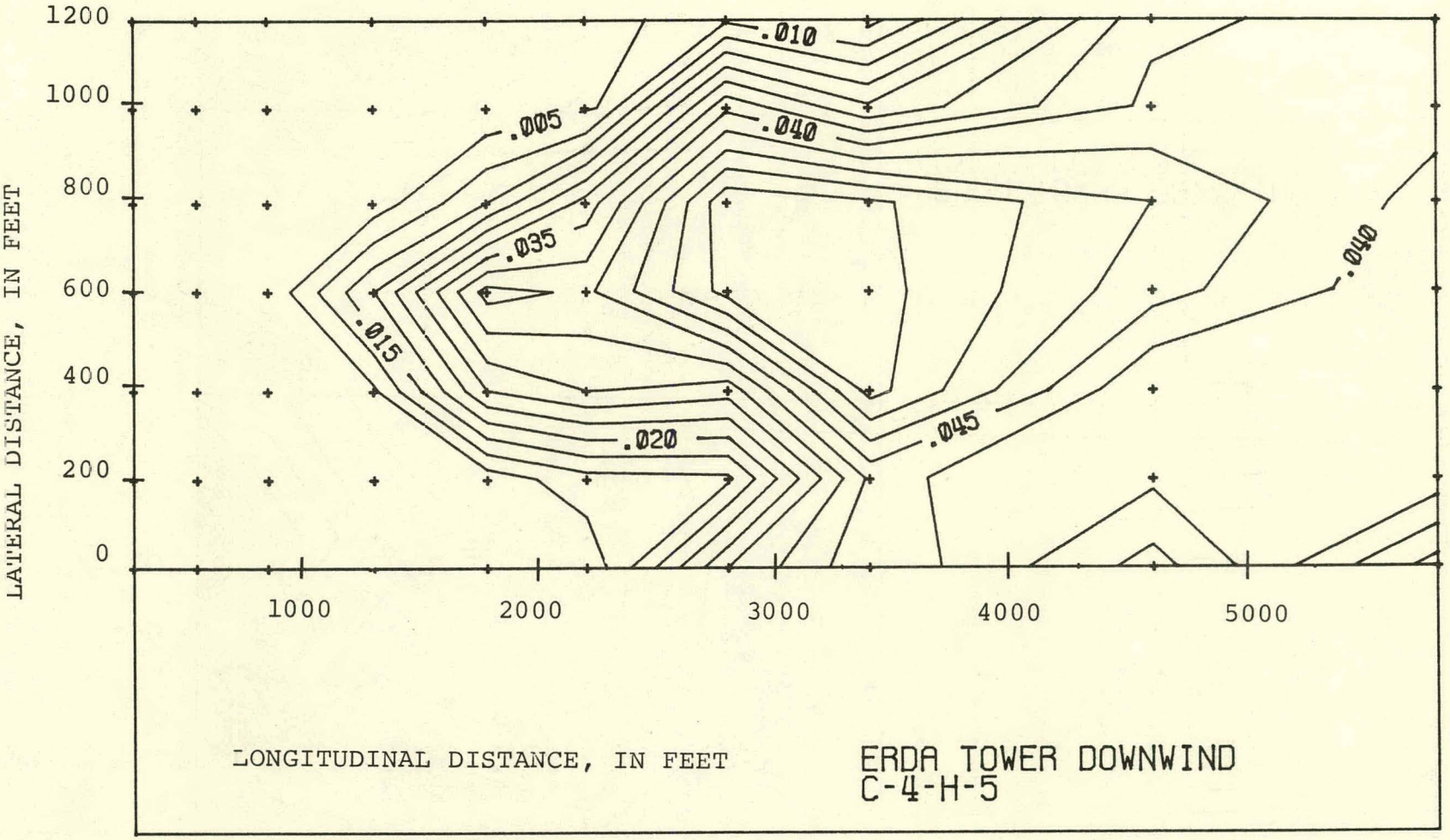

(f) Horizontal Distribution, 480 Feet Above the Ground

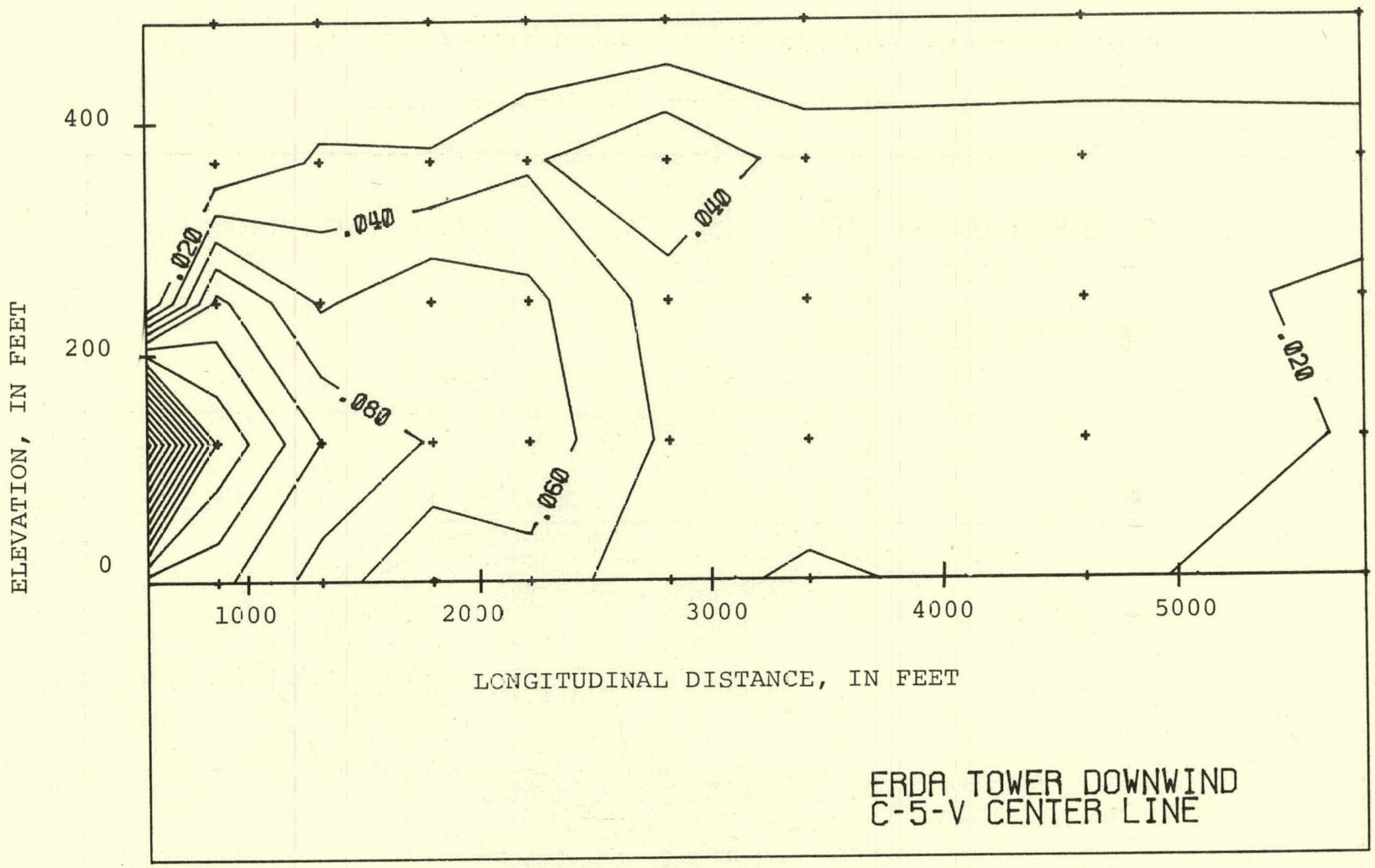

(a) Vertical Distribution

FIGURE 4.27 Temperature Distribution for Run C-5. V_a = 28.0 MPH.

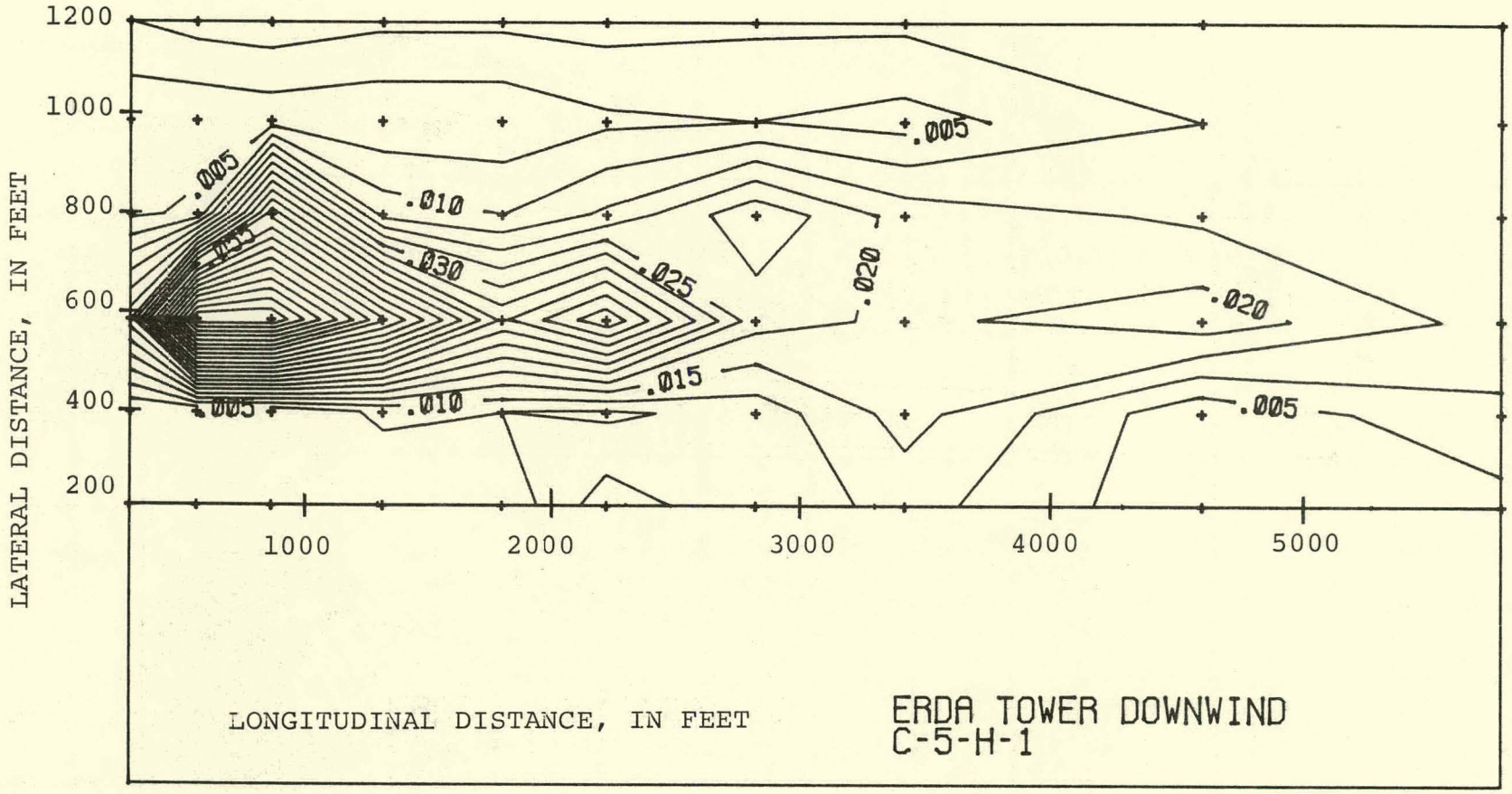

(b) Horizontal Distribution, Ground Level

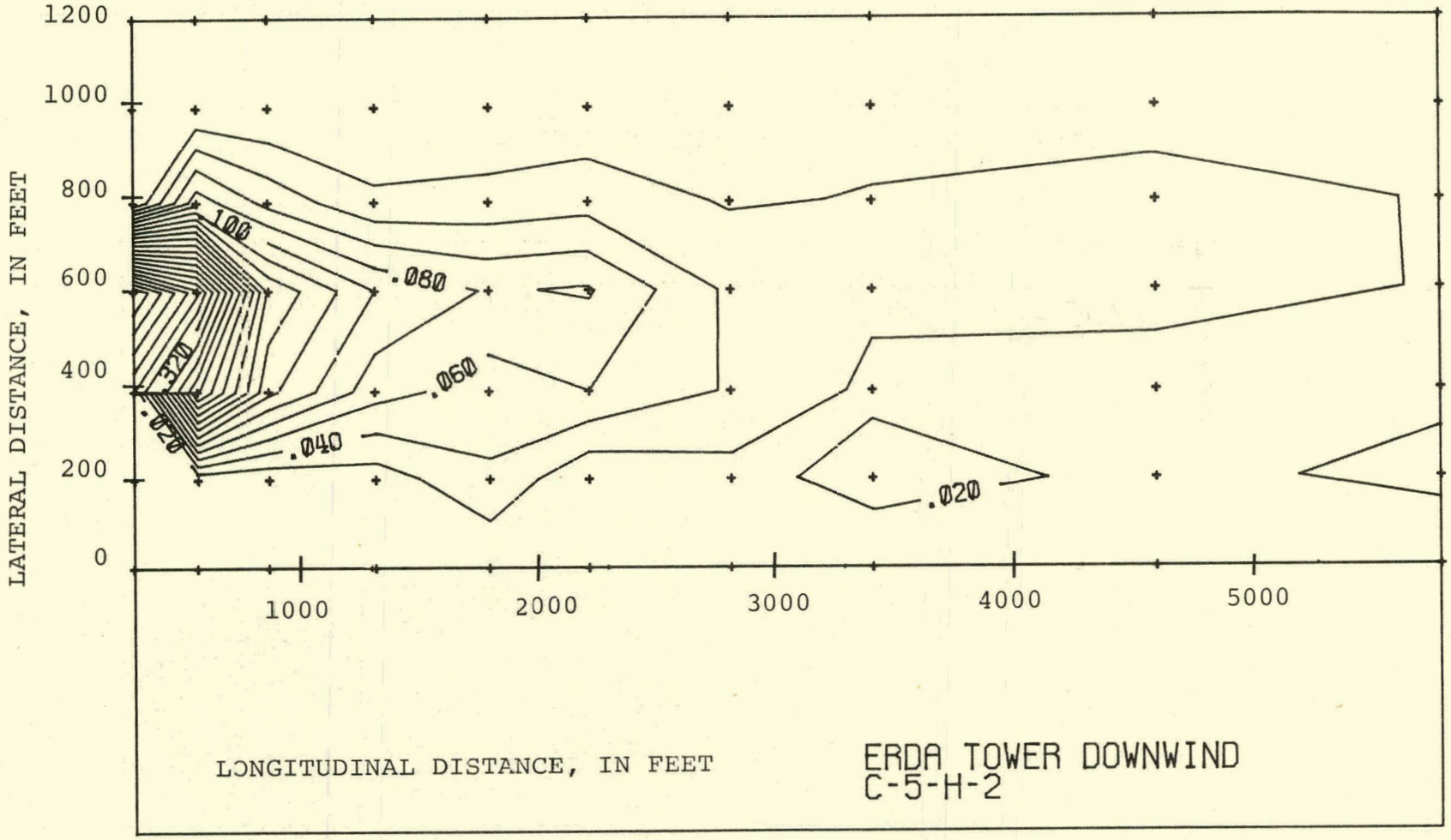

(c) Horizontal Distribution, 120 Feet Above the Ground

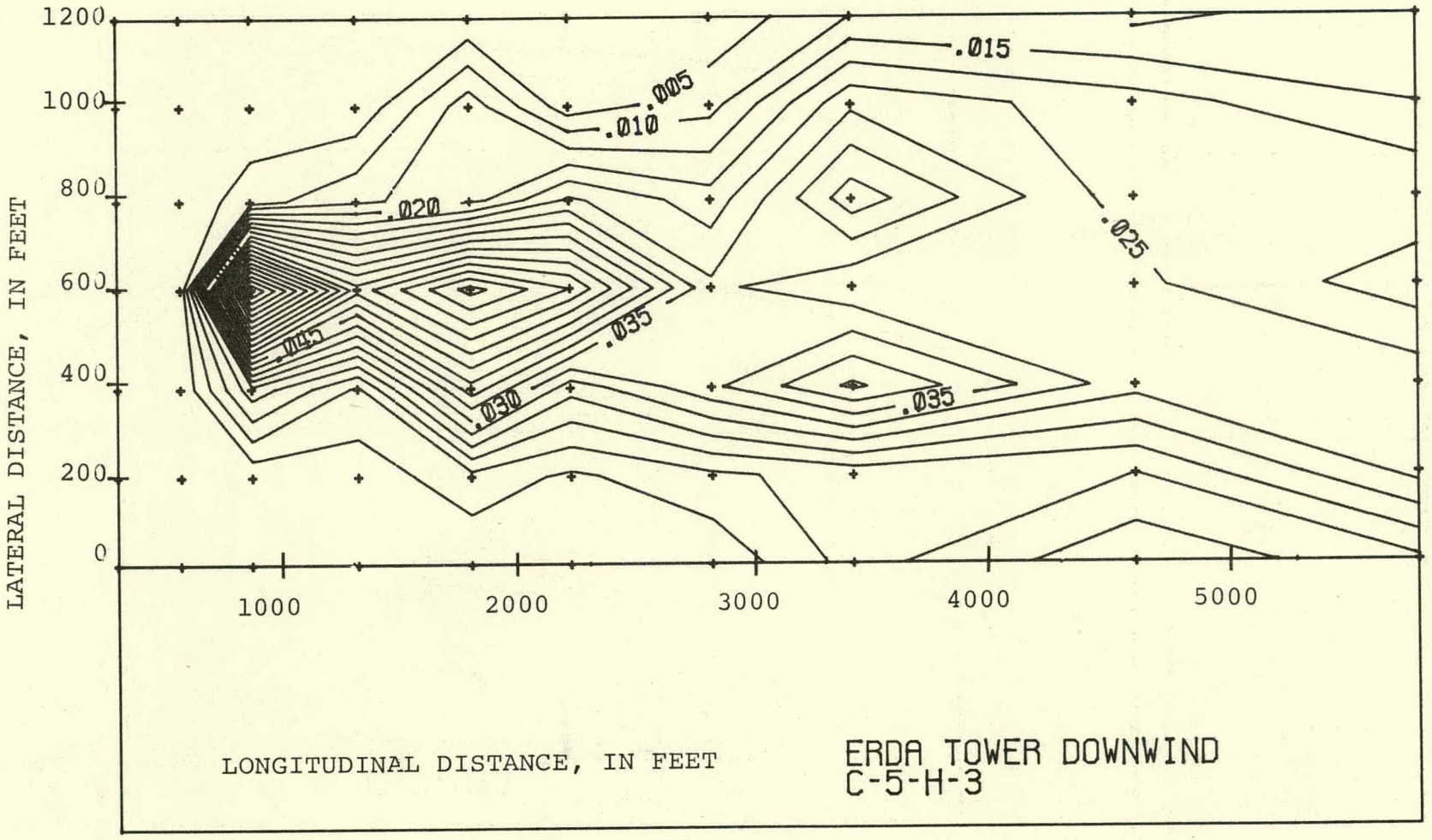

(d) Horizontal Distribution, 240 Feet Above the Ground

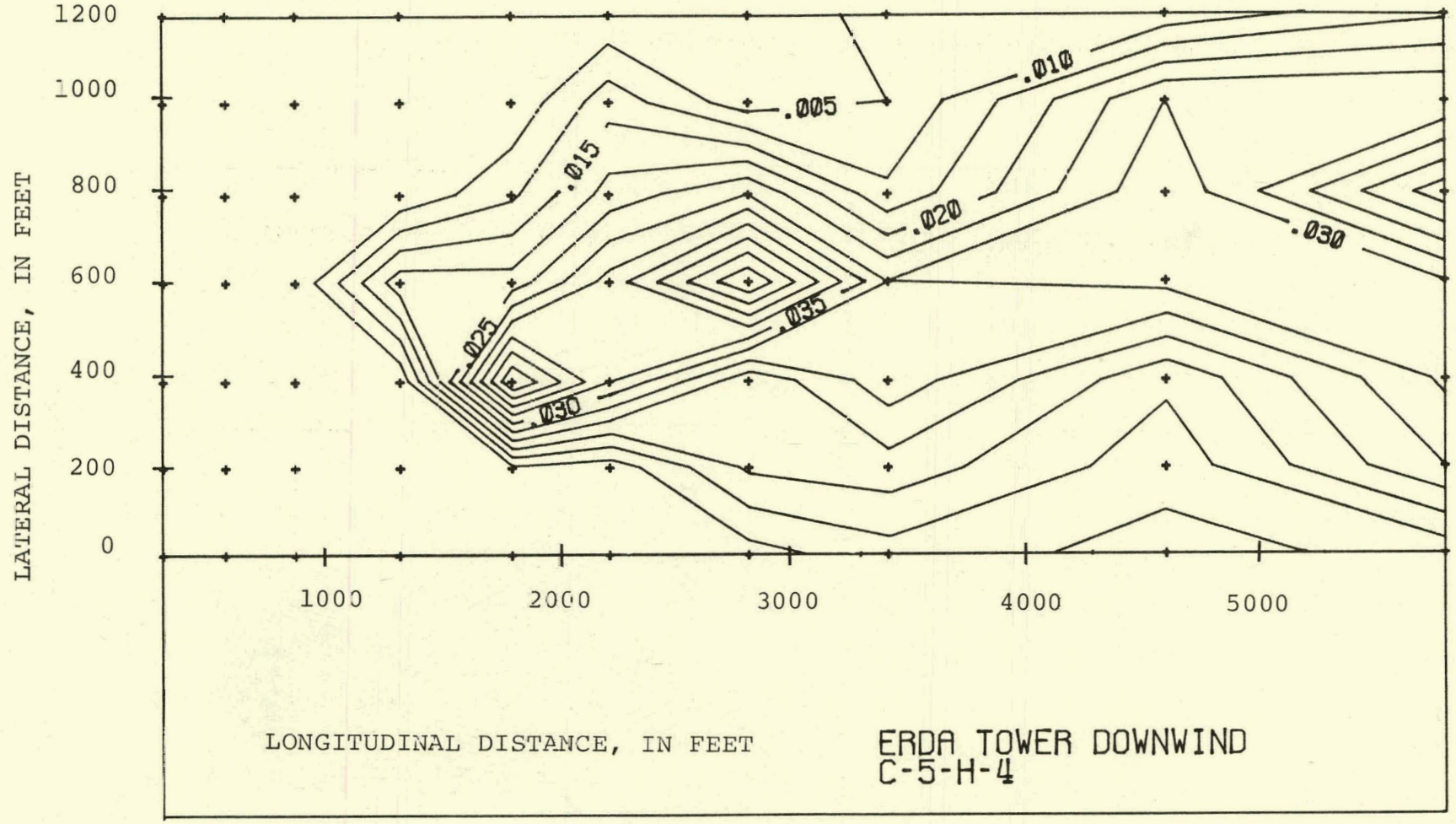

(e) Horizontal Distribution, 360 Feet Above the Ground

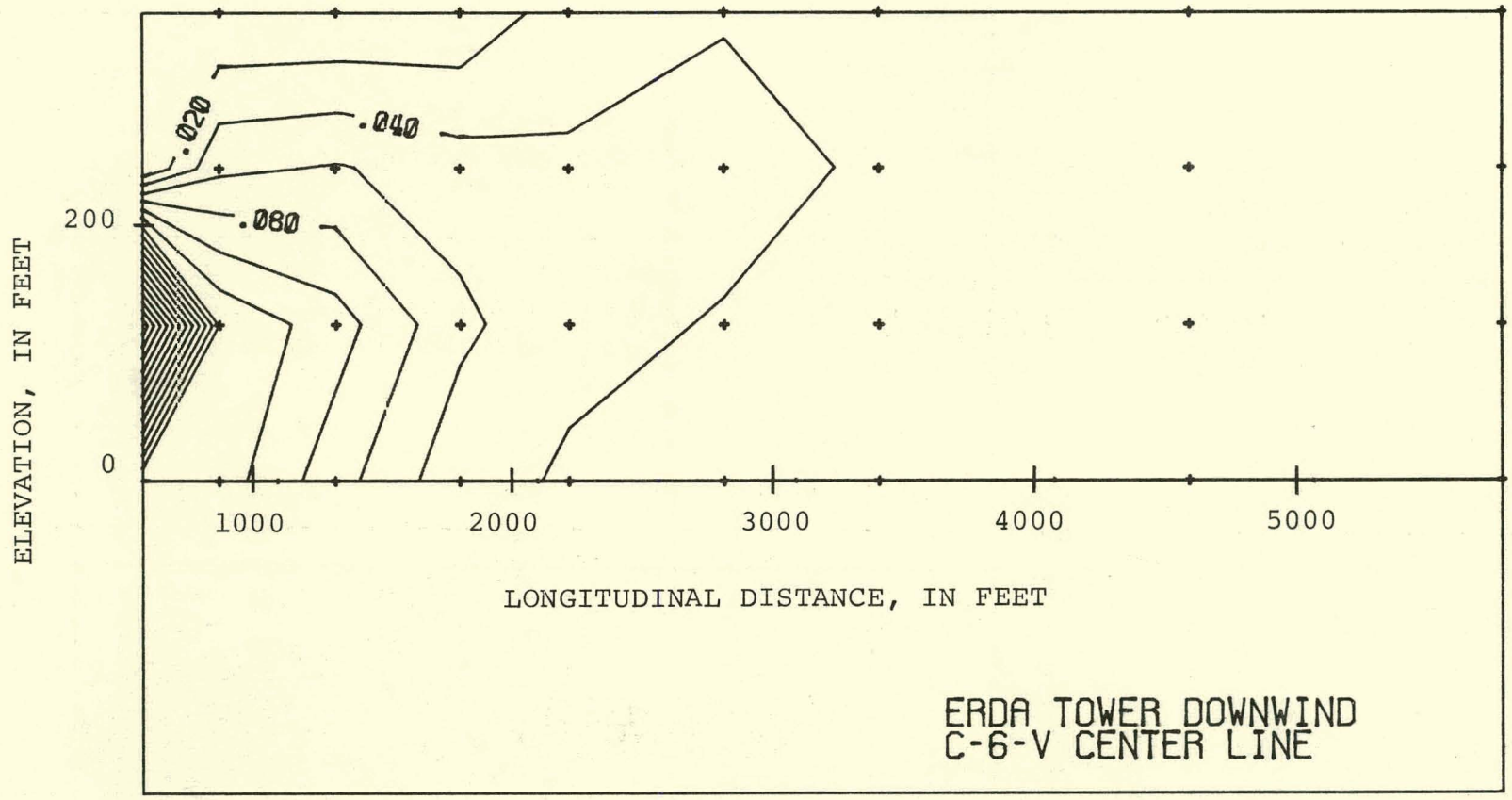

(a) Vertical Distribution

FIGURE 4.28 Temperature Distribution for Run C-6. V_a = 36.0 MPH.

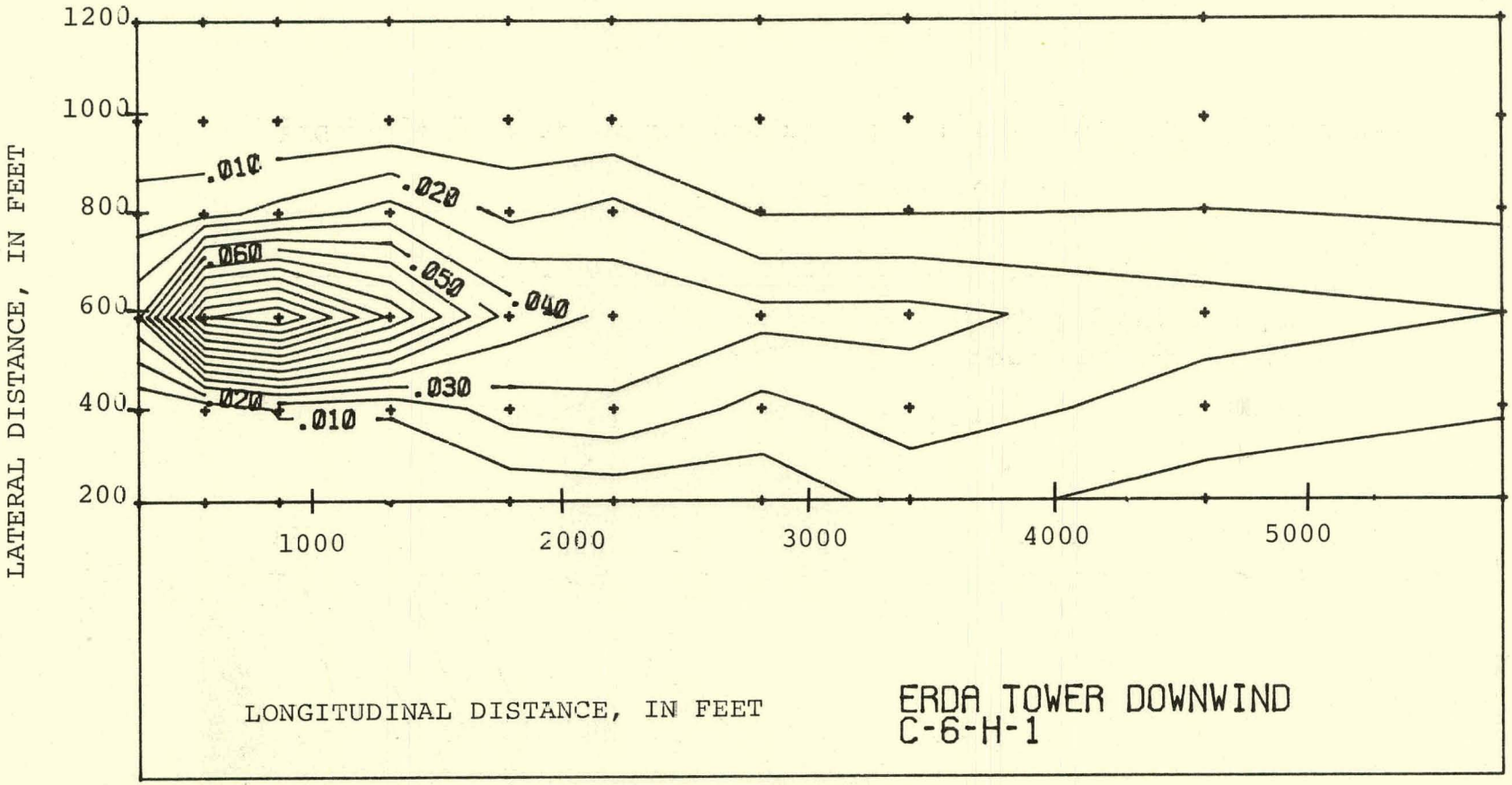

(b) Horizontal Distribution, Ground Level

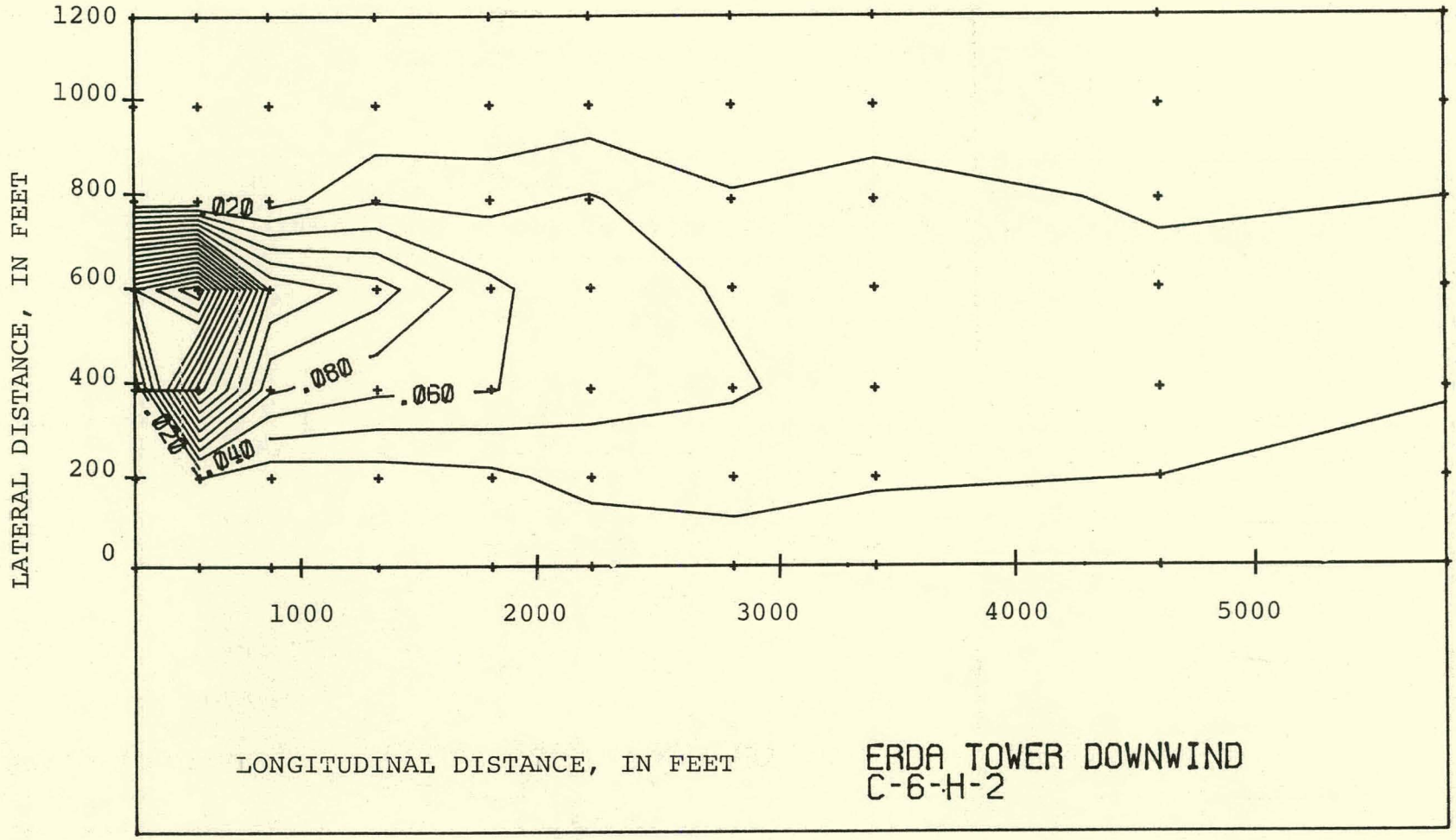

(c) Horizontal Distribution, 120 Feet Above the Ground

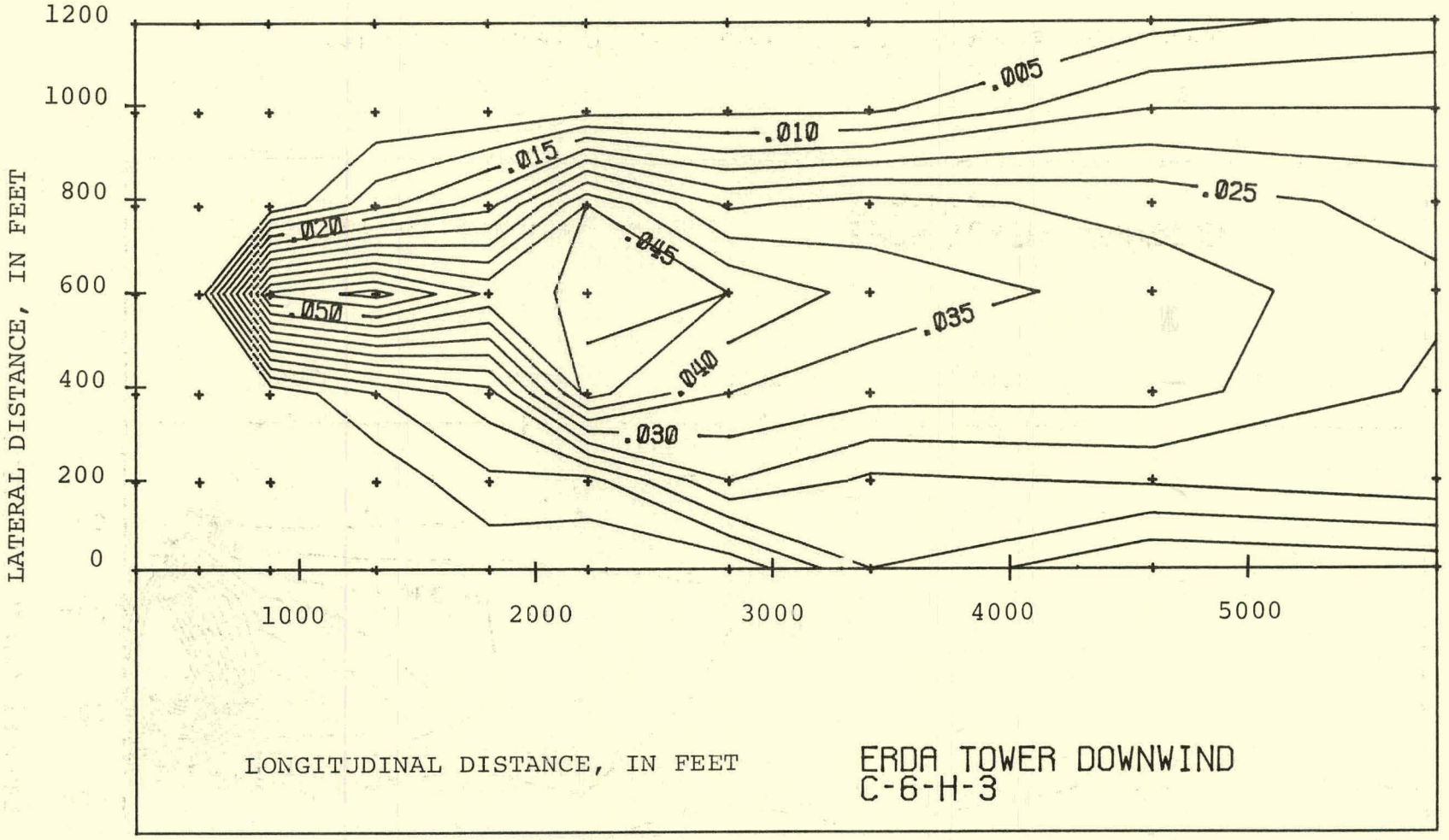

(d) Horizontal Distribution, 24) Feet Above the Ground

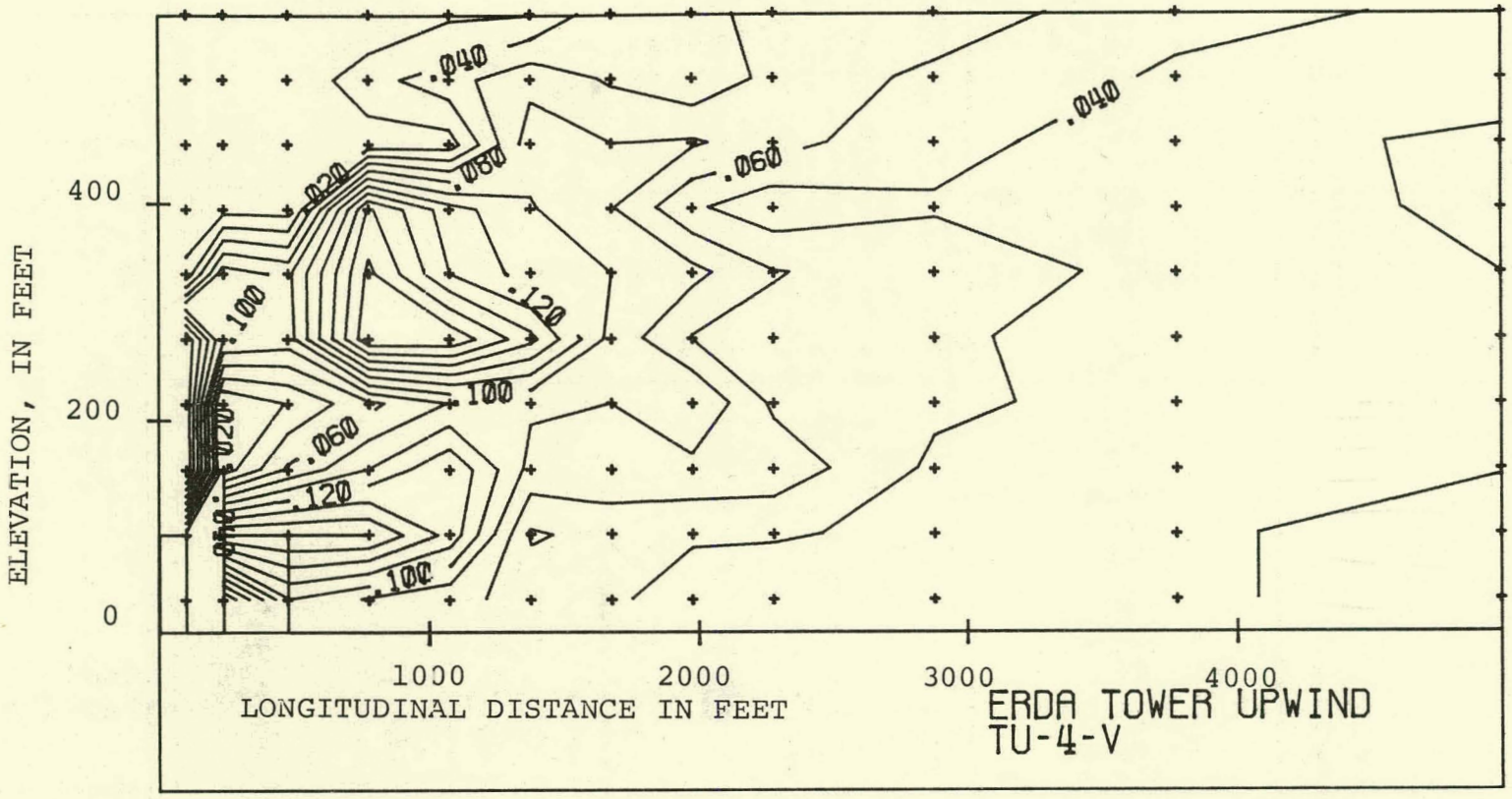

(a) Vertical Distribution

FIGURE 4.29 Temperature Distribution for Run TU-4. V_a = 19.6 MPH.

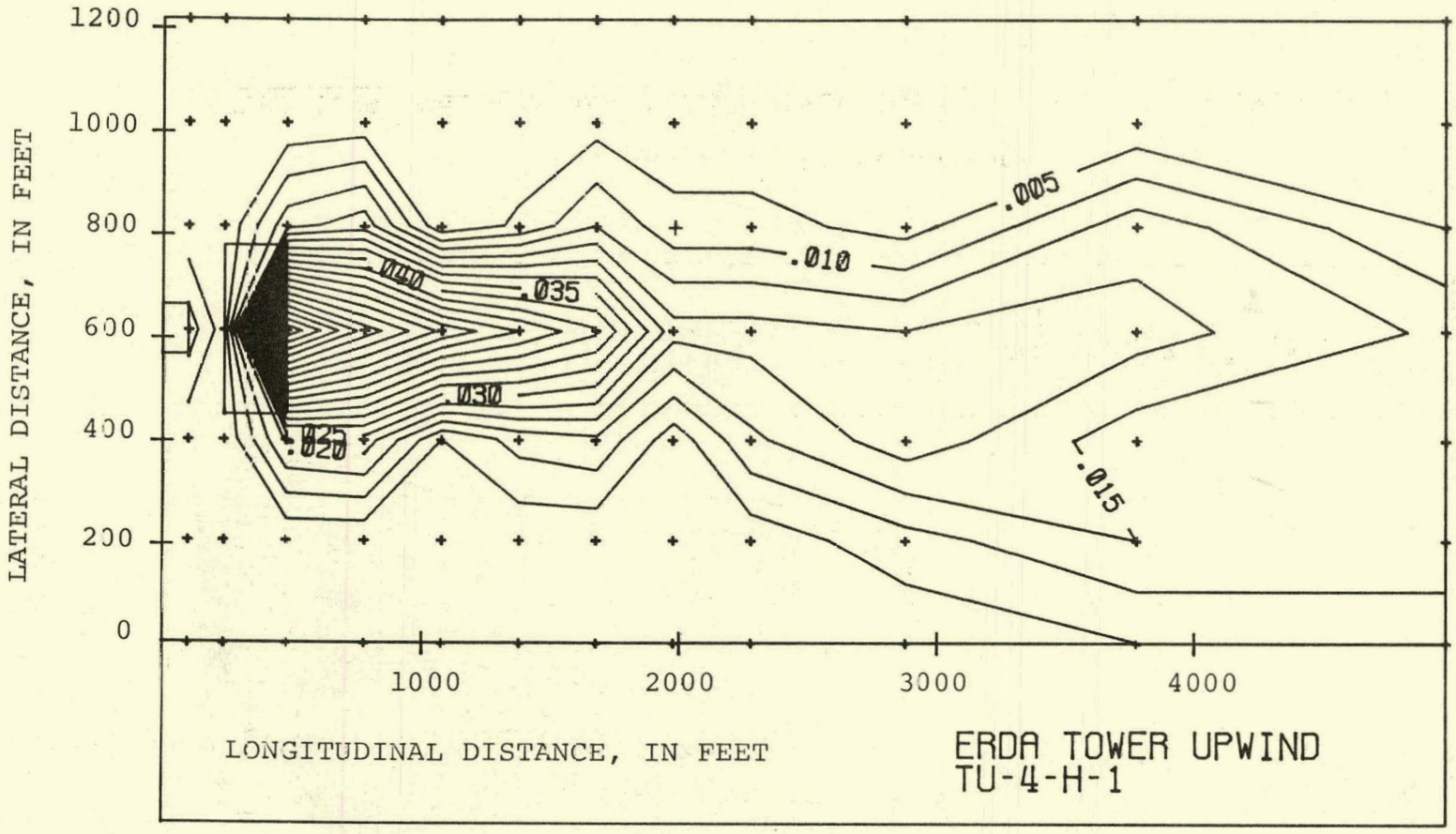

(b) Horizontal Distribution, 30 Feet Above the Ground

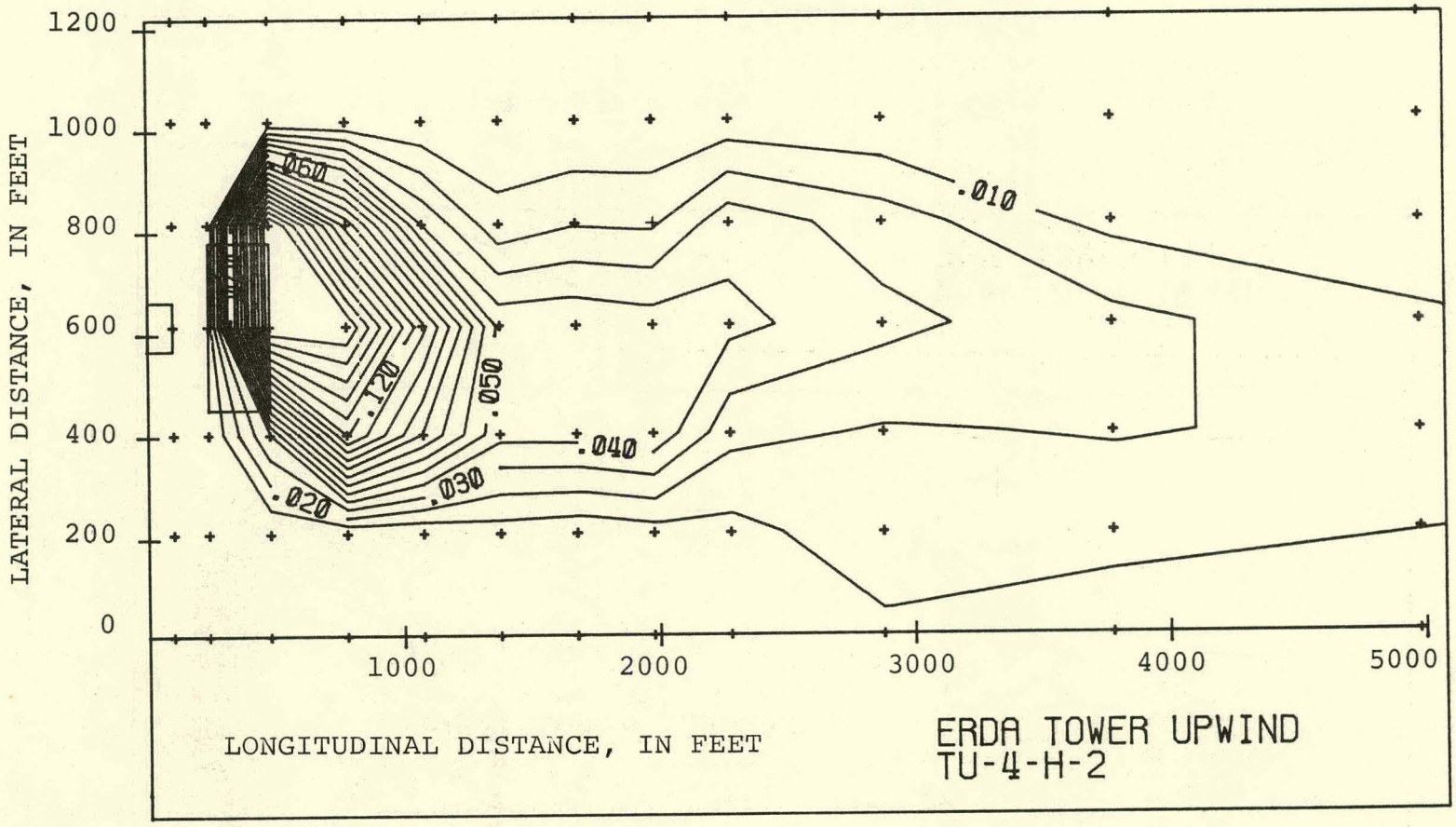

(c) Horizontal Distribution, 90 Feet Above the Ground

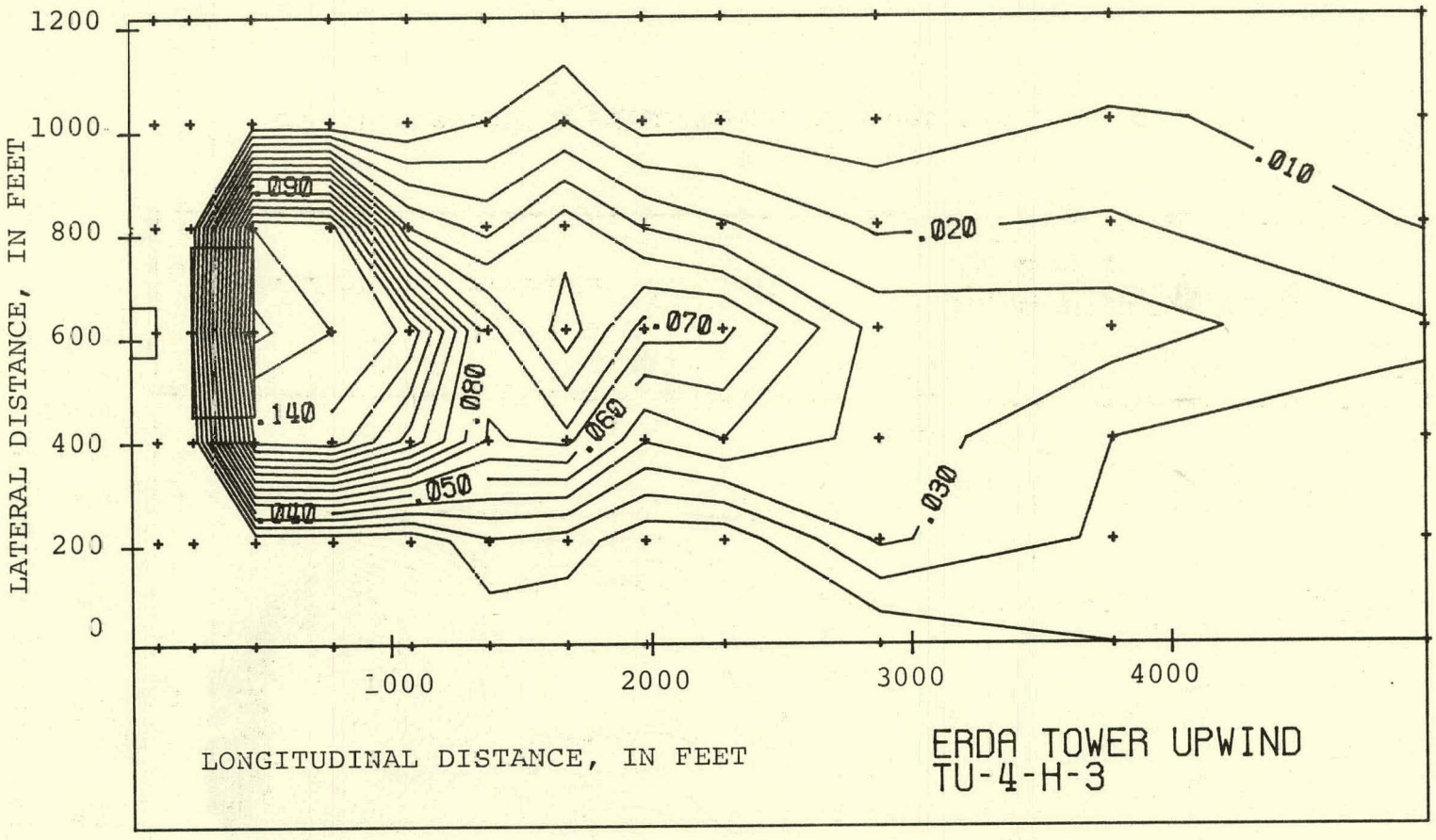

(d) Horizontal Distribution, 150 Feet Above the Ground

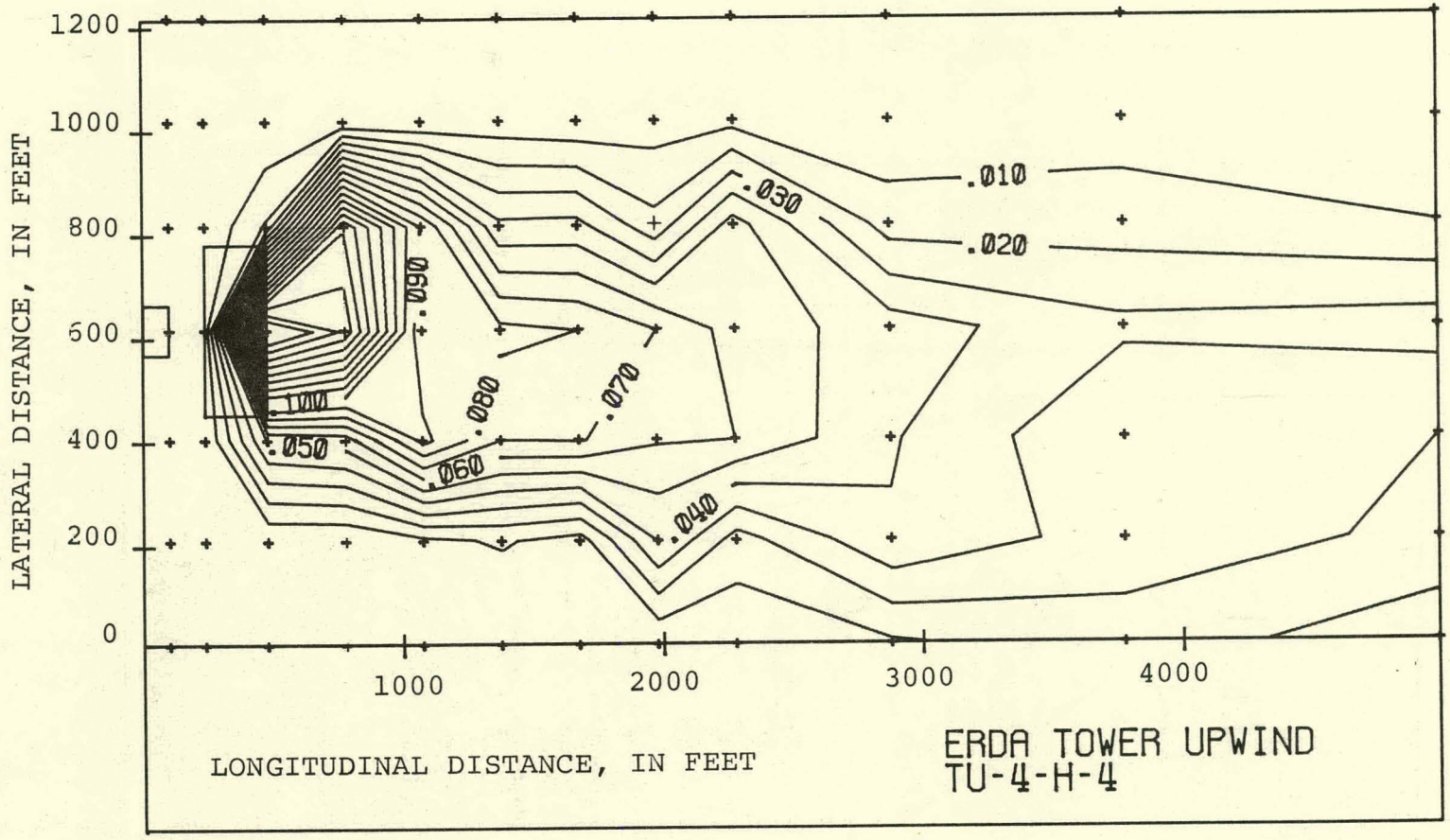

(e) Horizontal Distribution, 210 Feet Above the Ground

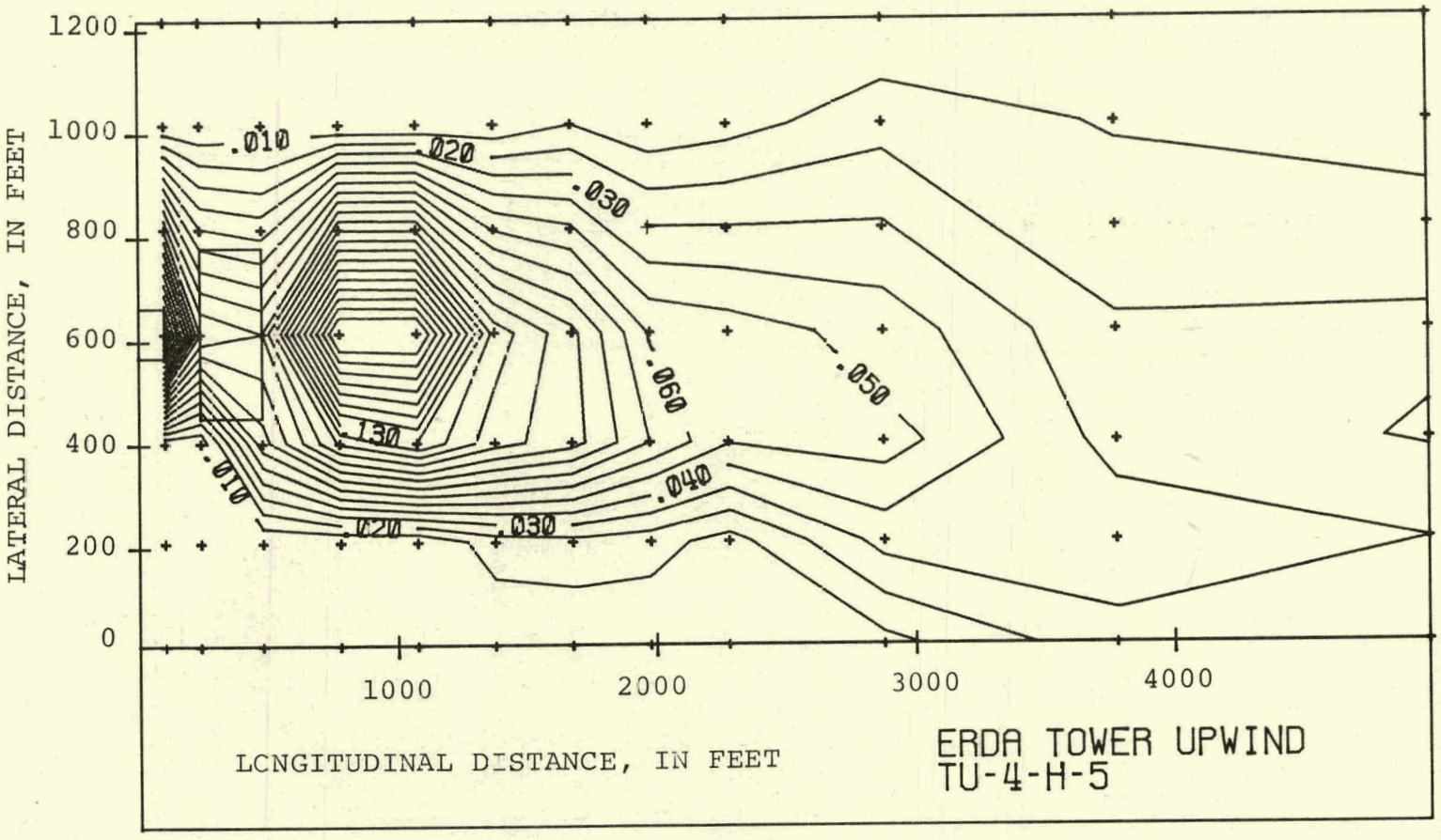

(f) Horizontal Distribution, 270 Feet Above the Ground

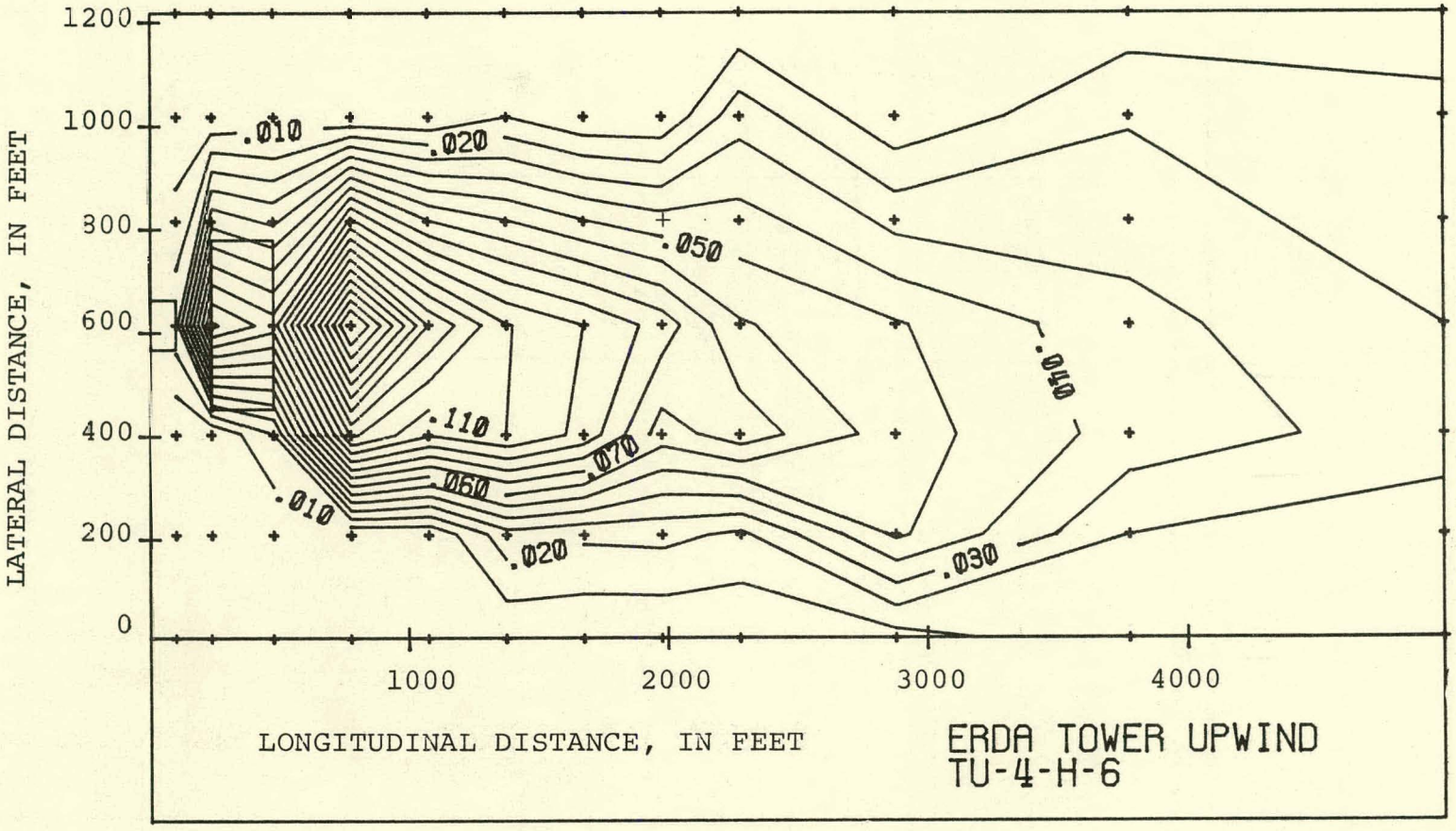

(g) Horizontal Distribution, 330 Feet Above the Ground

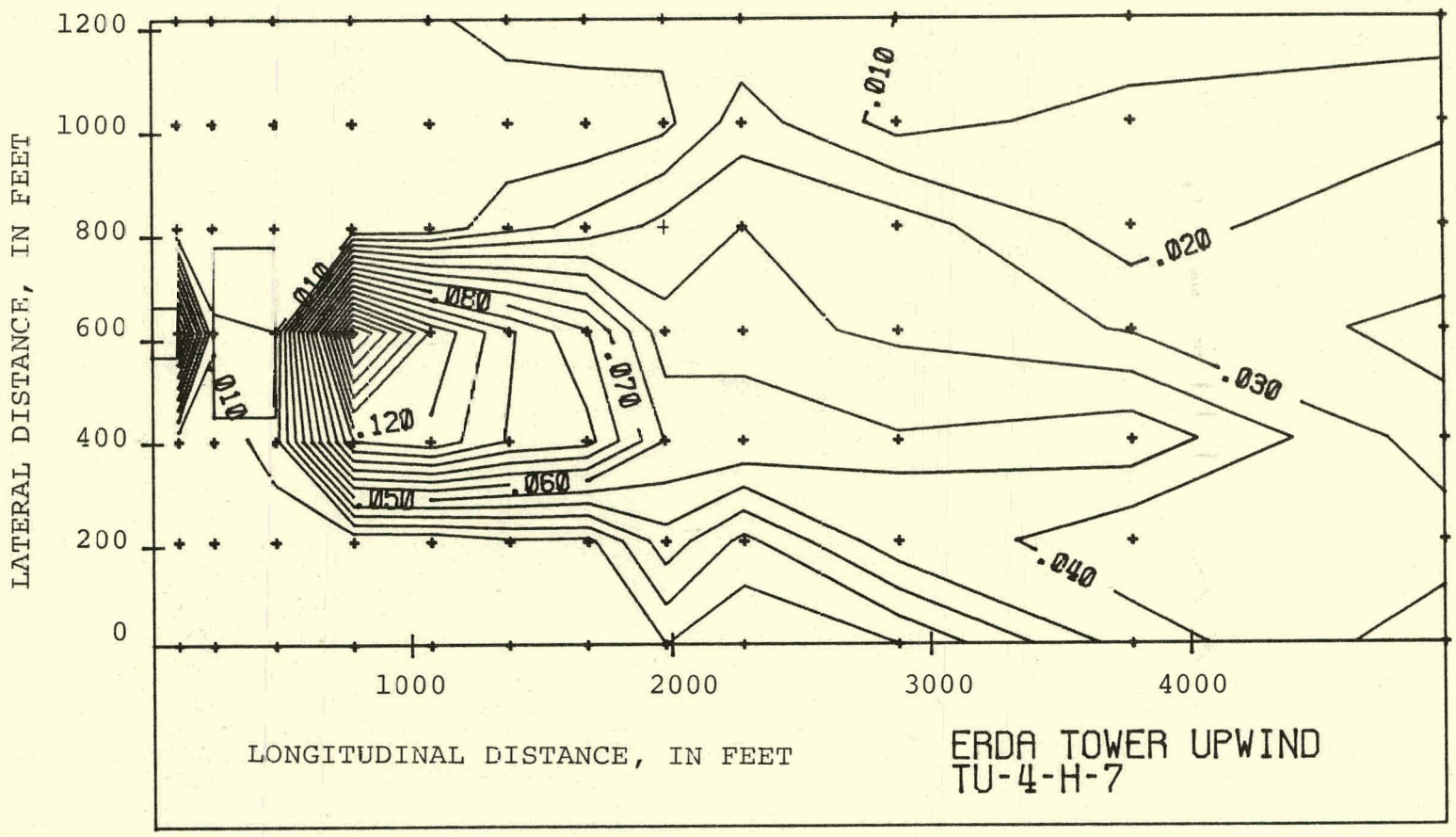

(h) Horizontal Distribution, 390 Feet Above the Ground

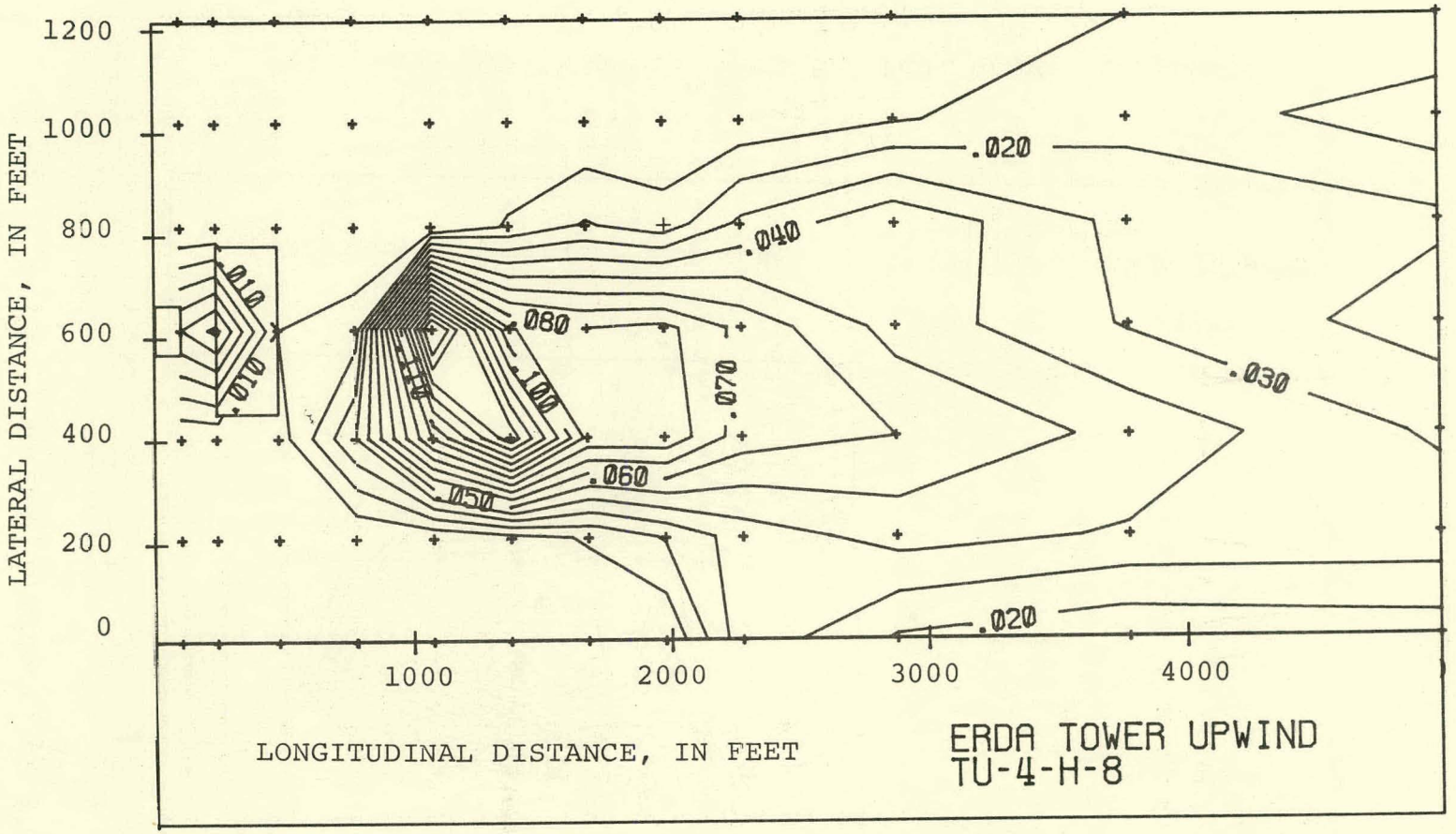

(i) Horizontal Distribution, 450 Feet Above the Ground

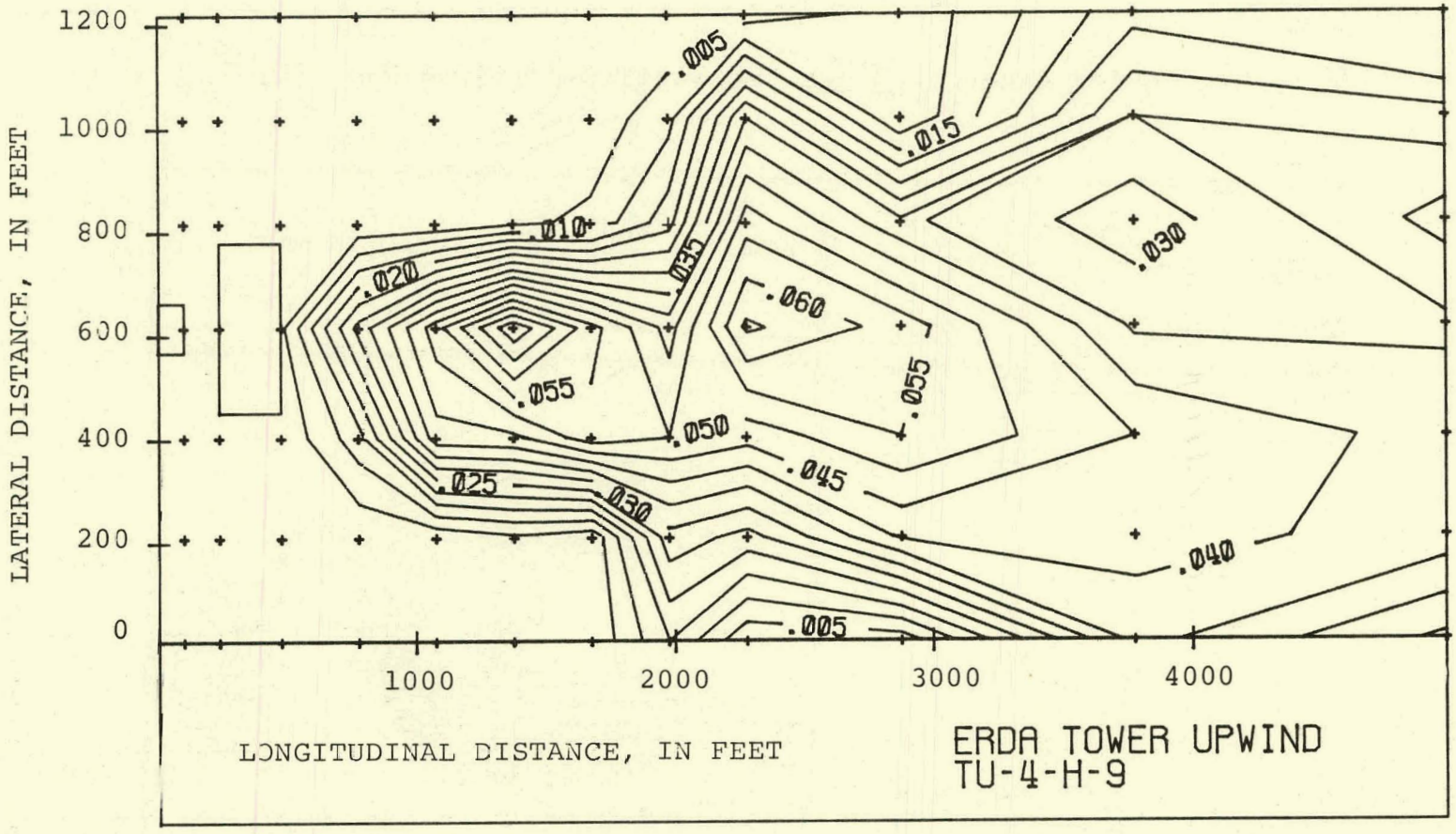

(j) Horizontal Distribution, 510 Feet Above the Ground

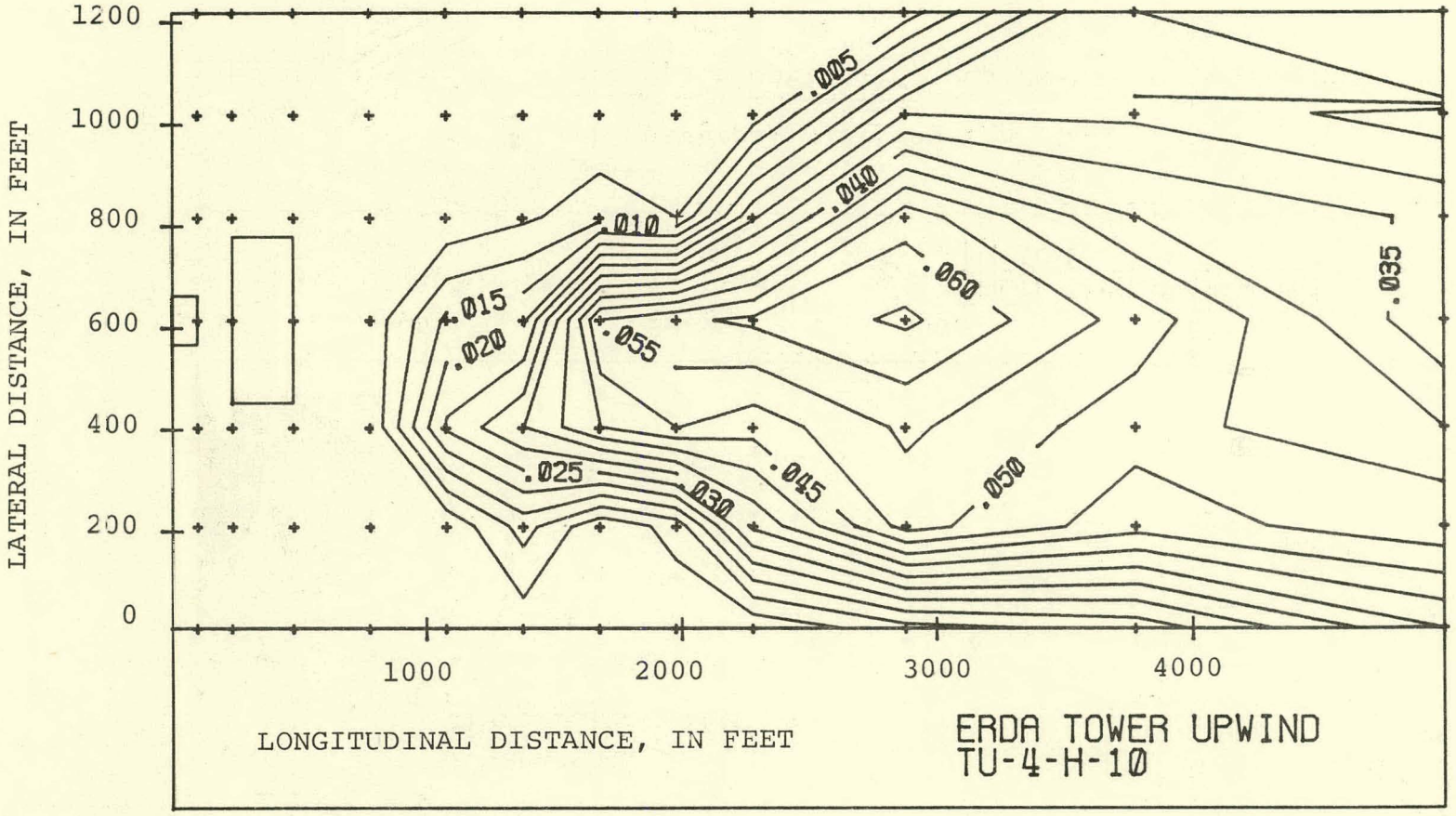

(k) Horizontal Distribution, 570 Feet Above the Ground

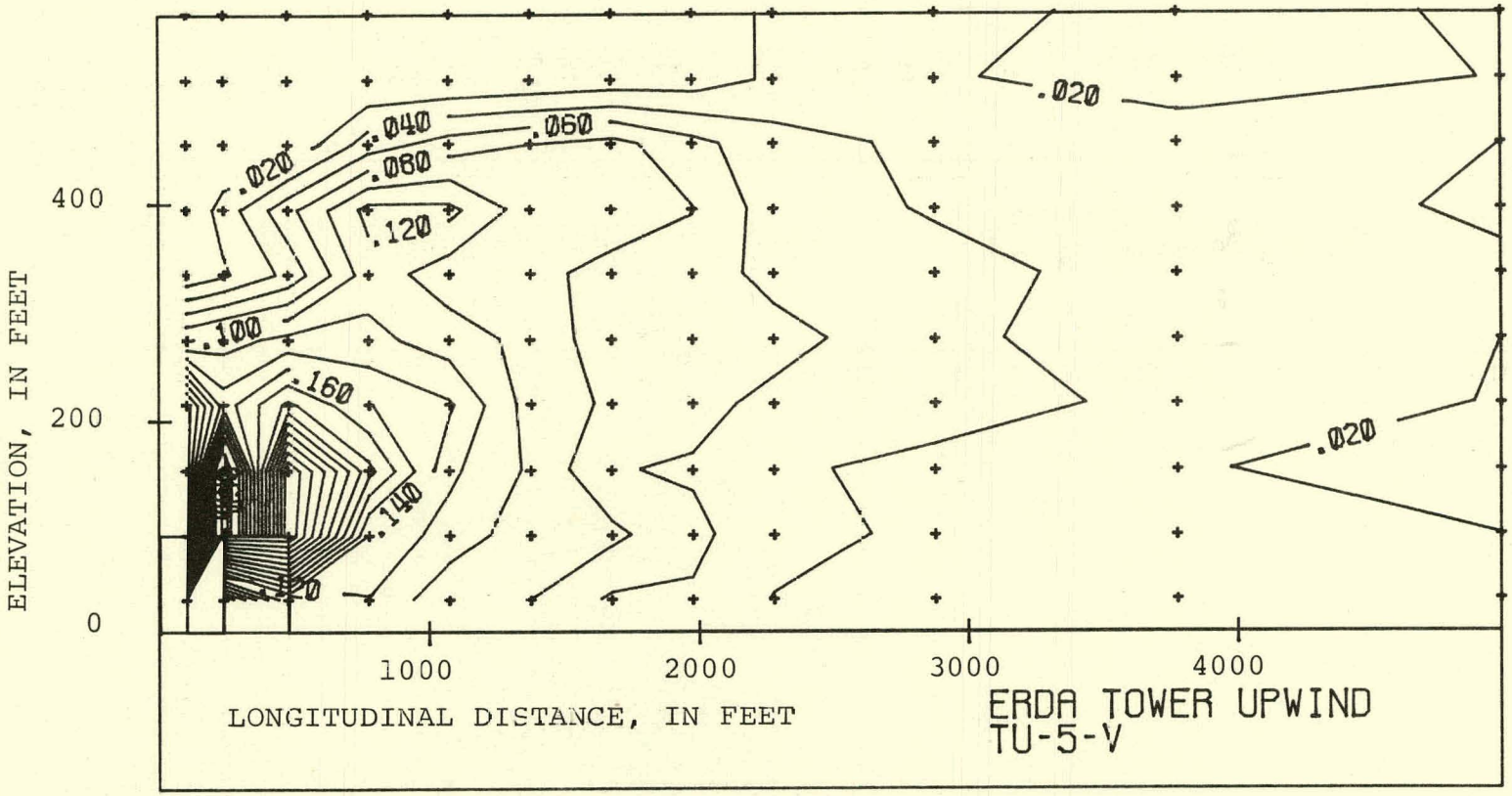

(a) Vertical Distribution

FIGURE 4.30 Temperature Distribution for Run TU-5. V_a = 29.8 MPH.

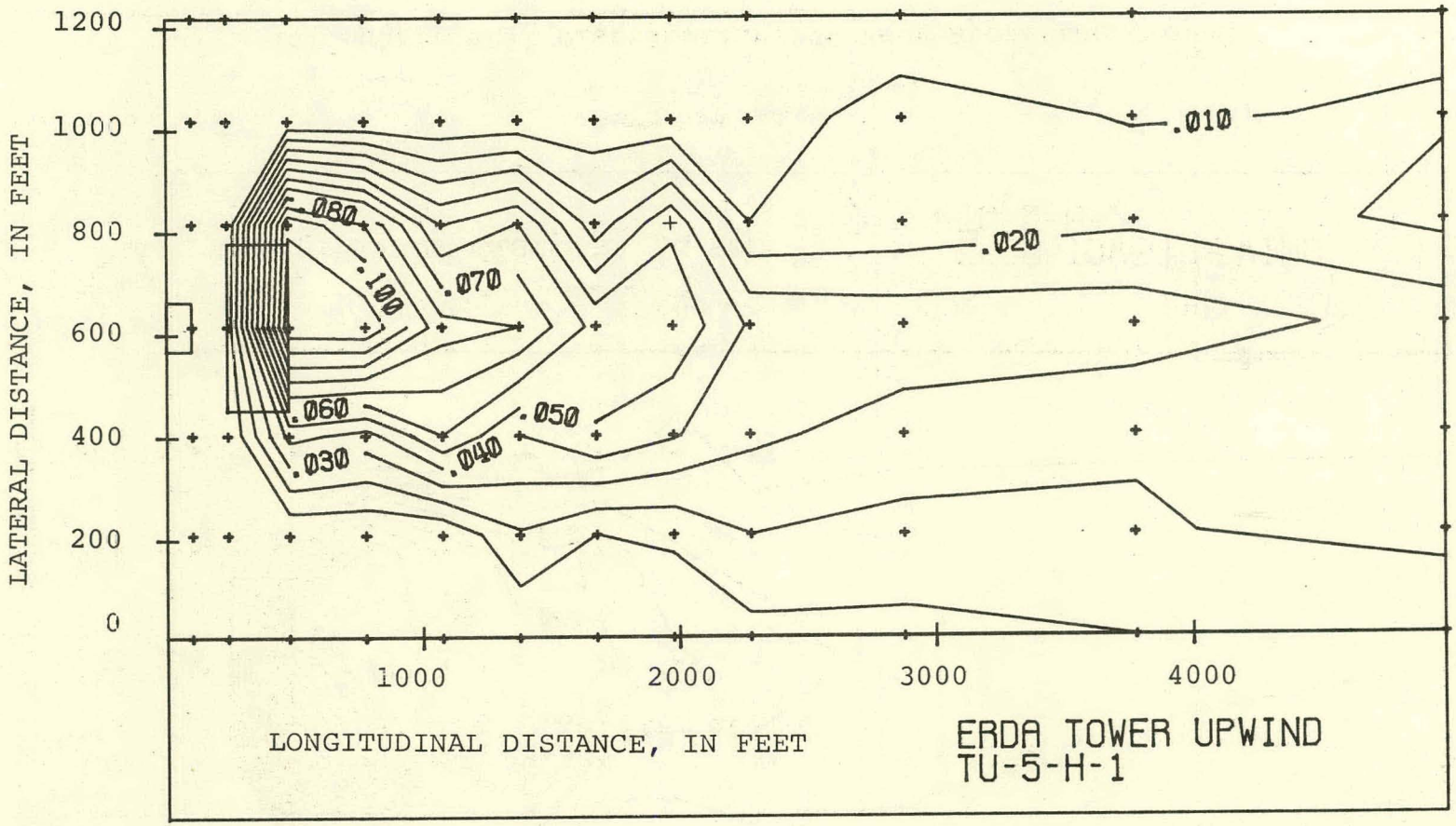

(b) Horizontal Distribution, 30 Feet Above the Ground

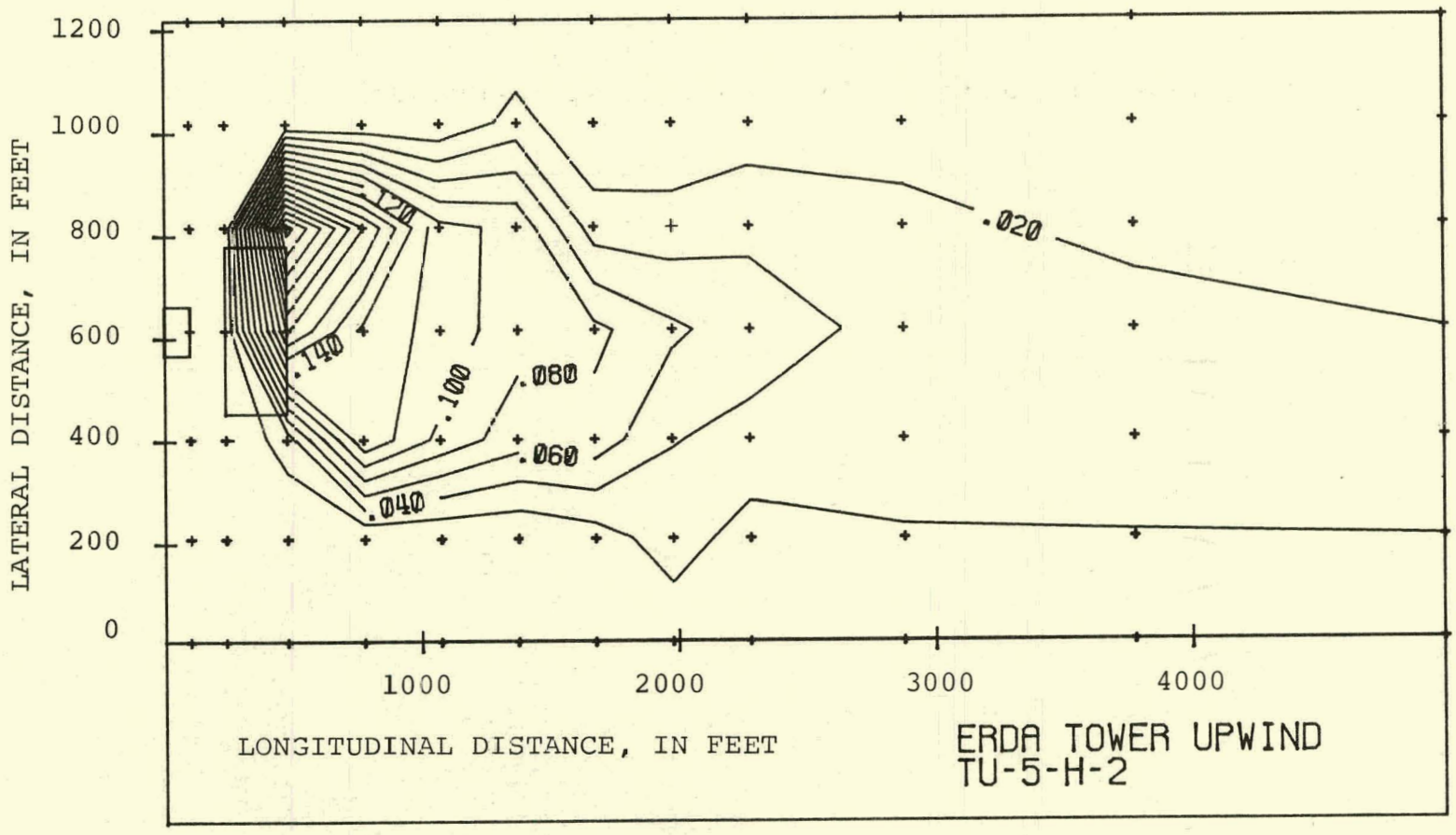

(c) Horizontal Distribution, 90 Feet Above the Ground

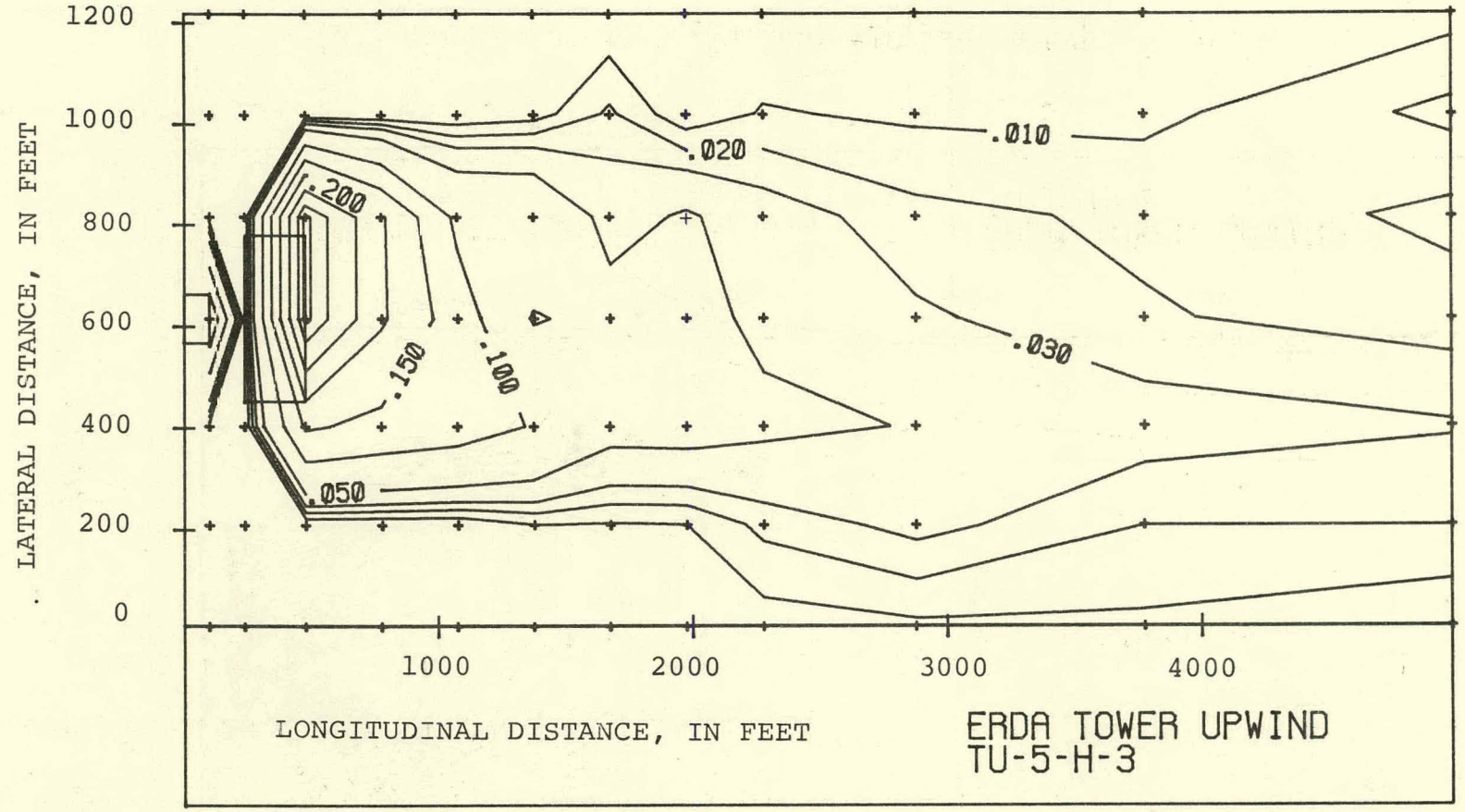

(d) Horizontal Distribution, 150 Feet Above the Ground

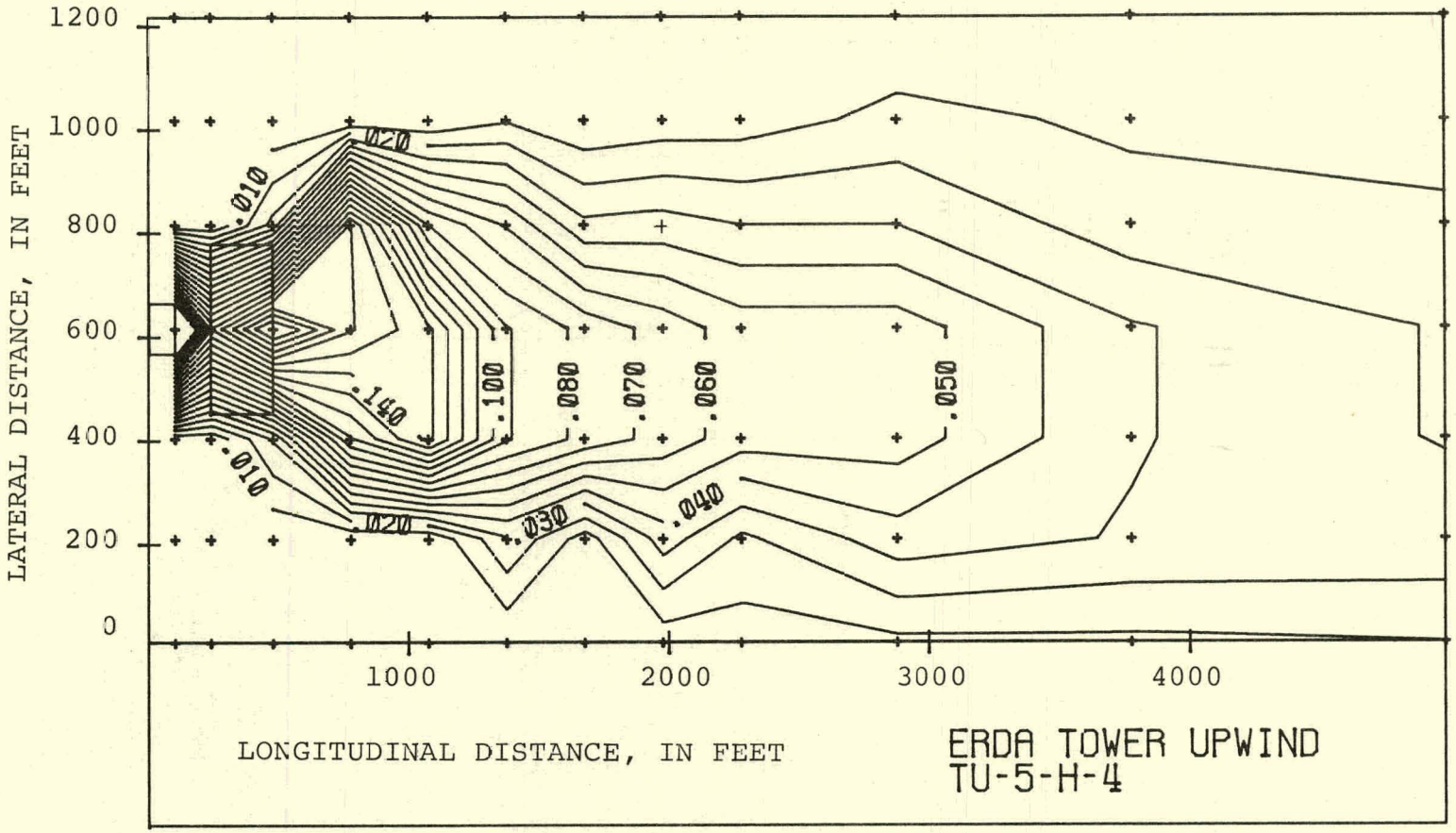

(e) Horizontal Distribution, 2_0 Feet Above the Ground

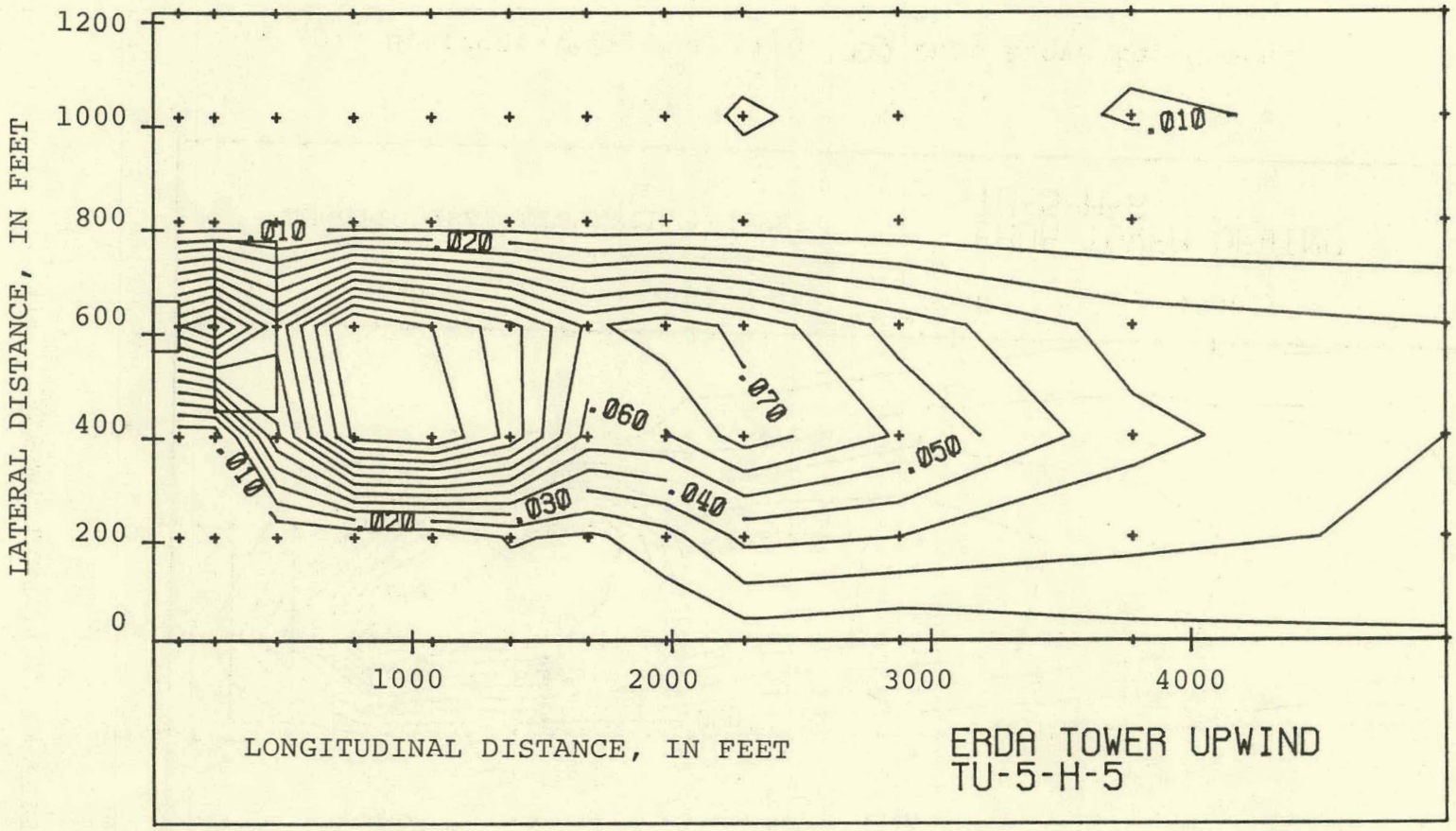

(f) Horizontal Distribution, 270 Feet Above the Ground

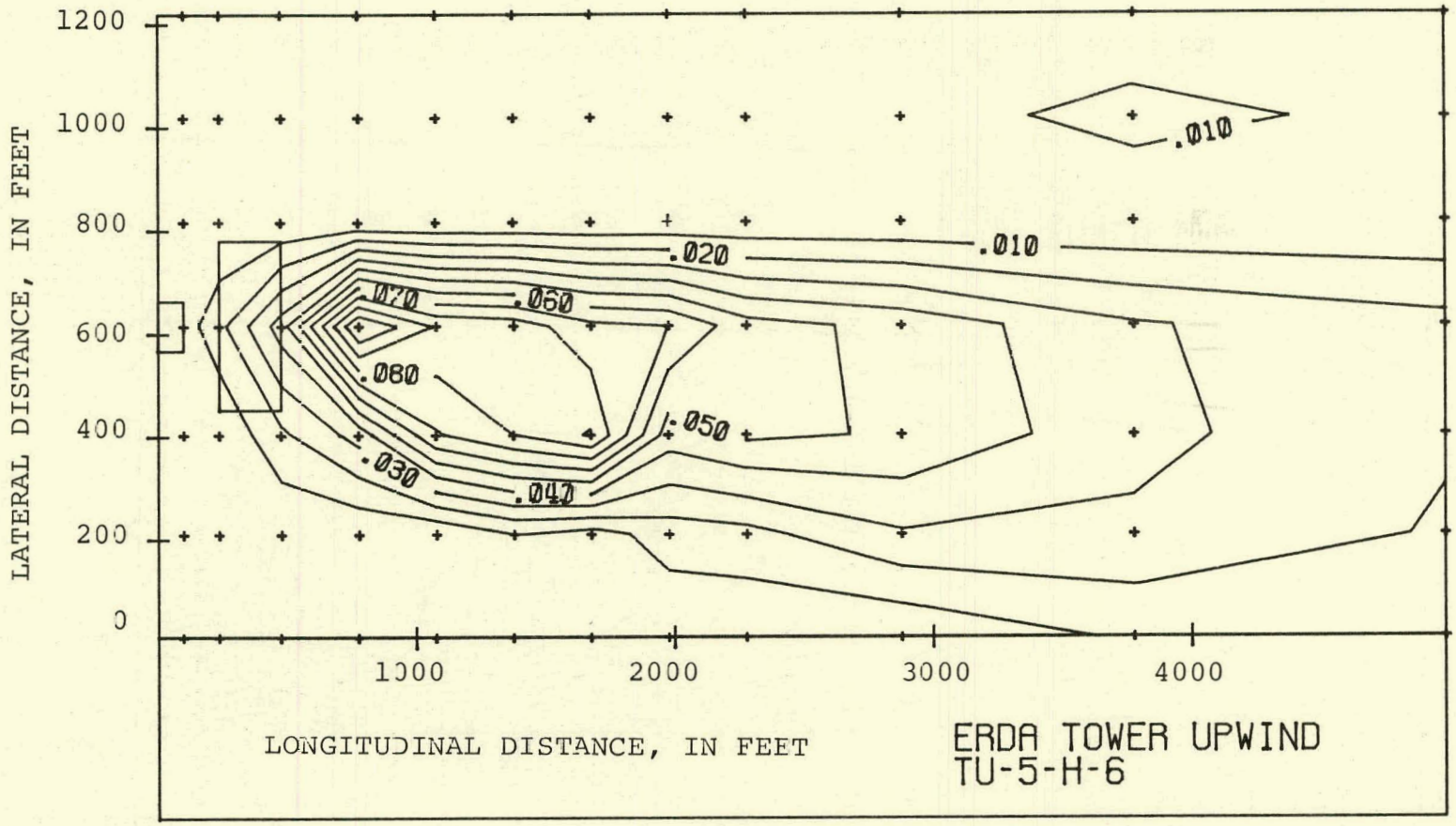

(g) Horizontal Distribution, 330 Feet Above the Ground

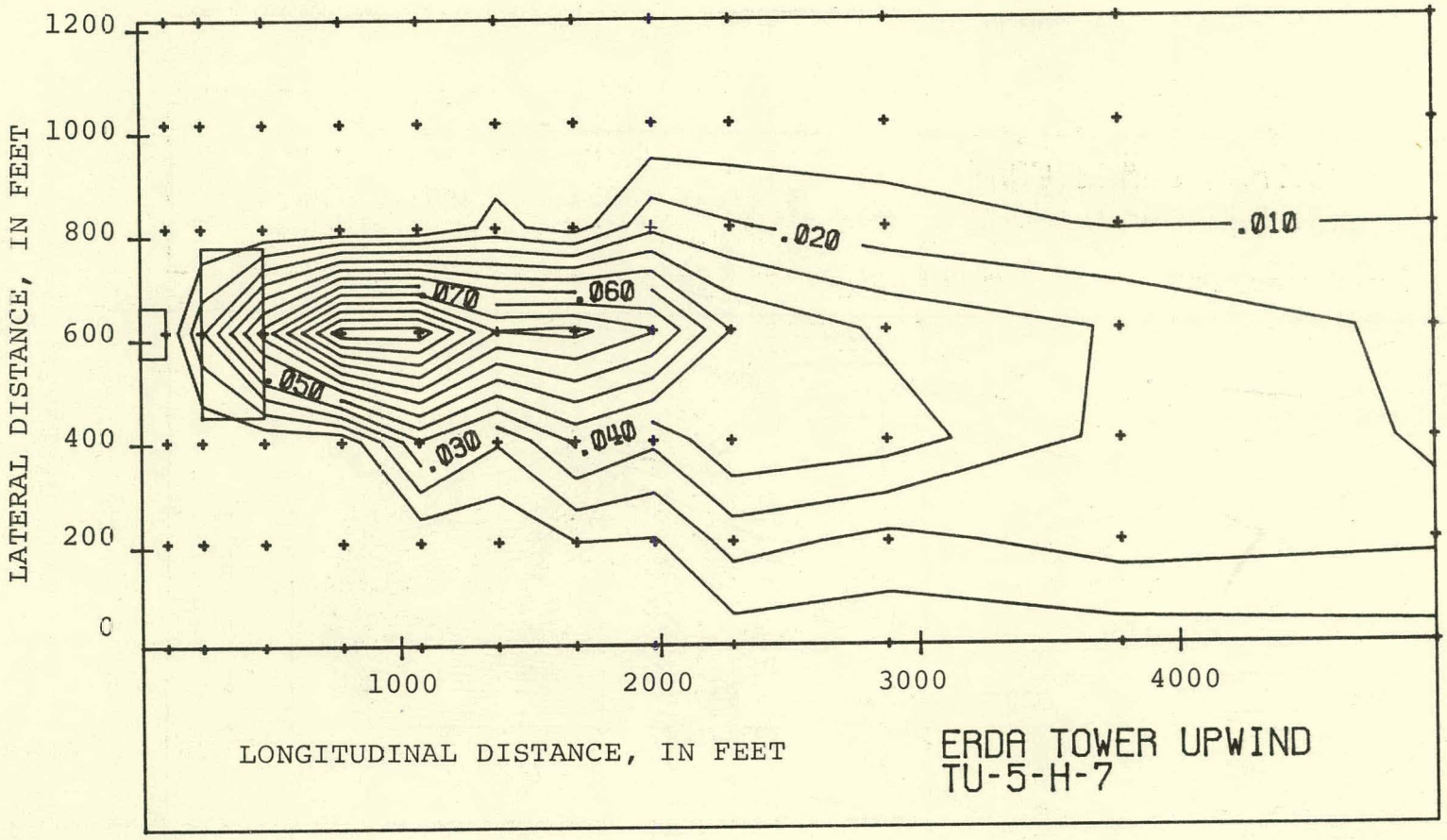

(h) Horizontal Distribution, 390 Feet Above the Ground

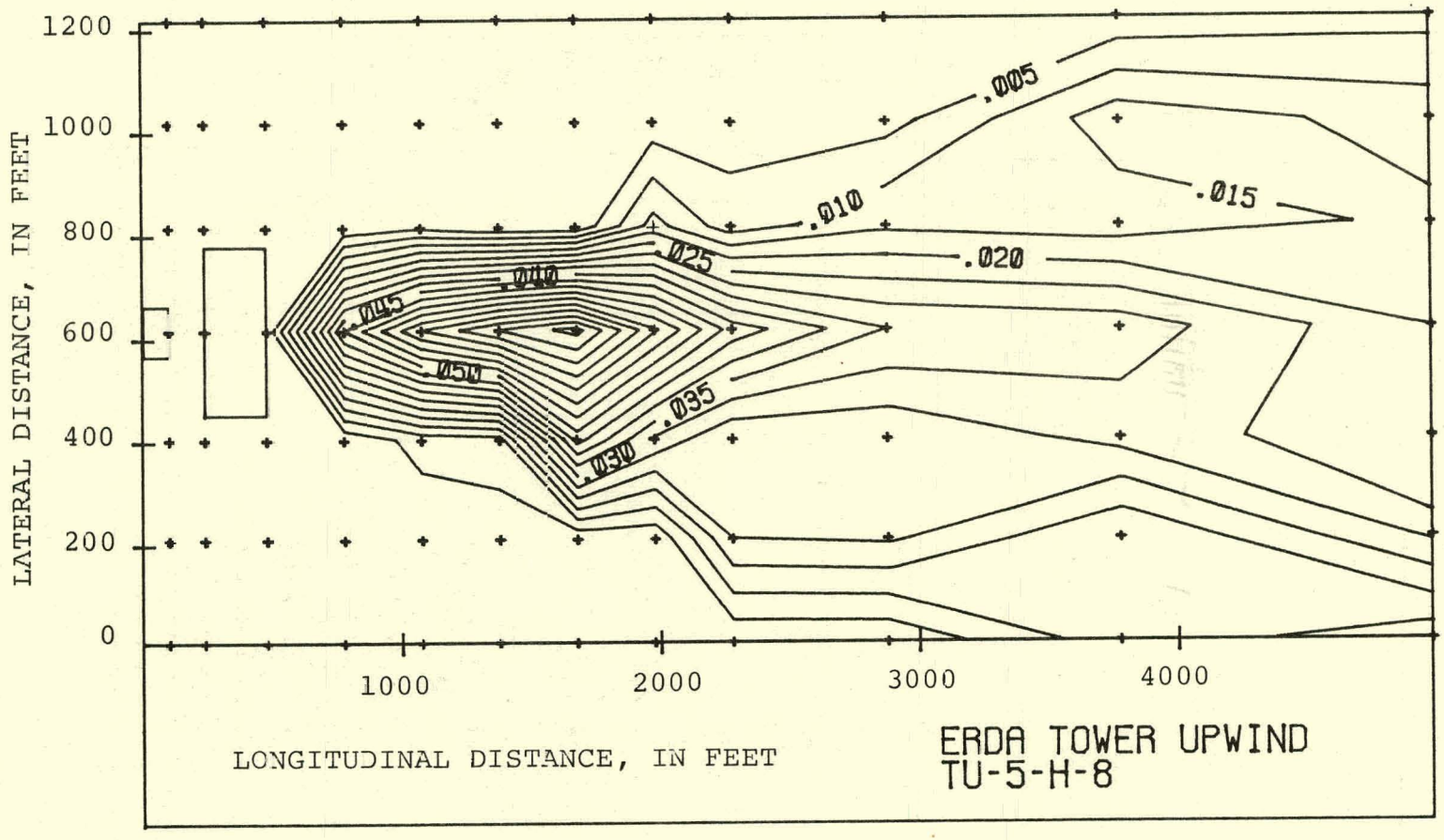

(i) Horizontal Distribution, 450 Feet Above the Ground

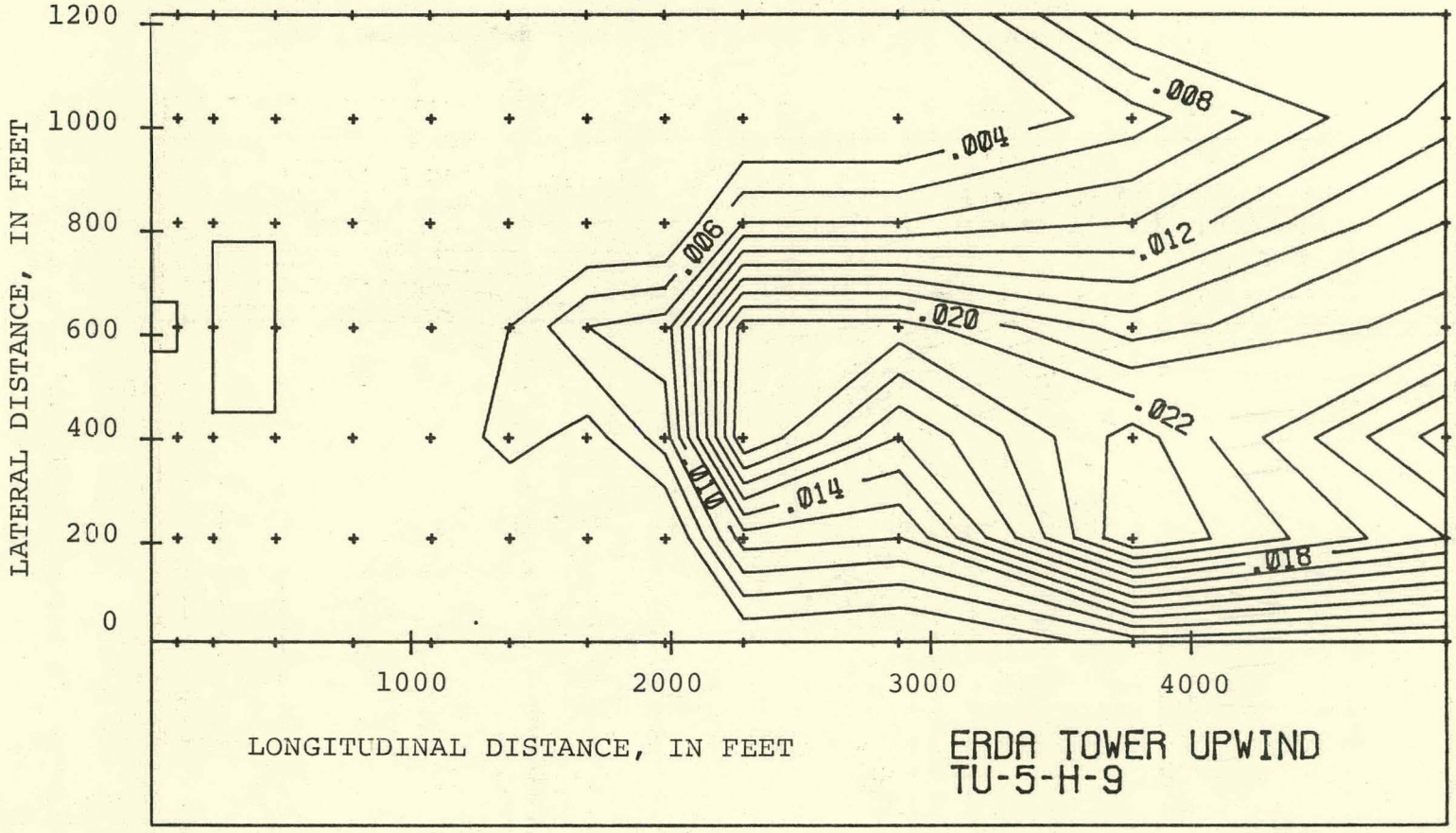

(j) Hcrizontal Distribution, 510 Feet Above the Ground

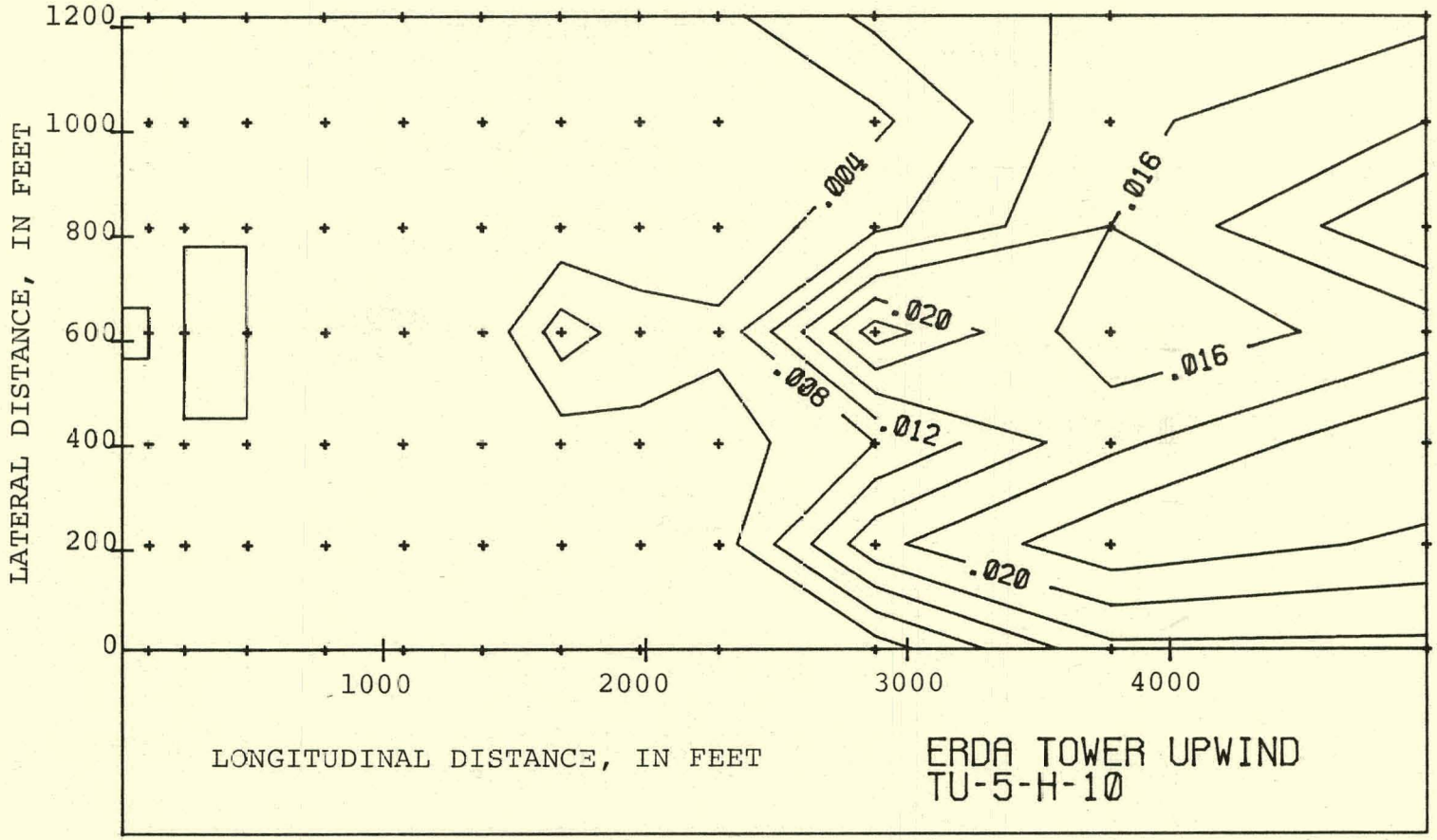

(k) Horizontal Distribution, 570 Feet Above the Ground

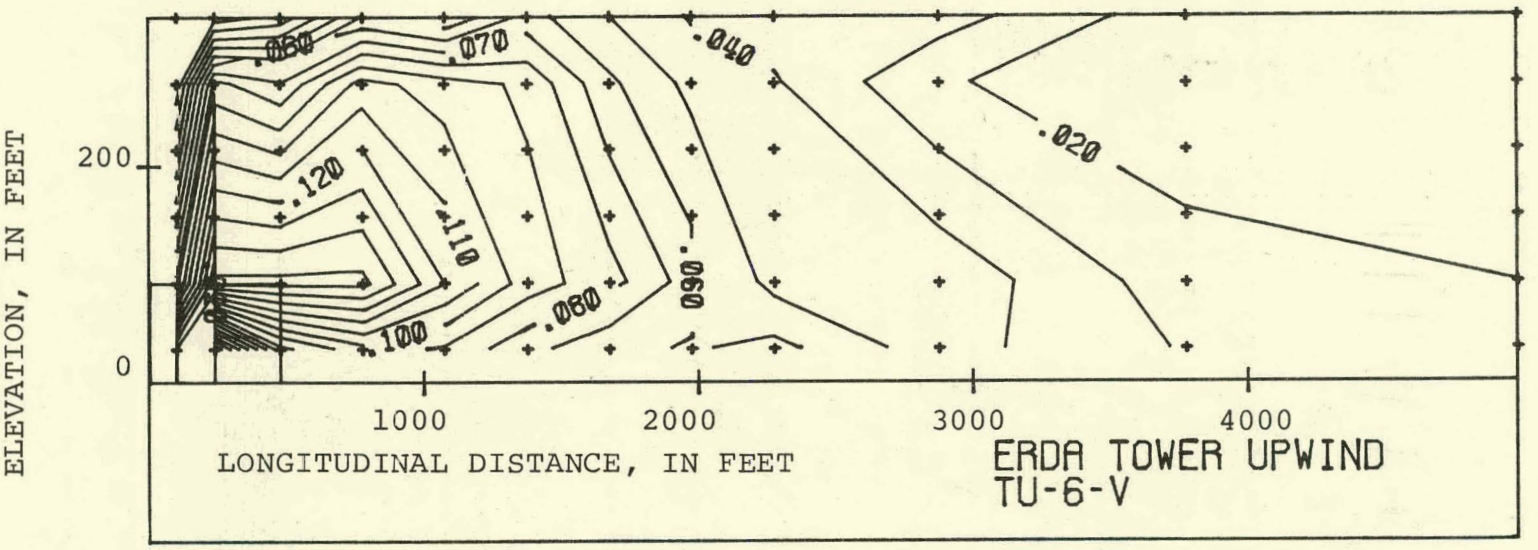

(a) Vertical Distribution

FIGURE 4.31 Temperature Distribution for Run TU-6. V_a = 39.1 MPH.

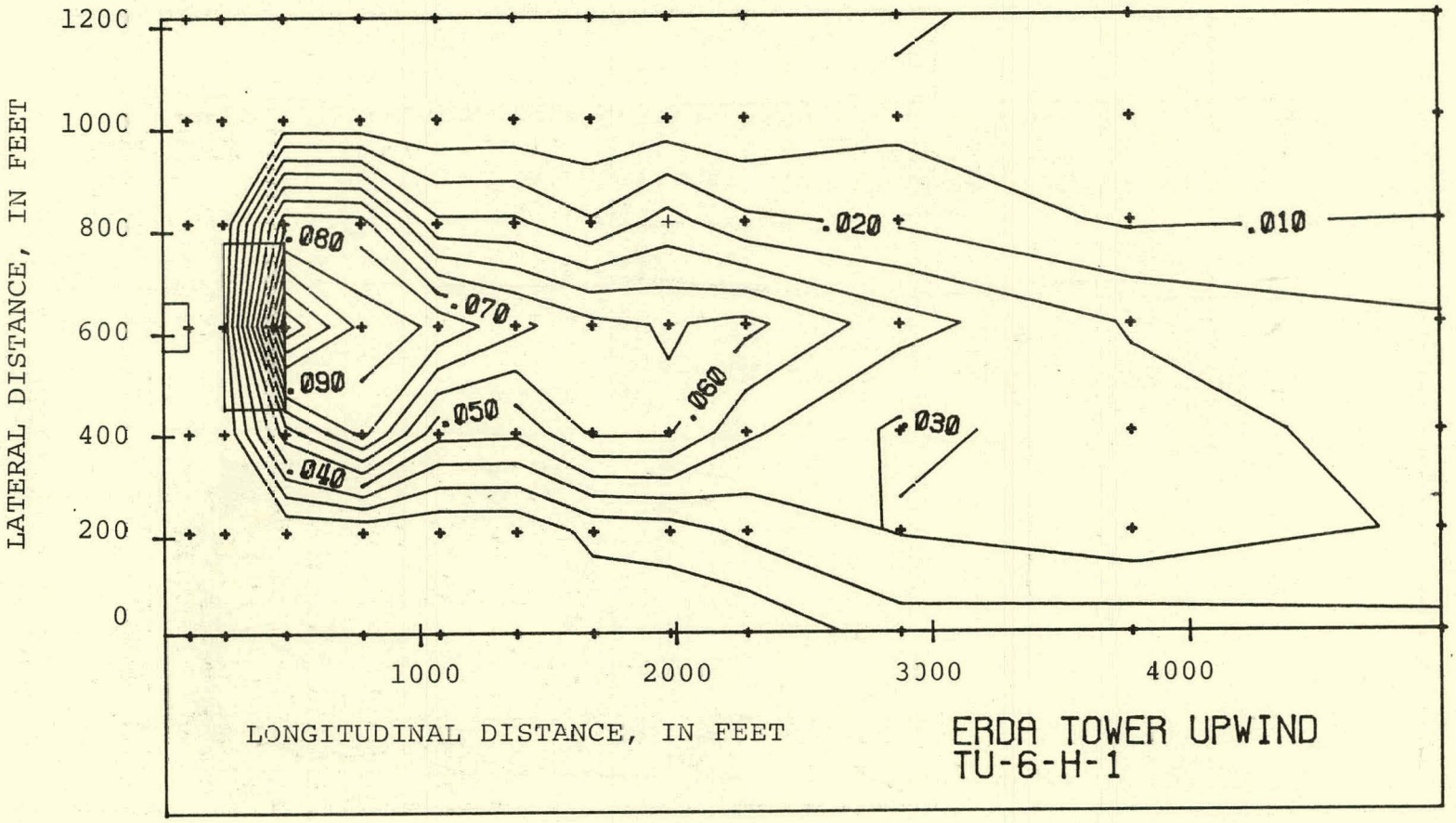

(b) Horizontal Distribution, 30 Feet Above the Ground

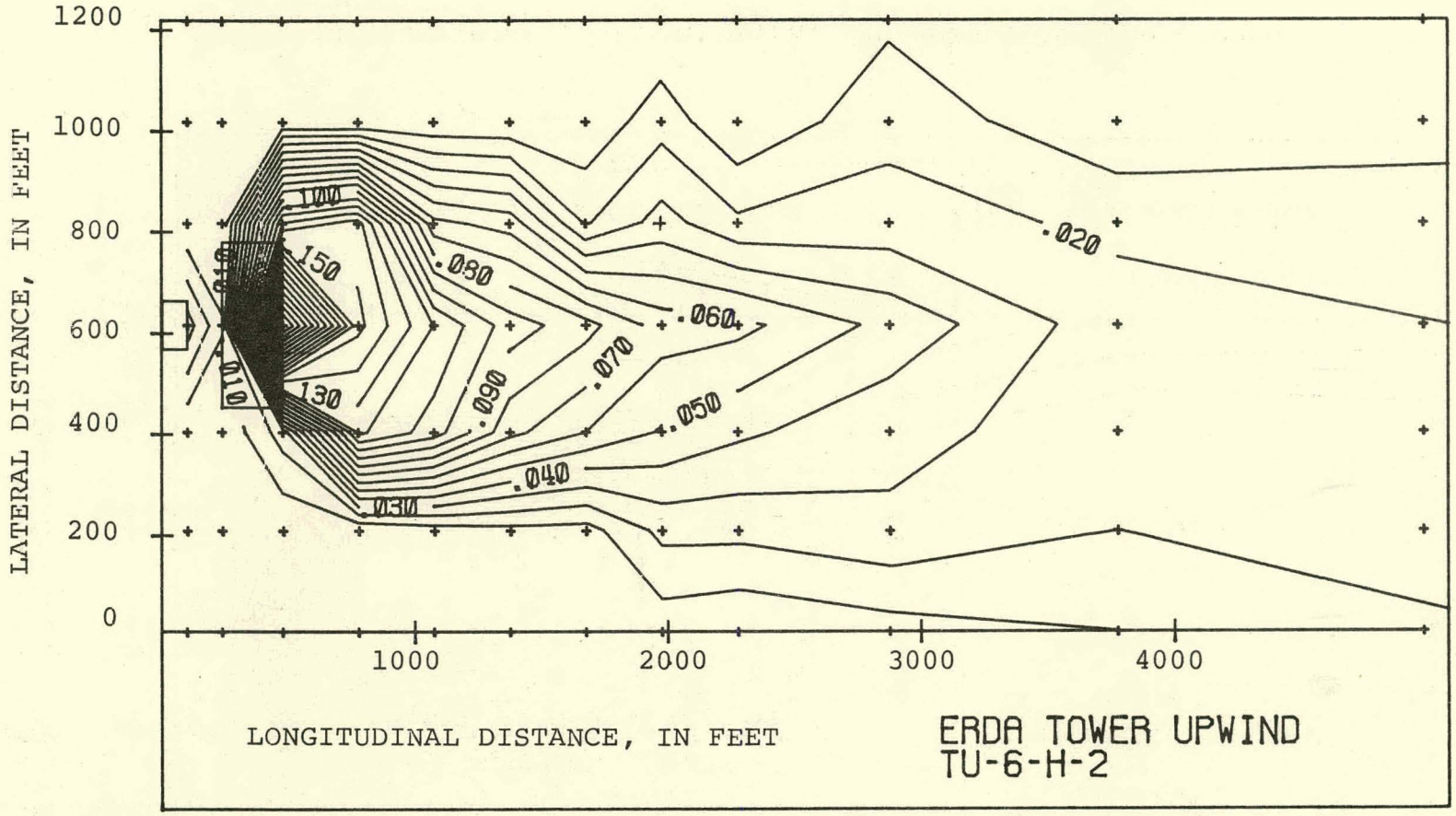

(c) Horizontal Distribution, 90 Feet Above the Ground

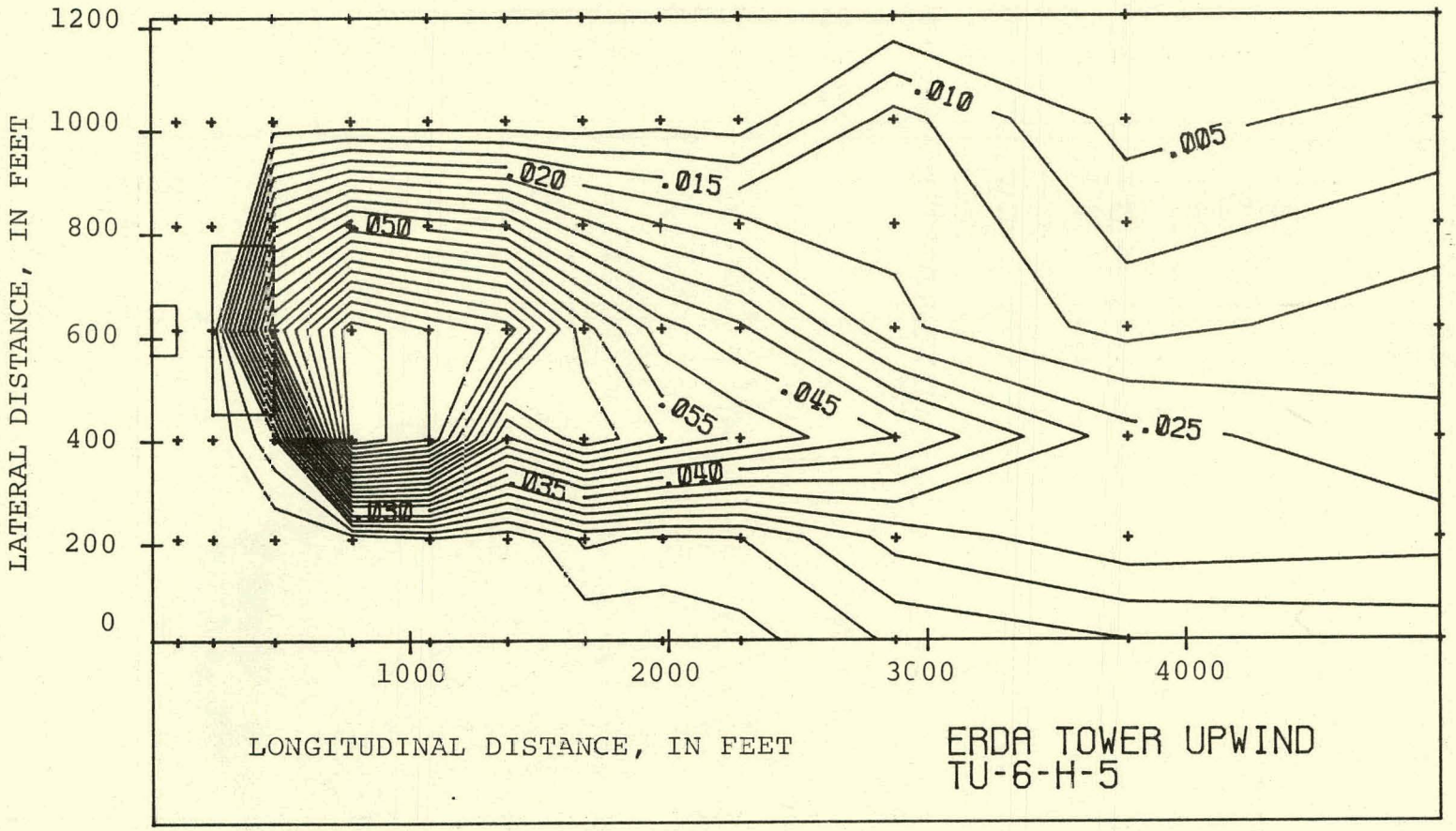

(d) Horizontal Distribution, 270 Feet Above the Ground

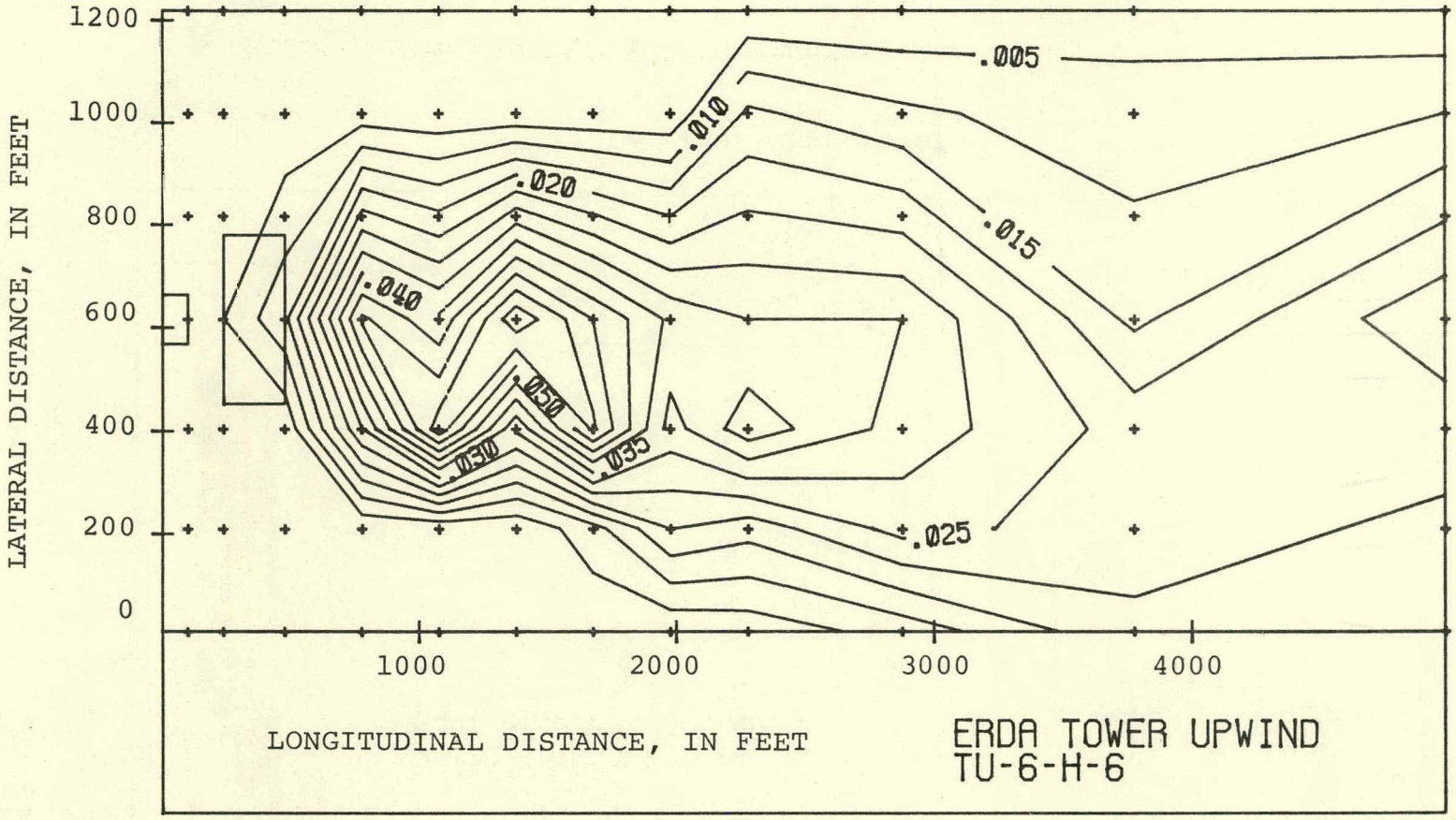

(e) Horizontal Distribution, 330 Feet Above the Ground

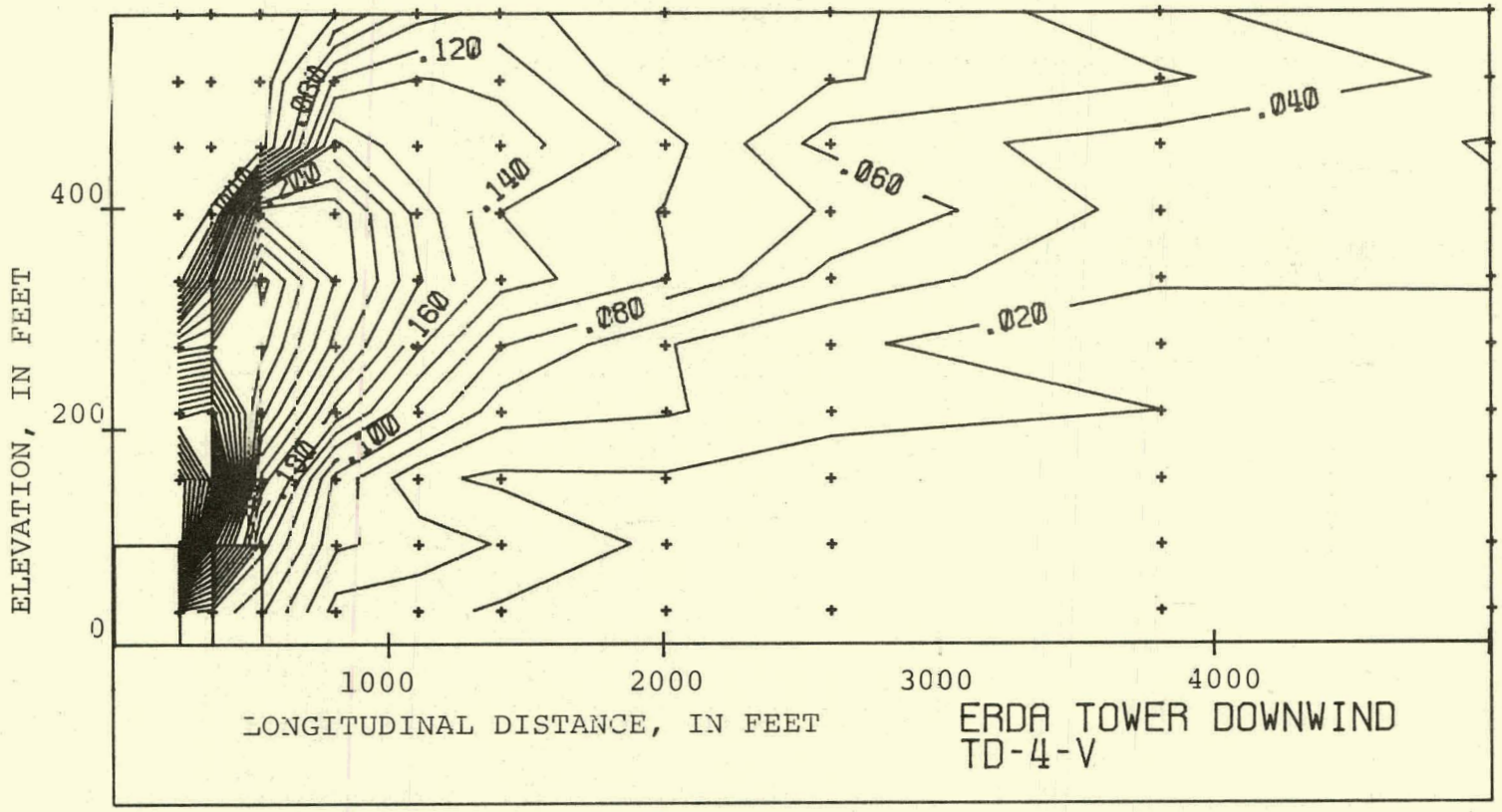

(a) Vertical Distribution

FIGURE 4.32 Temperature Distribution for Run TD-4. V_a = 19.8 MPH.

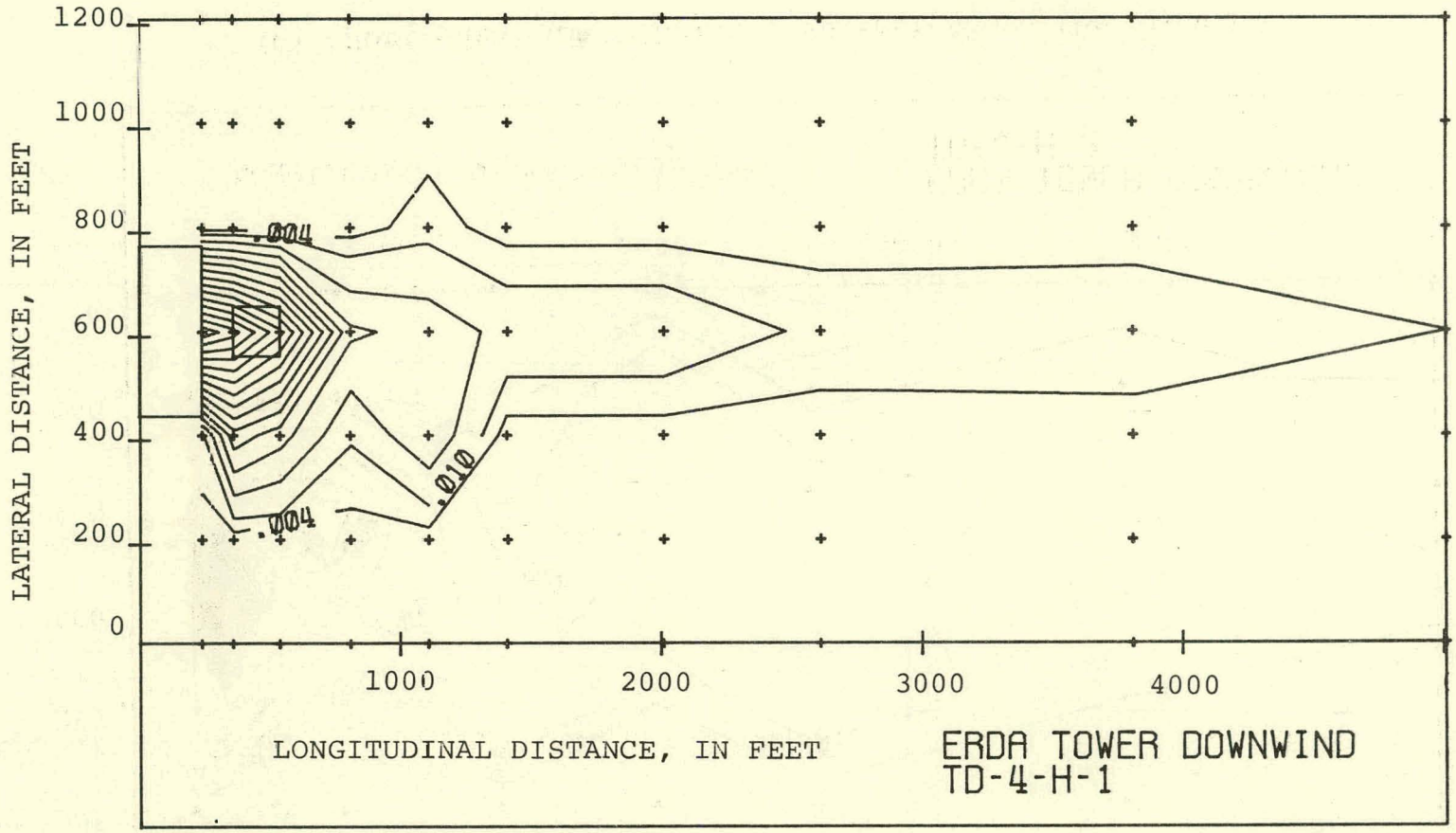

(b) Horizontal Distribution, 30 Feet Above the Ground

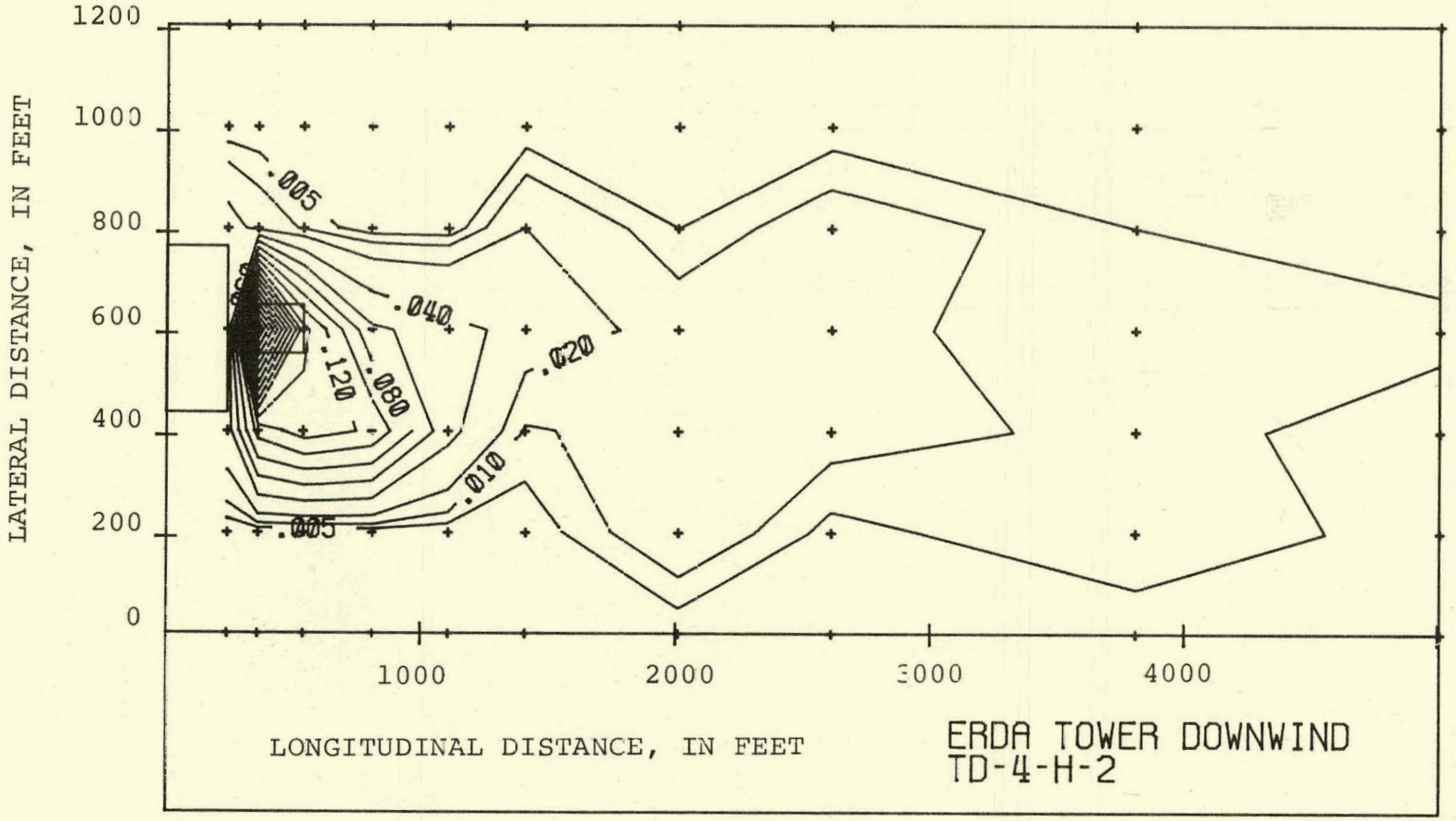

(c) Horizontal Distribution, 90 Feet Above the Ground

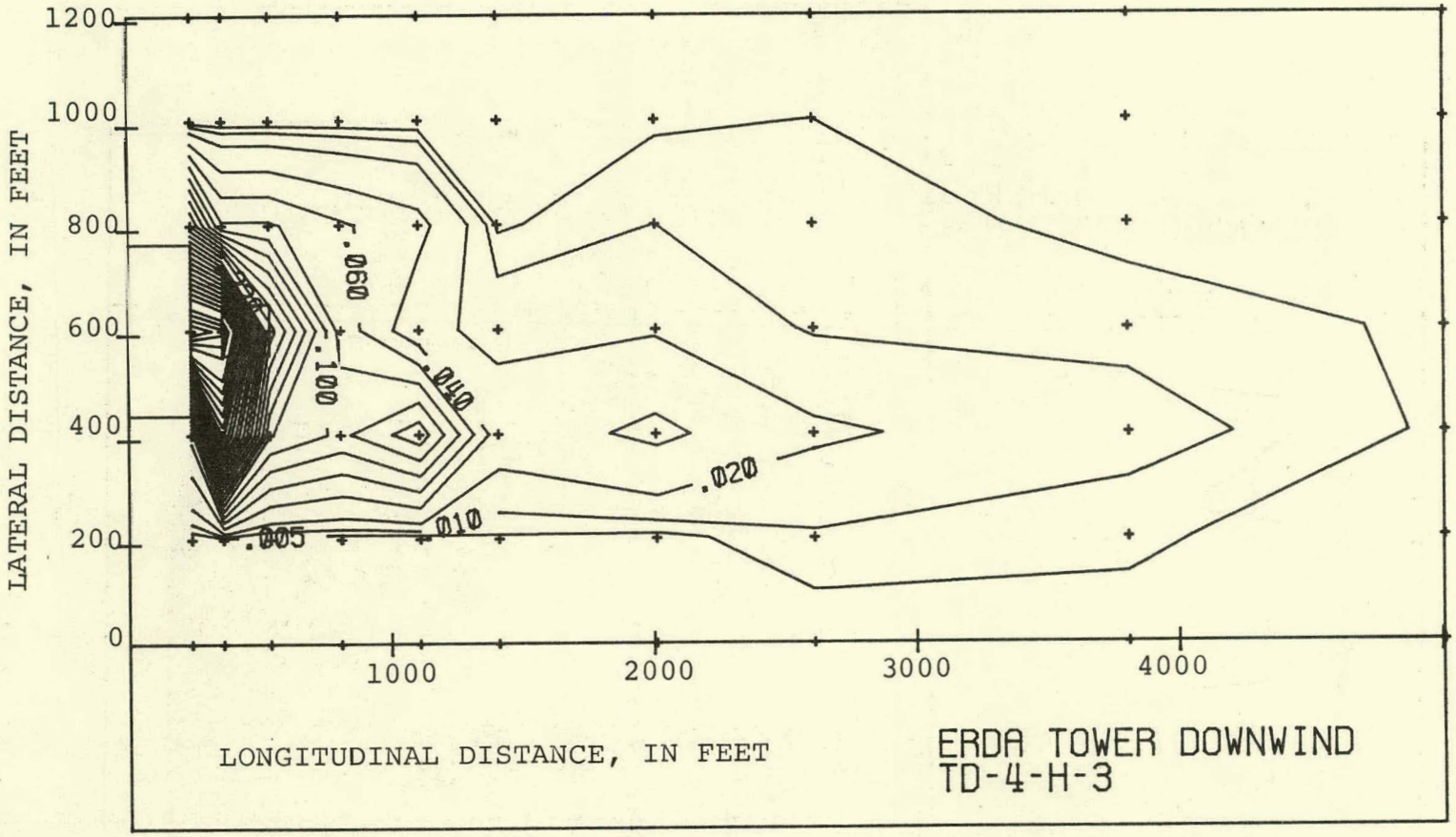

(d) Horizontal Distribution, 150 Feet Above the Ground

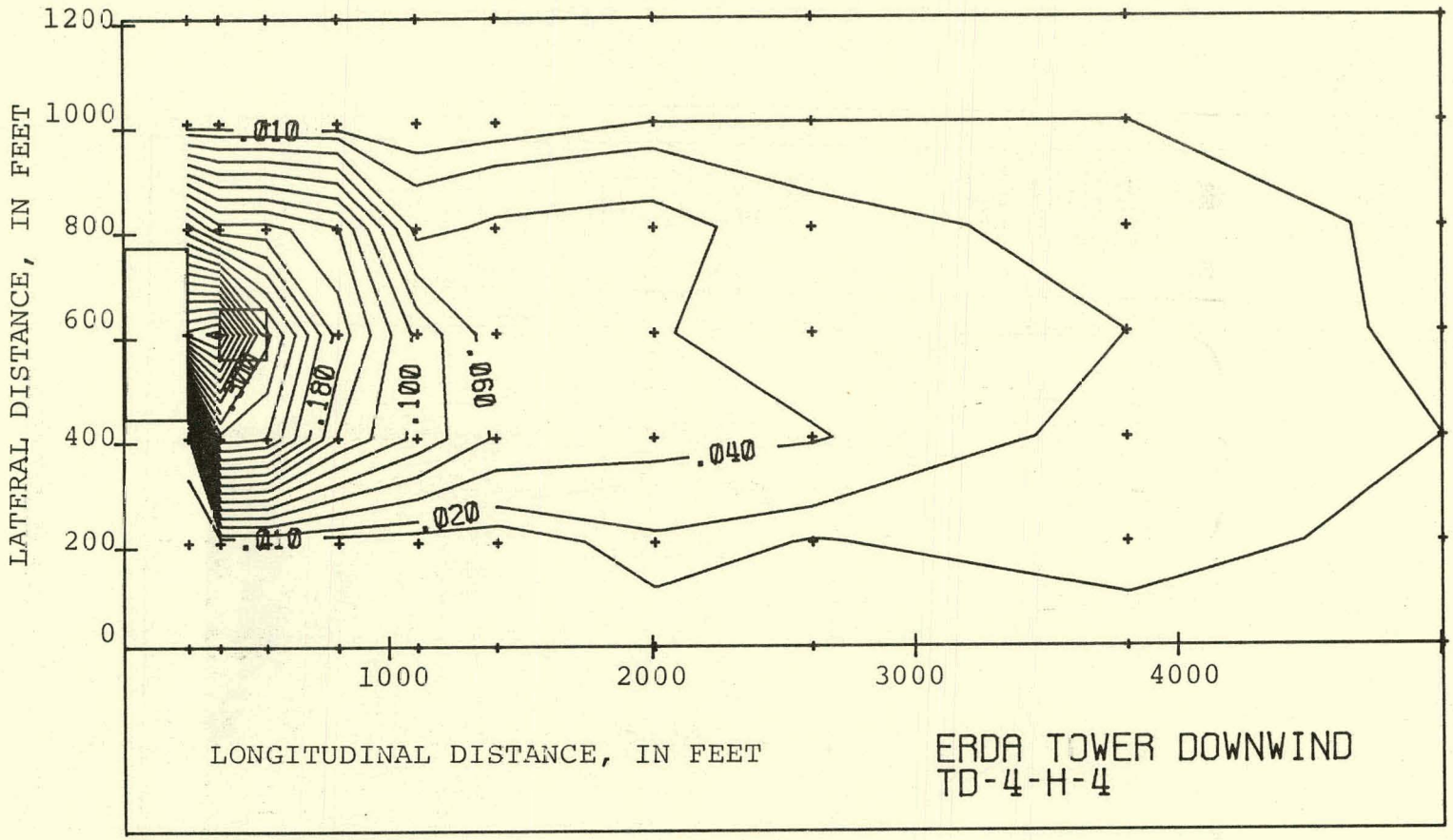

(e) Horizontal Distribution, 210 Feet Above the Ground

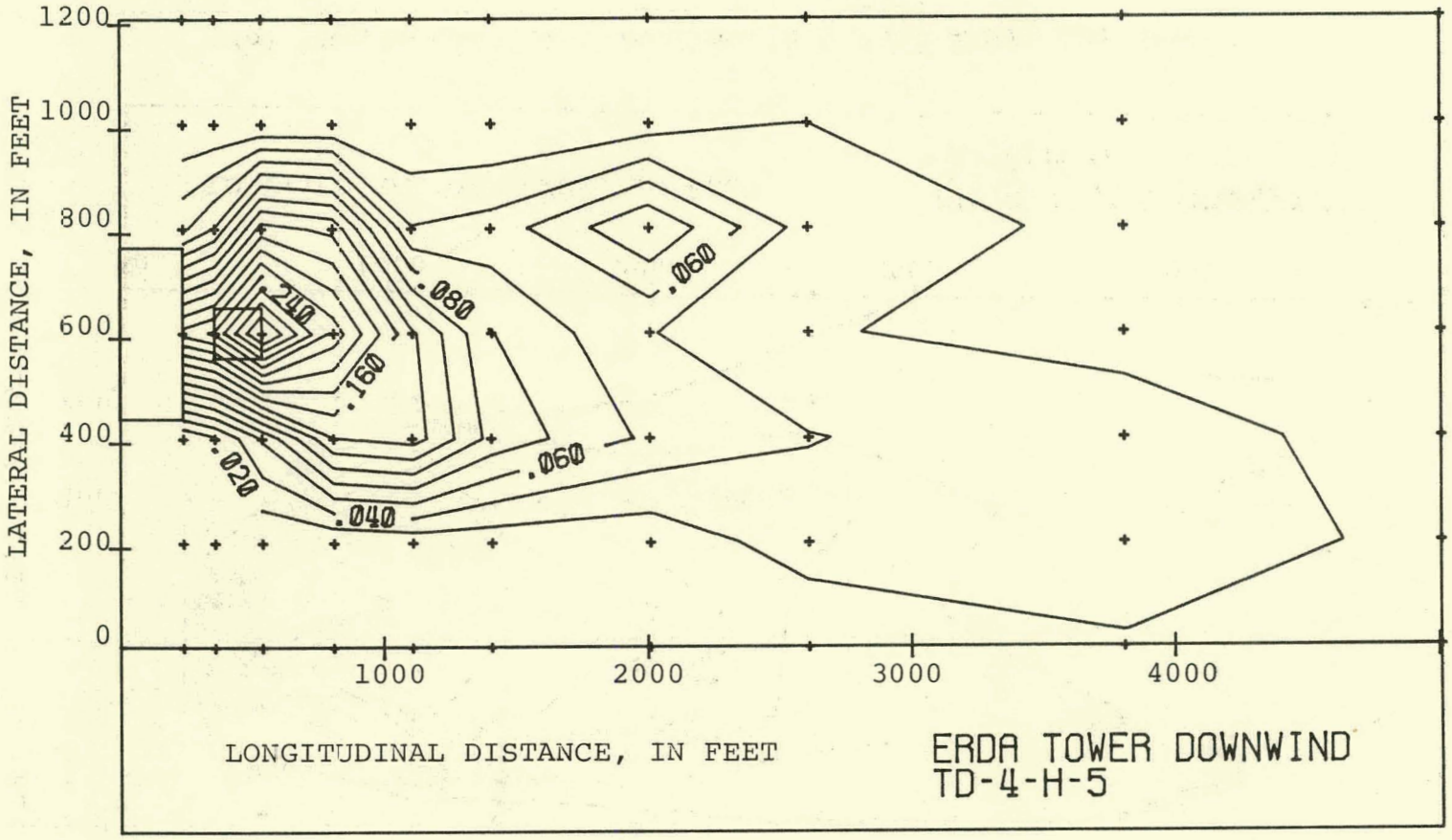

(f) Horizontal Distribution, 270 Feet Above the Ground

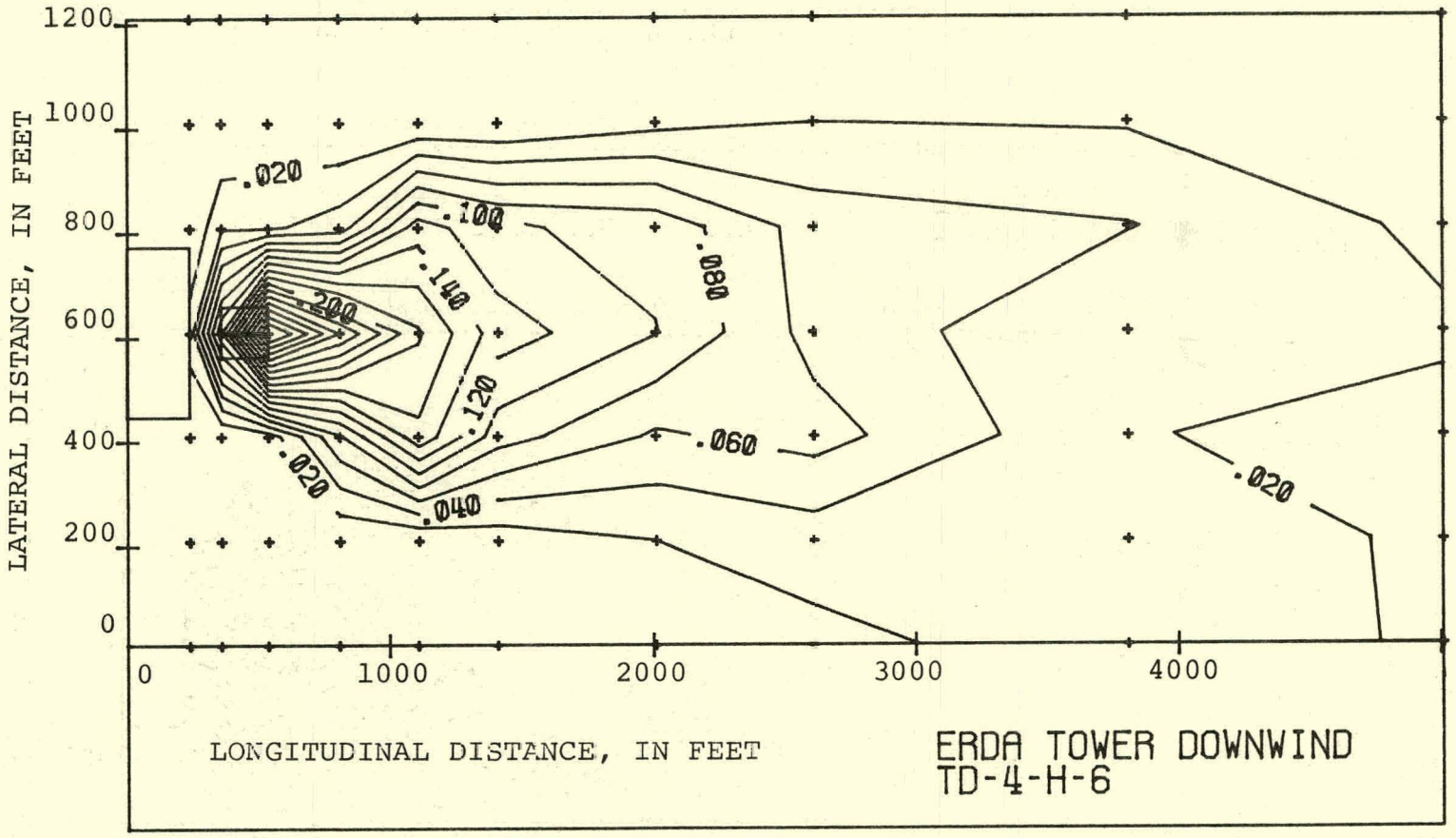

(g) Horizontal Distribution, 330 Feet Above the Ground

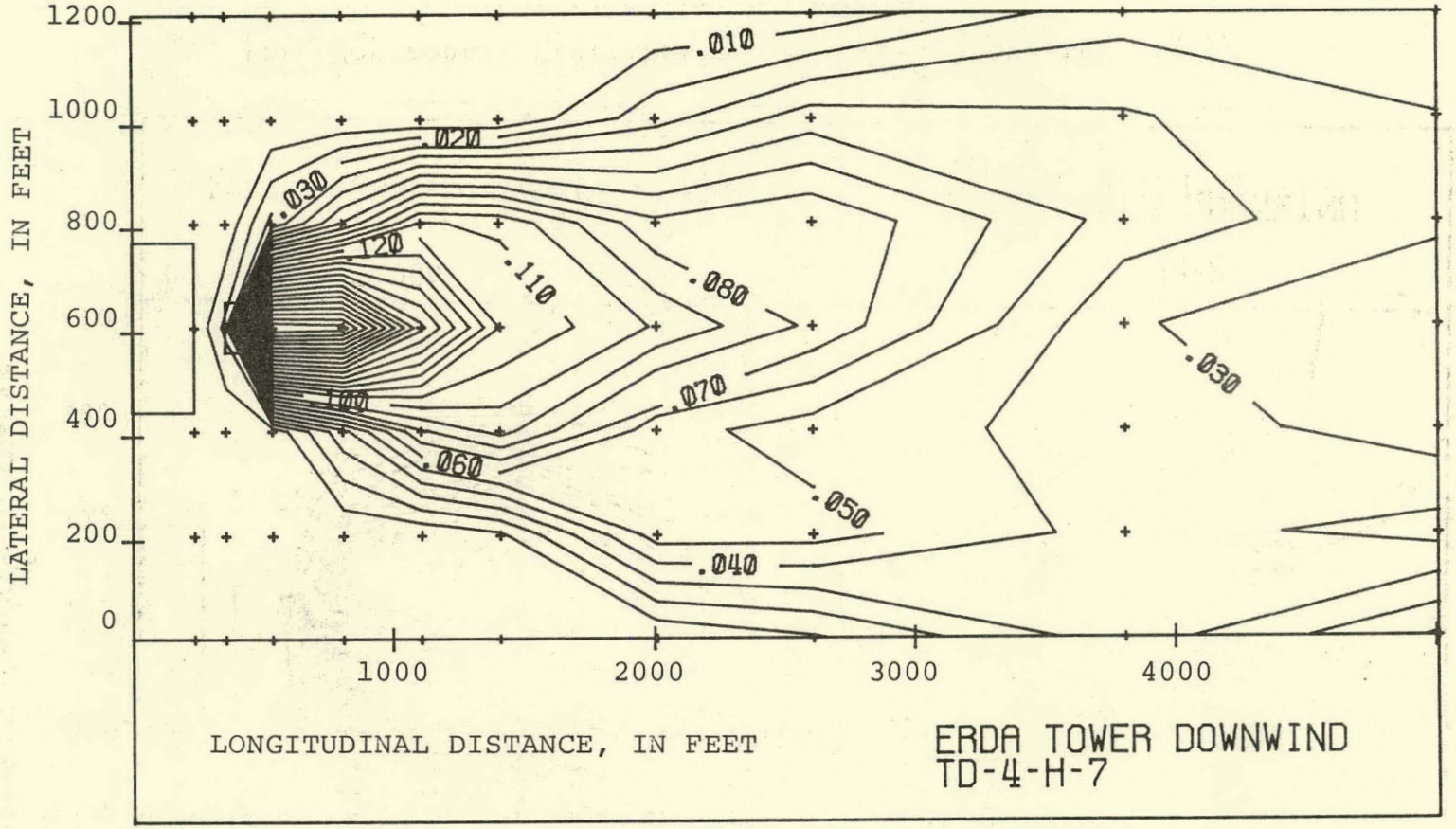

(h) Horizontal Distribution, 390 Feet Above the Ground

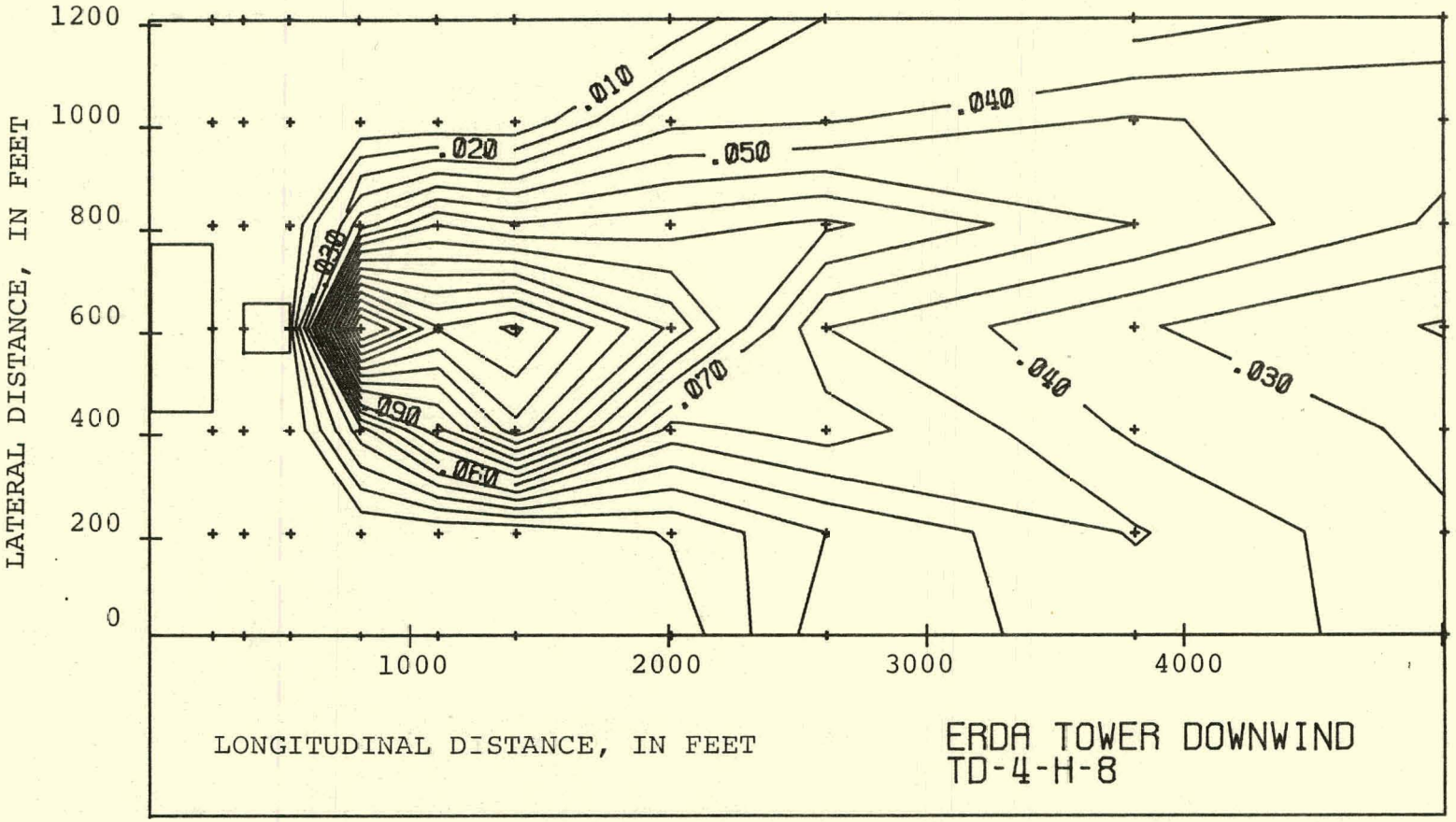

(i) Horizontal Distribution, 450 Feet Above the Ground

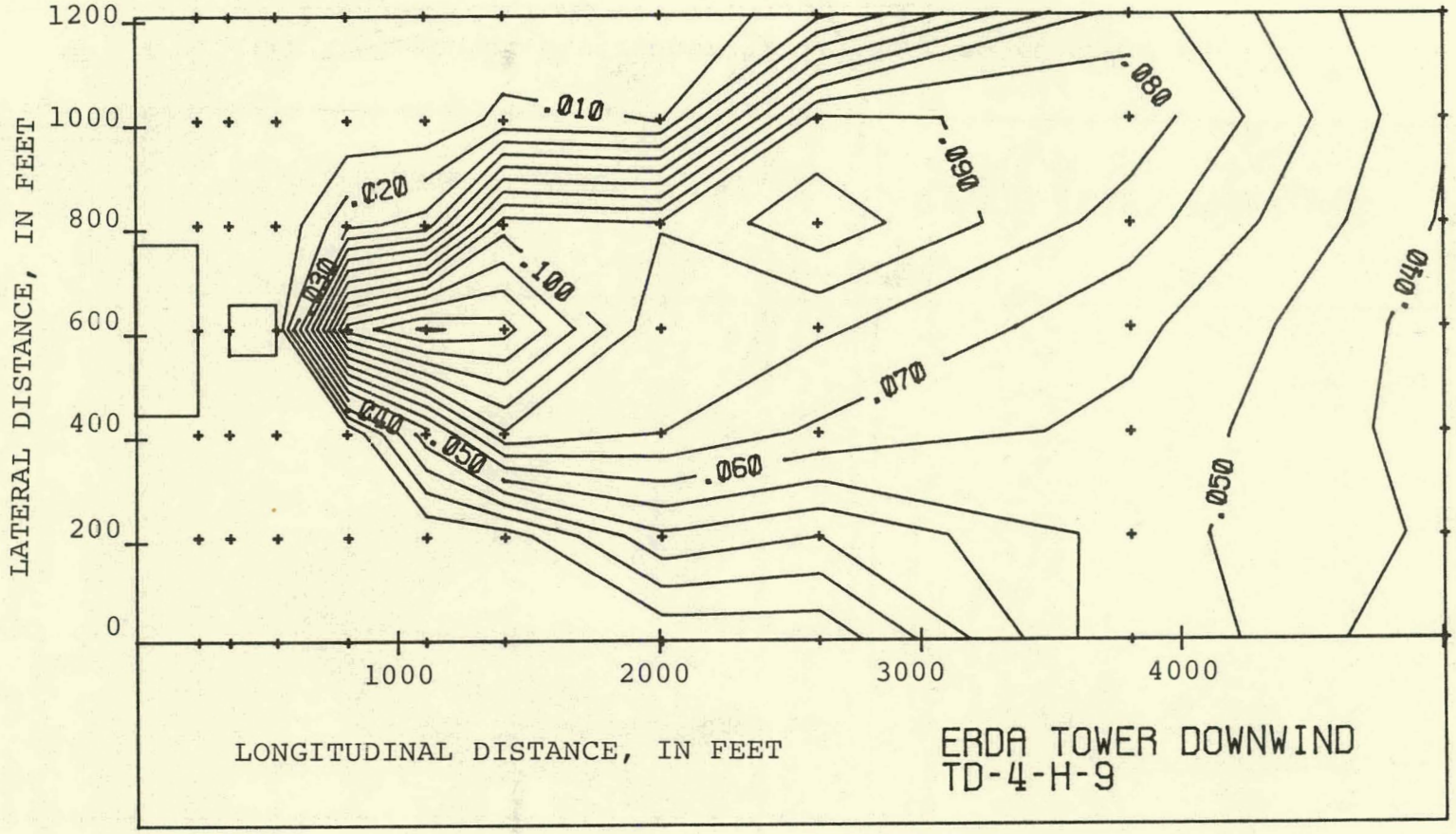

(j) Horizontal Distribution, 510 Feet Above the Ground

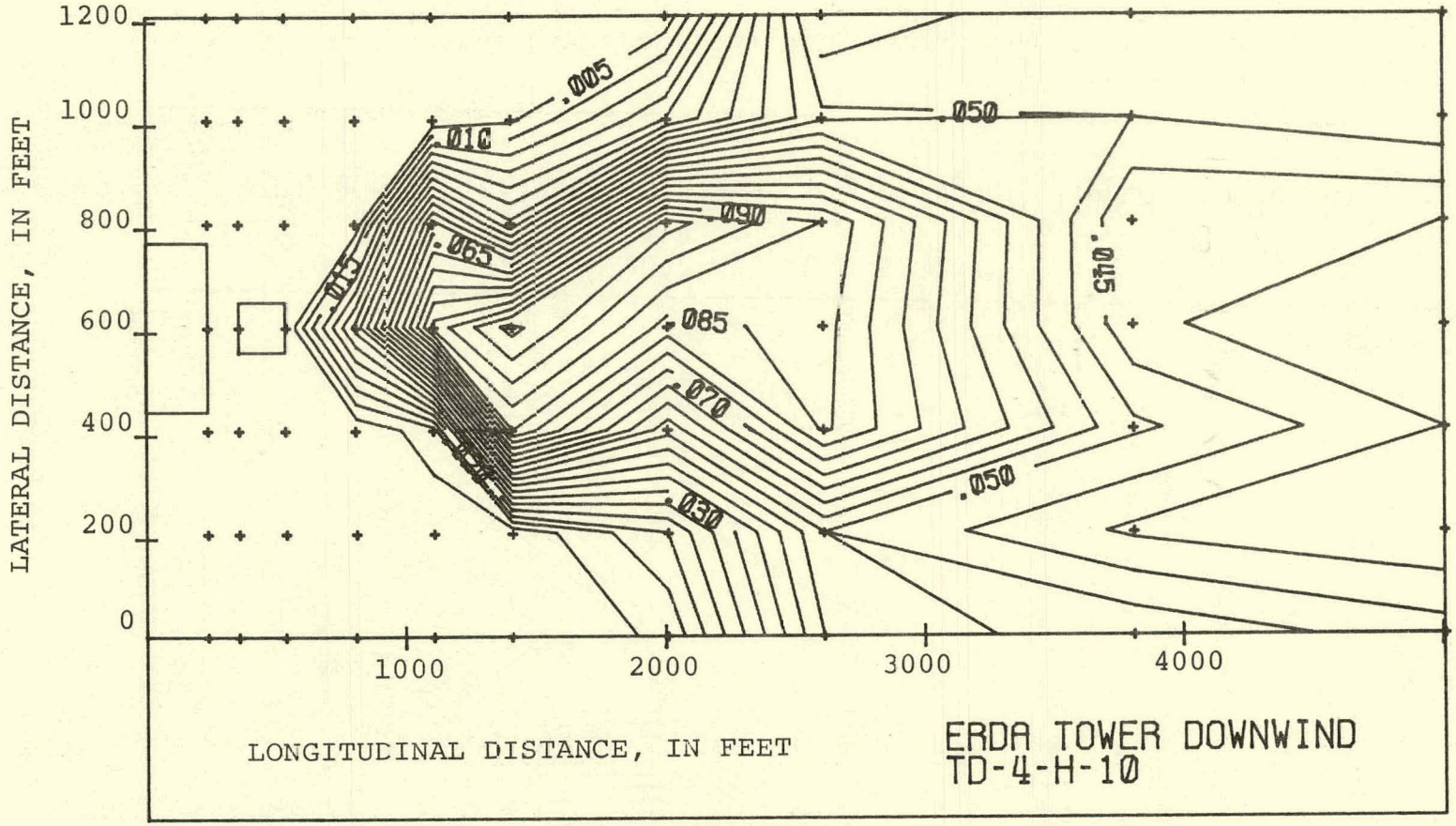

(k) Horizontal Distribution, 570 Feet Above the Ground

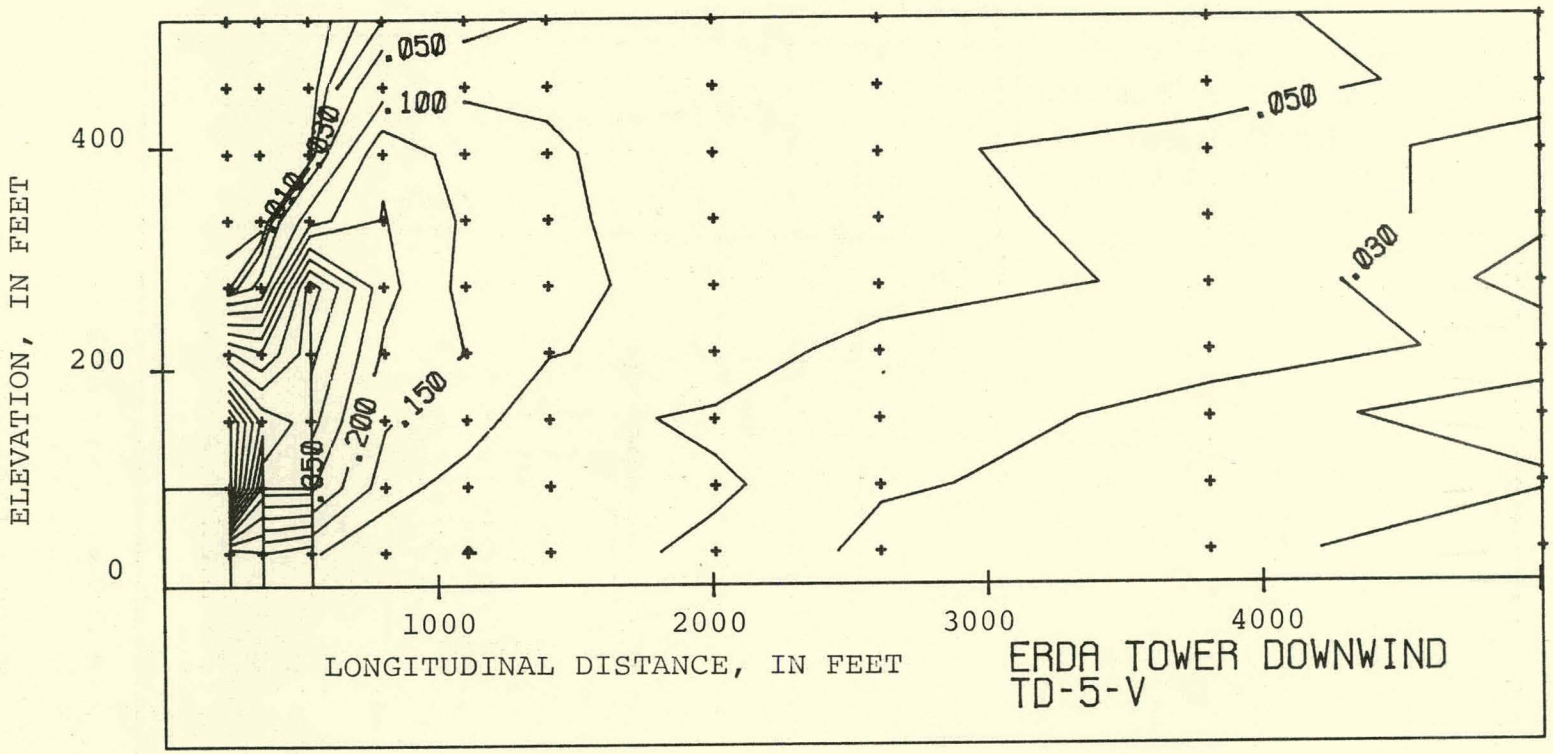

(a) Vertical Distribution

FIGURE 4.33 Temperature Distribution for Run TD-5. V_a = 29.2 MPH.

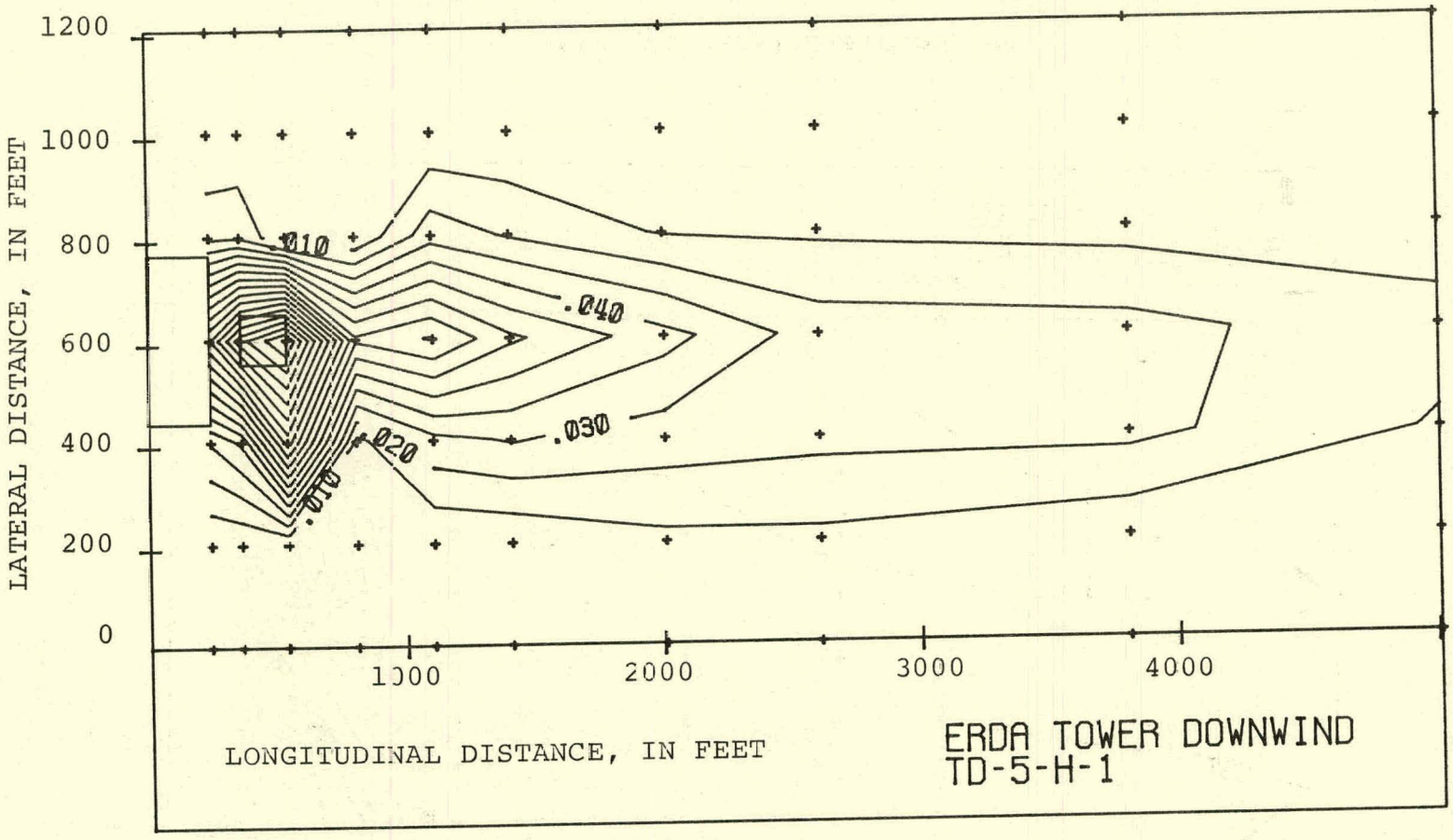

(b) Horizontal Distribution, 30 Feet Above the Ground

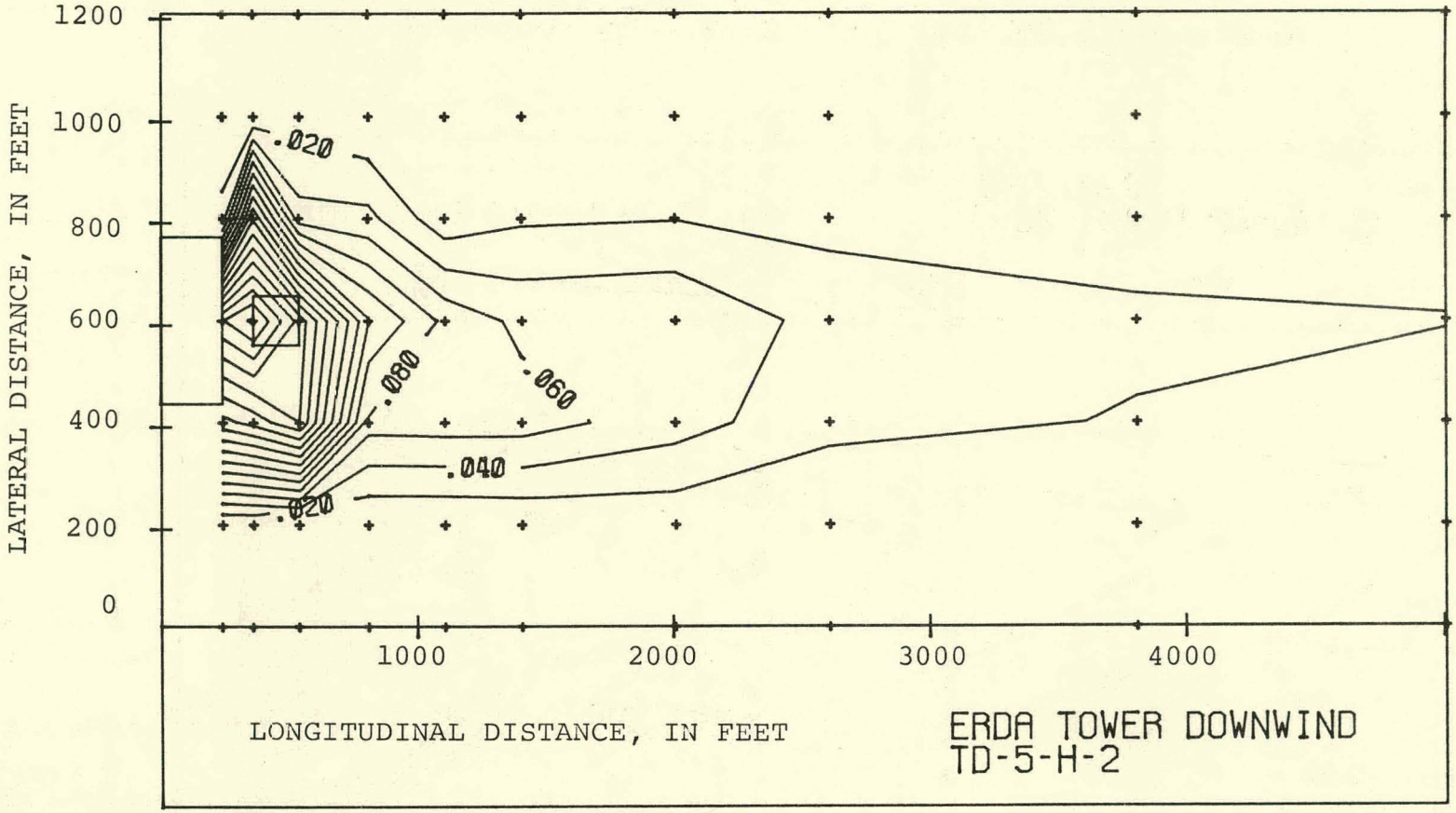

(c) Horizontal Distribution, 90 Feet Above the Ground

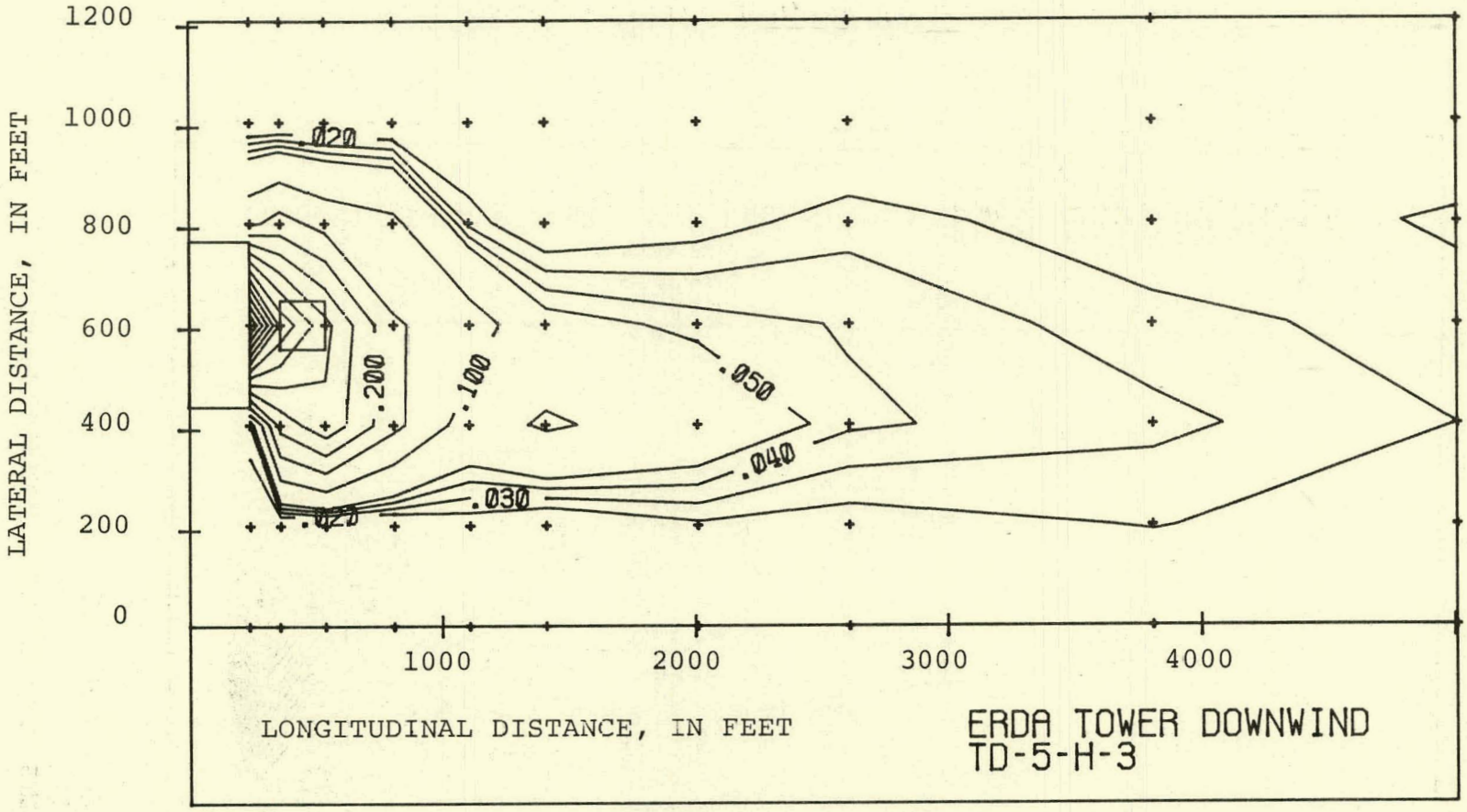

(d) Horizontal Distribution, 150 Feet Above the Ground

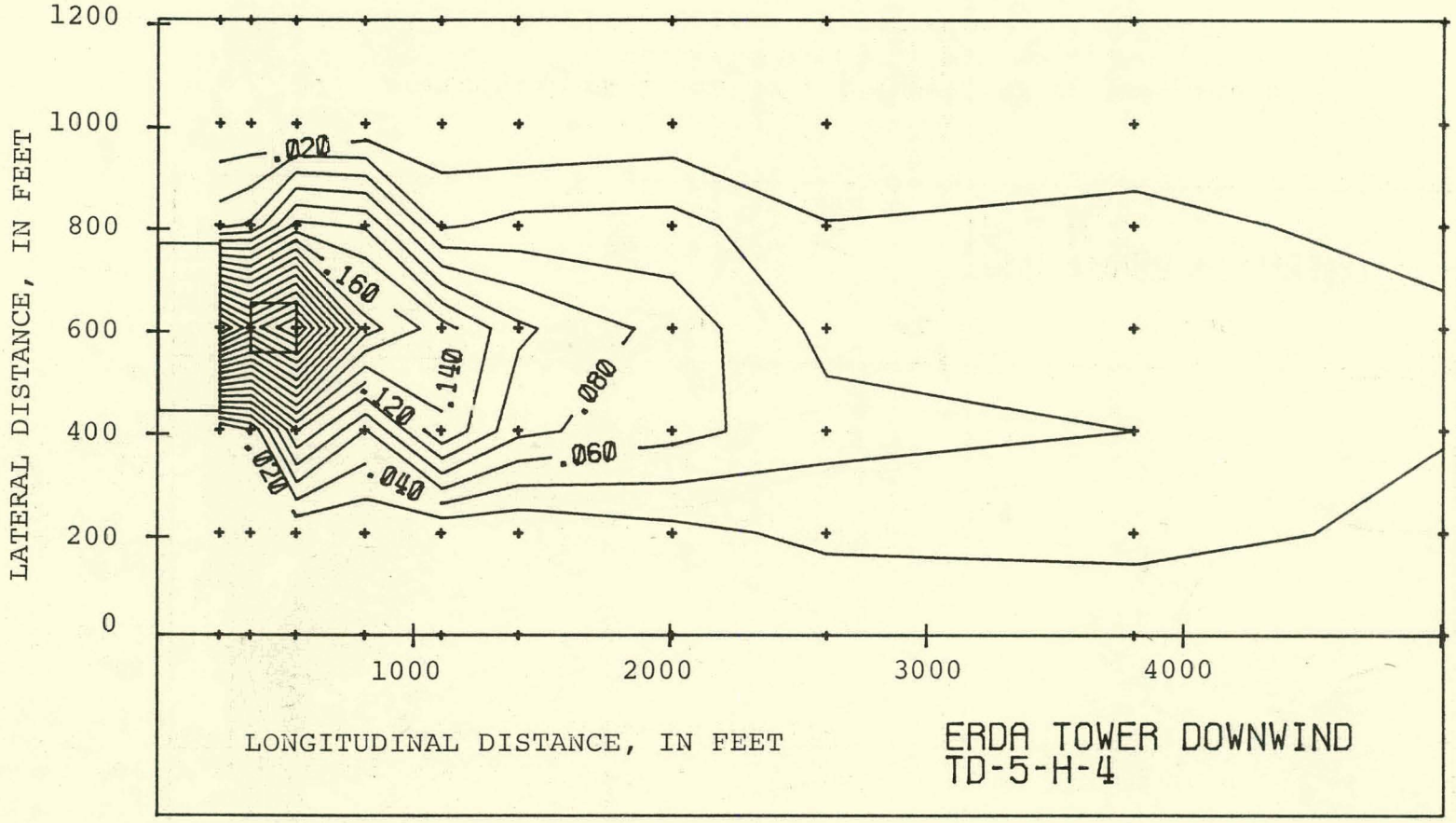

(e) Horizontal Distribution, 210 Feet Above the Ground

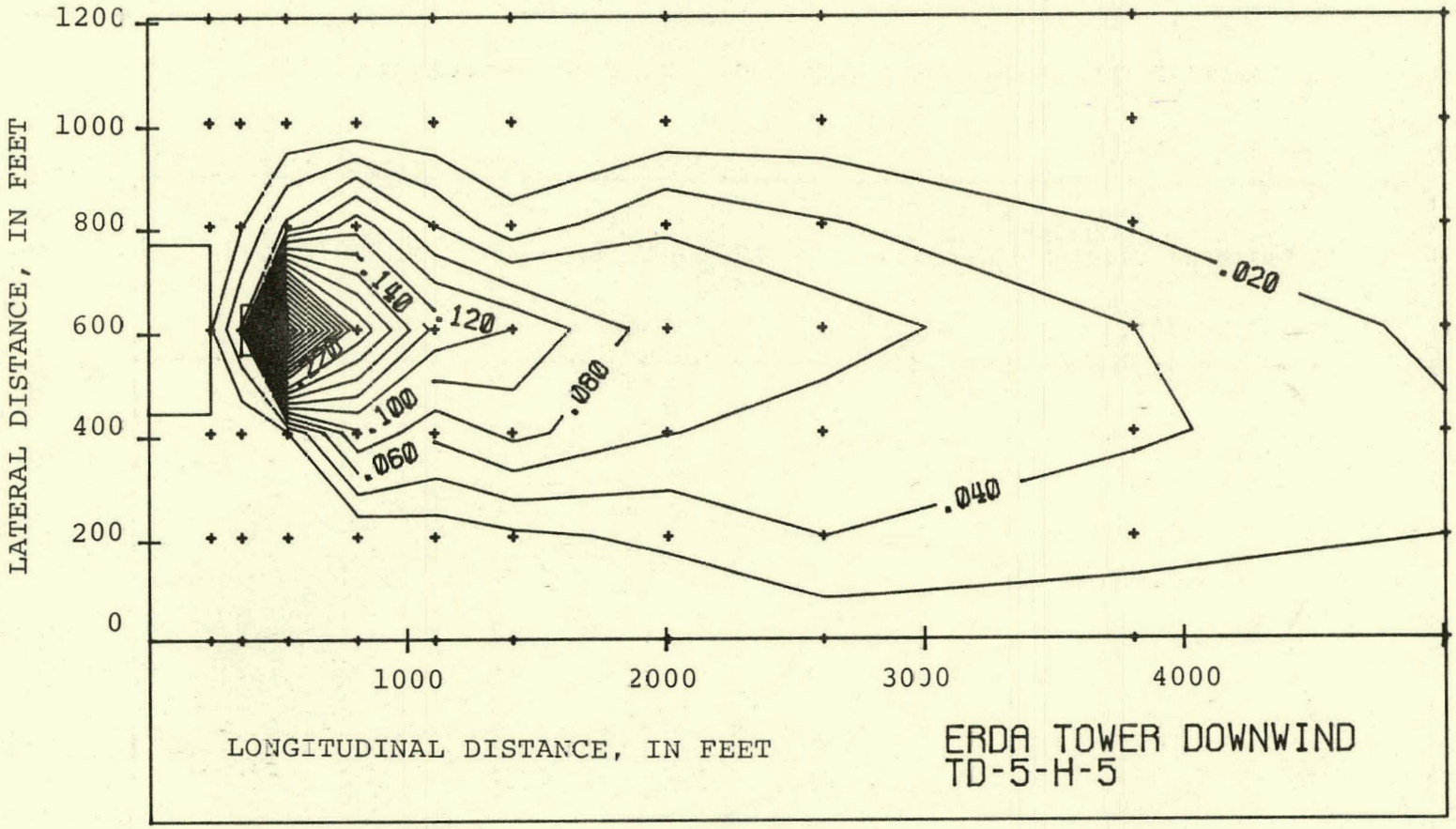

(f) Horizontal Distribution, 270 Feet Above the Ground

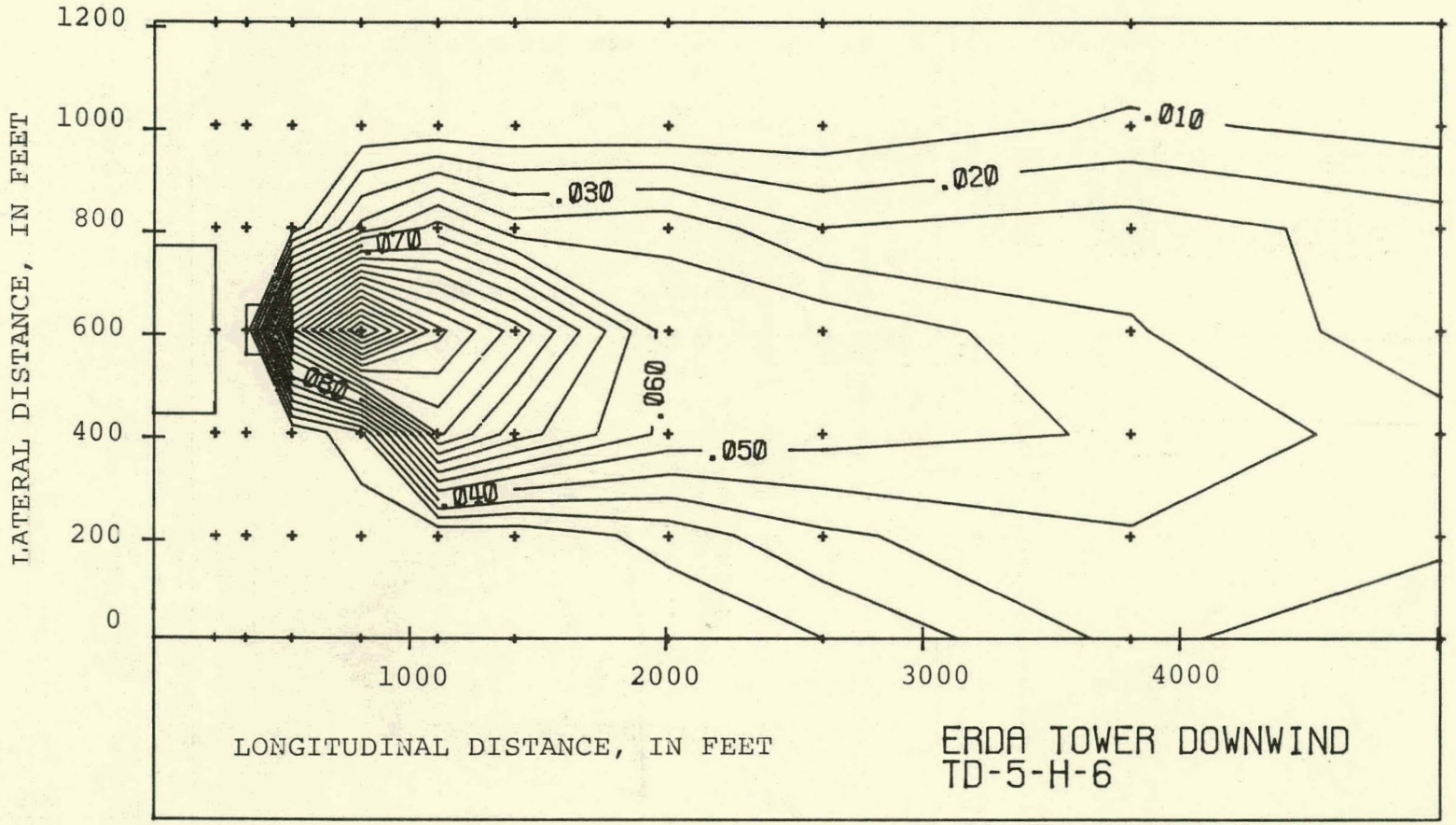

(g) Horizontal Distribution, 330 Feet Above the Ground

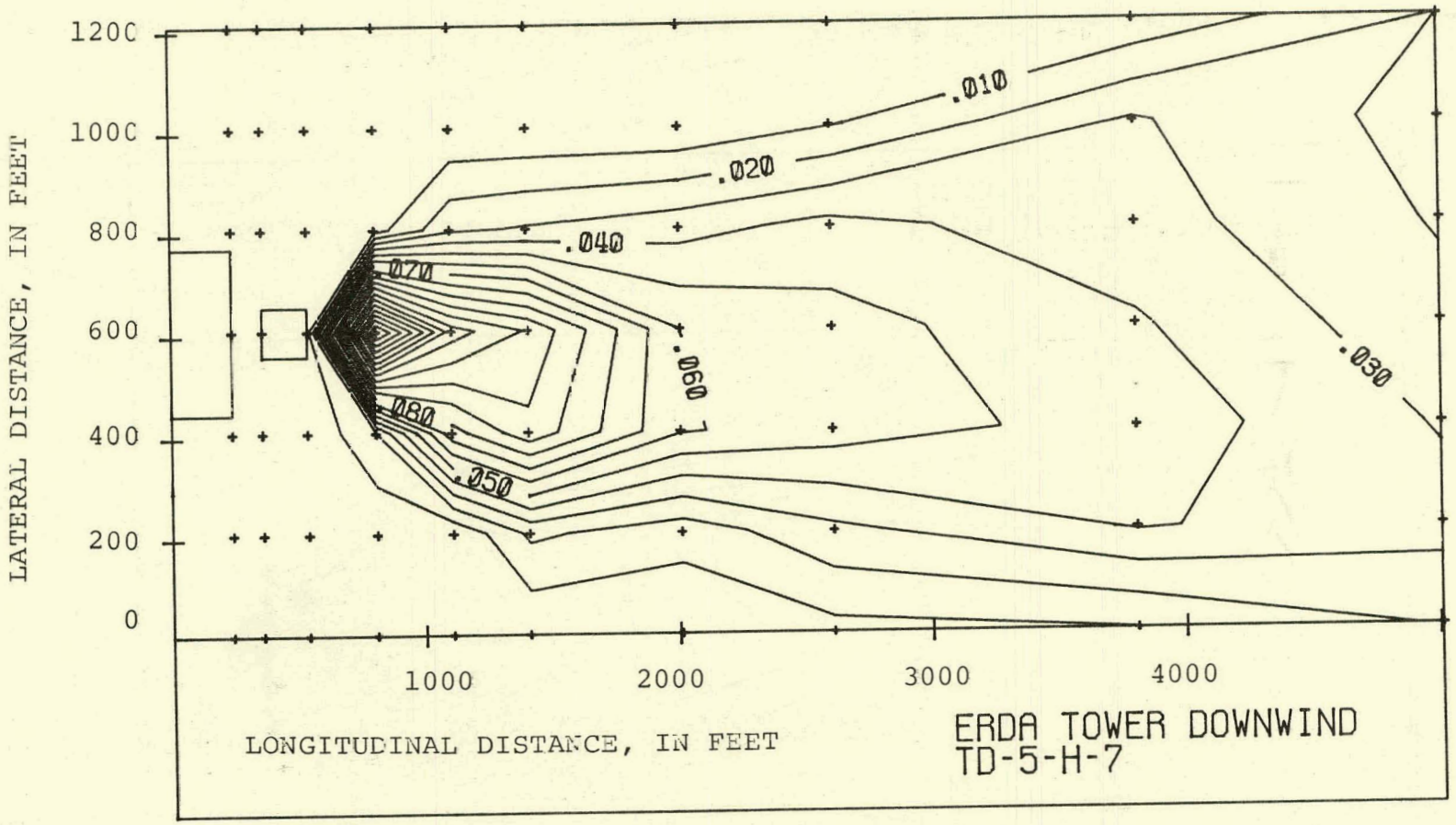

(h) Horizontal Distribution, 390 Feet Above the Ground

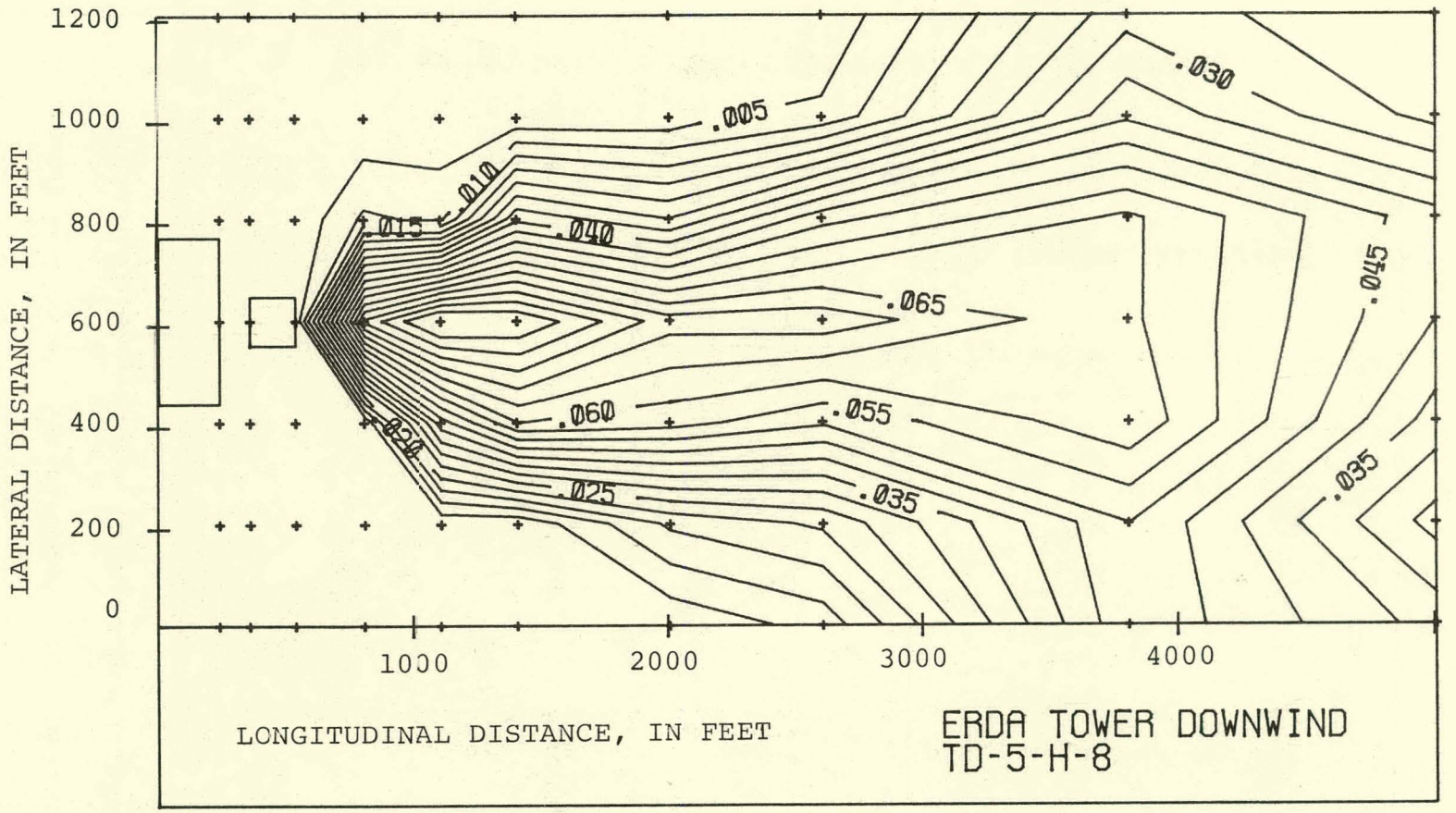

(i) Horizontal Distribution, 450 Feet Above the Ground

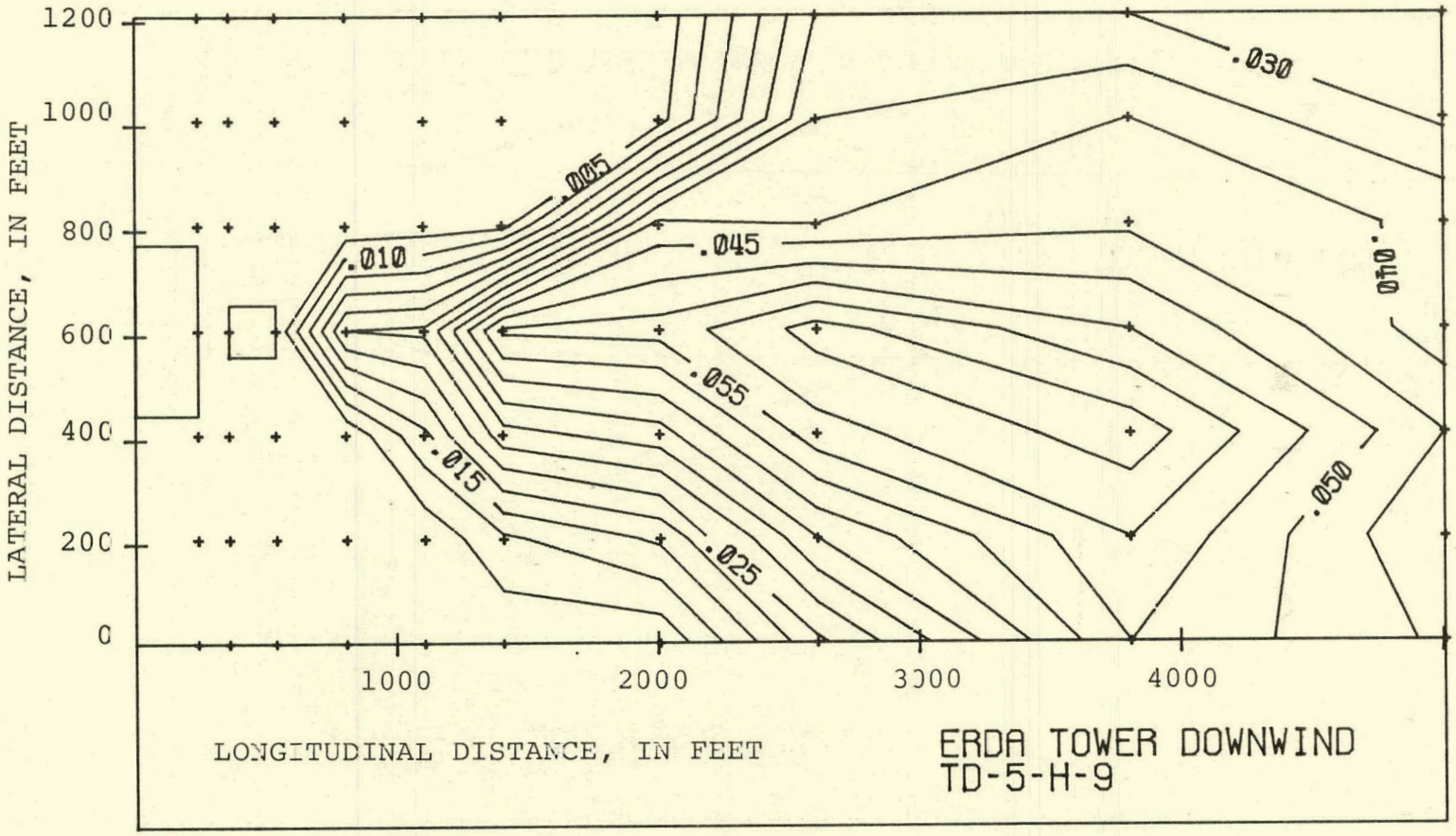

(j) Horizontal Distribution, 510 Feet Above the Ground

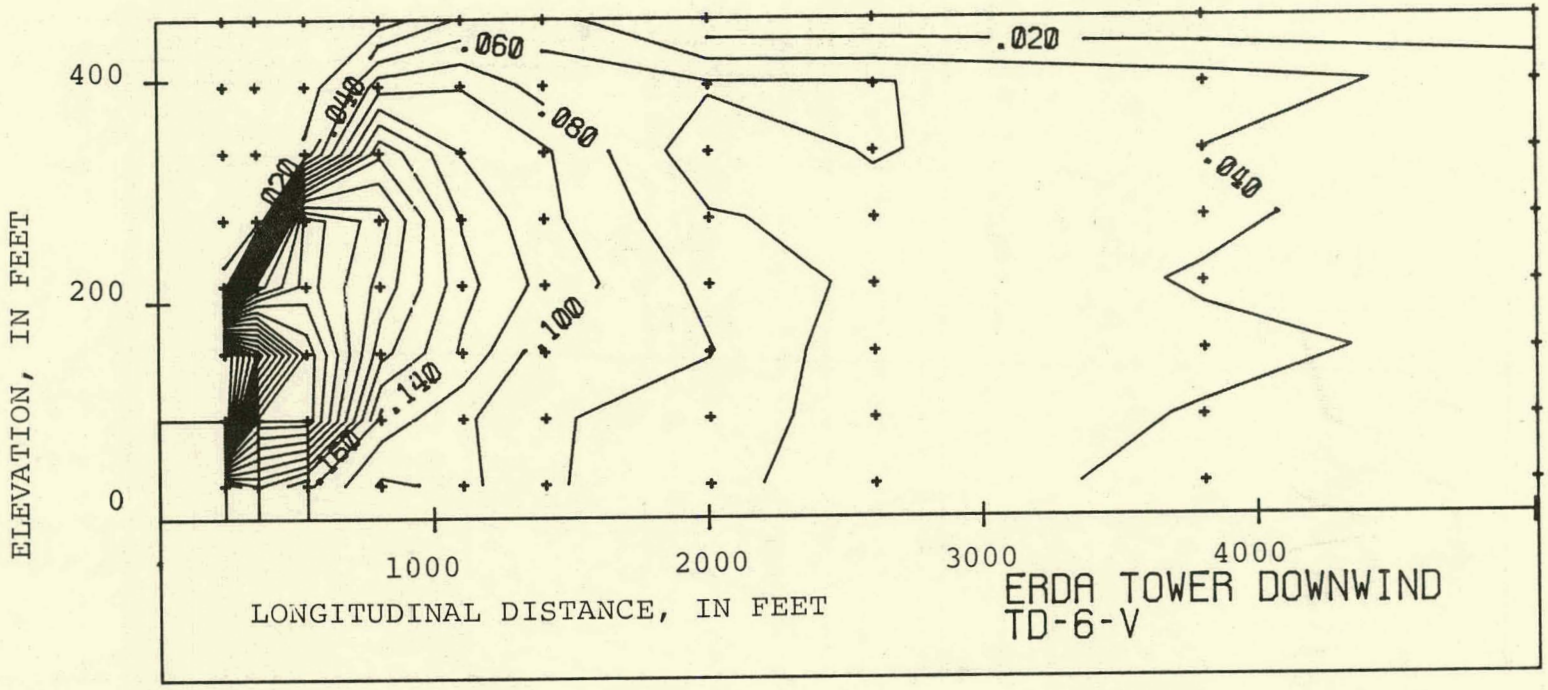

(a) Vertical Distribution

FIGURE 4.34 Temperature Distribution for Run TD-6. V_a = 37.1 MPH.

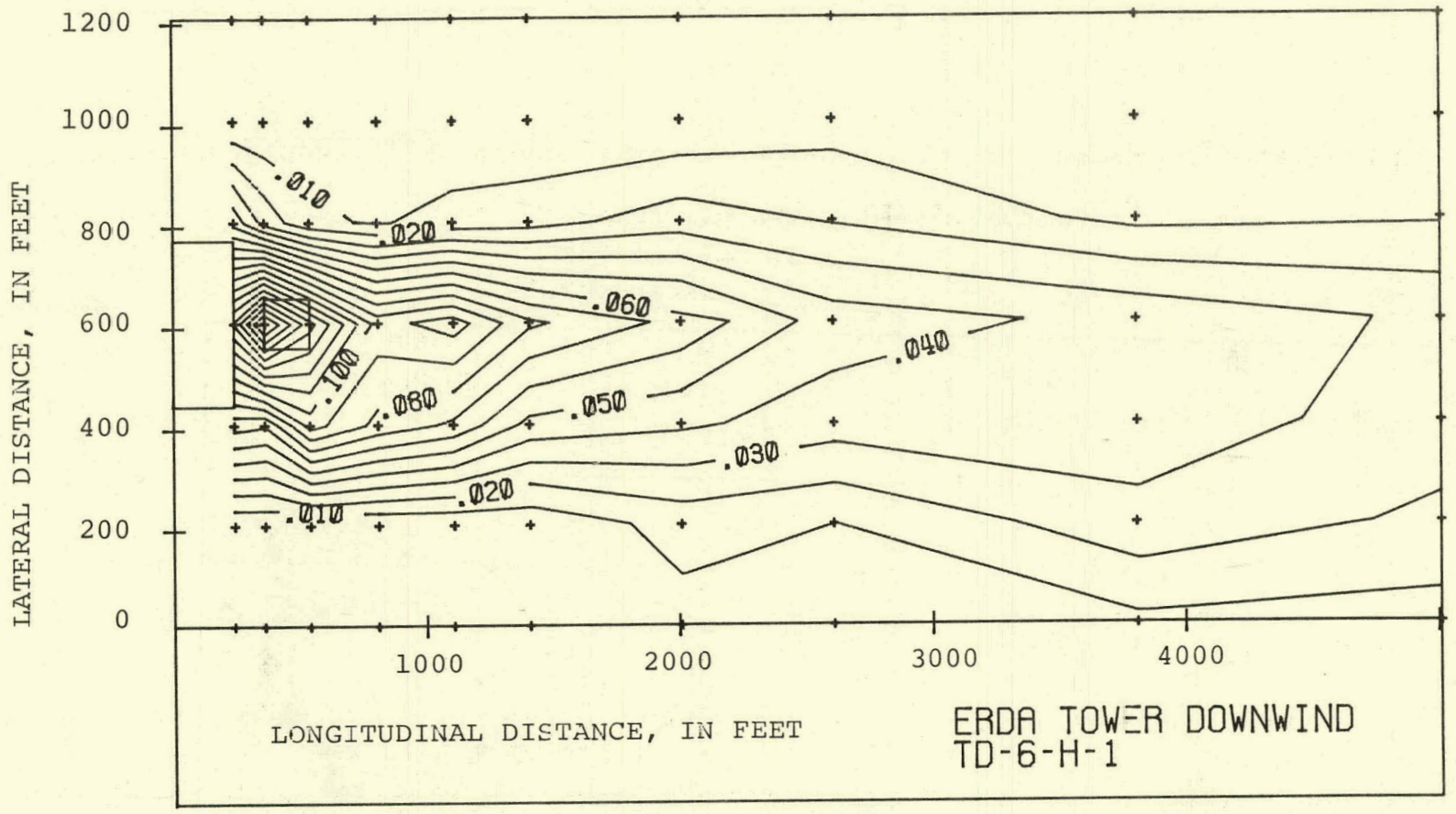

(b) Horizontal Distribution, 30 Feet Above the Ground

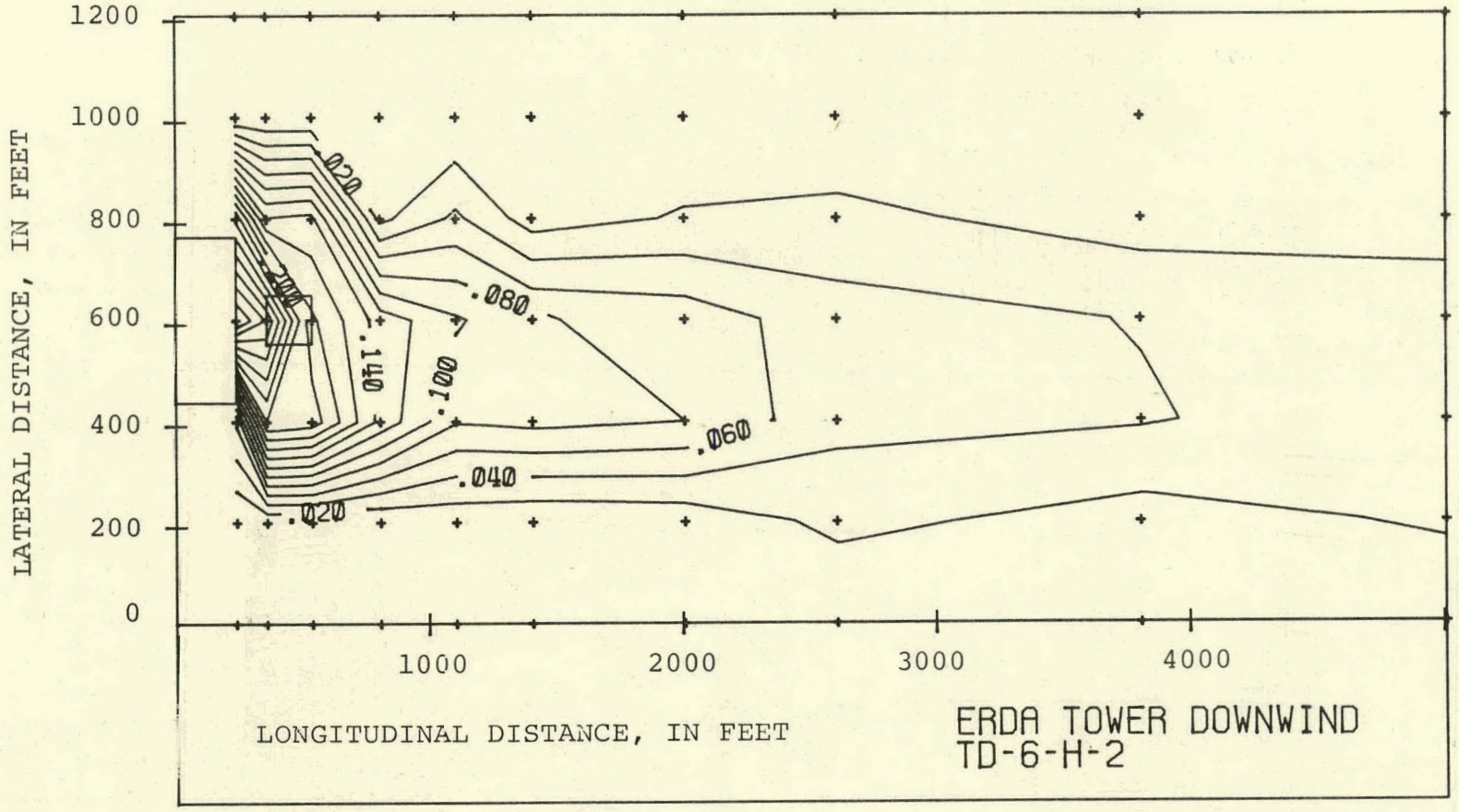

(c) Horizontal Distribution, 90 Feet Above the Ground

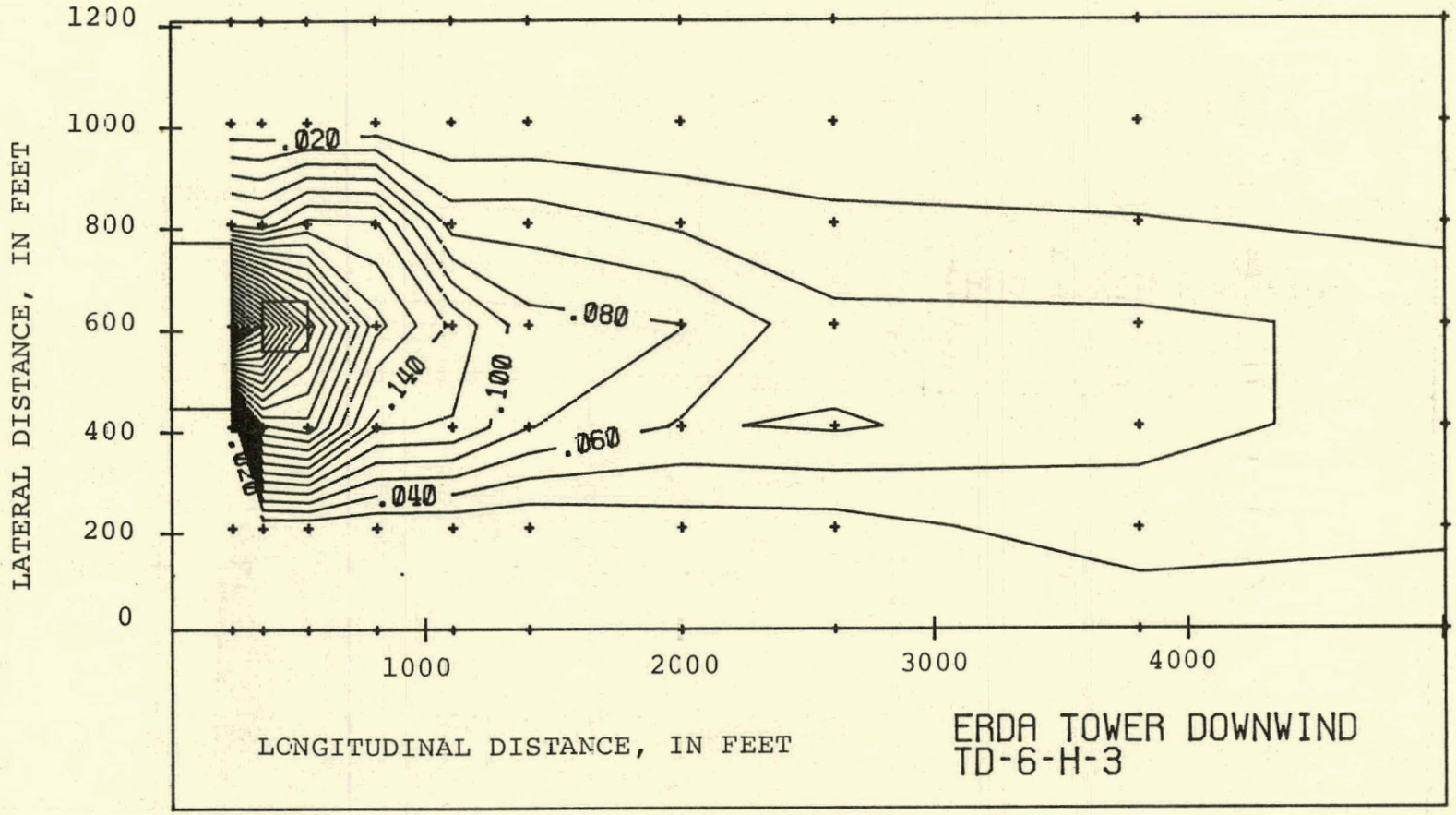

(d) Horizontal Distribution, 150 Feet Above the Ground

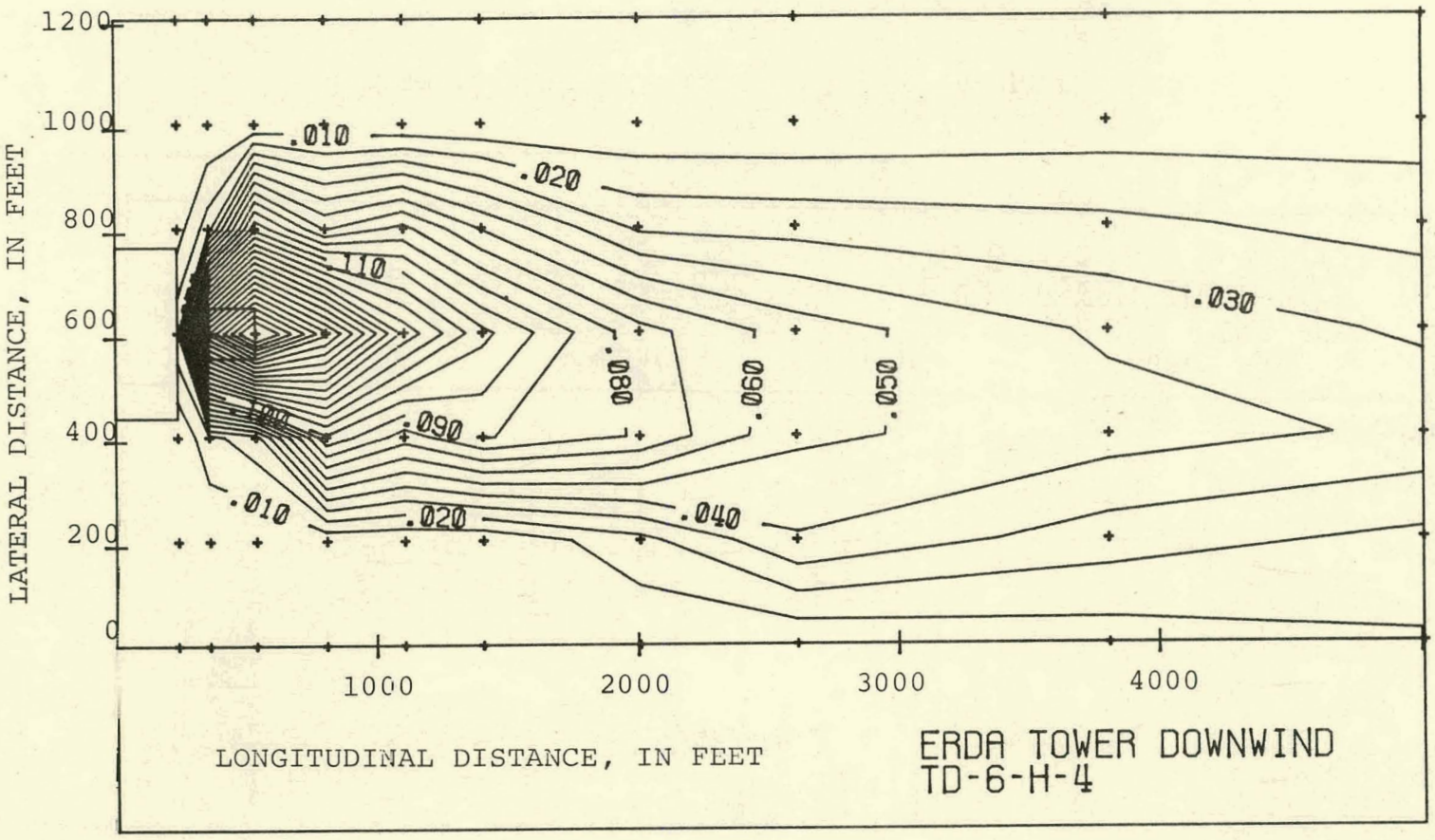

(e) Horizontal Distribution, 210 Feet Above the Ground

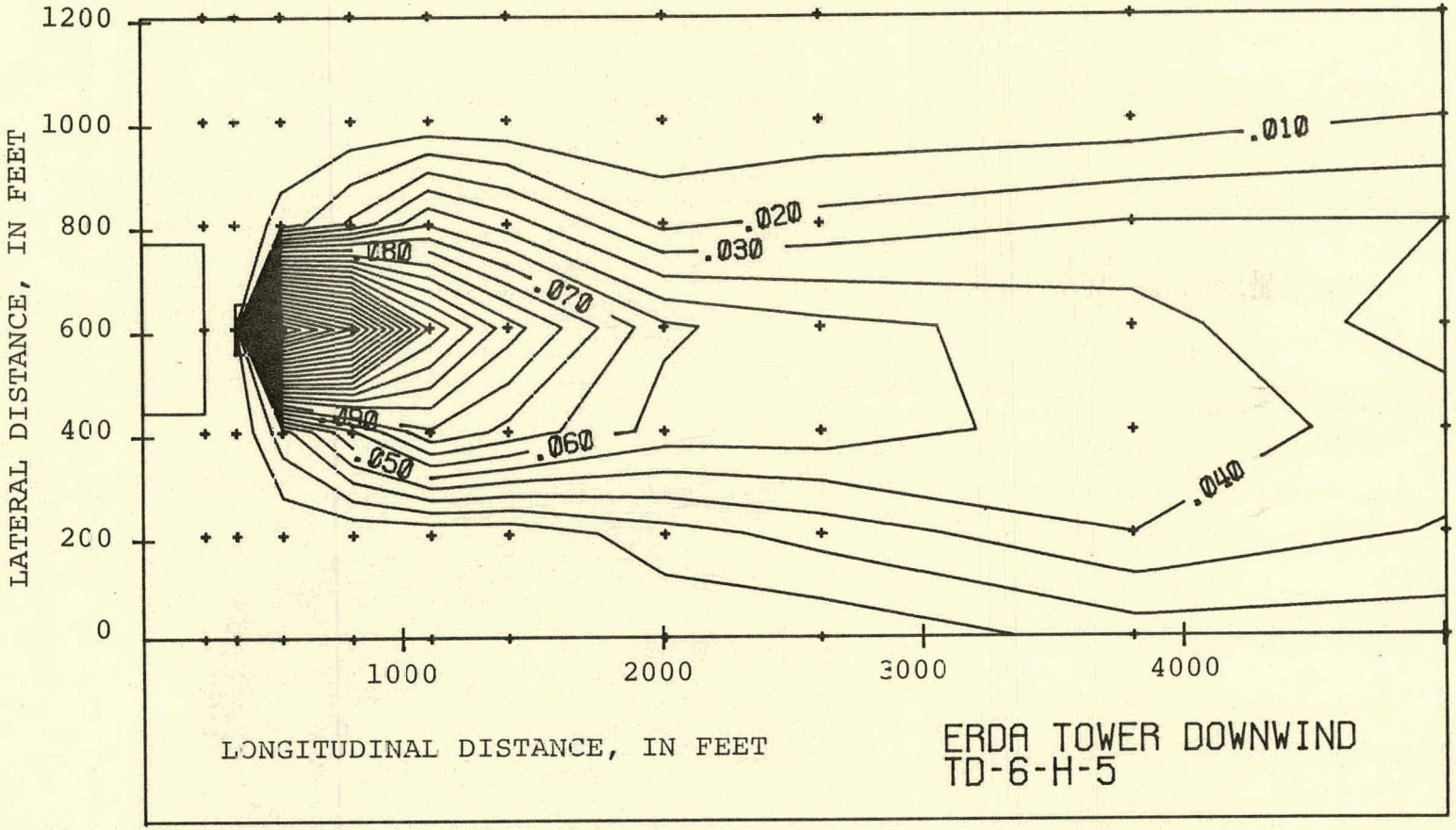

(f) Horizontal Distribution, 270 Feet Above the Ground

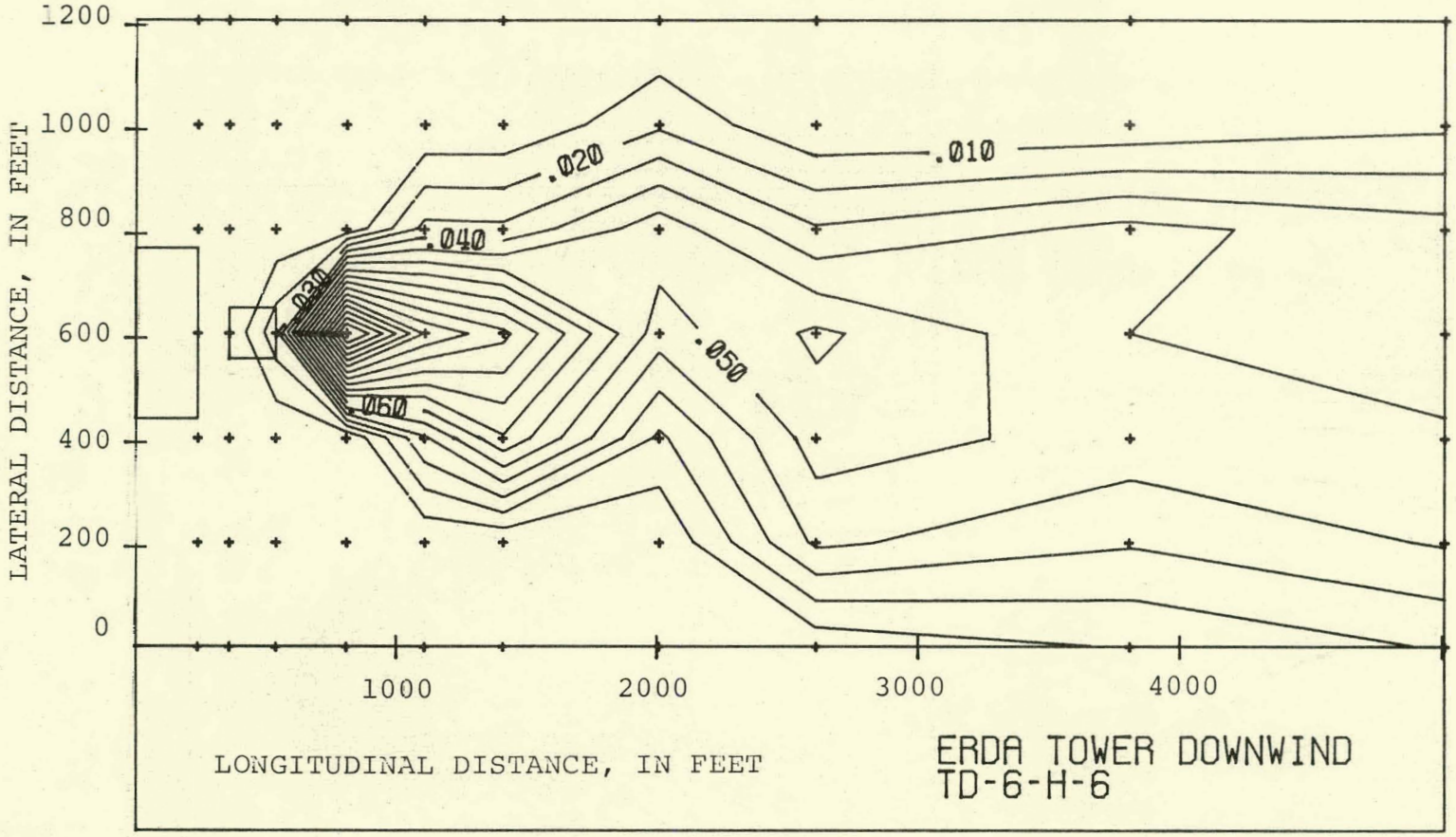

(g) Horizontal Distribution, 330 Feet Above the Ground

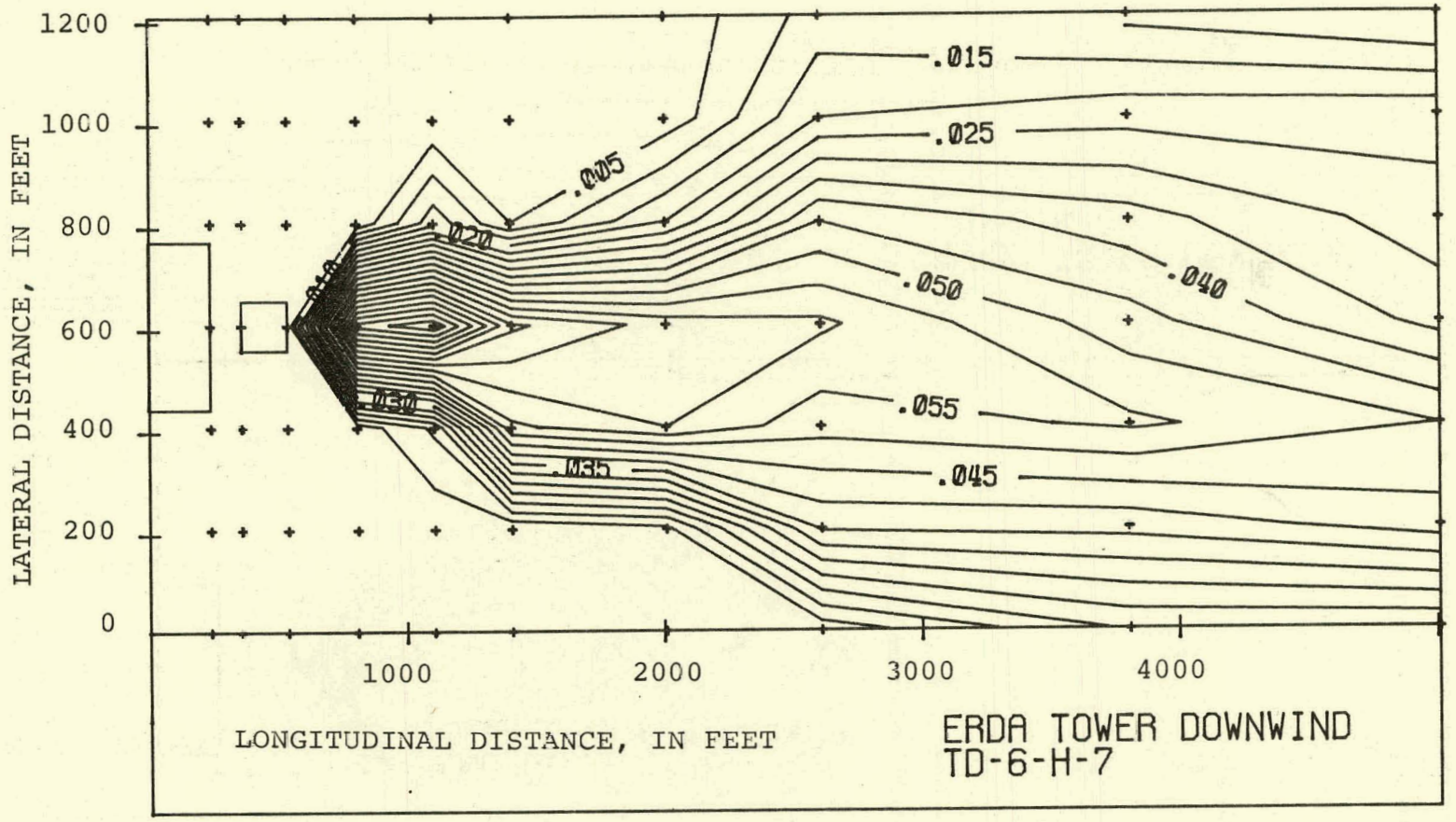

(h) Horizontal Distribution, 390 Feet Above the Ground

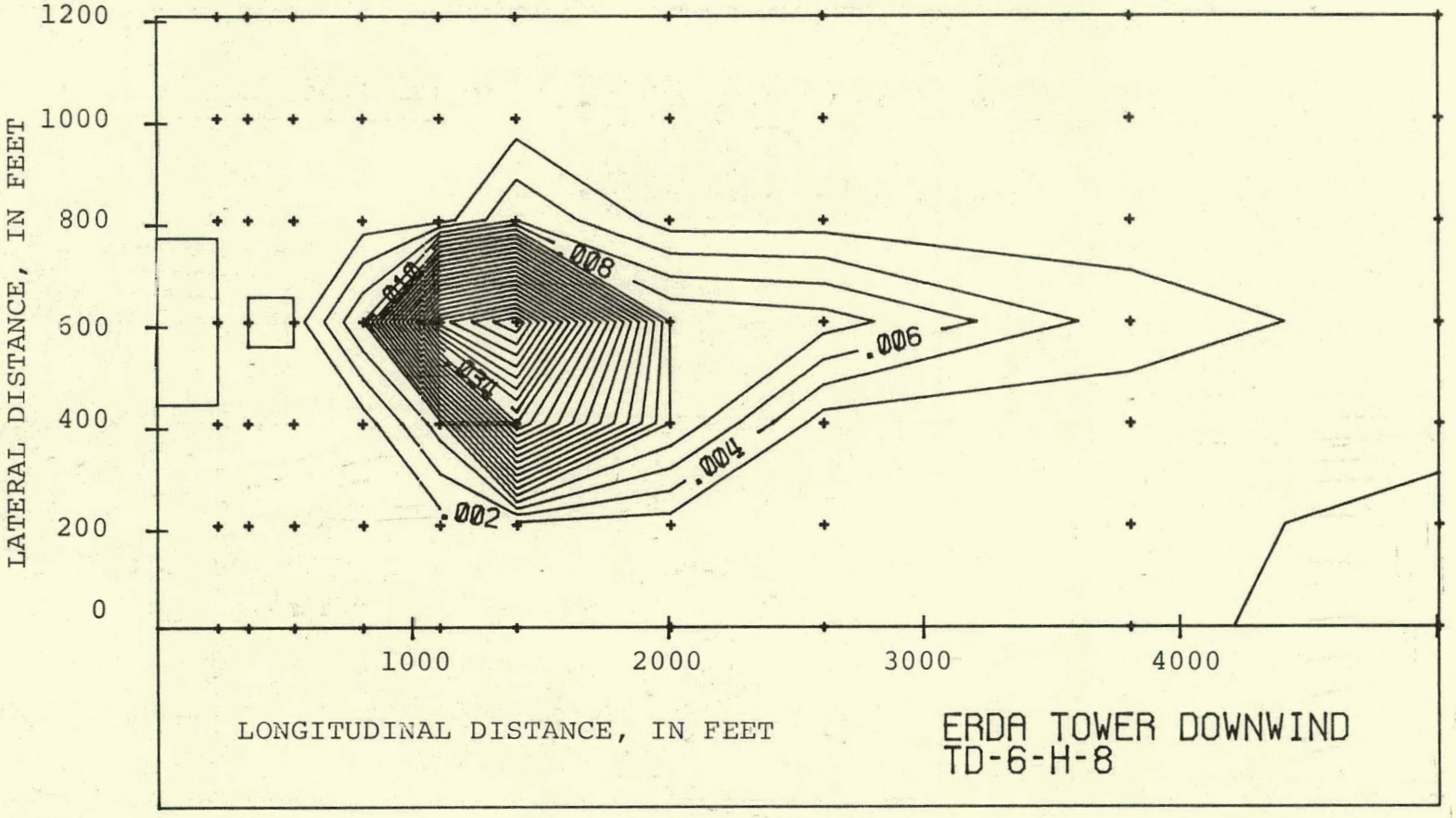

(i) Horizontal Distribution, 450 Feet Above the Ground

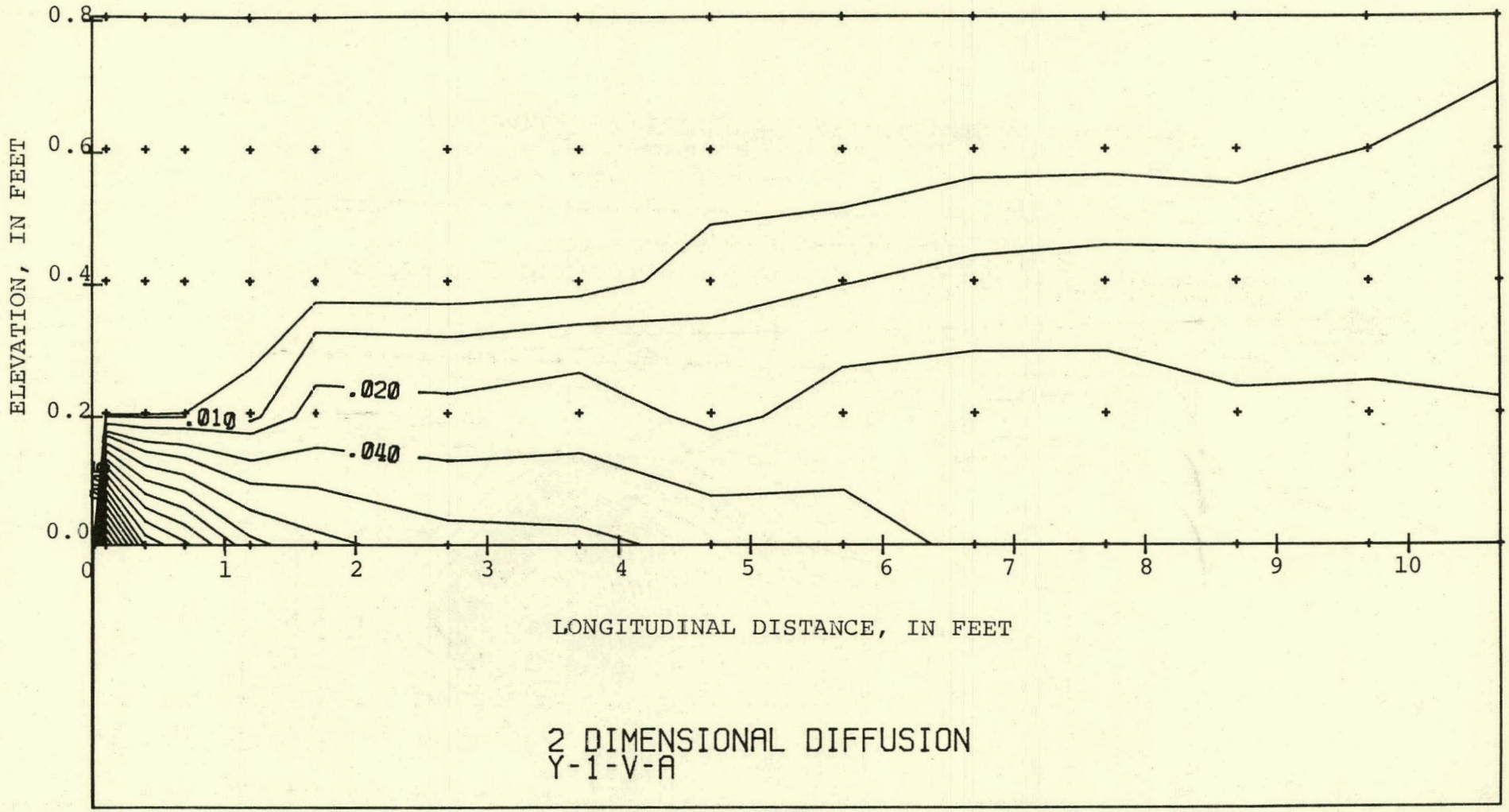

(a) Vertical Distribution of the Average Water Temperature

FIGURE 4.47 Vertical Temperature Distribution for Run Y-1. $K = 0.72$, $F_D = 6.7$, $R_j = 910$, and $R_a = 19.9 \times 10^4$

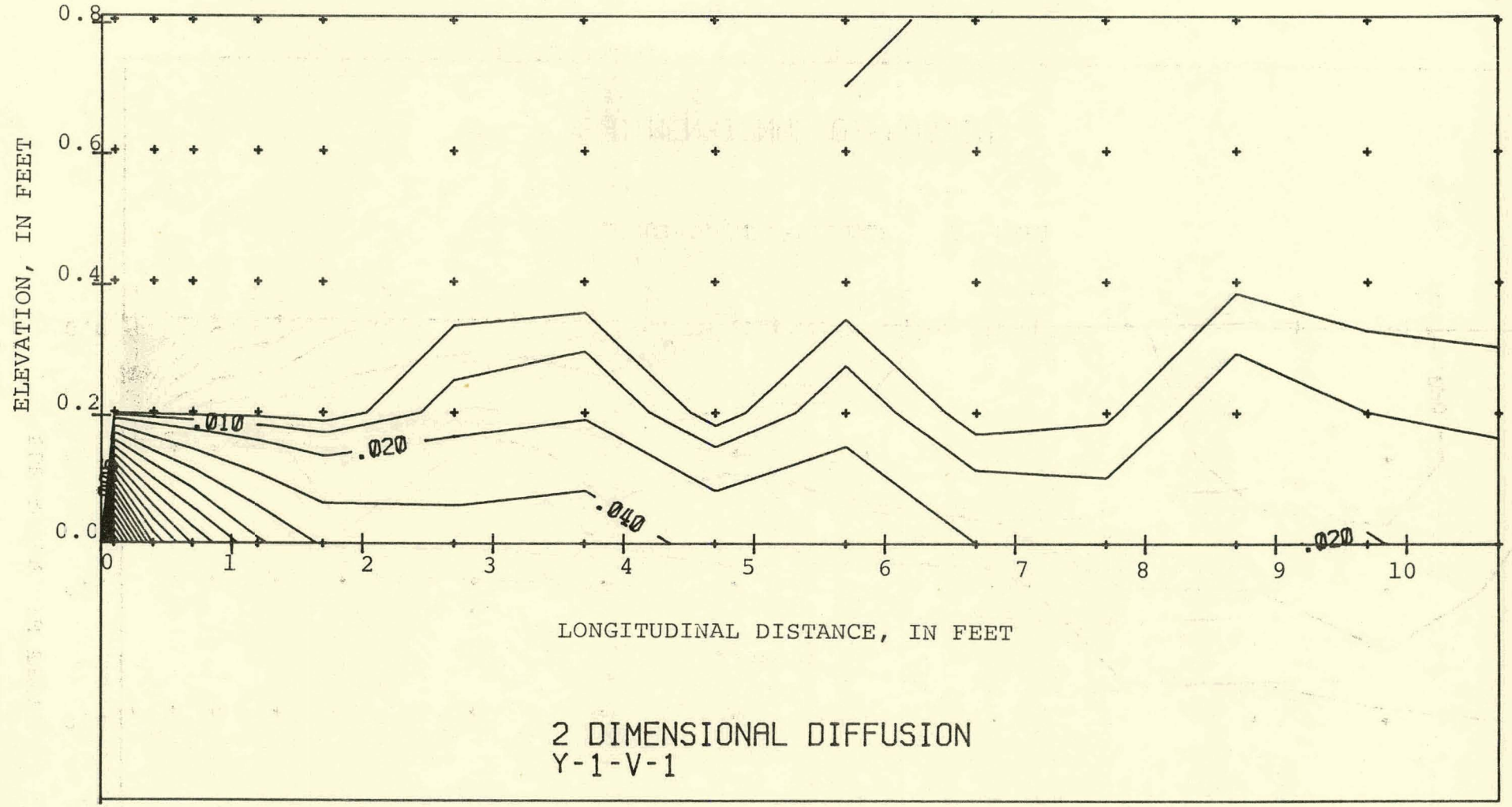

(b) Vertical Distribution of Water Temperature at Cross-Section 1

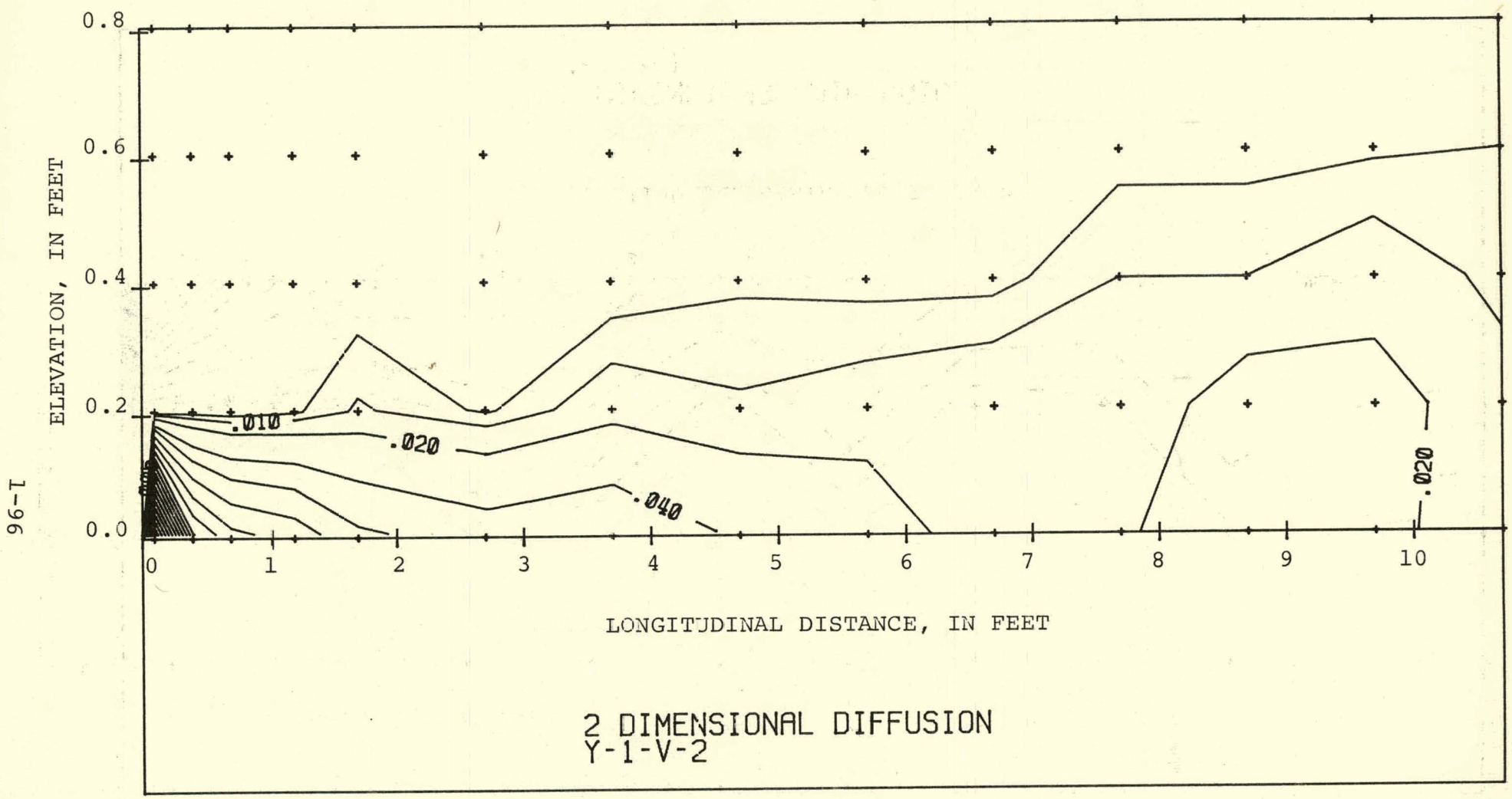

(c) Vertical Distribution of Water Temperature at Cross-Section 2

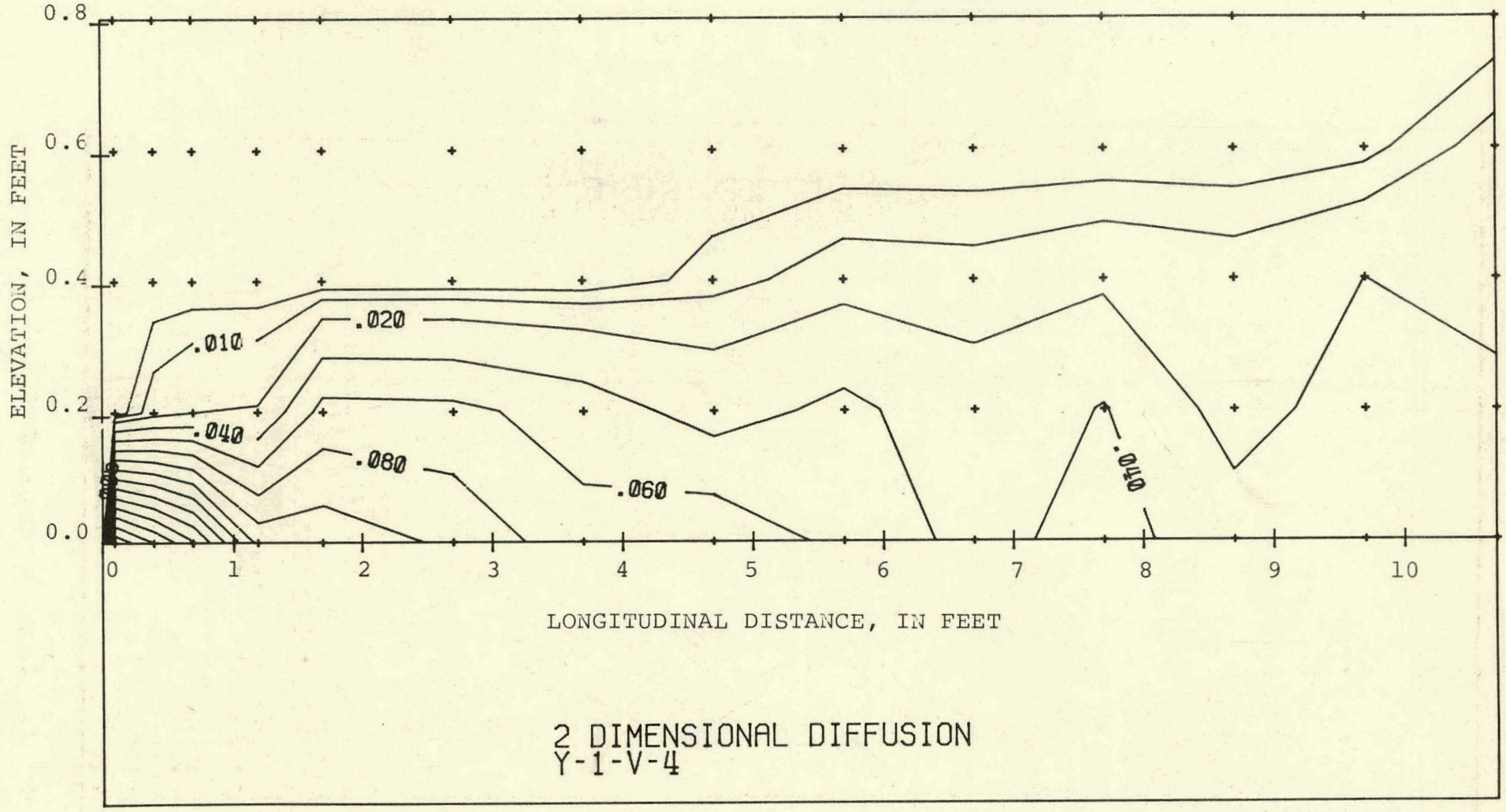

(d) Vertical Distribution of Water Temperature at Cross-Section 3

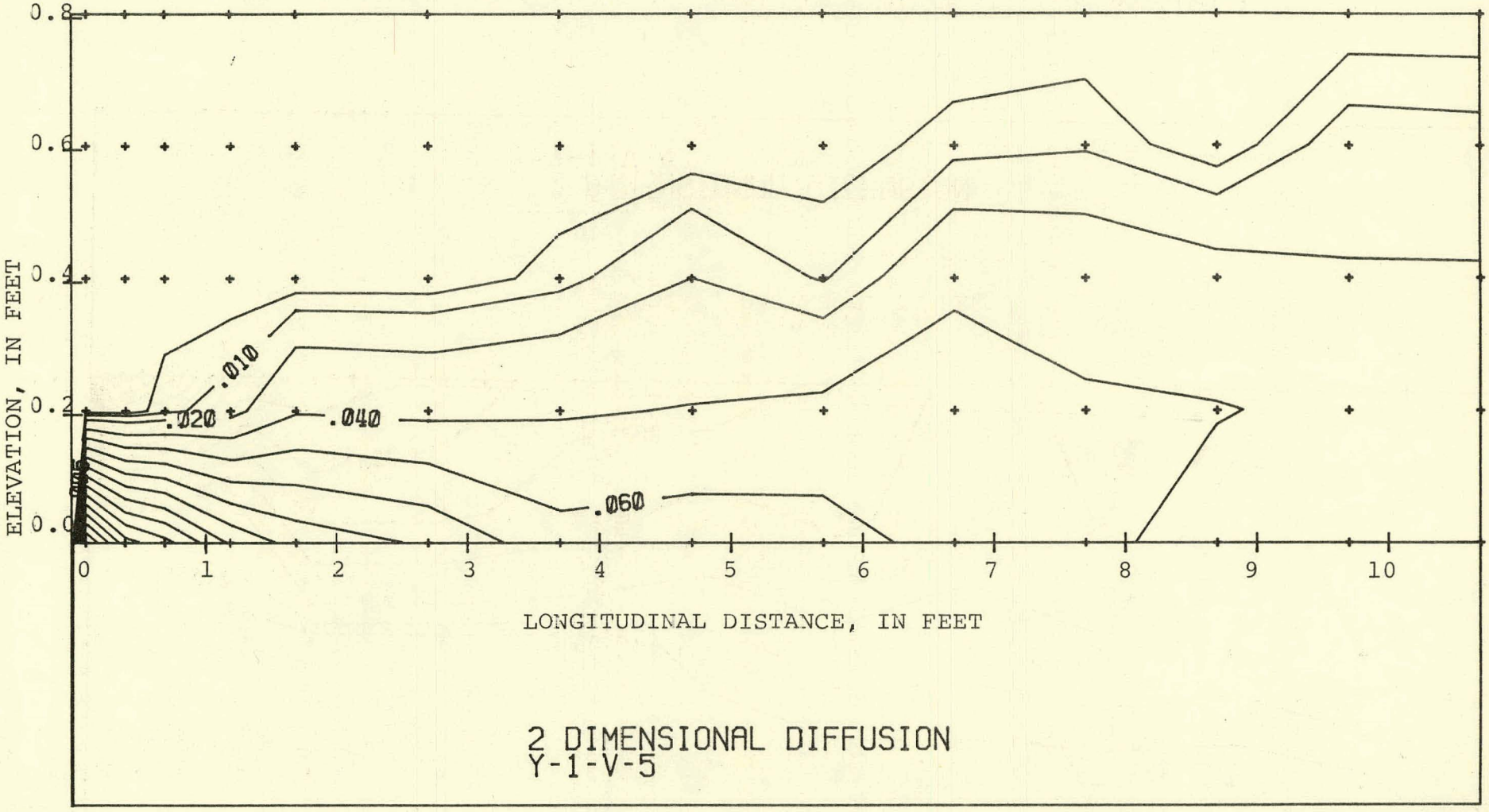

(e) Vertical Distribution of Water Temperature at Cross-Section 4

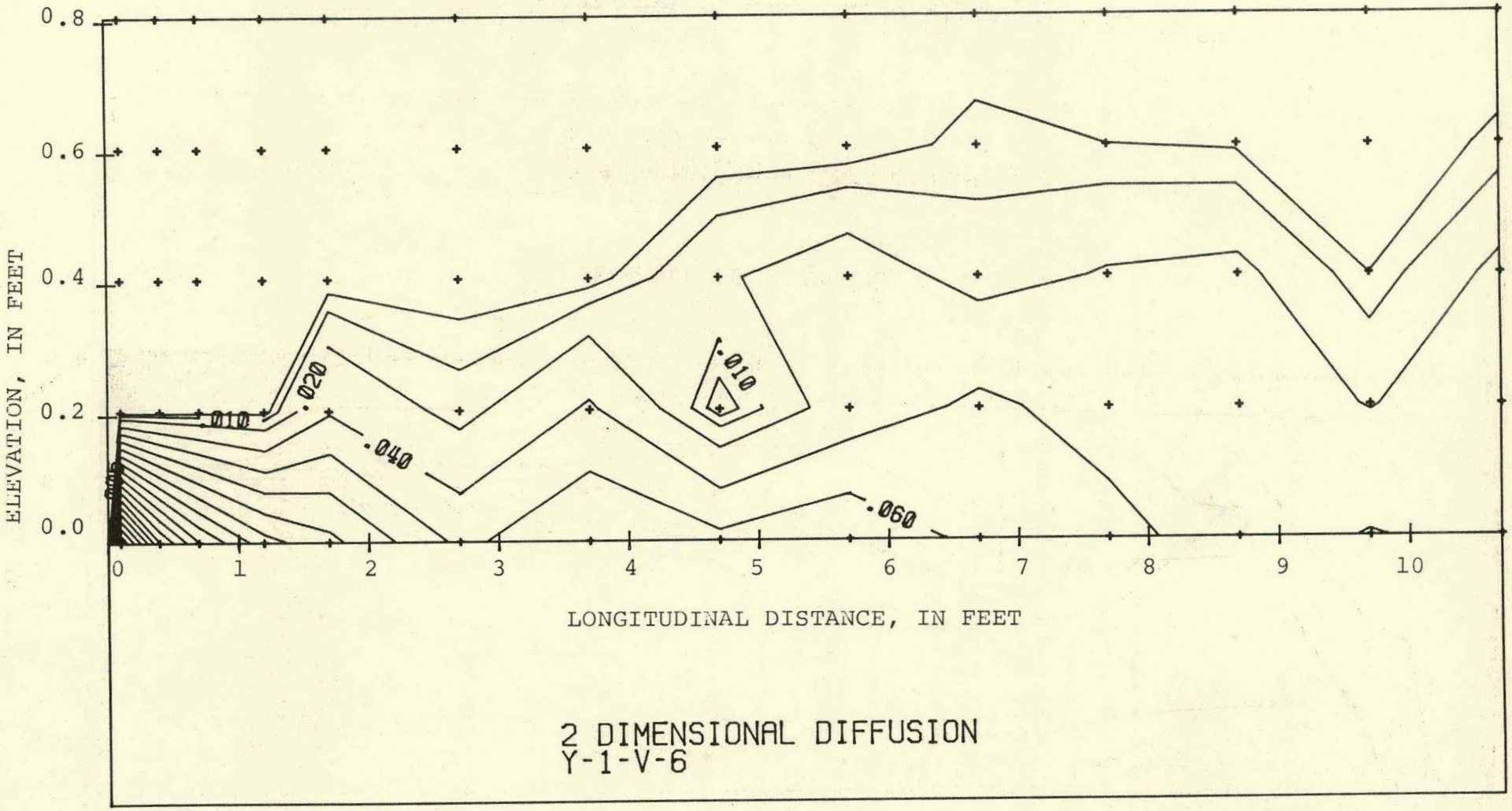

(f) Vertical Distribution of Water Temperature at Cross-Section 5

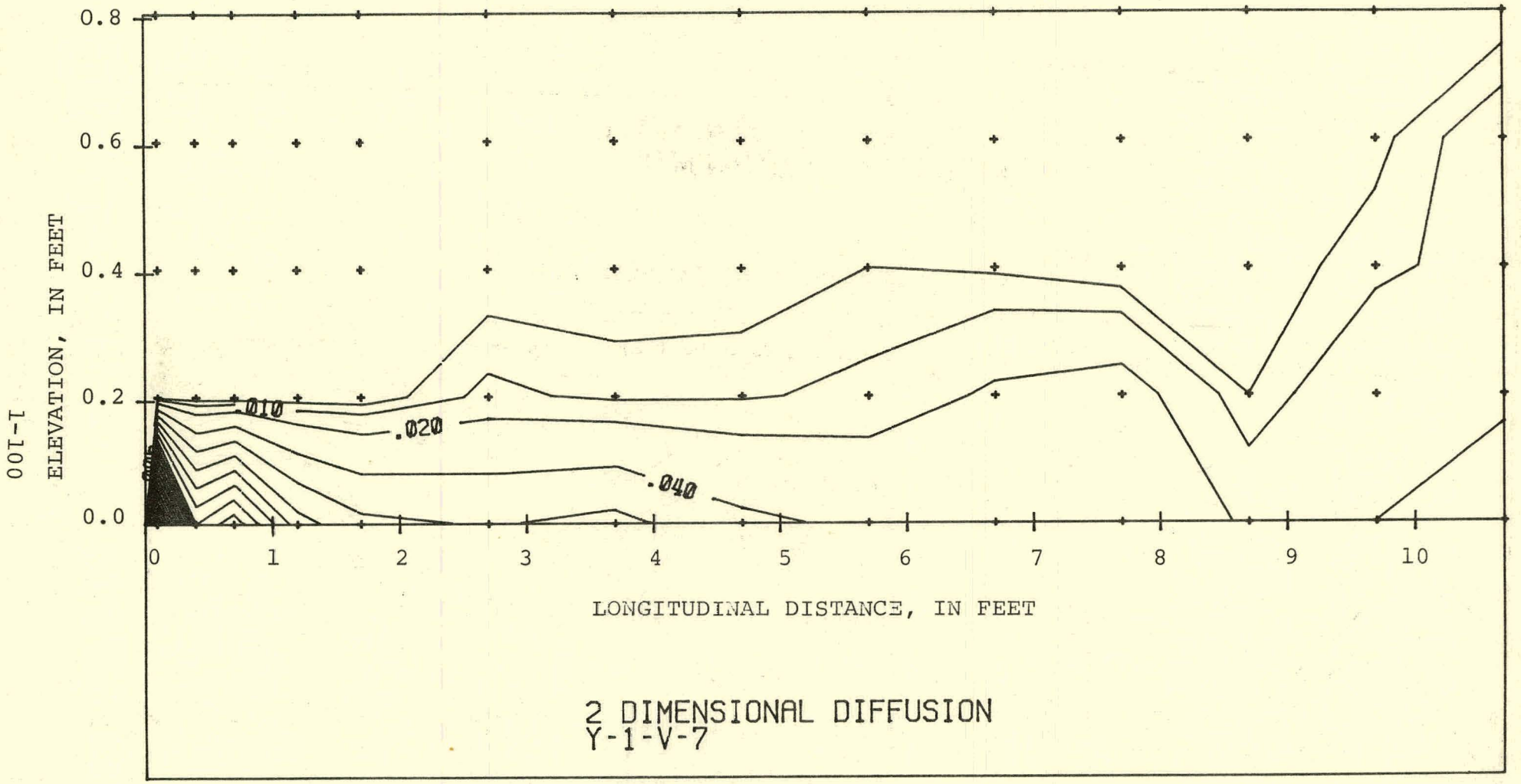

(g) Vertical Distribution of Water Temperature at Cross-Section 6

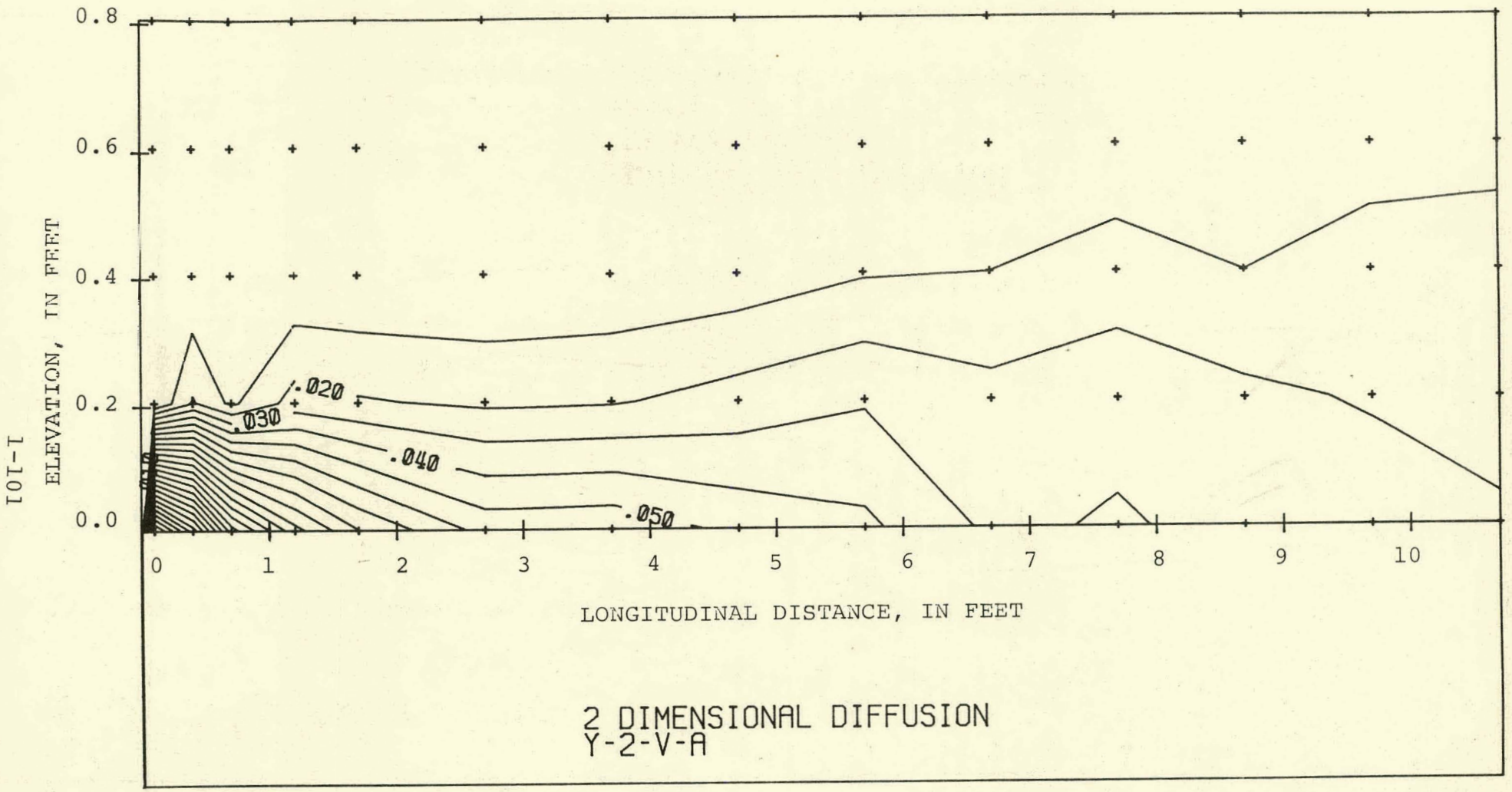

(a) Vertical Distribution of the Average Water Temperature

FIGURE 4.48 Vertical Temperature Distribution for Run Y-2. $K = 0.72$, $F_D = 4.5$, $R_j = 1130$, and $R_a = 19.9 \times 10^4$

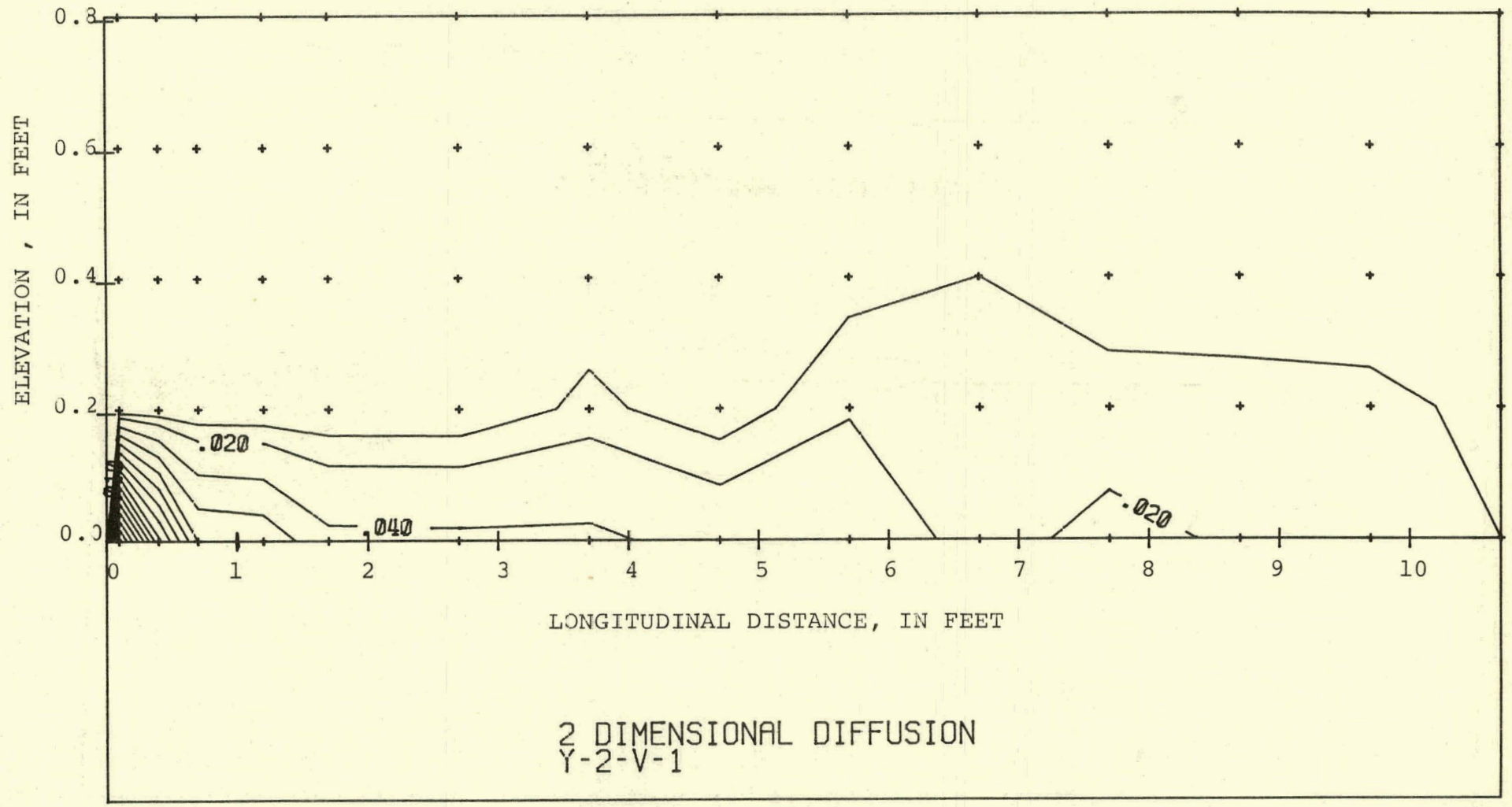

(b) Vertical Distribution of Water Temperature at Cross-Section 2

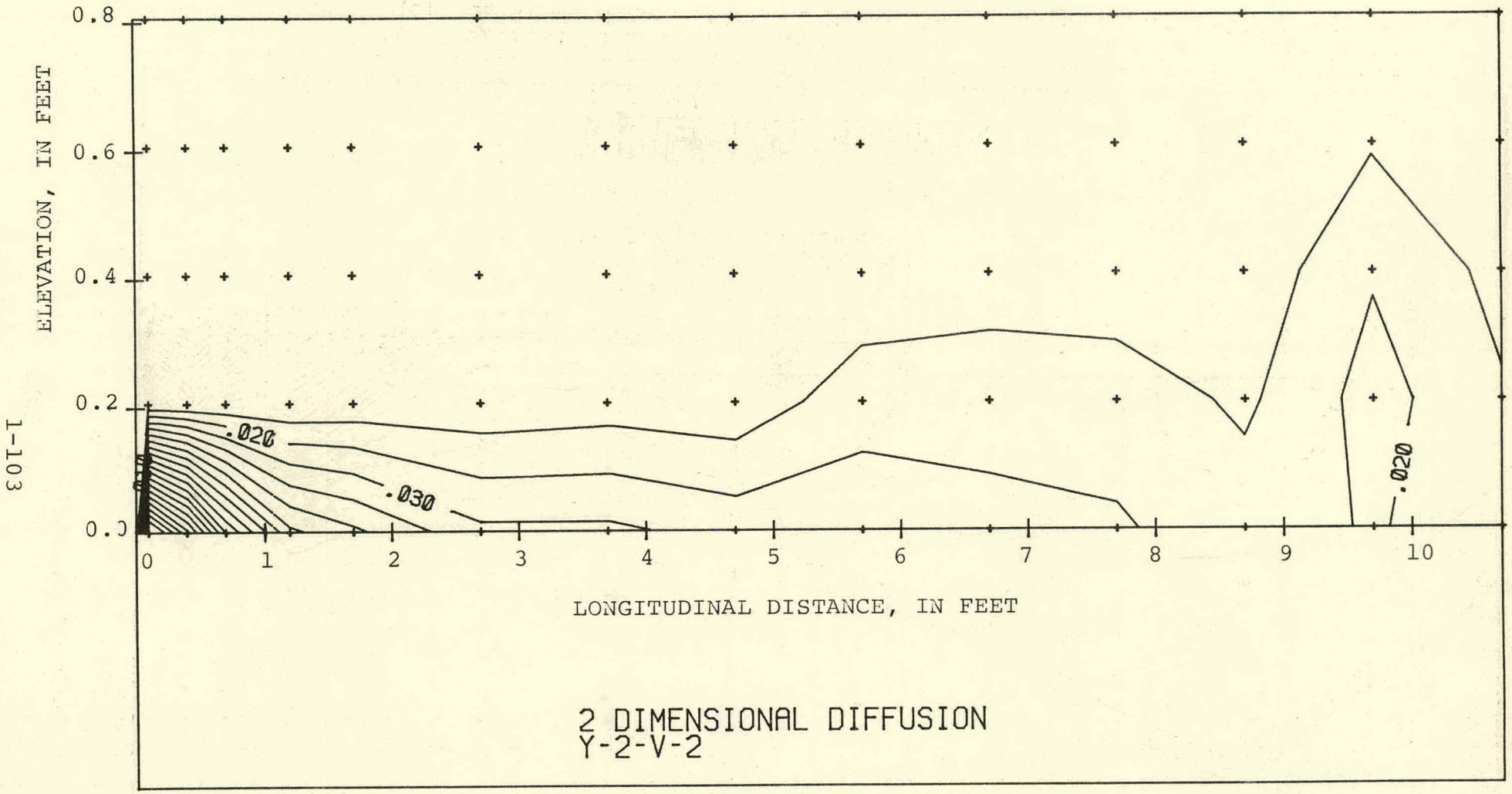

(c) Vertical Distribution of Water Temperature at Cross-Section 3

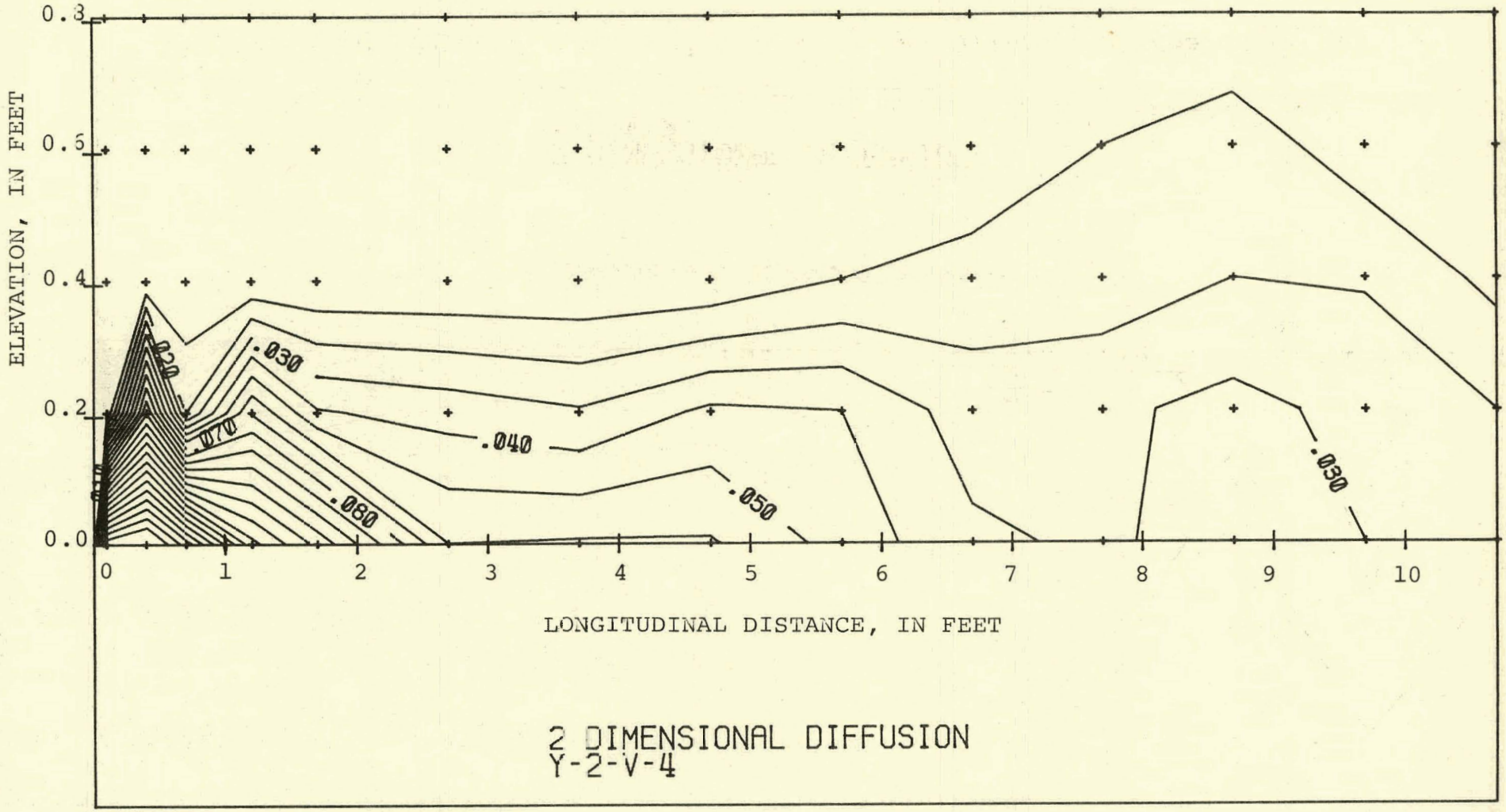

(d) Vertical Distribution of Water Temperature at Cross-Section 4

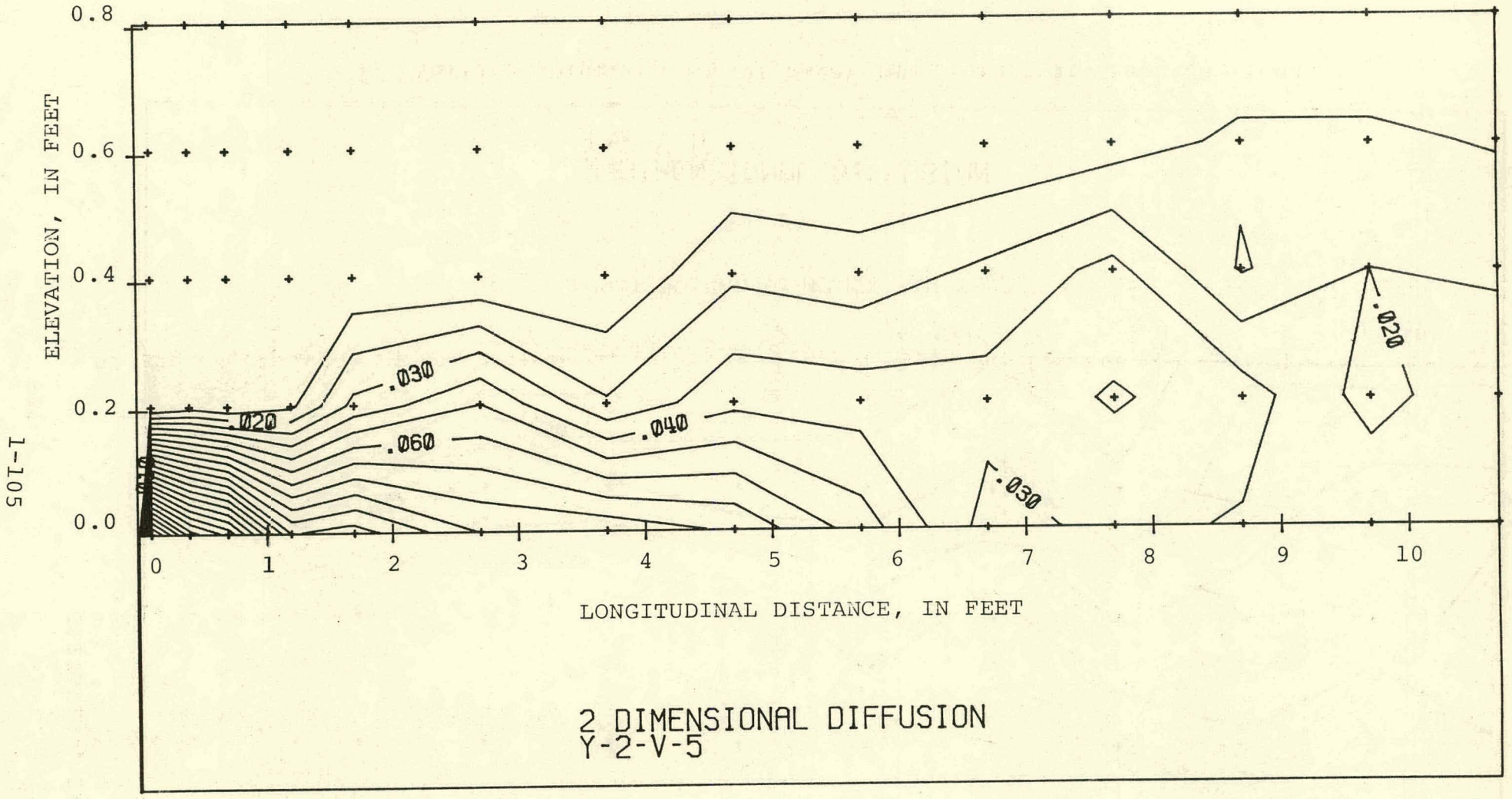

(e) Vertical Distribution of Water Temperature at Cross-Section 5

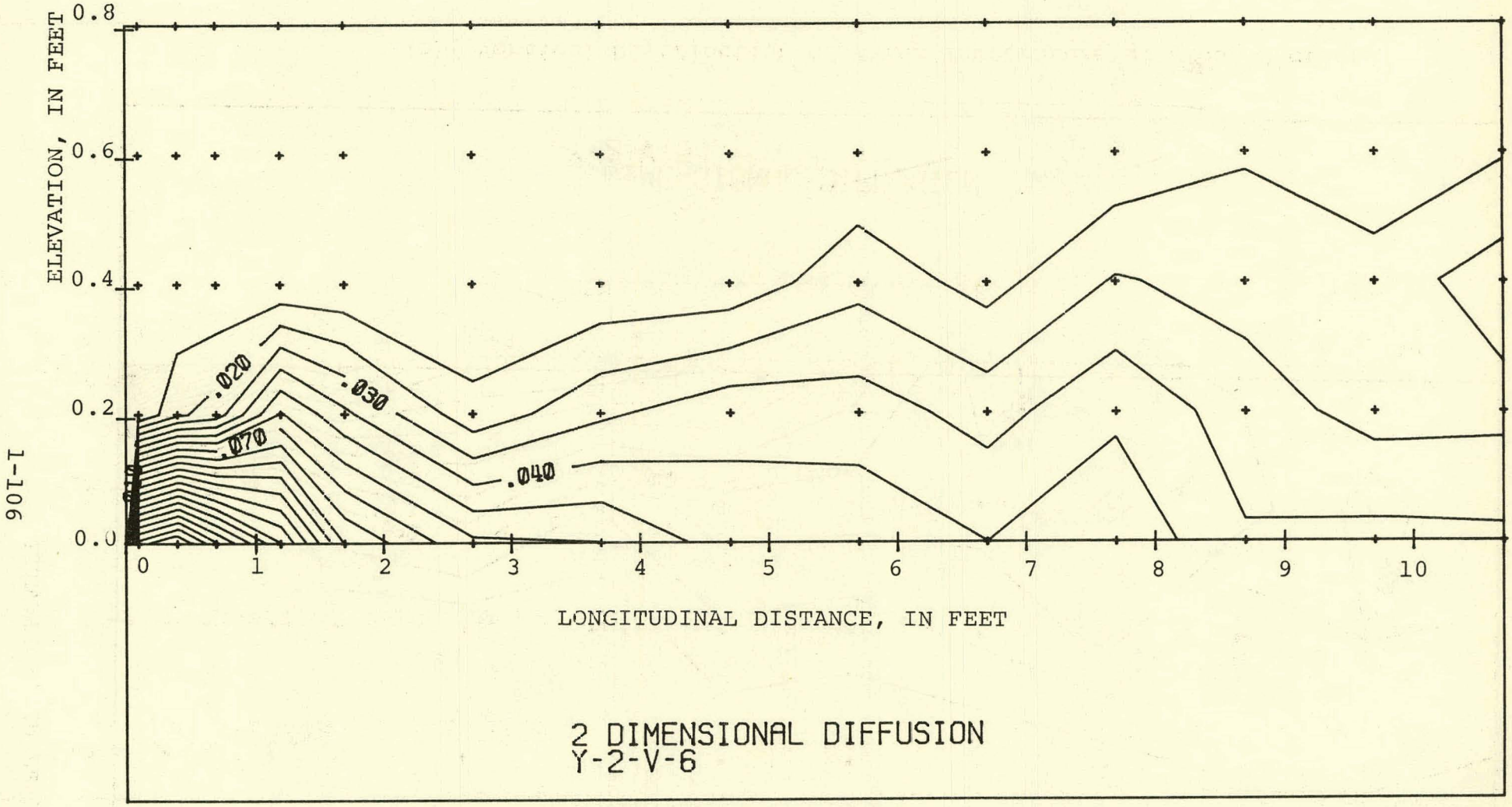

I-106

(f) Vertical Distribution of Water Temperature at Cross-Section 6

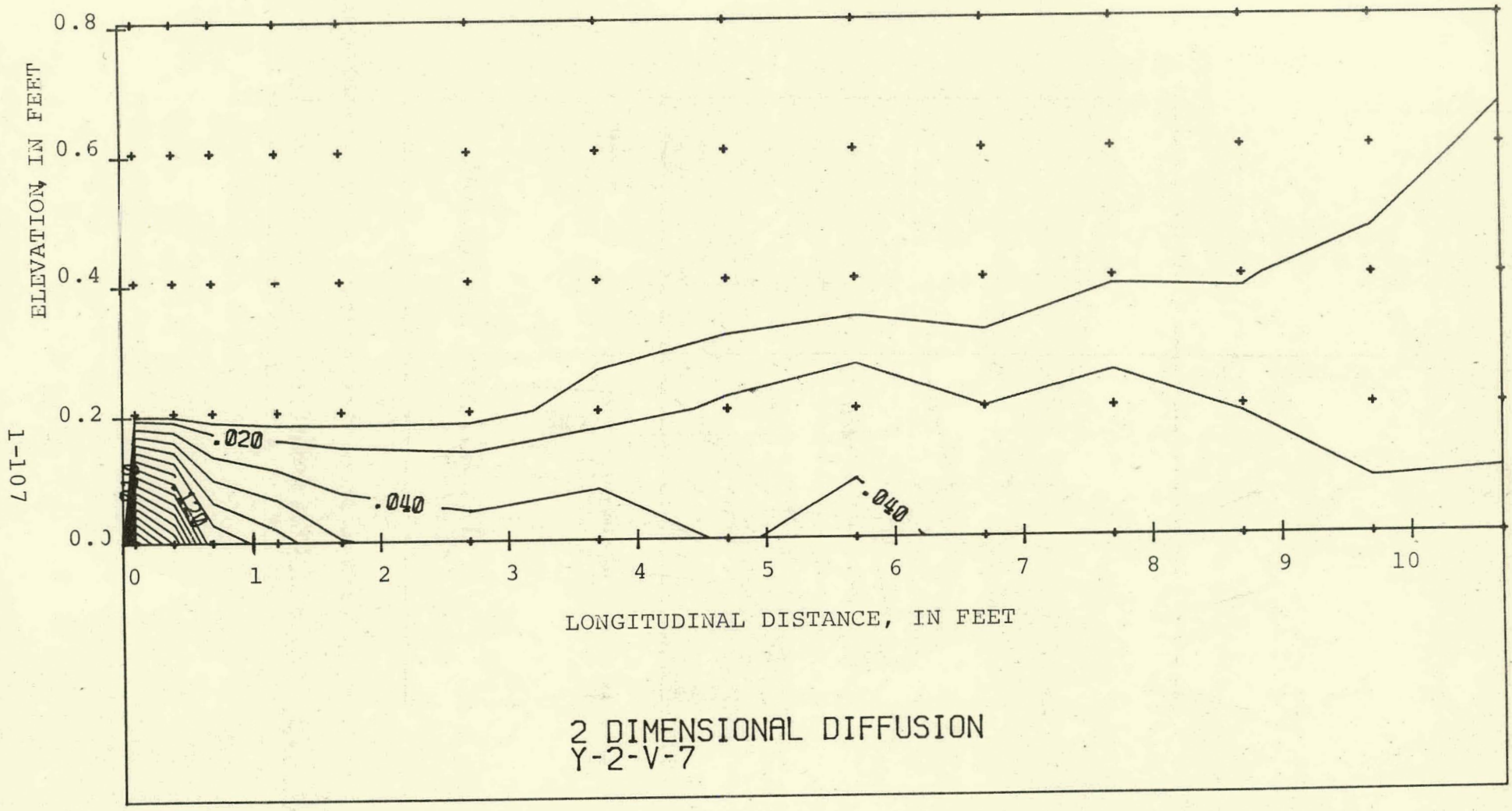

(g) Vertical Distribution of Water Temperature of Cross-Section 7

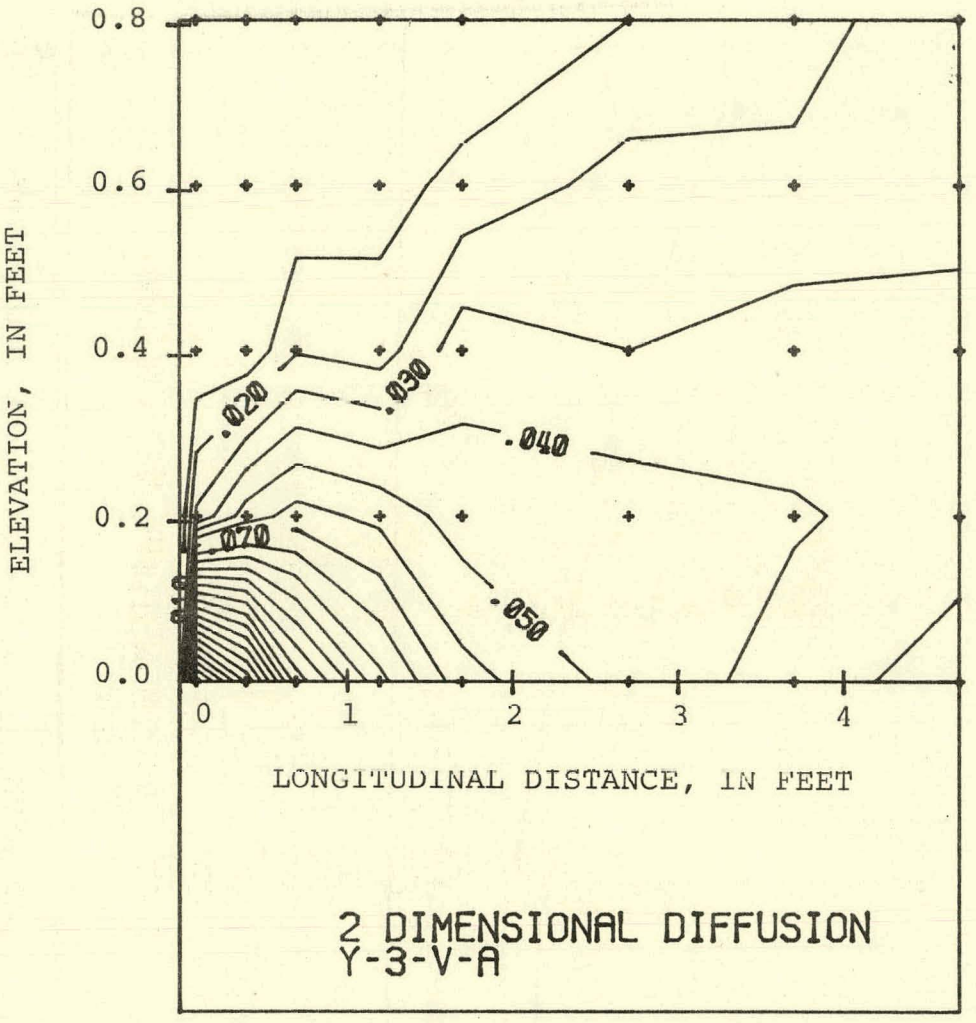

(a) Vertical Distribution of the Average Water Temperature

FIGURE 4.49 Vertical Temperature Distribution for Run Y-3. $K = 1.65$, $\mathbb{F}_D = 4.5$, $\mathbb{R}_j = 1130$, and $\mathbb{R}_a = 8.6 \times 10^4$

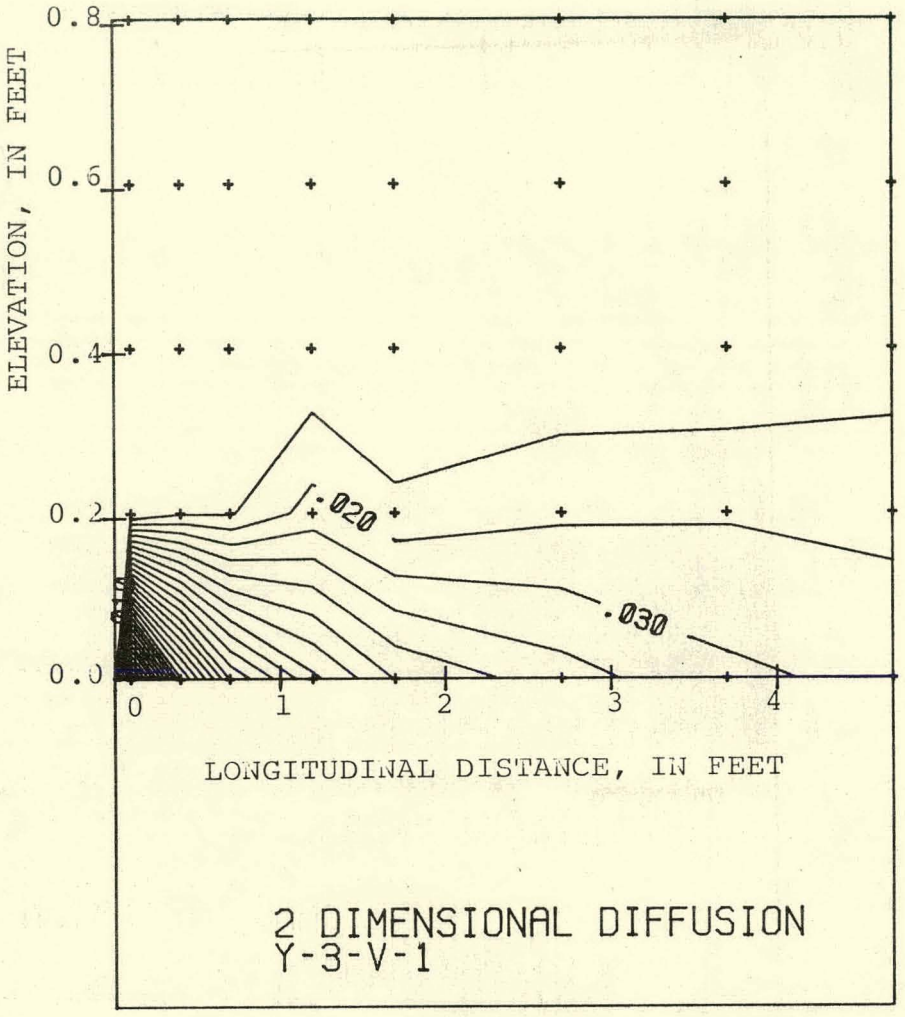

(b) Vertical Distribution of Water Temperature at Cross-Section 2

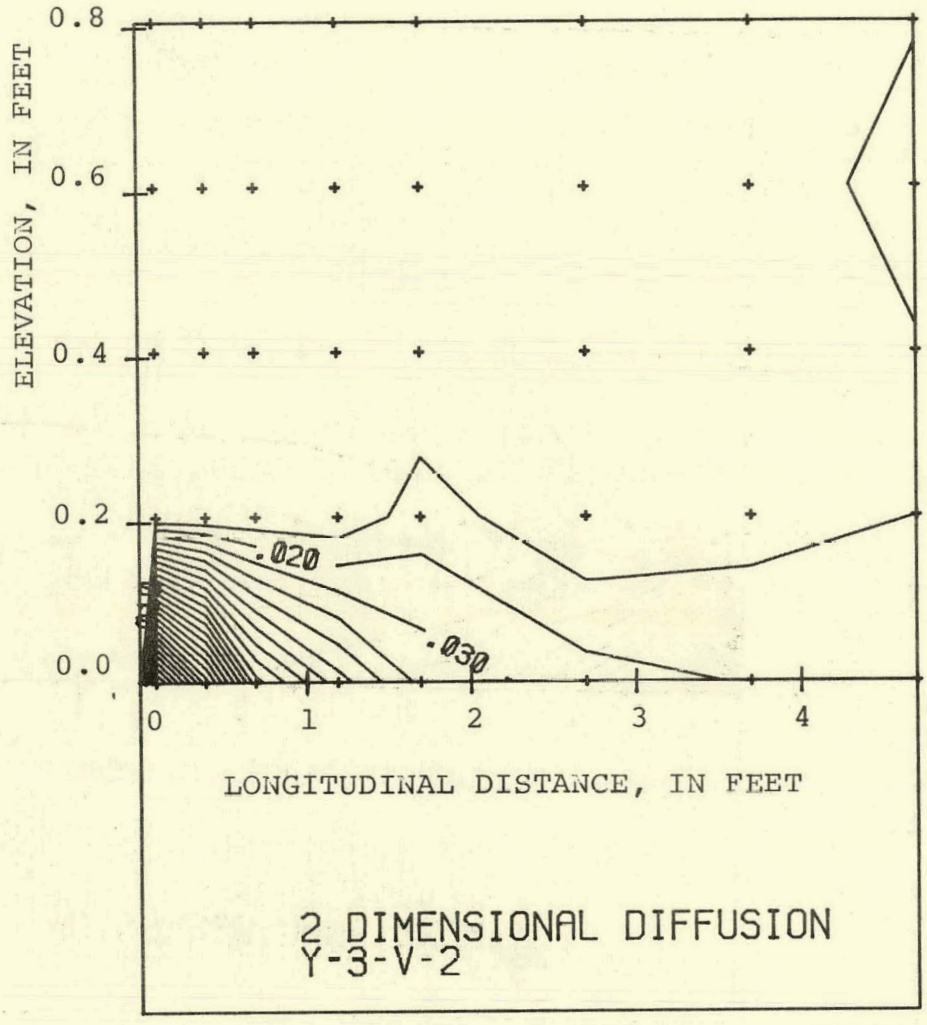

(c) Vertical Distribution of Water Temperature at Cross-Section 3

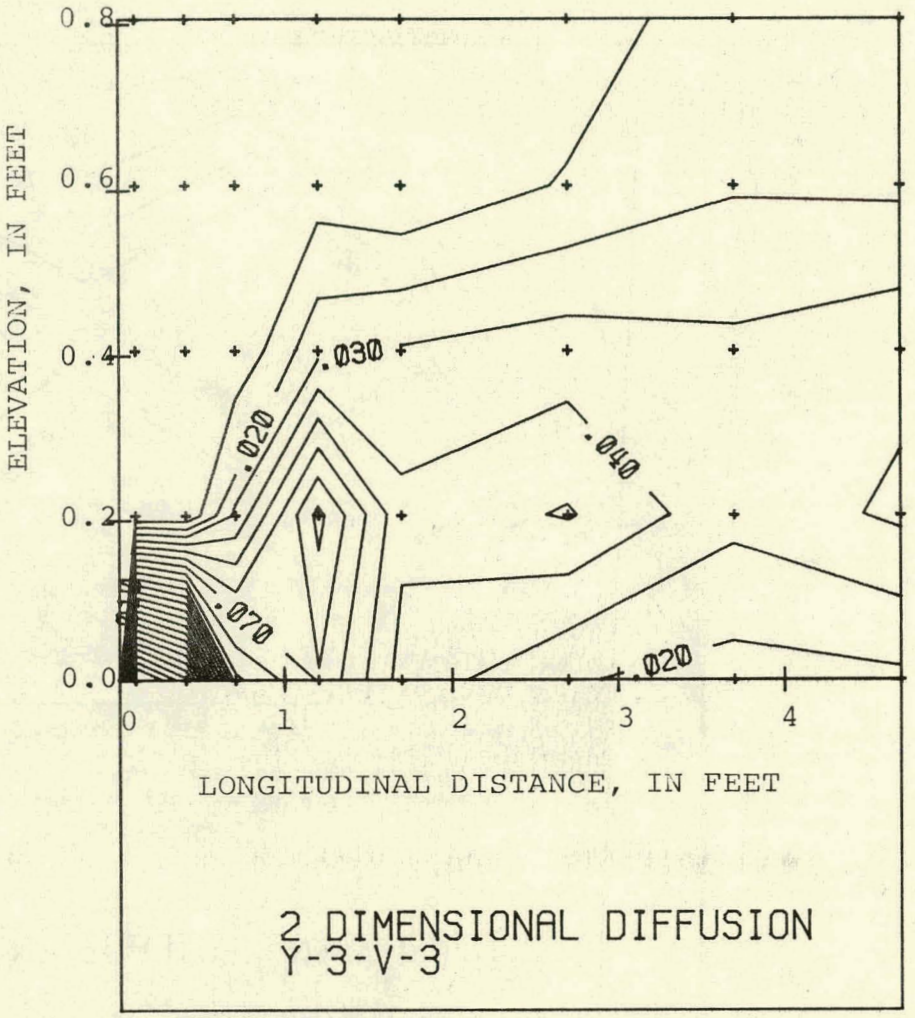

(d) Vertical Distribution of Water Temperature at Cross-Section 4

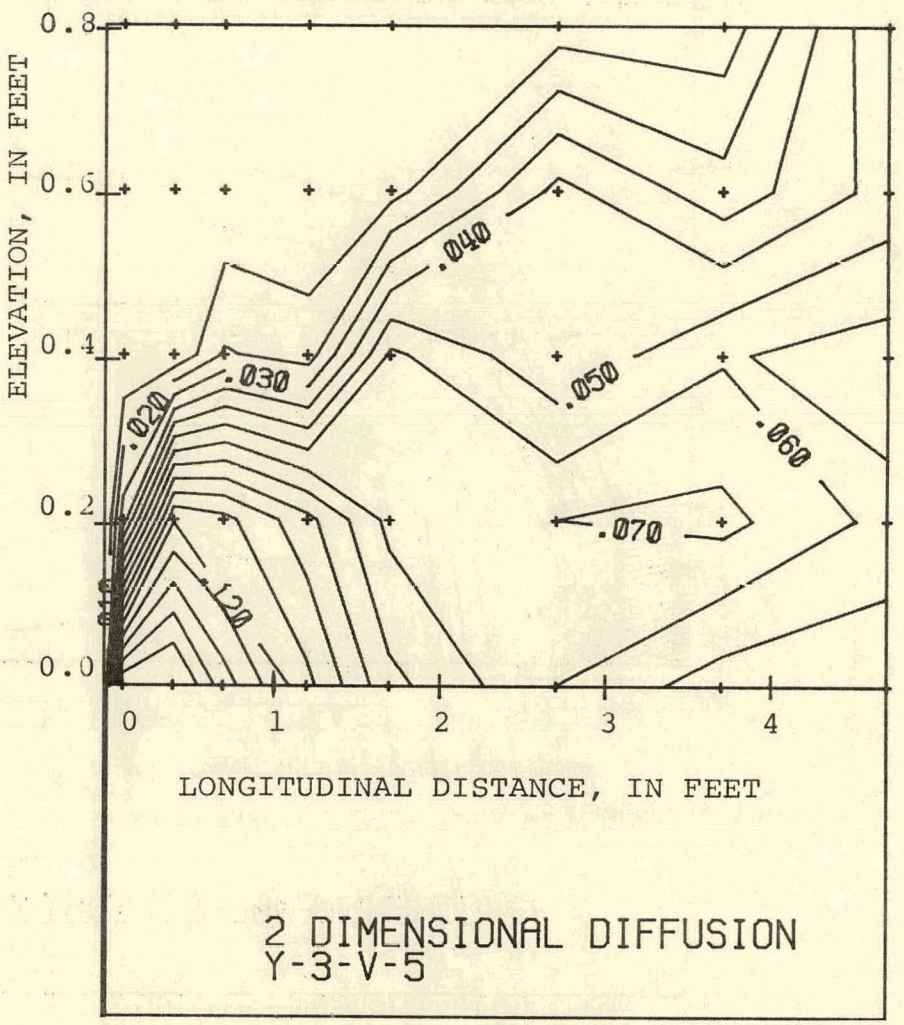

(e) Vertical Distribution of Water Temperature at Cross-Section 5

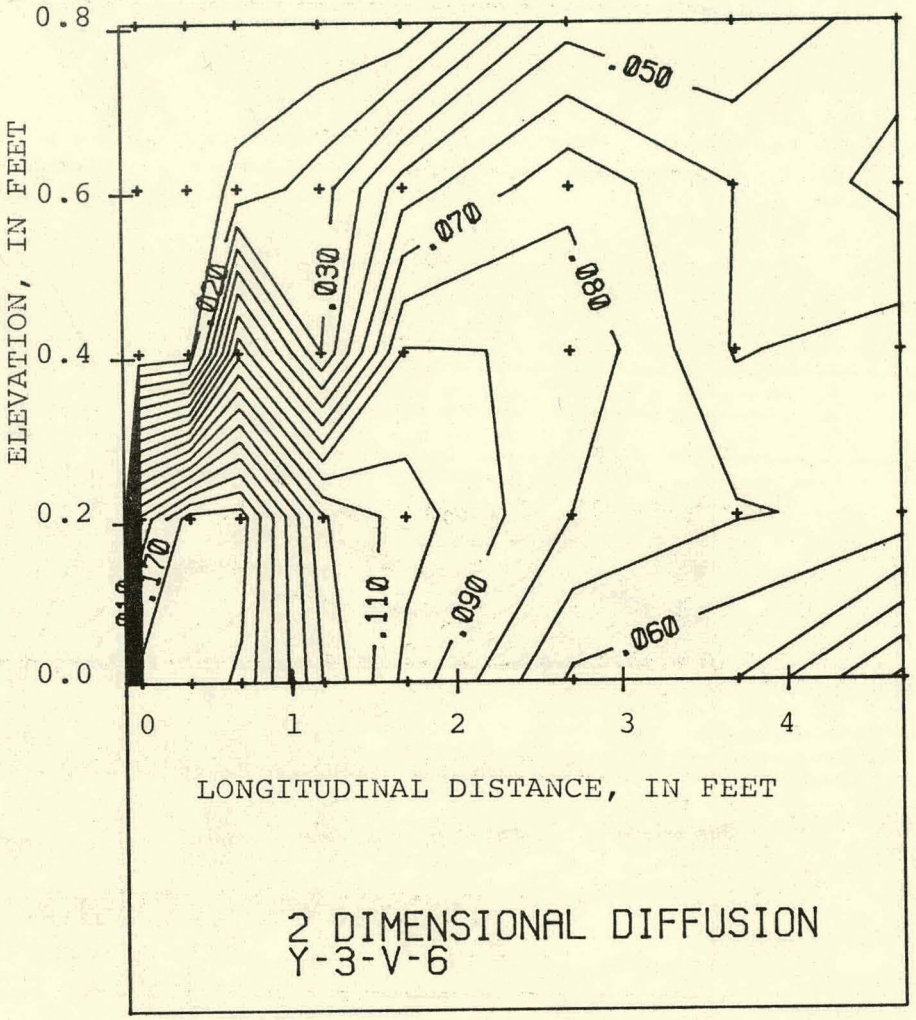

(f) Vertical Distribution of Water Temperature at Cross-Section 6

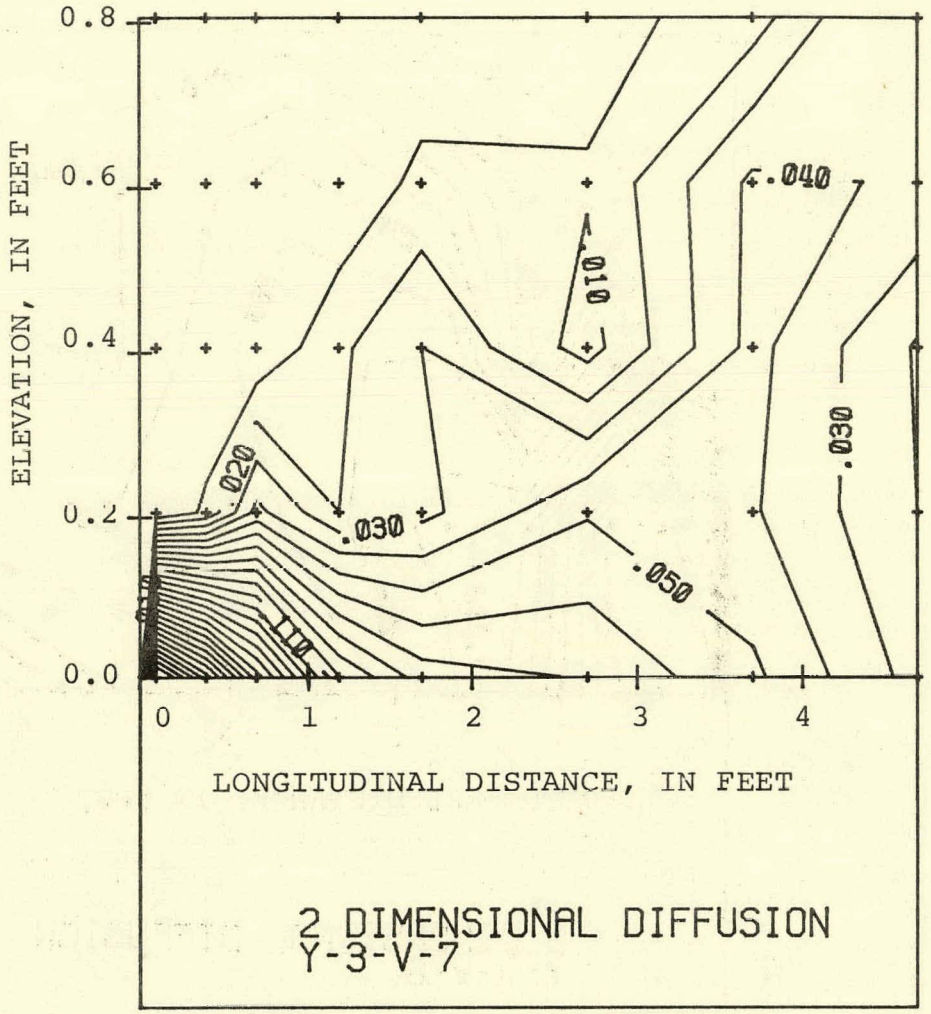

(g) Vertical Distribution of Water Temperature at Cross-Section 7

APPENDIX 2

REFERENCES

REFERENCES

1. B. E. Boyack, and D. W. Kearney, "Plume Behavior and Potential Environmental Effects on Large Dry Cooling Towers," GULF-GA-A12346, National Technical Information Service, Springfield, VA, February 1973.

2. W. G. Hoydysh, G. H. Storm, and R. R. Cirillo, "An Experimental Investigation of Air Recirculation Characteristics of Air Cooled Condenser Arrays on a Process Building," GAT-Z-4148 Category UC-38, National Technical Information Service, U. S. Department of Commerce, July 1971.

3. T. L. Chan, S. T. Hsu, J. T. Lin, K. H. Hsu, N. S. Huang, S. C. Jain, C. E. Tsai, T. E. Croley II, H. Fordyce, and J. F. Kennedy, "Plume Recirculation and Interference in Mechanical Draft Cooling Towers," IIHR Report No. 160, Iowa Institute of Hydraulic Research, The University of Iowa, Iowa City, IA, April 1974.

4. M. E. Smith, "Recommended Guide for the Prediction of the Dispersion of Airborne Effluents," ASME Committee on Air Pollution Control, ASME, May 1968.

5. G. A. Briggs, "Plume Rise," National Technical Information Service, Springfield, VA, 1969.

6. J. T. Lin, H. T. Liu, and Y. H. Pao, "Laboratory Simulation of Plume Dispersion in Stably Stratified Flows over a Complex Terrain," Flow Research Report No. 29, Flow Research Inc., February 1974.

7. B. W. Nichols and C. W. Hirt, "Transient Three-Dimensional Fluid Flow in the Vicinity of Large Structures," LA-DC-72-711, Los Alamos Scientific Laboratory, Los Alamos, NM, 1972.

8. L. S. Caretto, et al., "Two Calculational Procedures for Steady, Three-Dimensional Flow with Recirculation," Department of Mechanical Engineering Report EF/TN/A/47, Imperial College, London, 1972.

9. H. B. Zien, "Problems of Air Flow Through Large Natural Draft Cooling Towers," PB-227 815, National Technical Information Service, Springfield, VA, April 1972.

10. J. Taft, "A Numerical Model for the Investigation of Moist Buoyant Cooling Tower Plumes," SSS-R-74-2110, Systems, Science and Software, La Jolla, CA, February 1974.

11. J. P. Trepp, "A Two-Dimensional Hydrodynamic Model for Cooling Tower Plumes," Proceedings of a Symposium of International Atomic Energy Agency at Oslo, Norway, pp. 37-44, August 26-30, 1974.

APPENDIX 3

NOMENCLATURE

APPENDIX 3. NOMENCLATURE

a: Distance between the open coal mine pit to the cooling towers

b: Depth of the open mine pit

C: Constant

D: Cooling tower stack diameter

d: Ambient model flow depth and its corresponding prototype height

F: Plume buoyancy flux

f: Functional relationship

F_D: Densimetric Froude number defined by equation 3.4

F_o: Reference densimetric Froude number

F_x: Drag Force in longitudinal direction

F_z: Drag Force in vertical direction

g: Gravitational acceleration

ITD: Initial temperature difference

K: Velocity ratio of the heated effluent to the ambient flow defined by equation 3.7 and eddy diffusion coefficient for heat

K_1: Coefficient in equation 4.6

K_2: Coefficient

L: Reference length

P: Pressure

P^o: P/ρ_o

PR_x: Horizontal reference Prandtl number

PR_z: Vertical reference Prandtl number

q: Heat source

Q_D: Heat rejection capacity of a cooling tower

R: Recirculation ratio defined by equation 4.1 and gas content

r: Radial coordinate

R_a: Ambient flow Reynolds number defined by equation 3.5

R_j: Jet Reynolds number defined by equation 3.6

RE_x: Horizontal reference Reynolds number

RE_z: Vertical reference Reynolds number

T: Temperature

t: Time

T_a: Ambient flow temperature

T_i: Cooling tower input water temperature

T_w: Withdrawal water temperature of a cooling tower

U: Nondimensional longitudinal velocity (u/v_o)

u: Longitudinal velocity

V: Nondimensional vertical velocity (v/v_o)

v: Vertical velocity

V_a: Ambient velocity

V_j: Heated effluent velocity

v_o: Reference velocity

X: Longitudinal coordinate and nondimensional longitudinal coordinate (x/L)

x: Longitudinal coordinate

x_o: Representative longitudinal length = 10 feet

Y: Lateral coordinate

Z: Vertical coordinate and nondimensional vertical coordinate (z/L)

z: Vertical coordinate

Γ: Concentration of constituent

γ_d: Dry adiabatic lapse rate

Δ: $(\rho_o-\rho)/(\rho_o-\rho_r)$

ΔT: Difference between the temperature at any point in the flow field and that of the ambient flow

ΔT_a: Temperature difference within the ambient flow at different elevations

ΔT_o: Temperature difference between the heated effluent and the ambient flow

ΔZ: Elevation difference

$\Delta\rho$: Difference between the density at any point in the flow field and that of the ambient flow

$\Delta\rho_o$: Density difference between the heated effluent and the reference ambient fluid

ε: Eddy diffusion coefficient for momentum

ν_a: Kinematic viscosity of the ambient fluid

ν_d: Kinematic viscosity of the heated effluent

ξ: Binary function

ρ: Fluid density

ρ_a: Reference ambient fluid density

ρ_o: Reference ambient density

ρ_r: Reference density

Ψ: Nondimensional steam function, (ψ/Lv_o)

ψ: Stream function

Ω: Nondimensional vorticity, $(\omega L/v_o)$

ω: Vorticity

DISTRIBUTION

OFF-SITE

No. of Copies

1 Energy Research and Development Administration
ERDA Chicago Patent Group
9800 S. Cass Avenue
Argonne, IL 60439

A. A. Churm

1 Energy Research and Development Administration
Office of Assistant General Counsel for Patents
Washington, DC 20545

10 Energy Research and Development Administration
Division of Nuclear Research and Application
Washington, DC 20545

G. A. Newby, Acting Director (1)
G. W. Cunningham, Acting Deputy Director for Technology (1)
A. J. Pressesky, Acting Assistant Director for Technology (1)
D. H. Groelsema, Chief, Engineering and Component Development Branch (1)
J. D. Nulton, Engineering and Component Development Branch (4)
T. Beresovski, Chief, Advanced Concepts Evaluation Branch (1)
W. F. Savage, Advanced Concepts Evaluation Branch (1)

1 Energy Research and Development Administration
Division of Biomedical and Environmental Research
Environmental Programs
Washington, DC 20545

J. B. Blanton, Physical Oceanographer

1 Energy Research and Development Administration
Division of Reactor Development and Technology
Environmental and Sanitary Engineering Branch
Washington, DC 20545

288 Energy Research and Development Administration
Technical Information Center

1 Allied Chemical Company
550 Second Street
Idaho Falls, ID 83401

B. R. Dickey

1 Allis-Chalmers Power System, Inc.
1135 S. 70th Street
West Allis, WI 53214

J. S. Joyce

1 Aluminum Company of America
Alcoa Technical Center
Alcoa Center, OH 15069

R. Ollie

1 American Electric Power
2 Broadway
New York, NY 10004

H. J. Janzon

1 Arizona Public Service Company
2121 West Cheryl Drive
Phoenix, AZ 85021

T. Woods

1 Babcock & Wilcox
Fossil Power Division
20 S. Van Buren
Barberton, OH 44203

M. W. Peterson

1 Baltimore Gas & Electric Co.
Gas & Electric Bldg.
Baltimore, MD 21203

G. C. Creel

1 Baltimore Aircoil Co., Inc.
P. O. Box 7322
Baltimore, MD 21227

E. Schinner

1 Battelle-Geneva
7 Route De Drizi
1227 Geneva, Switzerland

J. P. Budliger

1 Battelle Institute eV.
6000 Frankfurt/Main 90
Postfach 900160
Germany

K. Simhan

1 Battelle Memorial Institute
505 King Avenue
Columbus, OH 43201

1 Bechtel Corporation
P. O. Box 60860, Terminal Annex
Los Angeles, CA 90060

P. Leung

1 Bechtel Corporation
P. O. Box 3965
San Francisco, CA 94119

G. R. Retti

1 R. W. Beck & Associates
400 Prudential Plaza
Denver, CO 80202

J. P. Rossie

1 Black Hills Power and Light Company
P. O. Box 1400
Rapid City, SD 57701

B. Westre

1 Burns & Roe, Inc.
320 Fulton Avenue
Hempstead, NY 11550

M. J. Hroncich

1 Carolina Power & Light Company
336 Fayettesville Street
Raleigh, NC 27602

J. Sell

1 Catalytic Construction Corporation
P. O. Box 11402
Charlotte, NC 28029

J. Morse

1 Commonwealth Edison
One First Plaza
P. O. Box 767
Chicago, IL 60690

R. H. Holyoak

1 Consolidated Edison Company of New York, Inc.
4 Irving Place
New York, NY 10003

C. L. Newman

1 Cornell University
Ithaca, NY 14850

F. K. Moore

1 Curtiss Wright Corporation
One Passaic Street
Wood Ridge, NJ 07075

R. C. Haberski

1 Corps of Engineers
U.S. Army Engineering Waterways Experiment Station
Vicksburg, MS 39180

G. H. Hilt, Director

1 Corps of Engineers
North Pacific Division
Water Quality Section
210 Custom House
Portland, OR 97209

B. Doyle

1 Corps of Engineers
North Pacific Division
Portland District Office
Portland, OR 97209

R. Waits, Chief of Hydrology

1 Corps of Engineers
North Pacific Division
Seattle District Office
4735 East Marginal Way South
Seattle, WA 98134

N. McDonald

1 Corps of Engineers
North Pacific Division
Walla Walla District Office
Bldg. 602, City-County Airport
Walla Walla, WA 99362

W. E. Sivley, Chief of Engineering Division

1 U.S. Department of Commerce
National Oceanic and Atmospheric Administration
Environmental Research Laboratories
Boulder, CO 80302

Director

1 U.S. Department of Interior
Office of Water Research and Technology
Washington, DC 20242

E. D. Eaton, Deputy Director

1 Duke Power Company
P. O. Box 2178
Charlotte, NC 28201

S. K. Blackley

1 Ecodyne Cooling Products Co.
San Rosa, CA 95403

J. K. Swindt

2 Electric Power Research Institute
3412 Hillview Avenue
P. O. Box 10412
Palo Alto, CA 94304

J. Maulbetsch
S. A. Schurr, Director of Energy Systems,
Environmental and Conservation Division

1 Empire State Electric Energy Research Corporation
1250 Broadway
New York, NY 10001

L. Geller

1 Environmental Protection Agency
Office of Research and Development
Office of Air, Land and Water Use
Washington, DC 20460

T. A. Murphy

1 Environmental Protection Agency
Air Quality Planning & Standards
Research Triangle Park, NC 27709

B. J. Steigerwald

2 Environmental Protection Agency
Pacific Northwest Water Laboratory
200 S. W. 35th Street
Corvallis, OR 97330

M. Shirazi
F. H. Rainwater

1 Environmental Protection Agency
Region X
1200 Sixth Avenue
Seattle, WA 98101

C. V. Smith, Jr.

1 Environmental Protection Agency
Region IX
100 California Street
San Francisco, CA 94111

P. DeFalco, Jr.

1 Franklin Institute
Twentieth & Parkway
Philadelphia, PA 19103

A. M. Rubin

1 GEA Airexchangers, Inc.
46 Worthington Drive
Maryland Heights, MD 63043

B. Davis

1 General Atomics
P. O. Box 81608
San Diego, CA 92138

D. A. Nelson

1 General Electric Company
Large Steam Turbine Division
300 Nott Street
Schenectady, NY 12301

E. H. Miller

1 Gilbert Associates, Inc.
525 Lancaster Avenue
Reading, PA 19603

J. F. Sebald

1 Heat Transfer Research, Inc.
1000 S. Fremont Avenue
Alhambra, CA 91802

J. E. Taboric

2 Hudson Products
6855 Horwin Drive
Houston, TX 77036

E. C. Smith
M. W. Larinoff

1 Italimpianti - Societa Italiana Impianti p.a.
Piaza, Piccapietra 9
18121 Genoa, Italy

C. Rocco

1 Los Angeles Department of Water and Power
111 N. Hope Street
Los Angeles, CA 90012

J. L. Mulloy

1 Louisiana Power & Light Co.
142 Delaronde St.
New Orleans, LA 70174

R. J. Meyer

1 Marley Company
5800 Fox Ridge Drive
Mission, KS 66202

R. Landon

1 Massachusetts Institute of Technology
77 Massachusetts Avenue
Cambridge, MA 02139

L. R. Glicksman

1 Niagara Blower
405 Lexington Avenue
New York, NY 10017

W. Kals

1 New York University
University Heights
New York, NY 10453

W. G. Hoydysn

1 Northeast Utilities
P. O. Box 270
Hartford, CT 06101

R. H. Meyer

7 U.S. Nuclear Regulatory Commission
Washington, DC 20555

R. Overstreet
R. Codell
D. Schrieber
Hydrologic Engineering Section, Site Analysis Branch
Division of Technical Review

R. T. Jaske
M. L. Ernst, Project Director
Nuclear Energy Center Special Study
Office of Special Studies

J. Davis
A. Joseph
Office of Nuclear Regulatory Research

1 Oregon State University
Department of Mechanical Engineering
Corvallis, OR 97330

L. P. Davis

1 Oregon State University
Department of Chemical Engineering
Corvallis, OR 97330

C. E. Wicks

1 Pacific Gas and Electric
77 Beale Street
San Francisco, CA 94106

F. F. Mautz

1 Pacific Power and Light Company
Public Service Building
Portland, OR 97204

P. G. Humphries

1 PFR Engineering Systems
1417 South Georgia Street
Los Angeles, CA 90015

T. Rozenman

1 Power Generation Cooling Systems
4714 - 52nd Street South
Seattle, WA 98118

A. C. Smith

1 Public Service of Colorado
5900 East 39th Avenue
Denver, CO 80207

R. F. Walker

1 Public Service of New Mexico
Corporate Planning Department
Albuquerque, NM 87103

E. D. Kist

1 Research Cottrell
Hamon Cooling Tower Division
P. O. Box 750
Bound Brook, NJ 08805

G. E. Collins

1 Reynolds Aluminum Company
Reynolds Metallurgical Research Laboratory
Richmond, VA 23261

B. Caruthers

1 Prof. Ing. Carlo Roma
Piazza delle Muse 8
Rome, Italy

1 San Diego Gas and Electric
101 Ash Street
San Diego, CA 92107

R. G. Lacy

1 Seattle City Light
1015 Third Avenue
Seattle, WA 98104

R. L. Skone

1 Southern California Edison
2244 Walnut Grove Avenue
Rosemead, CA 91770

J. Rasband

1 Consultant Engineer
74 Trinity Place, Suite 511
New York, NY 10006

P. Sporn

1 Stearns and Rogers
700 South Ash Street
Denver, CO 80222

J. Y. Parce

1 Stone & Webster Engineering Corporation
225 Franklin Street
Boston, MA 02107

D. H. Guild

1 Tampa Electric Co.
P. O. Box 111
Tampa, FL 33601

H. T. Wilson

1 Texas Electric Service Co.
115 W. Seventh Street
Fort Worth, TX 76102

W. Keel

1 Utah Power and Light
1407 West North Temple
Salt Lake City, UT 84103

J. H. Hutchinson

1 Union Carbide Corporation
ORGDP - K-25
P. O. Box D
Oak Ridge, TN 37803

G. J. Kidd

1 United Engineers & Constructors
IVB Building
1700 Market Street
Philadelphia, PA 19105

G. A. Engelson

1 University of Iowa
Hydraulic Research Institute
Iowa City, Iowa 52242

J. F. Kennedy

1 Virginia Electric & Power Co.
700 E. Franklin Street
Richmond, VA 23261

S. Ragone

1 Washington Public Power Supply System
3000 George Washington Way
Richland, WA 99352

D. D. Tillson

1 Washington State Department of Ecology
Olympia, WA 98504

J. Biggs, Director

1 West Associates
Sierra Pacific Power Company
100 E. Moana Lane
Reno, NV 89510

G. H. Soule

2 Westinghouse Electric Corporation
Steam Turbines Division
Lester Branch
P. O. Box 9175
Philadelphia, PA 19113

K. A. Oleson
G. J. Silvestri

ON-SITE

No. of Copies

3 Atlantic Richfield Hanford Company

D. J. Brown
R. E. Isaacson
ARHCO File

3 Energy Research and Development Administration
Richland Operations Office

P. G. Holsted
B. J. Melton
Technical Information Library

5 United Nuclear Industries, Inc.

T. E. Dabrowski
A. E. Engler
N. R. Miller
W. G. Westover
UNI File

1 Westinghouse Hanford Company
Hanford Engineering Development Laboratory

J. Fletcher

122 Battelle-Northwest

R. T. Allemann
T. W. Ambrose
D. B. Cearlock
D. W. Dragnich
D. E. Deonigi/J. W. Currie (2)
J. G. DeStreese
D. W. Faletti
J. W. Finnigan
B. C. Fryer
C. H. Henager
A. B. Johnson/D. Pratt (2)
W. S. Kelly
R. S. Kemper/P. A. Ard (2)
C. J. Knoll
W. V. Loscutoff
R. P. Marshall/R. L. Dillon (2)
D. E. Olesen
Y. Onishi (50)
L. T. Pedersen
H. C. Riches/J. B. Schuette (2)
J. S. Stoakes
A. M. Sutey
D. S. Trent (5)
M. Vagins
R. A. Walter
R. L. Watts
R. D. Widrig
R. K. Woodruff
F. R. Zaloudek
File - B. M. Johnson (30)
Technical Information (3)
Technical Publications (2)